SUPPRESSION OF ARTIFACTS IN IMPEDANCE CARDIOGRAPHY

Thesis
submitted in partial fulfillment of the requirements
for the degree of

Doctor of Philosophy

by

Vinod Kumar Pandey
(Roll No. 01430001)

under the supervision of

Prof. P. C. Pandey

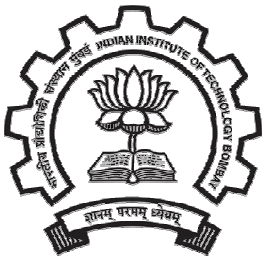

Biomedical Engineering Group
School of Biosciences and Bioengineering
Indian Institute of Technology Bombay

July 2009

DECLARATION

I declare that this written submission represents my ideas in my own words and where others' ideas or words have been included, I have adequately cited and referenced the original sources. I also declare that I have adhered to all principles of academic honesty and integrity and have not misrepresented or fabricated or falsified any idea/data/fact/source in my submission. I understand that any violation of the above will be cause for disciplinary action by the Institute and can also evoke penal action from the sources which have thus not been properly cited or from whom proper permission has not been taken when needed.

Vinod Kumar Pandey
Roll no. 01430001

Date: 22.07.2009

Indian Institute of Technology Bombay

CERTIFICATE OF COURSE WORK

This is to certify that Mr. Vinod Kumar Pandey (Roll No. 01430001) was admitted to the candidacy of Ph.D. Degree in January 2003, after successfully completing all the courses required for the Ph.D. Degree Programme. The details of the course work done are given below.

Sr. No.	Course No.	Course Name	Credits
1	BM 602	Biostatistics	6
2	BM 603	Physiology for Engineers	6
3	BM 607	Physiological Measurements and Quantitative Physiology	10
4	BM 632	Medical Instrumentation	6
5	BM 661	Signals and Systems for Biomedical Engineering	3
6	BMS 601	Seminar	4
7	BMS 801	Seminar	4
8	EE 603	Digital Signal Processing and its Applications	6
9	EE 616	Electronic Systems Design	6
10	EE 617	Sensors in Instrumentation	6
11	EE 712	Embedded Systems Design	6
		Total Credits	63

I.I.T. Bombay
Dated:

Dy. Register (Academic)

Vinod K. Pandey / Supervisor: Prof. P. C. Pandey, "Suppression of artifacts in impedance cardiography", *Ph.D. Thesis*, Biomedical Engineering Group, School of Biosciences and Bioengineering, IIT Bombay, 2009.

Abstract

Impedance cardiography is a noninvasive technique for monitoring stroke volume, based on sensing variation in the thoracic impedance, $z(t)$, due to the blood flow. Time derivative of the thoracic impedance is known as the impedance cardiogram (ICG) and is used for estimating ventricular ejection time (T_{lvet}), the ICG peak ($(-dz/dt)_{max}$), stroke volume, and some other cardiovascular indices. Respiration and motion artifacts cause base line drift in the sensed impedance waveform, particularly during or after exercise, and this drift results in errors in estimation of the parameters. Objective of the research reported in this thesis is to investigate techniques for removal of the artifacts from ICG for estimation of stroke volume and other cardiovascular indices, without smearing the beat-to-beat variations.

A baseline restoration circuit and signal processing technique for suppression of artifacts are developed and investigated. The baseline restoration circuit, based on amplitude tracking, is developed for partly removing the artifacts for effective utilization of the input dynamic range of the signal acquisition hardware. The signal processing techniques developed and investigated are based on adaptive filtering and wavelet based denoising. A signal related to respiration is sensed by a thermistor based airflow sensor and is used as the reference input for the respiratory artifact cancellation. For a better approximation of the respiratory artifact, cubic spline fitting is applied on the sensed impedance signal in synchronism with the respiratory phases. Adaptive filtering is not suitable for suppression of motion artifact because of practical difficulty in obtaining reference signal related to the various motions causing variation in the thoracic impedance. A wavelet based denoising technique, not requiring a reference signal, is investigated for removal of respiratory and motion artifacts. These artifact suppression techniques are evaluated on signals with simulated artifacts and signals acquired from several volunteers with normal health.

For validation of the techniques under a clinical setting, Doppler echocardiography is used as the reference. The values of stroke volume estimated from impedance cardiography were compared with those obtained from Doppler echocardiography, on beat-to-beat basis, for subjects with normal health and ward referral patients. Artifact suppression resulted in increased correlation, low scatter from linear regression, and a decrease in the mean bias and the standard deviation of the differences, showing that the artifact suppression techniques can be used with impedance cardiography instrument for continuous monitoring of stroke volume and other cardiovascular parameters.

Contents

List of figures

List of Tables

List of symbols

$(-dz/dt)_{max}$	maximum of the negative of the derivative of the impedance during the systole
c	intercept of linear regression line
$e(n)$	error output of adaptive filter
H	subject's height
L	distance between voltage sensing electrodes
m	slope of linear regression line
M	tap length of the adaptive filter
T_{lvet}	left ventricular ejection time
w_n	adaptive filter coefficient
$W(m,n)$	wavelet detail coefficient
$z(t)$	change in the thoracic impedance
$Z(t)$	total sensed thoracic impedance
Z_o	basal impedance across thorax
ΔV	stroke volume
ρ	resistivity of blood
μ	step size for adaptation in adaptive filter
Δz	impedance change
δ	weight correction factor in Bernstein's formula
ε	root mean square error for linear regression
$\Psi_{m,n}(t)$	wavelet function

List of abbreviations

A/D	analog-to-digital
ACI	acceleration index
AFER	adaptive filtering by using estimated respiration
AFSR	adaptive filtering by sensing respiration
Corr.	correlation coefficient
CSA	cross-sectional area
CWT	continuous wavelet transform
D/A	digital-to-analog
DWT	discrete wavelet transform
ECG	electrocardiogram
echo	Doppler echocardiogram
EMG	electromyogram
FIR	finite impulse response
HI	Heather index
ICG	impedance cardiogram
LMS	least mean square
m.b.	mean bias
NLMS	normalized LMS
PCG	phonocardiogram
PEP	pre-ejection period
rms	root mean square
s.d.	standard deviation
s.d.d	standard deviation of differences
SAR	signal-to-artifact ratio
SFLC	Scaled Fourier linear combiner
SNR	signal-to-noise ratio
STR	systolic time ratio
SV	stroke volume
TFI	thoracic fluid index
UP	unprocessed signal
VTI	velocity time integral
WBD	wavelet based denoising

Chapter 1

INTRODUCTION

1.1 Problem overview

The stroke volume is the amount of blood pumped by the left ventricle of the heart in one contraction. The cardiac output is the amount of blood pumped by heart in one minute, and hence it is given as the product of the stroke volume and the heart rate. It gives valuable diagnostic information about cardiovascular functioning (Kerr *et al*., 1998; Korhonen *et al*., 1999; Siebert *et al*., 1999; Nelson and Janerot-Sjöberg, 2001; Siebert *et al*., 2004; Liu *et al*., 2004). Unlike heart rate variability and blood pressure variability, stroke volume variability has not been widely used as a cardiac diagnostic tool, mainly because of the difficulty in getting accurate estimation of stroke volume on a beat-to-beat basis over a long period of time.

Impedance cardiography is a noninvasive technique for monitoring changes in the impedance of the thorax due to blood flow. In this technique, a high-frequency (20-400 kHz) and low-amplitude current (< 5 mA) is injected into the thorax using a pair of electrodes. The resulting voltage waveform, sensed across the same or another pair of voltage sensing electrodes, gets amplitude modulated due to variations in the thoracic impedance. It is demodulated to obtain the impedance variation ($z(t)$) and it can be used, with the help of an appropriate impedance model of the thorax, for estimating stroke volume and several other cardiovascular indices (Kubicek *et al.*, 1966; Kubicek *et al.*, 1967; Kubicek *et al.*, 1974; Kubicek, 1989; Patterson, 1989; Sramek, 1994). Several studies have shown that the values of the stroke volume and some of the indices estimated using impedance cardiography have a good correlation with those obtained using dye dilution, thermodilution, CO_2 rebreathing, and Doppler echocardiography methods (Lababidi *et al.*, 1971; Aust *et al.*, 1982; Wang *et al.*, 1989; Northridge *et al.*, 1990; Pappas *et al.*, 1994; Kizakevich *et al.*, 1994; Woltjer *et al.*, 1996; Verhoeve *et al.*, 1998; Greenberg *et al.*, 2000; Treister *et al.*, 2004; Fortin *et al.,* 2005). As impedance cardiography is a noninvasive and a low cost technique, it has a great potential in cardiovascular diagnostics.

Negative derivative of the thoracic impedance, $-dz/dt$, is known as the impedance cardiogram (ICG). The stroke volume is generally calculated using Kubicek's formula (Kubicek *et al.*, 1966; Kubicek *et al.*, 1967; Kubicek *et al.*, 1974; Patterson, 1989; Kubicek, 1989) or one of its several modifications (Sramek *et al*., 1983; Sherwood *et al*. 1990; Verdu, 1994; Bernstein and Lemmens, 2005), using two parameters: (i) the left ventricular ejection time (T_{lvet}) and (ii) peak of the ICG ($(-dz/dt)_{max}$). In Kubicek's formula, it is assumed that the resistivity of blood is constant during the cardiac cycle and aortic blood flow is a square wave pulse lasting until the end of the systole. The product of $(-dz/dt)_{max}$ and T_{lvet} is thus directly proportional to the systolic pulsatile change in the aortic blood volume. However, actual aortic blood flow profile significantly differs from a square pulse, and it varies across individuals. Further, blood flow results in a change in the orientation of the erythrocytes and hence in a change in the blood resistivity during the cardiac cycle (Visser *et al.*, 1976; Sakamoto and Kanai, 1979; Visser, 1989; Thomas *et al.*, 1991; Sramek, 1994). Contribution of various blood vessels in the thoracic region is not well established. These factors have limited the development of a model for a precise and accurate estimation of the stroke volume and other indices for cardiovascular diagnosis.

Another problem with impedance cardiography is that sensing of the variation in the thoracic impedance due to blood flow is influenced by respiration and motion artifacts. Respiratory artifact is the variation in the sensed thoracic impedance caused primarily by changes in the thoracic cage during inhale and exhale phases of respiration. While, motion related artifacts are due to body movement and thoracic dimension changes. The spectra of the motion and respiratory artifacts partly overlap with that of the ICG. These artifacts have a large amplitude as compared to the impedance variation due to the blood flow, and cause a baseline drift in the sensed impedance waveform. Presence of these artifacts in the signal restricts proper use of the input dynamic range of the analog-to-digital (A/D) converter and severely affects the estimation of the various indices, particularly during stress test or during post-exercise relaxation. Ensemble averaging is generally employed for suppressing the artifacts, but it suppresses beat-to-beat variations. It also tends to suppress or blur some of the important points in the ICG waveform and may cause errors in the estimation of the various parameters.

1.2 Research objective

The research objective is to investigate techniques for suppression of the artifacts in the signal sensed by impedance cardiography, for the estimation of stroke volume and other cardiovascular indices without smearing the beat-to-beat variations.

A baseline restoration circuit is developed for fast estimation and partial removal of the baseline drift, before digitizing the signal, for effective utilization of the input dynamic range of the A/D converter. Signal processing techniques, based on adaptive filtering and wavelet based denoising, are investigated for cancellation of the artifacts in the acquired signals. In the adaptive filter based technique, a reference signal is needed for artifact cancellation. For removing respiratory artifact, respiration is sensed by a thermistor based airflow sensor placed in front of the nostrils. There are limitations in applying this technique for removal of motion artifacts, due to practical limitations in obtaining a reference signal related to various motions that may cause variation in thoracic impedance. Application of wavelet based denoising technique without involving a reference signal is investigated for removal of respiratory and motion artifacts.

A quantitative evaluation of the artifact suppression is carried out by applying these techniques on the artifact-free ICG recordings added with simulated artifacts at different levels, for recordings from 23 healthy volunteers. Suppression of the actual artifacts is investigated by applying the techniques on the signals acquired under the conditions of high heart rate variability and artifacts, from 52 healthy volunteers during post-exercise relaxation. For the validation of the techniques, under a clinical setting, Doppler echocardiography is used as a reference technique. Simultaneous recordings of ICG and Doppler echocardiogram were carried out from nine subjects with normal health and five subjects with cardiovascular disorders. Agreement between the values of stroke volume and some of the indices as estimated from the two techniques are examined.

1.3 Thesis outline

Chapter 2 presents an overview of the fundamentals of impedance cardiography inluding impedance model of the thorax, electrode systems, and various artifacts present in the impedance signal. This is followed by a review of the signal processing techniques for artifact cancellation. At the end of this chapter, the techniques to be investigated and the methods for their evaluation and validation are presented.

Chapter 3 presents a baseline restoration circuit for effective utilization of the input dynamic range of the A/D converter. Chapter 4 presents the techniques based on adaptive filtering for removal of respiratory artifacts. The wavelet based denoising technique is presented in Chapter 5. Results from analysis of the recordings taken, in a clinical setting, from the subjects with normal health and those with cardiac disorders are presented and discussed in Chapter 6. The estimated stroke volume and some of the cardiac indices from impedance cardiography are compared with the values obtained from Doppler echocardiography, which provides a reference for beat-to-beat variations. Chapter 7 gives a

summary of the work done, conclusions drawn from the present research, and some suggestion for further work.

Extended results and supplementary information are provided in the appendices. An overview of some of the commercially available impedance cardiograph instruments are presented in Appendix A. Hardware details of the impedance cardiograph developed in our lab, and used for recording the signals during the research, are presented in Appendix B. Appendix C presents analysis results related to the techniques based on adaptive filtering for removing simulated respiratory artifacts, and on actual recordings from the healthy volunteers. Appendix D gives the analysis results for the wavelet based denoising technique. Detailed results from clinical evaluation of the signal processing techniques are given in Appendix E. Forms used for recording background information and consent of the participating subjects are presented in Appendix F.

Chapter 2

FUNDAMENTALS OF IMPEDANCE CARDIOGRAPHY

2.1 Introduction

The stroke volume is the amount of blood pumped by the left ventricle of the heart in one contraction (Vander *et al.*, 1980; Guyton, 1991; Ross and Wilson, 2006). The cardiac output is the amount of blood pumped by heart in one minute, and hence it is given as the product of the stroke volume and the heart beat rate. Cardiac disorders like valvular heart disease, congenital heart disease, disorder in pacemaker cells, blockage in arteries, pulmonary edema, etc. may lead to a decrease in the stroke volume. Beat-to-beat variation in stroke volume and left ventricular ejection time provide diagnostic information about cardiovascular functioning (Kerr *et al*., 1998; Korhonen *et al*., 1999; Siebert *et al*., 1999; Nelson and Janerot-Sjöberg, 2001; Siebert *et al*., 2004; Liu *et al*., 2004). Unlike heart rate variability and blood pressure variability, stroke volume variability has not been widely used as a cardiac diagnostic tool, mainly because of the difficulty in getting accurate estimation of stroke volume on a beat-to-beat basis over a long period of time.

The established methods for estimating stroke volume, Fick's dye dilution and thermo dilution methods, are invasive and need catheterization and provide only an average stroke volume (Lababidi *et al.*, 1971; Wang *et al.*, 1989; Pappas *et al.*, 1994; Woltjer *et al.*, 1996; Webster, 1998; Fortin *et al.*, 2005). Electromagnetic flowmeters employ sensor probes across the thoracic aorta (Browning *et al.*, 1969; Hirakawa *et al.*, 1975; Webster, 1998). The measurements obtained are sensitive to the velocity distribution of the flowing blood. The CO_2 rebreathing method is a noninvasive technique for measuring the cardiac output, but changes in the breathing rate and deep breathing during measurement can introduce error in the estimation of the cardiac output. Doppler echocardiography is used to noninvasively measure the stroke volume and some other cardiovascular indices (Fisher *et al.*, 1983; Huntsman *et al.*, 1983; Christie *et al.*, 1987; Northridge *et al.*, 1990; Arora *et al.*, 2007). But this technique needs a radiologist or a skilled operator to operate the instrument and poses

technical difficulties in getting Doppler images during stress test and can not be used for monitoring the indices over extended periods (Daley *et al.*, 1985; Gardin *et al.*, 1986).

The electrical resistivity of blood is lower than that of other body tissues (Geddes and Baker, 1967; Baker, 1989). The blood volume changes in the thoracic region during the cardiac cycle, while the volume of other body tissues remains almost the same. During systole, heart pumps blood into the pulmonary circulatory system and the systemic circulatory system. The pulmonary circulation supplies blood for oxygenation in the lungs, and the systemic circulation supplies the oxygenated blood, through the aortic artery, to various parts of the body. Due to the increase of blood volume in the thoracic region the impedance of the thorax decreases (Kubicek *et al.*, 1966; Kubicek *et al.*, 1967; Kubicek *et al.*, 1974; Patterson, 1989; Kubicek 1989). By sensing this signal, the stroke volume can be estimated and it can be used for estimating the stroke volume and the cardiac output.

Impedance cardiography is a non-invasive technique for monitoring cardiac related impedance changes in the thoracic impedance (Kubicek *et al.*, 1966; Kubicek *et al.*, 1967; Kubicek *et al.*, 1974; Zhang *et al.*, 1986; Qu *et al.*, 1986; Patterson, 1989; Kubicek, 1989; Deshpande *et al.*, 1990; Sramek, 1994; Jensen *et al.*, 1995; Sherwood *et al*, 1998; Song and Kim, 2003; Bernstein and Lemmens, 2005). The impedance is generally measured using four band electrodes placed around the thorax, by passing a high frequency (20-400 kHz) low amplitude current (< 5 mA) between the outer two electrodes and picking up the resulting amplitude modulated voltage across the inner two electrodes. The voltage is demodulated to get the impedance signal $Z(t)$. The maximum value of the impedance, with the lowest volume of blood in the thorax, is known as the basal impedance Z_o. The variation in the impedance, $z(t)$, from the basal value is related to the variation in the blood volume, and its negative derivative ($-dz/dt$) is known as the impedance cardiogram (ICG).

This chapter gives an overview of variation in the thoracic impedance, impedance model of the thorax, electrode systems and instrumentation for impedance cardiography, clinical studies related to impedance cardiography, and the artifacts present in the thoracic impedance signal, followed by a review of the signal processing techniques for artifact cancellation. At the end of the chapter, the techniques to be investigated are proposed, and the methods for their evaluation and validation are presented.

2.2 Variations in the thoracic impedance

Variations in the thoracic impedance are caused by several physiological events including blood volume change in the thorax, air volume change in the lungs, and heart movement (Kubicek *et al.*, 1966; Kubicek *et al.*, 1967; Karnegis and Kubicek, 1970; Kubicek *et al.*, 1974; Harley and Greenfield, 1969; Patterson, 1989; Wang *et al*., 1991; Sramek, 1994; Jensen

et al., 1995; Song and Kim, 2003). Bonjer *et al.* (1952) conducted an experiment in anaesthetized dogs by encasing the heart in an insulating sheet of rubber. They found that the volume changes in the heart itself generally play a very minor role in the variation in the thoracic impedance. Mohapatra (1981) has reported experiments to investigate the origin of the variation in thoracic impedance and has concluded that these variations reflect both a change in the blood velocity as well as a change in the blood volume. The heart by itself does not contribute to change in the thoracic impedance because its physical volume is less than 10% of the thoracic volume and effects of variation in its impedance are shielded by aorta and vena cava (Bonjer *et al.*, 1952; Lewis, 1974; Sramek, 1994). Geddes and Baker (1972) investigated the effect of 2 ml saline injection into the ventricles and the pulmonary artery of dogs on thoracic impedance changes. It was observed that injection into the ventricles produced a larger change in the impedance, and it was concluded that contraction of both the right and the left ventricle can cause a change in the thoracic impedance. In an another experiment, soon after the death of the dog, they artificially induced volume changes of the heart and rhythmic perfusion of the systemic and the pulmonary circulation with a mechanical fluid pump. The results showed that the changes in the impedance were due to expulsion of the blood from the heart during the ventricular contraction.

Kubicek (1989) conducted studies on a dog whose left ventricle pumped only once every two ejections of the right ventricle (left mechanical alternas). A change in the thoracic impedance was observed when the left ventricle contracted. It was also observed that the $(-dz/dt)_{max}$ was synchronized with the peak blood flow in the aorta, as measured by an electromagnetic flow-meter. Pappas *et al.* (1994) used thermodilution and impedance cardiography on eight rabbits, and found a high correlation between cardiac outputs estimated from the two techniques. Recently, Gaw *et al.* (2008) have reported a mathematical model to explain the flow dependence of the electrical conductivity of blood during pulsatile flow through rigid tubes.

In the four-electrode arrangement for impedance cardiography as shown in Fig 2.1, current is injected through the outer electrodes. Electrically non-conducting ribs running perpendicular to the current path and the contents of the intra-thoracic space contribute to the basal impedance Z_O. The two major conductive pathways vena cava and thoracic aorta are parallel with the current flow. These two vessels have high conductivity in comparison to the other thoracic tissues and it is estimated that they conduct more than 50% of the injected current (Sramek, 1994). The remaining injected current flows through the intercostal muscle and less conductive lung tissues. Change in the resistance of the lung is due to changing volume of air in the alveolar space. Variations in the thoracic impedance have several origins: (1) cardiovascular activity, (2) orientation of erythrocytes, (3) respiration, and (4) motion.

1) *Cardiovascular activity*: Most of the high frequency measurement current flows through the thoracic aorta and the inferior and the superior vena cave. The contraction of the ventricles results in pressure and volume change in the aorta and the pulmonary artery. Vena cava does not exhibit pulsating blood flow in synchronism to the heart beat. Hence, most of the variation in the thoracic impedance originates from the thoracic aorta and the pulmonary artery (Bonjer *et al.*, 1952; Kubicek *et al.*, 1966; Kubicek *et al.*, 1967; Kubicek *et al.*, 1974; Patterson, 1989; Kubicek, 1989; Wang *et al.*, 2001).

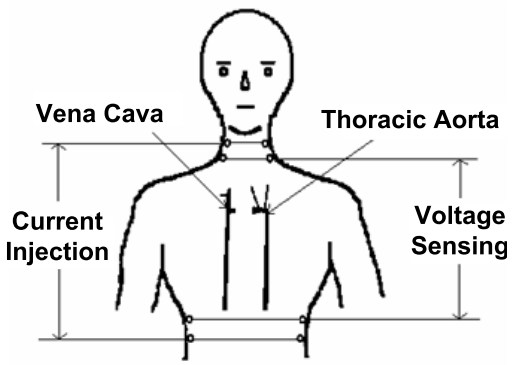

Fig 2.1 Four-electrode arrangement for impedance cardiography (adapted from Sramek, 1994).

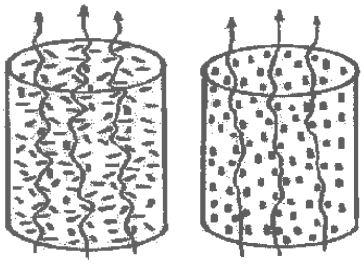

(a) (b)

Fig 2.2 (a) Randomly oriented erythrocytes at the end of diastole, **(b)** Oriented erythrocytes at high blood velocity (adapted from Sramek, 1994).

2) *Orientation of erythrocytes*: During pulsating flow of the blood, its effective conductivity changes (Visser *et al.*, 1976; Visser, 1989; Sramek, 1994). The erythrocytes (red blood cells) have a disc like shape. Prior to the aortic valve opening, the erythrocytes have arbitrary orientation within plasma and the current lines have extended path length as shown in Fig 2.2(a). Due to acceleration in blood flow, after opening of the aortic valve, erythrocytes generally get aligned with the flow direction. As the injected high frequency current is parallel to the main axis of the thoracic aorta, current lines become straight and shorter, as shown in Fig. 2.2(b), and the thoracic impedance decreases.

3) *Respiration*: Respiration also contributes to a change in the thoracic impedance (Miyamoto *et al*., 1981; Muzi *et al.*, 1985; Zhang *et al.*, 1986; Hurwitz *et al.*, 1990; Raza *et al.*, 1992; Wang *et al.*, 1991; Barrows *et al.*, 1995; Ouyang *et al.*, 1998; Webster, 1998; Yamamoto *et al.*, 1998; Ernst *et al.*, 1999; Riese *at al.,* 2003; Krivoshei *et al.*, 2008). Due to respiration, the intra-thoracic pressure changes. During inspiration, the intra-thoracic pressure is negative, which in turn produces not only an inrush of air into the lungs but also an increase in venous return to the thorax. Changes in thoracic cage dimensions during inhalation and exhalation cause variation in the sensed thoracic impedance. This part of the variation in the thoracic impedance is known as respiratory artifact. For sensing the variation in the thoracic

impedance, impedance pneumography can be used for apnea monitor (Wilson *et al.*, 1982; Sahakianh and Kuokh, 1985).

4) *Motion*: Due to body movements and breathing, thoracic dimensions change, resulting in a change in the current distribution and a change in the position of electrodes with respect to thoracic cage. The resulting variation in the thoracic impedance is known as motion artifact (Qu *et al.*, 1986; Barrows *et al.*, 1995; Rosell and Webster, 1995).

2.3 Impedance model of the thorax and estimation of the parameters

Nyboer *et al*. (1950) proposed a bioimpedance model for use in impedance plethysmography for monitoring the electrical impedance of a cylindrical region of the body, *e.g*. an arm or a leg. Modeling the region as a cylindrical conductor, they derived a formula for calculating the increment in the blood volume from the corresponding decrease in the impedance (Nyboer *et al*., 1950; Nyboer, 1970). This technique later received clinical importance because of the work by Kubicek *et al.* (Kubicek *et al.*, 1966; Kubicek *et al.*, 1967; Kubicek *et al.*, 1974; Patterson, 1989; Kubicek, 1989). Kubicek *et al.* modified the model for stroke volume estimation from thoracic impedance measurement, assuming that the source of impedance change were lungs, which receive the blood from right ventricle during the systole (Kubicek *et al.*, 1966; Kubicek *et al.*, 1974; Patterson, 1989; Kubicek, 1989).

The thoracic region is modeled as a conductor of fixed length L, variable cross-sectional area S, with volume given as

$$V = L\,S \tag{2.1}$$

With resistivity ρ, the resistance of the region is given as

$$R = \rho\frac{L}{S} \tag{2.2}$$

An increase in the volume of the blood in the region results in an effective increase in the cross-sectional area and hence a decrease in its resistance. By substituting value of S from Eqn. 2.2 into Eqn. 2.1, blood volume in the region is given as

$$V = \rho\frac{L^2}{R} \tag{2.3}$$

Hence, a fractional change in the volume is related to a fractional change in the resistance as

$$\frac{\Delta V}{V} \approx -\frac{\Delta R}{R} \tag{2.4}$$

Substituting the value of V from Eqn. 2.3 in Eqn. 2.4, we get

$$\Delta V \approx -\rho\frac{L^2}{R^2}\Delta R \tag{2.5}$$

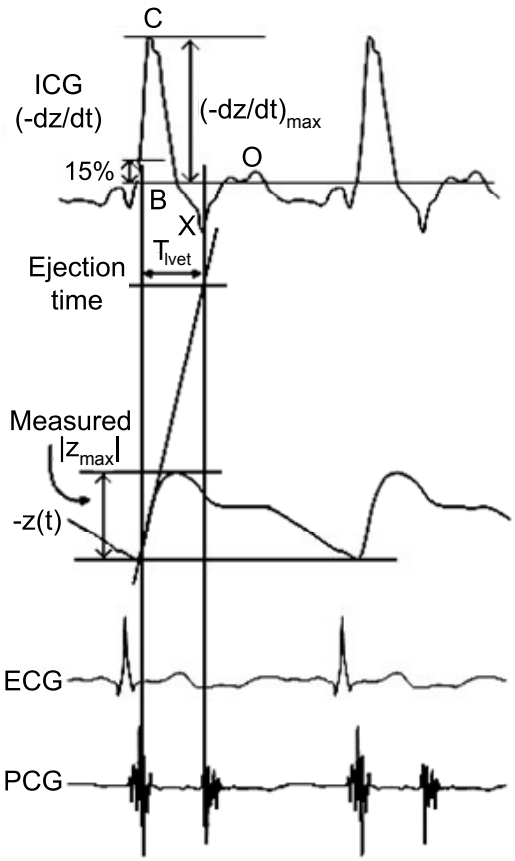

Fig. 2.3 Typical waveforms in impedance cardiography: $-z(t)$ and $-dz/dt$ along with electrocardiogram (ECG) and phonocardiogram (PCG); for calculation of ΔZ using forward-slope extrapolation method (adapted from Patterson, 1989).

Impedance is measured by injecting ac current using a pair of electrodes and measuring the resulting voltage. The impedance at the frequency used for sensing is nearly resistive (Rosell *et al.*, 1995) and hence we can write

$$\Delta V = -\rho \frac{L^2}{Z^2}(\Delta Z) \tag{2.6}$$

The value of the impedance with the lowest quantity of blood is known as the basal impedance Z_o, and hence the time varying impedance can be written as

$$Z(t) = Z_0 + z(t) \tag{2.7}$$

where $z(t) \leq 0$ and $|z(t)| << Z_o$. Hence the change in the blood volume can be estimated from the maximum change in the impedance $\Delta Z = -|z|_{max}$ as

$$\Delta V = \rho \frac{L^2}{Z_0^2}(|z|_{max}) \tag{2.8}$$

Negative of the slope of the impedance variation, *i.e.*, *-dz/dt*, is known as the impedance cardiogram. Figure 2.3 shows $z(t)$ and *-dz/dt* waveforms along with the associated electrocardiogram (ECG) and phonocardiogram (PCG) waveforms. The ICG waveform has three characteristic points: B, C, and X. Point B and point X denote the aortic valve opening and closing respectively and these points are associated with the first and the second heart sounds. The point C corresponds to the point of maximum rate of impedance change $(-dz/dt)_{max}$. The point O indicates the time of opening of the mitral valve and it represents a rapid ventricular diastole. The time interval between points B and X is the left ventricle ejection time (T_{lvet}) and it gives duration of the mechanical systole.

The basal impedance Z_o is usually about 25 Ω and impedance changes $z(t)$ caused by cardiovascular activity is less than about 2 % of the basal impedance (Witsoe *et al.*, 1969; Kubicek *et al*., 1974; Patterson, 1989). The impedance change ΔZ (= $|z|_{max}$) refers to the decrease in the impedance caused by the increase in blood volume. In order to take care of the blood that leaves the thoracic region during the ejection phase, a forward slope extrapolation method was developed by Kubicek *et al.* (Kubicek *et al.*, 1966; Kubicek *et al.*, 1974; Patterson, 1989). As shown in Fig 2.3, a straight line is drawn from the steepest part of $z(t)$ signal until the end of the ejection phase. In this model, it is assumed that the blood flow is a square wave pulse, *i.e.,* it is constant over the blood ejection phase, and blood starts significantly leaving the thoracic region sometime after the aortic valve opens. Hence, the maximum rate of change is proportional to the blood flow. Thus, ΔZ is obtained as the product of the ICG peak and the left ventricle ejection time, which is determined from the last upward crossing of ICG before the large systole peak to the second heart sound. Hence, Eqn. 2.6, for estimating the stroke volume becomes,

$$\Delta V = \rho \frac{L^2}{Z_o^2} \left(-\frac{dz}{dt} \right)_{\max} T_{lvet} \tag{2.9}$$

where, ΔV = stroke volume (mL), ρ = resistivity of blood (Ω-cm), L = the length of the modeled conductor (cm), Z_o = the basal impedance (Ω), $(-dz/dt)_{max}$ = the maximum of the derivative of the impedance during the systole (Ω/s) , T_{lvet} = left ventricle ejection time (s). Equation 2.9 is generally known as the Kubicek's formula for estimating the stroke volume.

There have been several questions on the validity of the fixed length conductor model of the thorax (Visser *et al.*, 1976; Sakamoto and Kanai, 1979; Traugott, 1981; Visser, 1989; Thomas *et al.*, 1991; Sramek, 1994; Raaijmakers *et al.*, 1995). Several modifications have been proposed to correct the estimate, for different contributions of the different blood vessels, blood flow profiles, electrical current configurations, and changes in blood

conductivity due to change in the orientation of erythrocytes with the rate of blood flow. Sramek *et al.* (1983, cited in Van De Water *et al.*, 2003) approximated L as 17% of the patient's height (H) and changed the cylindrical model to a frustum. The stroke volume is estimated as

$$\Delta V = \left(\frac{(0.17H)^3}{4.2} \right) \frac{1}{Z_o} \left(-\frac{dz}{dt} \right)_{\max} T_{lvet} \tag{2.10}$$

where, H is the patient's height in cm. In this formula, blood resistivity ρ has been eliminated. Also, this formula uses a percentage of body height and not the distance between sensing electrodes, hence inaccuracy due to error in measuring the distance between sensing electrodes is eliminated. For improving the accuracy of the estimated stroke volume, Bernstein (1986) introduced an empirically determined weight correction factor δ, derived by taking ratio of the actual weight and the ideal weight for the subject's height, as follows

$$\Delta V = \delta \left(\frac{(0.17H)^3}{4.2} \right) \frac{1}{Z_o} \left(-\frac{dz}{dt} \right)_{\max} T_{lvet} \tag{2.11}$$

It is to be noted that despite several modifications for estimation of stroke volume, these formulas use the same two parameters $(-dz/dt)_{max}$ and T_{lvet}.

In addition to estimating $(-dz/dt)_{max}$ and T_{lvet}, the ICG waveform has been used for calculating several other indices (Summers *et al.*, 1999; Modak and Banerjee, 2004; Peng *et al.*, 2004; Thompson *et al.*, 2004). The thoracic fluid index (TFI) is representative of total fluid volume in the thorax comprised of both the intra-vascular and the extra-vascular fluid (Saunders,1988), and it is defined as

$$\text{TFI} = 1/Z_o \tag{2.12}$$

The velocity index (VI) is related to the peak velocity of blood in the aorta, it is given as

$$\text{VI} = \left(\frac{-dz}{dt} \right)_{\max} / \text{ TFI} \tag{2.13}$$

As mentioned earlier, the value of $(-dz/dt)_{max}$ has been found to be related to the peak aortic blood flow (Kubicek, 1989). The acceleration index (ACI) is the peak acceleration of blood flow in the aorta, which occurs within the first 10 - 20 ms after the opening of the aortic valve, and it is defined as

$$\text{ACI} = \left(\frac{d^2 z}{d^2 t} \right)_{\max} / \text{ TFI} \tag{2.14}$$

Pre-ejection period (PEP) is defined as the time interval from the beginning of the electrical stimulation of the ventricles to the opening of the aortic valve (electrical systole), *i.e.*, time interval from the beginning of the Q wave of the ECG to the B point of the ICG. It is

the period of isovolumic ventricular contraction and hence it is a measure of contractility of the heart (Modak and Banerjee, 2004; Peng *et al.*, 2004). Systolic time ratio (STR) is the ratio of the electrical systole (PEP) to the mechanical systole (T_{lvet}), and it is given as

$$\mathrm{STR} = \mathrm{PEP} / T_{lvet} \tag{2.15}$$

A higher STR may indicate the presence of left ventricular dysfunction in chronic heart failure because the isovolumetric contraction time of the ventricles takes longer in relation to the ejection time of the ventricles (Modak and Banerjee, 2004; Thompson *et al.*, 2004). STR are useful in diagnosing valve disease, angina pectoris, pericardial disease, coronary artery disease, and mitral valve disease (Lewis, 1975; Lewis *et al.*, 1977). Heather index (HI) is defined as

$$\mathrm{HI} = \left(-\frac{dz}{dt} \right)_{\max} \; / \; T_{Q-C} \tag{2.16}$$

where $T_{Q\text{-}C}$ is the time interval between the Q-wave of ECG and the C-point of ICG. The STR, ACI, and HI provide a measure of systolic contractility (Lewis, 1975; Summers *et al.*, 1999; Peng *et al.*, 2004). Summers *et al.* (1999) simultaneously measured HI and cardiothoracic ratio (longest observed length of the cardiac silhouette divided by the transthoracic length at the same level) for monitoring acute congestive heart failure.

In the ICG waveform shown in Fig. 2.3, the characteristic points used for parameter estimation can be clearly identified. However, the waveform varies markedly across individuals (DeSouza and Panerai, 1981). Point B in the ICG, at the onset of rapid upstroke of ICG, denotes the onset of left ventricular ejection. Lababidi *et al.* (1971) showed that the point B corresponds to the maximum amplitude of the first heart sound. Other studies, using simultaneous recording of ICG and echocardiogram, have also indicated a correspondence between point B with onset of the left ventricle ejection (Rusmussen *et al.*, 1975, cited in Buell, 1988; Petrovick *et al.,* 1980; Stern *et al.,* 1985). The lowest point in ICG, point X, corresponds to the closure of the aortic valve. It is usually seen as a sharp notch, as seen in Fig. 2.3, in synchronism with the second heart sound (Lababidi *et al.,* 1970; Patterson, 1989) and generally can be easily recognized.

Kubicek *et al.* (1966) introduced a method for determining left ventricle ejection time (T_{lvet}) from the zero crossing or a deflection point just preceding the $(-dz/dt)_{max}$ of ICG (point B) to the negative peak of the ICG waveform (point X). However, it was observed that the point B sometimes falls above zero crossing (Lamberts *et al.*, 1984; DeMarzo and Lang, 1996). Kubicek *et al.* (1970) modified the algorithm for detection of point B, by marking it as the instant of 15% of $(-dz/dt)_{max}$ value. Inaccuracy in the detection of onset of left ventricle ejection, from ICG, directly affects the estimation of stroke volume and some of the indices (DeMarzo *et al.*, 1996). Reference to maximum deflection of first heart sound may be helpful

for avoiding ambiguity in locating the B-point. The value of $(-dz/dt)_{max}$ is the maximum rate of change of $z(t)$ and is marked as the peak in ICG, within a given cardiac cycle following the QRS complex of ECG. This value is usually taken as absolute value of $(-dz/dt)_{max}$ relative to the zero crossing. However, in some of the studies, it has been defined as the value of $(-dz/dt)_{max}$ with reference to the point B (Boer *et al.,* 1979; Mohapatra, 1981).

2.4 Electrode system

A typical ICG system uses a four-electrode configuration for reducing the effect of skin-to-electrode impedance in the sensed signal. The equivalent resistor network for 4-electrode configuration is shown in Fig. 2.4**,** with E1-E4 representing the electrodes. For measuring impedance change Z_x, a current source is connected across the outer terminals of the network. Impedances $Z_{i1,}$ $Z_{i2,}$ $Z_{v1,}$ Z_{v2} represent electrode-tissue interface impedances. Impedances Z_a and Z_b are the tissue impedances of the regions between the current and the voltage electrodes. The differential amplifier with a gain A, for the measurement of V_x, has very high input impedance, *i.e.*, $Z_{in} >> (Z_x + Z_{v1} + Z_{v2})$. The output voltage is $V_o = A\ I\ Z_x$ and it is not affected by the other impedances. For the reasons of economy and convenience in application, some impedance cardiographs use two electrodes. In this case, the current density is higher near the electrode than elsewhere in the tissue and the measured impedance becomes more dependent on the tissue near the electrodes than elsewhere in the body. Moving the electrodes closure to the main source of the impedance variation (aorta) may provide a more accurate measurement. Both the electrode configurations use surface electrodes, either in the form of

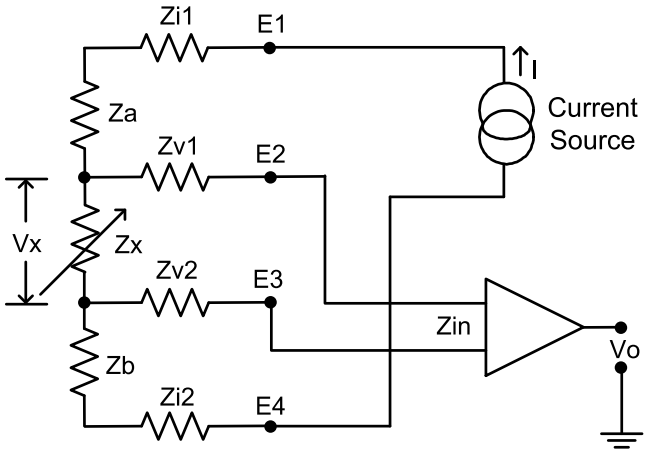

Fig 2.4 Resistor model of four-electrode configuration used in impedance cardiography.

bands or spot electrodes.

Band electrodes: Kubicek *et al.* (1966) used a 4-electrode configuration with circumferentially placed band electrodes and this configuration has been widely used. Typically, the current is passed between a circumferential electrode high on the neck and another roughly at the level of the umbilicus, while the voltage is measured between an electrode around the base of the neck and one at the xyphoid level. Each electrode usually consists of a disposable strip of adhesive tape having thin strip of aluminum coated mylar, forming the electrode along the centre (Witsoe *et al.*, 1969). Use of electrode gel is optional (Witsoe *et al.*, 1969). Several studies have been conducted regarding the placement of sensing electrodes (Miyomoto *et al.*, 1981; Edmunds *et al.*, 1982; Veigl and Judy, 1983; Ferrigno *et al.*, 1986; Qu *et al.*, 1986). In some of the studies, forehead position has been used for the upper injection electrode (Verdu, 1994). Watanabe *et al.* (1981, cited in Penney *et al.*, 1985) used half band electrodes in impedance cardiography. Lambert *et al.* (1984) reported a considerable change in amplitude of $z(t)$ and ICG due to variation in distance between the sensing electrodes. For reproducible stroke volume estimates, they suggested using an approximate distance of 24 cm between the sensing electrodes, and a separation of at least 3 cm between the sensing and the injection electrodes.

Spot electrodes: Band electrodes are used for providing a nearly uniform current density in the thoracic region, but they pose practical difficulties in correct placement and may be uncomfortable for some patients. Further, motion causes variation in the contact impedance at different points along the bands, resulting in a change in the current distribution, which can result in a large motion artifact. Similar problem may also be contributed by band electrodes during sensing, because the sensed voltage gets dominated by points along the band electrodes with low contact impedance (Verdu, 1994). Spot electrodes have small area, and current distribution may become non-uniform, with higher current density near the injection electrodes, *i.e.*, the impedance variation near the electrodes will contribute more to the modulated output voltage. The main advantage of the spot electrodes is that their location can be selected to minimize motion artifacts. Several studies have been conducted for replacement of band electrodes with spot electrodes (Penney *et al.*, 1984; Qu *et al.*, 1986; Boomsma *et al.*, 1989; Sherwood *et al.*, 1992; Gotshall and Sexson, 1994; Woltjer *et al.*, 1996; Barde *et al.*, 2006). Possibility of a non-uniform current distribution across the thorax is the main concern in using spot electrodes. Several electrode arrays have also been introduced using disposable spot electrodes.

Penney *et al.* (1985) used 2-channel impedance cardiograph for simultaneously recording of ICG from spot and band electrodes. Two spot electrodes were placed at the back of the neck, separated by 6 cm and centered about prominence of the seventh cervical vertebra. The other two electrodes were placed at the end of the ninth inter-costal space: one

near the mid-clavicular line and the other one at 8 cm from the first, in tenth inter-costal space near mid-auxiliary line. A good correlation was observed between the signals from the two techniques, in terms of peak and shape of the waveform.

Qu *et al.* (1986) investigated the use of a four-spot electrode array for reducing motion artifact. Motion artifacts were found to be minimum when the electrodes were placed in the sagittal plane of the body. One current injection electrode was placed on the back of the neck over the fourth cervical vertebra and the other one on the back over the ninth thoracic vertebra. One voltage sensing electrode was placed on front of the neck, 4 cm above the clevicle and the other one over the sternum at the fourth rib. They found that if the spot electrode array deviates from the center region of the chest the signal-to-artifact ratio (SAR) drastically reduces. The placement of the array of spot electrodes on the abdomen also resulted in reduced signal-to-artifact ratio. Zhang *et al.* (1986) compared the results from the band and spot electrodes. The values of the correlation coefficients between the cardiac output measured by CO_2 rebreathing and impedance cardiography was found to be 0.97 (n = 76) with the band electrodes and 0.95 (n = 78) with the spot electrodes).

Woltjer *et al.* (1996) used a 16-spot electrode array and compared stroke volume obtained using the spot electrodes and the band electrodes. No significant differences were observed in the stroke volume obtained with both the arrays. Bernstien and Lemmens (2005) replaced each band electrode by a pair of spot electrodes. Using this electrode configuration and by using Sramek-Bernstien formula for cardiac output estimation from ICG, a high correlation (r = 0.88, n = 94) was reported between the cardiac output values estimated from ICG and thermodilution method for critically ill patients. The results are similar to those reported in an earlier study by Appel *et al.* (1986) on critically ill patients (r = 0.83, n = 16).

These studies suggest that the spot electrodes may be used as an alternative to the band electrode, despite the concern for non-uniform current distribution.

2.5 Instrumentation for impedance cardiography

The frequency and current amplitudes used for measuring thoracic impedance should be selected to avoid any physiological effects. The impedance is generally measured by passing a high frequency (20-400 kHz), low amplitude current (< 5 mA) across the thorax. In this frequency range, the impedance is nearly resistive and the tissues are not excitable, except possibly at very high current levels (Grimnes and Martinsen, 2000). If a frequency much higher than 400 kHz is used, current distribution is confined near to the skin, and contribution of the various organs to the thoracic impedance will not be observed. At frequencies much lower than 20 kHz, there may be physiological effects due to excitation of cells (Baker, 1989). Also, at lower frequencies skin-to-electrode impedance is high which may introduce problem of dynamic range and more electrode related artifacts (Rosell *et al.*, 1995).

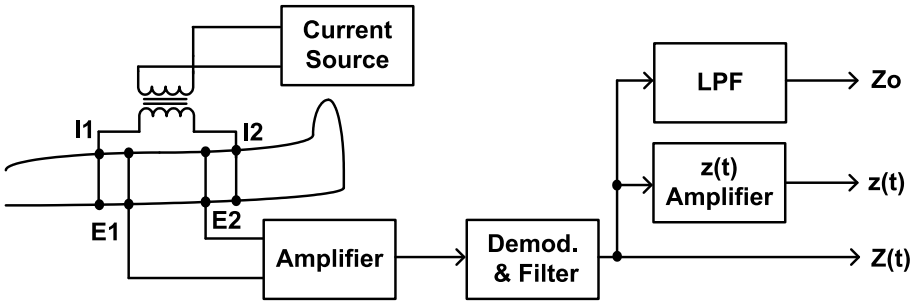

Fig 2.5 Impedance plethysmograph developed by Nyboer *et al*. (adopted from Nyboer, 1970).

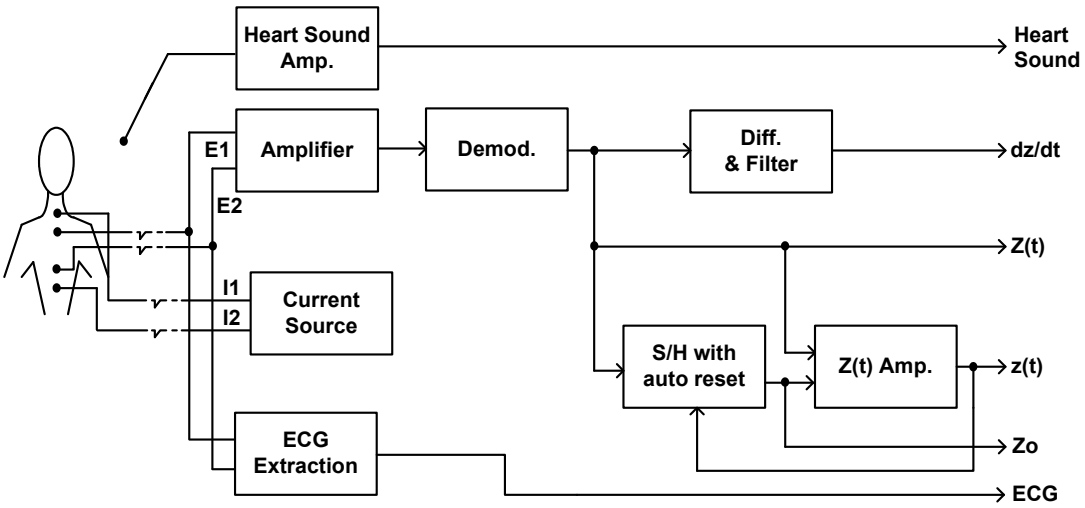

Fig 2.6 Impedance cardiograph developed by Kubicek *et al.* (1974).

Nyboer developed an impedance plethysmograph for measuring impedance variation in a limb (Nyboer, 1970), as shown in Fig. 2.5. Four-electrode configuration is employed for reducing the effects of skin-to-electrode impedance and for a uniform current density in the selected segment. Two electrodes, I1 and I2, are used for injection of current, and the other two electrodes, E1 and E2, are used for sensing the voltage drop across them. The amplitude of the sensed voltage is directly proportional to the electrical impedance of the segment between electrode E1 and E2. The amplification and detection of sensed voltage yields the output $Z(t)$ which is varying impedance $z(t)$ superimposed on the basal impedance Z_o. Varying impedance $z(t)$ is obtained by subtracting basal impedance Z_o from the total measured impedance $Z(t)$.

Using an approach similar to that in Nyboer's plethysmograph, Kubicek *et al.* developed an impedance cardiograph instrument (Kubicek *et al.*, 1966; Witsoe *et al.*, 1969; Kubicek *et al.*, 1974). The block diagram of the instrument, known as the Minnesota

impedance cardiograph, is shown in Fig. 2.6. The current is injected into the thorax with a pair of electrodes I1 and I2 and the voltage developed across the thorax is picked up by another pair of electrodes E1 and E2. Because of time varying impedance $z(t)$ in the region between sensing electrodes the amplifier output is an amplitude modulated voltage. This signal is fed to a demodulator which provides an output proportional to $Z(t)$, sum of basal impedance Z_o, and time varying component $z(t)$. Motion and respiration cause changes in thoracic dimensions and introduce artifacts in the $z(t)$ signal. These artifacts have a large amplitude and result in a baseline drift. For restoring the baseline, a sample-and-hold based baseline restoration circuit was introduced by Kubicek *et al.* (Witsoe *et al.*, 1969; Kubicek *et al.*, 1974). In this circuit, two comparators were used to set thresholds and whenever the ICG signal crosses the range defined by these thresholds, output was pulled to a value within the range. The baseline drift that does not cross these threshold ranges was not compensated. A successive approximation register (SAR) based baseline restoration circuit was later reported by Qu *et al.* (1986).

In an ICG instrument developed by Kizakevich *et al.* (1988), a crystal controlled square wave generator, at 100 kHz, followed by a band-pass filter and voltage-to-current converter was used for providing a stable sinusoidal excitation. The sensing circuit included synchronous demodulator, low pass filter, and sample-and-hold based baseline restoration circuit. Low pass filtered output of synchronous demodulator resulted in basal impedance Z_o, while sample and hold based baseline restoration circuit provided varying component of the impedance $z(t)$. Differentiation of z(t) gave the ICG output. Analog outputs of the instrument were digitized with a microprocessor based circuit and ensemble averaging was carried out in digital domain to suppress the artifacts. In an instrument reported by Jindal *et al.*, dz/dt was normalized by dividing it with Z_o, and the peak amplitude of this waveform was taken as blood flow index (BFI) (Bhuta *et al.*, 1990; Jindal *et al.*, 2004).

Fortein *et al.* (2005) used two direct digital synthesis (DDS) chips to generate two stable ac current of 40 kHz. Second DDS chip was used to generate quadtrature signal. These two current sources were fed into a transformer to ensure isolation from the sensing circuit. Cables used for current injection were shielded to reduce pick-ups and interference. Sensed voltage was demodulated by a synchronous detector followed by a PI-feedback controller to maintain injection current amplitude at 400 μA.

There are a number of impedance cardiograph instruments commercially available: HIC-2000, HIC-3000, HIC-4000, NCcardiac outputM3, BioZ, Niccomo, CircMon, TEBcardiac output, THRIM, LifeGard, Philips Impedance Cardiograph, etc. Most of these instruments have a microcontroller/ microprocessor/ DSP/ PC for estimation of stroke volume and other cardiac indices. Some of the instruments (*e.g.* HIC-2000, HIC-3000, HIC-4000, and

THRIM) provide analog outputs of the waveform for post-processing of the signals. A brief description of some of these instruments is given in Appendix A.

2.6 Clinical studies

Several studies for the validation of the stroke volume obtained using impedance cardiography have been reported. Harley *et al.* (1968) reported a correlation of 0.26, for 24 patients with heart disease, between cardiac output measured by impedance cardiography and thermal dilution method.

Lababidi *et al.* (1971) compared cardiac output estimated by dye dilution and Minnesota impedance cardiograph (model 202). In 20 children without shunts or valvular insufficiency, 5.5% mean difference was observed in cardiac outputs measured by Fick's dye dilution and impedance cardiography. In 21 children, with left to right shunts cardiac output estimated from ICG showed good correlation (r = 0.92) with pulmonary blood flow. In 13 subjects with aortic insufficiency, there was a mean difference of 50% in the cardiac output estimated by Fick's dye dilution and impedance cardiography. The authors concluded that impedance cardiography should not be used in the aortic insufficiencies.

Keim *et al.* (1976) reported a correlation of 0.49 between stroke volume estimated from impedance cardiography and Fick's dye dilution method, for 17 cardiac patients. Secher *et al.* (1979) measured stroke volume, in 12 women before and during Caesarean section, to compare impedance cardiography with the thermodilution method. Correlation coefficients were 0.77 and 0.55 before and during anaesthesia respectively. Slope of the regression line, before anesthesia was found to be 1.07 and during anesthesia the slope was 0.45.

Aust *et al.* (1982) measured stroke volume simultaneously by Minnesota impedance cardiograph (model 400) and M-mode echocardiography, for six healthy volunteers. Recordings were carried out over a two hour period, for assessing cardiovascular response to the drug Amezinium Metilsulfate and placebo, in the supine position and when tilted 80^{o} head-up for 10 minutes. There was a high correlation (r = 0.83) between the estimates from the two methods. Muzi *et al.* (1985) reported correlation of 0.87 ($p < 0.01$) for cardiac outputs estimated by thermodilution and impedance cardiography for 14 patients admitted in intensive-care unit.

Wang *et al.* (1989) used a microprocessor based hardware for real time monitoring of stroke volume and cardiac output. Ensemble averaging was used for reducing muscle noise, 60 Hz interference, and respiratory artifacts in real time. They compared the outputs estimated using this instrument and thermodilution from 10 healthy volunteers, 4 critically ill patients, and 8 healthy exercising volunteers. Correlation coefficients for the output estimated by the two methods were found to be high for all the three groups: 0.93, 0.94 and 0.95 respectively.

Kizakevich *et al.* (1993) measured T_{lvet} and other cardiac indices by impedance cardiography and Doppler echocardiography, before, during, and after exercise, in 31 hospitalized patients with chest pain syndrome admitted for coronary angiography. Correlation between the values obtained using impedance cardiography and Doppler techniques, for aortic valve opening, timing for peak ejection velocity, aortic valve closure, ICG acceleration, and normalized ICG acceleration were 0.78, 0.86, 0.73, 0.74, and 0.79 respectively. Vandeer *et al.* (1999) compared cardiac output estimated by impedance cardiography and Doppler echocardiography, for 26 cardiac patients and the correlation coefficient was found to be 0.85.

Perrino *et al.* (1994) used the instrument BoMed NCCOM3-R7 for measuring cardiac output of 43 patients, undergoing noncardiac surgery. The correlation coefficient for the values obtained from impedance cardiography and thermodilution was 0.84. Mean bias analysis, estimated from Bland-Altman method, showed a disagreement between the two methods. Yakimets and Jensen (1995) evaluated accuracy of the NCCOM-R7 impedance cardiograph instrument in estimating the stroke volume and the cardiac output for 17 patients undergoing coronary angiography and 28 patients after heart surgery using NCCOM-R7, Fick's dye dilution, and thermodilution methods. As compared to measurement from Fick's dye dilution and thermodilution methods, the impedance cardiography underestimated the stroke volume for all patients undergoing coronary angiography. Correlation coefficients for values obtained using impedance cardiography and Fick's dye dilution were 0.68 for resting condition and 0.22 during exercise. Correlation coefficients for the patients after heart surgery were 0.55 and 0.51 for observations taken at two different time. They concluded that impedance cardiography with the instrument used by them should not be used as a basis for clinical decision on the patients with heart disease without further investigations.

Woltjer *et al.* (1996) compared stroke volume estimated by ICG and thermodilution on 24 stable patients who underwent diagnostic heart catheterization and found a correlation coefficient of 0.69. After excluding the data from the patients with an aortic valve disorder, correlation was found to be 0.87. No significant mean difference between the two methods was reported and it was suggested that impedance cardiography might be a clinically useful tool for diagnosing heart failure. Fortein *et al.* (2005) conducted validation studies on congestive heart failure (CHF) patients, waiting for heart transplantation. A high correlation ($r = 0.88$, $n = 16$, $p < 0.001$) was found between the cardiac output estimated using impedance cardiography and thermodilution. Other studies also showed a high correlation between cardiac output from ICG and one of the clinically established methods (Charloux *et al.*, 2000; Bellerdinelli *et al.*, 1996). Several studies have shown good reproducibility of impedance cardiography variables before, during, and after exercise across the healthy subjects as well as

patients (Northridge *et al.*, 1990; Kizakevich *et al.*, 1994; Verhoeve *et al.*, 1998; Greenberg *et al.*, 2000; Van De Water and Miller, 2003; Treister *et al.*, 2004).

2.7 Suppression of respiratory and motion artifacts in ICG

The sensed impedance variation is a mixed representation of components related to changes in the blood volume, air volume, and thoracic dimensions. The thoracic impedance signal $z(t)$ is very small compared to the basal impedance, and it is influenced by respiration and motion artifacts which have much larger amplitudes. Use of baseline restoration circuit partly removes the respiratory and motion artifacts. The ICG signal bandwidth typically extends over 0.8 - 20 Hz. Respiration related artifact extends over 0.2 - 2 Hz, while motion related artifact have a band of 0.1 - 10 Hz (Webster, 1998). Thus the spectra of respiratory and motion artifacts partly overlap with that of the ICG. The artifact causes a variation in the baseline of the signal, and may introduce errors in calculating the parameters for estimating the stroke volume and other cardiac indices.

Holding the breath during recording can avoid respiratory artifacts, but it may change the stroke volume (Andersen and Vik-Mo, 1984; Ferrigno *et al.*, 1986; Du Quesnay *et al.*, 1987). Ensemble averaging has been widely used to suppress the respiratory and motion artifacts in impedance cardiography (Miyamoto *et al.*, 1981; Muzi *et al.*, 1985; Qu *et al.*, 1986; Zhang *et al.*, 1986; Riese *et al.*, 2003). In this technique, time frames in the ICG waveform are identified with reference to the R peak of ECG. Parameters T_{lvet} and $(-dz/dt)_{max}$ were calculated from ensemble averaged ICG waveform. The R-peak detection is generally carried out using Hamilton and Tompkins algorithm (Hamilton and Tompkins, 1986). Ideally, ensemble averaging enhances the coherent components and suppresses the non-coherent components with a zero mean. However, it suppresses beat-to-beat variation and transient changes in the signal. Because of heart rate variability, ensemble averaging tends to blur or suppress the less distinctive point B of the waveform and may result in error in its detection (Hurwitz *et al.*, 1990; Wang *et al.*, 1991; Raza *et al.*, 1992; Barrows *et al.*, 1995; Yamamoto *et al.*, 1998). Further, the time difference between point B of ICG and R-peak of ECG may change, resulting in smearing of ICG peaks. We have earlier reported a method based on cross-correlation analysis for estimation of ventricular ejection time T_{lvet} from PCG (Pandey and Pandey, 2005). It is particularly suited for use during exercise, or post-exercise relaxation, when cardiac activity is rapidly changing.

Hurvitz *et al.* (1990) used coherent ensemble averaging for enhancement of ICG, based on events in the waveform itself as the synchronization reference. The points B, C and X were first aligned in each frame and then the segments were ensemble averaged. Since the various events were already aligned before averaging, it provides better enhancement. This

technique is free from problems of beat-to-beat variation of cardiac events and event latency (Hurvitz *et al.*, 1990; Riese *et al.*, 2003). However, this technique can be applied only if points B, C, and X can be reliably detected in the artifact contaminated signal.

Yamamota *et al.* (1998) used a narrow bandpass IIR digital filter, centered around the heart rate. However, it introduces nonlinear phase distortion and attenuates high frequency components of ICG signal. Raza *et al.* (1992) used a high pass IIR digital filter with voluntary cardio-respiratory synchronization. In this technique, a high pass digital filter is programmed for a cutoff frequency that varies as a function of heart rate. Forward filtering followed by backward filtering was used to reduce phase distortion. The disadvantage of this technique is the possibility of distortion of the ICG signal acquired during exercise and post-exercise recordings.

An adaptive filter (Widrow *et al.*, 1975; Haykin and Widrow, 2003; Widrow and Stearns, 2005; Haykin, 2005) can be employed to dynamically change its transfer function to remove respiratory and motion artifacts. Adaptive filters have been extensively used in several biomedical applications for removing motion and other related artifacts (Sahakian and Kuo, 1985; Thakor and Zhu, 1991; Varanini *et al.*, 1991; Akkiraju and Reddy, 1992; Barrows e*t al.*, 1995; Tong *et al.*, 2002; Liu and Pecht, 2006; Tiinanen *et al.*, 2008). Barros *et al.* (1995) used an adaptive filter with scaled Fourier linear combiner for removal of movement artifact. ICG signal was expressed as a scaled Fourier series, with a period varying with the R-R interval of the ECG. A metronome was used to adjust respiratory and movement artifact at different frequencies. However, this technique may produce a distorted output due to variation in time difference between the electrical and mechanical activities of the heart. Ouyang *et al.* (1998) used a wavelet denoising technique for artifact cancellation. Coiflets wavelet (order 5) was used with soft thresholding to suppress the artifacts. The technique used auto-regressive model estimated on 8 s breath-hold signal. Krivoshei *et al.* (2008) used an orthonormal basis to separate the signal and the artifacts using the Jacobi weighting function in the standard Gram-Schmidt process. This technique can not track fast changes in the signal.

Ensemble averaging and coherent ensemble averaging restrict beat-to-beat estimation of stroke volume and other cardiac indices. There is a partial overlap between ICG and the artifact spectra and statistical properties of both vary. Hence non-adaptive digital filters (Raza *et al.*, 1992; Yamamoto *et al.*, 1998) are not very effective in removing respiratory and motion artifact from ICG signal. Spectral subtraction technique (Boll, 1979; Gong, 1995; Stahl *et al.*, 2000) which involves estimating noise magnitude spectrum and subtracting it from the contaminated spectrum, can not be used because of difficulty in dynamically estimating the respiratory and motion artifact spectra using average or quantile based estimation. Adaptive processing may be used for canceling the artifacts but sensing the reference signal, related to the artifacts, and combining them is a serious problem.

2.8 Scope of the research

The research objective is to investigate techniques for removal of the artifacts from ICG, for estimation of stroke volume and other cardiovascular indices without smearing beat-to-beat variations.

In impedance cardiography, impedance variation related to blood volume changes is superimposed on a large baseline which may drift over a large range. The baseline varies from subject to subject and it also depends on electrode placement. It may drift for the same subject due to movement and breathing. While amplifying the signal, the baseline drift needs to be removed to make effective use of the input dynamic range of the signal acquisition circuit. An automatic baseline restoration circuit has been developed as a part of instrumentation for the impedance cardiography for partly removing the artifacts before digitizing the signal and effective utilization of the input dynamic range of the A/D converter.

Signal processing techniques, based on adaptive filtering and wavelet based denoising, are investigated for removal of the artifacts. Adaptive filtering based technique needs a reference signal for artifact cancellation. Respiratory artifact is the variation in the sensed thoracic impedance, caused primarily by change in the dimension of thoracic cage during inhale and exhale phases of respiration. Hence, air flow during respiration is directly related to the respiratory artifact and it can be used to provide a reference for adaptive cancellation of respiratory artifact from the recorded thoracic impedance signal. Respiratory signal can be acquired during exercise. Hence beat-by-beat stroke volume calculation is possible, even if respiratory artifact has a large variation. There are limitations in applying this technique for removal of motion artifacts, due to practical limitations in obtaining the reference signal related to various motions that may cause variation in the thoracic impedance. Application of wavelet based denoising technique, without involving a reference signal, is investigated for removal of respiratory and motion artifacts. A quantitative evaluation of the artifact suppression is carried out by applying these techniques on artifact free recordings added with simulated artifacts at different levels, for a number of healthy volunteers.

The signal processing techniques are validated on the signals recorded from several subjects with normal health and subjects with cardiovascular disorders, under a clinical setting. Several studies, as reviewed earlier, have established Doppler echocardiography as a noninvasive technique for estimating the stroke volume. This technique permits beat-to-beat monitoring of the stroke volume. Estimates of the stroke volume from the impedance cardiogram are compared against those obtained by Doppler echocardiography. The signal from the impedance cardiography and Doppler echocardiogram are recorded simultaneously, to enable a comparison of average values and the beat-to-beat- variations, as obtained by the two methods.

Chapter 3

BASELINE RESTORATION CIRCUIT

3.1 Introduction

The variation in the sensed thoracic impedance has components related to the changes in (i) the blood volume due to cardiovascular activity and (ii) the air volume, the thoracic dimensions, and the skin-electrode interface impedances due to respiration and motion. The thoracic impedance signal $z(t)$ is typically less than about 2 % of the basal impedance (Witsoe *et al.*, 1969; Kubicek *et al*., 1974; Patterson, 1989). The respiratory and motion artifacts have much larger amplitudes and cause a large drift in the baseline of the signal, and hence these artifacts may introduce errors in calculating the parameters for estimating the stroke volume and other cardiac indices. The ICG signal bandwidth typically extends over 0.8 - 20 Hz. The Respiration related artifacts extend over 0.2 - 2 Hz, while motion related artifacts have a band of 0.1 - 10 Hz (Webster, 1998). The overlap between the spectra of the ICG signal and the artifacts makes it difficult to restore the baseline drift by high pass filtering the signal. It may be possible to employ digital signal processing for suppressing the baseline drift, but the drift needs to be at least partly removed before analog-to-digital (A/D) conversion in order to make effective use of the input dynamic range of the signal acquisition setup. A tracking based baseline restoration circuit is developed for fast estimation and removal of the baseline drift.

This chapter gives a brief review of baseline restoration circuit for balancing of offset drift, followed by the description of the proposed tracking based baseline restoration. The last section presents and discusses the test results.

3.2 Baseline restoration

Several circuits for automated balancing of offset drift have been reported, including bridge circuit (Matsuno *et al.*, 1986), automatic reset circuit (Shankar and Webster, 1984; Webster, 1998), self-balancing system (Cohen and Longini, 1971), successive approximation register (SAR) based method (Qu *et al.*, 1986), and integrator based baseline restoration circuit (Joshi and Pandey, 1994). The bridge based circuit does not permit removal of base line drift related

to artifacts. In the self-balancing system, the baseline drift is balanced by a ramp approximation using digital counter. It consists of a differential amplifier, threshold detector, counter, digital-to-analog (D/A) converter, and comparator. The counter output is given to the D/A converter and the difference between the D/A converter output and the input is amplified, to provide the baseline corrected output. Whenever the output voltage crosses a set threshold, a narrow pulse is generated to reset the counter, and the counter starts incrementing until the D/A converter output equals the analog input. For *n*-bit counter and D/A converter, the balancing may take up to 2^n clock pulses.

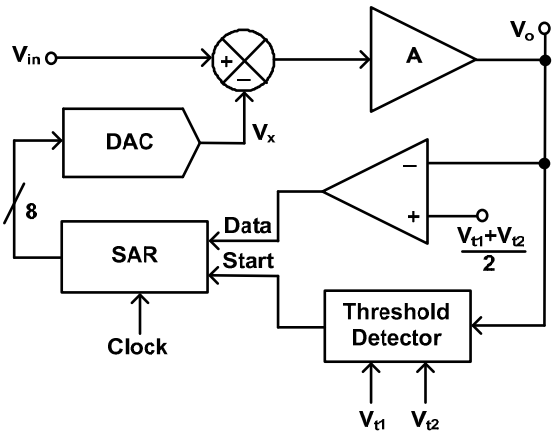

Fig. 3.1 A block diagram of successive approximation based baseline restoration circuit of Qu *et al.* (1986).

The automatic reset circuit reported by Shankar and Webster (1985, cited in Webster, 1998) used a difference amplifier for subtracting a correction voltage from the input, a sample-and-hold for sampling the input signal and providing the correction voltage, and two comparators to define the output voltage range. When the output voltage crosses the range set by the two thresholds in either direction, the sample-and-hold samples the input signal and holds it as the correction voltage which is fed back to the input of the difference amplifier to reset the output to zero. In this circuit, the hold error may introduce its own drift.

Qu *et al.* (1986) have reported a drift cancellation circuit, as part of an impedance cardiograph, using a difference amplifier, a successive approximation register (SAR), D/A converter, and a threshold detector as shown in Fig. 3.1. In this circuit, the SAR and D/A converter approximate the base line drift, which is subtracted from the input signal and the difference is amplified to give the output V_o. Whenever voltage V_o crosses the threshold range $[V_{t1}, V_{t2}]$ in either direction, a start pulse is given to SAR and successive approximation is initiated. Polarity of V_o with respect to the center of threshold range is used as data input for successive approximation to obtain a new estimate of the base line and output is brought to near the center of the range. For *n*-bit SAR and D/A converter, this circuit requires *n* clock cycles for drift correction and the output is not useable during this interval. Therefore this time interval should be short and correction should not take place too frequently.

In the circuit presented here, developed as a part of instrumentation for impedance cardiography, tracking has been used for estimation and removal of the baseline drift, and this

circuit requires only one clock cycle. This technique has been implemented using a microcontroller and a D/A converter.

3.3 Circuit description

The block diagram for the tracking based baseline restoration is shown in Fig. 3.2. The up/down counter and a D/A converter are used to track the baseline drift in the input signal, and the estimated drift V_x is subtracted from the input to give the drift balanced amplified output V_o. Two thresholds are selected corresponding to the desired range [V_{t1}, V_{t2}] of the signal or the input range of the signal acquisition setup. Whenever the output crosses the threshold range in either direction, a new estimation of the drift is carried out in the up/down counter depending on the direction of the drift. The estimate is output to the D/A converter and the baseline drift correction is carried out in one clock pulse. One quantization step of the D/A converter after amplification is set to half of the output threshold range. Hence, after crossing of the threshold in either direction, the signal is brought back in the middle of the two thresholds.

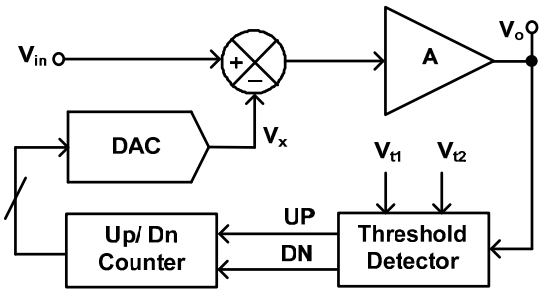

Fig. 3.2 Block diagram of the tracking based baseline restoration circuit.

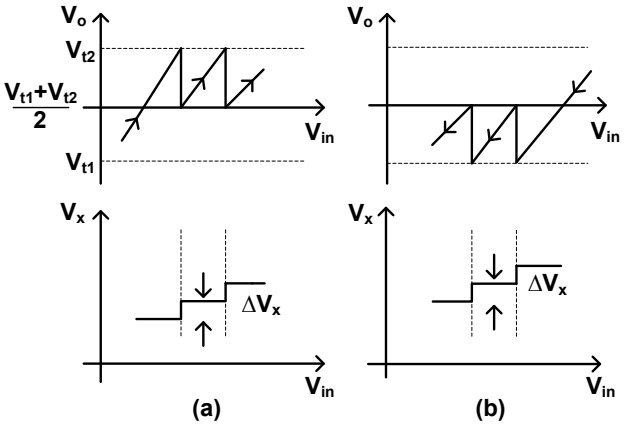

Fig. 3.3 Input-output relationship for **(a)** increasing input, and **(b)** decreasing input.

The relationship between the input voltage V_{in} and the output voltage V_o along with the correction voltage V_x is shown in Fig. 3.3, for (a) increasing input and (b) decreasing input. Drift cancellation has a hysteresis, and the actual output depends on the direction of the input change.

The circuit of the microcontroller based implementation is shown in Fig. 3.4. The circuit uses quad op amp TL084 (U1), 20-pin microcontroller AT89C2051 (U2), and 12-bit serial D/A converter TLV5618A (U3). The U3 is used as 8-bit D/A converter by masking the four LSBs. This circuit has been developed for baseline drift removal in an impedance cardiograph with ± 5 V supply, as briefly described in Appendix B.

The output of the DAC used in this circuit is unipolar (0 – 4.2 V) and hence for cancellation of bipolar drifts, a reference voltage V_r is added in the summer-amplifier stage, which has a provision for different gains for the input V_{in}, reference voltage V_r, and the correction voltage V_x. Op amp U1A is used as a summer-amplifier and its output is given as

$$V_o = A_s V_{in} - A_x (V_x - A_r V_r / A_x) \tag{3.1}$$

where

$$A_s = (R_2 \parallel R_3 / (R_1 + R_2 \parallel R_3))(1 + R_5 / R_4)$$
$$A_r = (R_1 \parallel R_2 / (R_3 + R_1 \parallel R_2))(1 + R_5 / R_4)$$
$$A_x = R_5 / R_4$$

Op amps U1B and U1C are used as comparators for comparing the output V_o with the threshold voltages V_{t1} and V_{t2}, which are set using a resistive divider. The port pins P1.2 and P1.3 of the microcontroller U2 are used to scan the threshold detector outputs. The tracking up/down counter of Fig. 3.2 is realized using software inside the microcontroller. The count

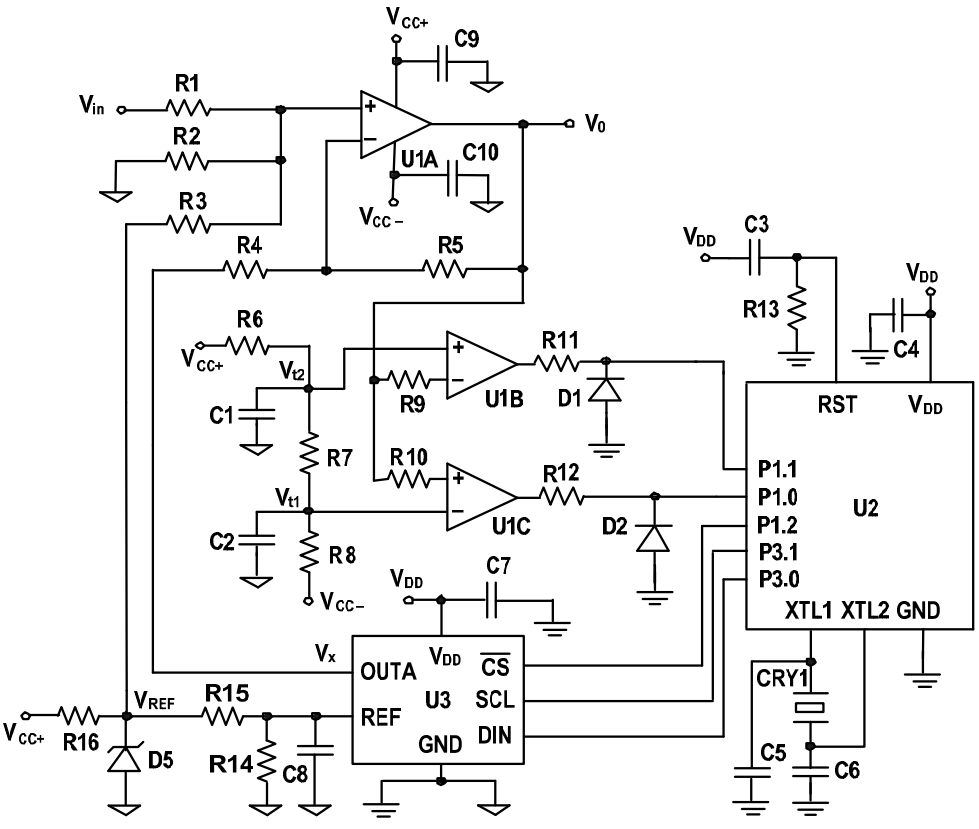

R1=R2=100 kΩ, R3=50 kΩ, R4=1 kΩ, R5=180 kΩ, R6=22 kΩ, R7=66 kΩ, R8=22 kΩ, R9=R10=R11=R12=10 kΩ, R13=15 kΩ, R14=R15=5.6 kΩ, R16=680 Ω, C1=C2=10 nF, C3=10 µF, C4=0.1 µF, C5=C6=22 pF, C7=C8=C9=C10=0.1 µF, CRY1: 24 MHz Crystal, D1,D2: 1N4148, D5: 4.2 V Zener, V_{cc+}= +5 V, V_{cc-}= –5 V, V_{DD}= +5 V, U1: TL084, U2: AT89C2051, U3: TLV5618A

Fig. 3.4 Circuit diagram of the microcontroller based baseline restoration circuit.

value is written as control byte to the D/A converter, interfaced serially to the microcontroller via serial peripheral interface (SPI), for varying its output over 0 – 4.2 V in 256 steps.

The input consists of the actual signal V_s superimposed on the baseline drift V_d. The input signal range is mapped to the output voltage, and hence the gain for the input signal is selected as $A_s = (V_{t2} - V_{t1}) / (V_{s\,max} - V_{s\,min})$. If the summer output $V_{o.}$ goes below the lower threshold V_{t1}, the up/down counter is decremented, and the D/A converter output V_x gets decreased by one step. Similarly, if V_o goes above the upper threshold V_{t2}, V_x is increased by one step. Thus the correction voltage V_x is given as

$$V_x(t_n+1) = \begin{cases} V_x(t_n) + \Delta V_x, & V_o(t_n) > V_{t2} \\ V_x(t_n) - \Delta V_x, & V_o(t_n) < V_{t1} \\ V_x(t_n), & \text{otherwise.} \end{cases} \tag{3.2}$$

For N steps in the D/A converter, the step voltage is $\Delta V_x = (V_{x\,max} - V_{x\,min})/N$. The gain for the correction voltage is $A_x = 0.5(V_{t2} - V_{t1})/\Delta V_x$. If the output V_o is within the range $[V_{t1}, V_{t2}]$,

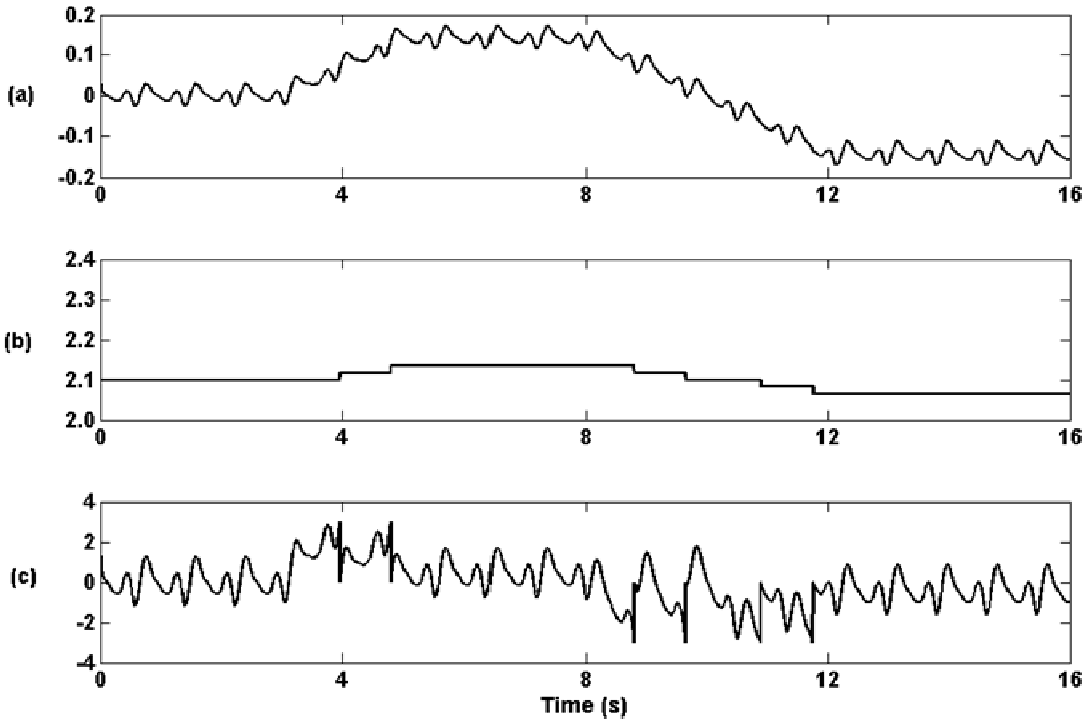

Fig. 3.5 Output of the baseline restoration circuit for the thoracic impedance signal $z(t)$ with large baseline shifts **(a)** input (in V), **(b)** correction voltage (in V), **(c)** output (in V).

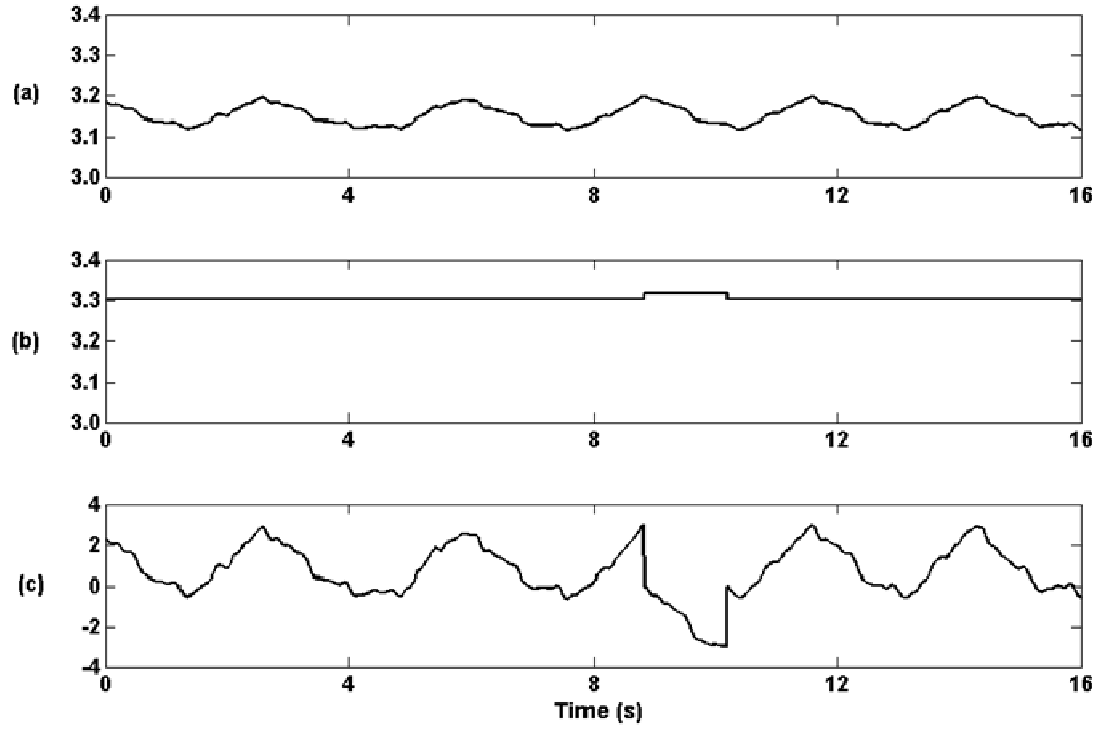

Fig. 3.6 Output of the baseline restoration circuit for the actual thoracic impedance signal $z(t)$ with large baseline shifts **(a)** input (in V), **(b)** correction voltage (in V), **(c)** output (in V).

both the comparator outputs are low, and the count in the counter is not changed and the correction voltage remains constant.

3.4 Test results and discussion

The thresholds and the amplification in the baseline restoration circuit can be set by considering the range of maximum excursion of the artifact-free signal and the input range of the A/D converter. Lower values of the thresholds result in a better use of the dynamic range of the A/D converter, but they may lead to more frequent activation of baseline correction. From a number of signal recordings, artifact-free signal was found to be below 40 mV. For this signal range, the thresholds were set as ± 3 V and it ensured that the baseline correction was not carried out too frequently. The component values as shown in Fig. 3.4 resulted in signal gain $A_S = 45$, correction voltage gain $A_X = 180$, and reference voltage gain $A_r = 90$. The time for restoring the drift is less than 1 ms. An example of drift cancellation by the implemented circuit is shown in Fig. 3.5. Input consists of 55 mV (p-p) thoracic impedance signal $z(t)$, with fundamental frequency of 1.2 Hz, superimposed on a slowly varying baseline drift, with a slope of 70 mV/s. The output waveform shows that the baseline is restored when the signal after amplification crosses the threshold range in either direction. The baseline correction introduces a discontinuity and hence the correction during the cardiac cycle makes

the output waveform during that cycle unsuitable for estimation of the parameters. Figure 3.6 shows the output obtained when baseline restoration circuit has been used in the impedance cardiograph instrument for recording the signals from a subject. The input signal is the variation in the thoracic impedance $z(t)$ superimposed on a slowly varying baseline drift due to respiration, superimposed on the basal impedance Z_o. In this example, two corrections happened between 8 s and 12 s.

To sum up, a tracking based circuit has been developed for fast restoration of baseline. The logic and interface of D/A converter are implemented in software on an 8-bit microcontroller for simplifying the hardware requirement. Although the circuit has been developed for impedance cardiography, it can be used for acquisition of other bio signals with large drifts or abrupt baseline shifts. This circuit is independent of the processor to which the signal acquisition unit is interfaced and can be used in setups with real time as well as offline processing. In the present implementation, tracking of baseline is initiated by the output going out of the defined range. Alternatively, the microcontroller can be programmed to carry out the tracking for drift cancellation at periodic intervals, which may be appropriate for certain applications.

Chapter 4

ADAPTIVE FILTERING FOR SUPPRESSION OF RESPIRATORY ARTIFACT

4.1 Introduction

This chapter presents investigations on the application of adaptive filtering for suppression of respiratory artifacts from the impedance signal for estimation of stroke volume and other cardiac indices on beat-to-beat basis. The contaminated ICG is applied as the primary input to the adaptive filter and a respiration signal sensed by a thermistor based airflow sensor is used as the reference. For improving the artifact cancellation, another technique is developed which estimates the reference signal from the sensed respiration and the ICG. The two techniques are referred to as: (i) adaptive filtering by sensing respiration (AFSR) and (ii) adaptive filtering by using estimated respiration (AFER). Both the techniques are applied on signal recordings from several volunteers and the results obtained are qualitatively examined. These techniques do not require any control of respiration. As adaptive filtering suppresses additive artifacts, it will not affect variations in the impedance signal caused by modulation of the stroke volume by the respiratory cycle.

The chapter begins with a brief review of application of adaptive filtering for suppressing different types of artifacts in biosignals. The following section presents the adaptive filtering based technique using the sensed respiratory signal as the reference. This is followed by a description of the adaptive filtering technique using the estimated respiration signal as the reference. These techniques are applied on signals acquired from several volunteers and results are presented and discussed in the following sections. Evaluation of the two techniques for suppression of artifacts in signals acquired in a clinical setting and validation of the results obtained by comparing them with those from Doppler echocardiography are presented later in Chapter 6.

4.2 Adaptive filtering of biosignals

Adaptive filtering is used in many biomedical applications for suppressing several types of artifacts (Widrow *et al*., 1975; Tompkins, 2002). Thakor and Zhu (1991) used an LMS based adaptive filter to remove various types of artifacts from the ECG signal. For removing slow varying baseline, a constant value was given as the reference to the one-tap length filter and the filter error (the difference between the primary input and filtered reference) was taken as the processed output. For removing 60 Hz noise, common mode signal at the right leg was used as the reference and filter error was taken as processed output. For reducing EMG noise, primary signal was ECG from the aVf lead and the reference was obtained by taking difference between the signals from the aVr and aVl leads. The filtered reference was taken as the processed output. For reducing motion artifact, the reference input was an impulse train with the start of each QRS-wave in the ECG represented by an impulse, and the filtered reference was taken as the processed output. Cascading of filter structures was used to remove baseline variation, 60 Hz noise, EMG noise, and motion artifacts from the recorded ECG. For arrhythmia analysis, the technique was effective in detection of P-wave, premature ventricular complexes, recognition of conduction block, arterial fibrillation, and paced rhythm. It was found to introduce distortion in the ST segment.

Burbank and Webster (1978) have shown that skin stretch is a major cause for motion artifact in ECG signals. Hamilton and Curley (1997) used skin stretch signal from a miniature displacement sensor, as the reference input to an LMS based adaptive filter. Artifact-free ECG signal and motion artifact, sensed by pressing the center of the electrode and stretching the skin around the electrode, were added together. The simulated signals were processed by the adaptive filter and Yule-Walker IIR filter. Sampling rate of 100 Hz was used. Adaptive filter with filter tap length of four resulted in noise reduction of -10.2 dB, while the Yule-Walker filter resulted in noise reduction of 7.7 dB. Tong *et al.* (2002) used an LMS based adaptive filter for suppressing motion artifact from ECG. Electrode motion, sensed by two anisotropic magnetoresistive sensors and three-axis accelerometer, was used as the reference signal to the adaptive filter. The technique was applied on artifact-free ECG added with motion artifacts, generated by pushing on the electrode, stretching the skin around the electrode, and pulling the ECG leads. Root mean square values, maxima, and minima of artifact-free ECG and processed ECG were compared to measure the artifact suppression. Reference signal from the three-axis accelerometer was found to give better artifact suppression than that from the magnetoresistive sensor.

Akkiraju and Reddy (1992) used an LMS based adaptive filter for removing ECG from EMG. The ECG and EMG signals were recorded from the same location. The contaminated EMG was the primary input to the adaptive filter, while ECG was the reference input. The EMG signals recorded from various other parts of the chest were processed and

amplitude spectrum of the recorded signal and the processed signal were compared to evaluate the technique. Magnitude spectrum of the processed EMG showed a reduction of approximately 85% in the ECG magnitude. Marque *et al.* (2004) used an adaptive filter for ECG removal from surface EMG recorded from the right erector spinae muscle at the level of the first lumbar vertebra (L1). The ECG, recorded by placing electrodes 15 cm apart from top to bottom of the left scapula, was used as the reference because its waveshape was found to be similar to that of the artifact. Five algorithms were investigated: LMS, normalized LMS (NLMS), least mean absolute value (LMAV), fast recursive least square (FRLS), and sign-sign (SIGN). Energy and mean power frequency were used to estimate effectiveness of the technique. Based on results from simulation, FRLS was found to be fastest in adapting filter parameters and most effective in removing the ECG.

Schuessler *et al.* (1995) used an adaptive filter for removal of cardiogenic oscillations from esophageal pressure signal. The reference signal was derived from QRS wave of the ECG signal. Filter weights were adjusted on the basis of cross-correlation between the reference signal and the primary signal. The technique was evaluated using simulated waveforms and actual signals. Mean square error and power spectrum of the signals were used to measure the noise suppression. A reduction of approximately 76% in the power spectrum at the frequency corresponding to the heart rate was reported. Cheng *et al.* (2001) used an LMS based adaptive filter for removal of the artifacts due to pressure change in the aorta and pericardium from the esophageal pressure signal related to the respiration. An airflow signal was used as the reference signal with the contaminated esophageal pressure being the primary input. Output of the adaptive filter was the cardiac signal, which was subtracted from the contaminated esophageal pressure to get cleaned esophageal pressure signal. The technique was applied on recordings from two rats. Processing improved the relative precision in the measurement of airway resistance by 12.5 to 68 %, indicating a reduction in the effect of cardiogenic artifact. Tiinanen *et al.* (2008) used a LMS based adaptive filter to suppress the effect of respiration from blood pressure. The respiration signal from a thermistor based sensor was used as the reference while the systolic blood pressure from a finger was taken as the primary signal. The technique was applied on the simulated recordings and the recordings obtained from healthy subjects. Power spectra of the artifact-free signal and the processed signal were compared and the spectral components of the artifact were found to have been suppressed in the processed output.

Sahakian and Kuo (1985) employed an impulse train, corresponding to the ECG R-wave, as the reference input to an LMS based adaptive filter to suppress the blood flow related component from the thoracic impedance signal in impedance pneumography. Processing of simulated signals showed that the technique was effective in suppressing the blood flow related components from the thoracic impedance signal. Rosell *et al.* (1995)

applied adaptive filtering for reducing motion artifacts in ventilation monitoring by using a two-frequency (57 kHz and 185 kHz) impedance plethysmograph. The components of the impedance signal related to ventilation and those related to nonventilatory movements were found to be different in the signals x_{LF} and x_{HF} sensed using the lower and higher carrier frequencies. The mean of x_{LF} and x_{HF} was used as the primary input to the RLS filter of order zero. The signal x_{HF} with a scaling factor was subtracted from x_{LF} and the resulting output was used as the reference. The scaling factor was obtained, using an LMS based zero-order filter, during a learning interval at the start of the signal acquisition with normal respiration and without any nonventilatory movements. Compared to the signal-to-artifact ratio in x_{LF}, the signal-to-artifact ratio (ratio of the rms values) in the processed output showed an improvement of 183% for arm movement, 133% for leg movement, and 34% for abdominal breathing.

Huang *et al.* (1991) used an LMS based adaptive filler to eliminate the noise caused by inflation and deflation of pressure cuffs from ICG signal during external counterpulsation (ECP: a noninvasive technique used to decrease pain from angina pectoris, by increasing diastolic blood flow and coronary blood flow, using serial inflation of three sets of pressure cuffs wraped around the calves, thighs, and buttocks). Five spot electrodes were used. The outer two electrodes for injecting current, the inner three electrodes for sensing the ICG and the reference signal, and one common electrode. The reference signal was bandpass filtered and applied as the reference input to the adaptive filter. Power spectra of primary, the reference, and the processed output were compared to see the effectiveness of the technique in processing signals from healthy adults during ECP. It was found that the spectral components, related to the inflation and deflation, were suppressed in processed output. The ICG signal was slightly distorted.

Barrows e*t al.* (1995) used an LMS based adaptive filter, based on scaled Fourier linear combiner (SFLC), to suppress respiration and movement artifacts from the ICG signal. The ICG signal was approximated as fifteen harmonics in a scaled Fourier series, with the period varying with the R-R interval of the ECG. The mean square error in the processed output was found to decrease significantly for simulated data with triangular wave as the ICG signal, artifacts consisting of respiratory and motion components simulated by harmonic spectra with randomly modulated frequencies and exponentially decreasing amplitudes, and random noise. For signals with the volunteer synchronizing the respiration in resting and post-exercise relaxation conditions, the magnitude spectrum showed attenuation of the artifact components.

4.3 Adaptive filtering by sensing respiration (AFSR)

Respiratory artifact is the variation in the sensed thoracic impedance, caused primarily by

changes in the intra-thoracic pressure and the dimension of the thoracic cage during inhale and exhale phases of respiration. Adaptive filtering, with a signal closely related to the respiratory artifact as the reference input, can be used for suppressing the artifact from the sensed signal ($z(t)$ or dz/dt). Several techniques have been reported for sensing respiration. A thermistor mounted on a mouthpiece is frequently used for measurements of breathing patterns (Weissman *et al*., 1984). Other techniques for measuring respiration, without using a mouthpiece, face mask, or a device about the head have also been reported (Reibold, 1974; Manus, 1986; Pennock; 1990). A piezoelectric element on an elastic belt is used for sensing the rate of change of the circumference of the rib cage or the rate of change of the circumference of the abdomen. It requires a constant tension in the elastic belt. Devices like strain gauges, mercury filled silastic rubber, and pneumatic tubes do not follow the dimensional changes instantaneously. Impedance sensing itself can be used for respiration monitoring but the sensed signal may contain an ICG component and hence may not be suitable as reference input for adaptive filtering.

We have used a thermistor based airflow sensor to measure air flow from the nostrils during the respiration. The sensed output is related to the intra-thoracic pressure changes modulating the thoracic impedance and hence it can be used as a reference for adaptive cancellation of the respiratory artifact. As the respiration can be continuously monitored, the technique can be applied for continuous suppression of the respiratory artifact. It is assumed that the adaptive filter can linearly transform the sensed respiratory signal to become sufficiently correlated to the respiratory artifact present in the impedance signal.

4.3.1 Adaptive cancellation scheme

A schematic of the adaptive respiratory artifact canceller is shown in Fig. 4.1. Signal $x(n)$, the thoracic impedance signal from the thoracic impedance sensor is the primary input. It can be expressed as sum of the true thoracic impedance signal $s(n)$ and the respiratory artifact $r_a(n)$. Reference signal $r(n)$ is obtained from the respiratory sensor and it is assumed to be related to $r_a(n)$ and does not have components related to the signal $s(n)$. In our setup, the respiratory sensor uses a thermistor to sense temperature variation because of airflow in front of the nostrils during the inhale and exhale phases of the respiration. The artifact is caused by the movement of the thoracic cage, and hence the sensed reference signal has a delay with respect to the artifact. To partly compensate for this delay, a delay of n_d samples is introduced in the path of the primary signal $x(n)$. Number of taps in the adaptive FIR filter should be large enough to properly track the actual delay.

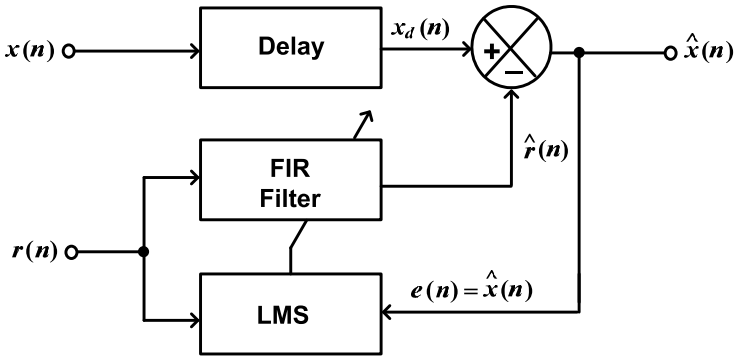

Fig. 4.1 Adaptive respiratory artifact canceller using sensed respiration (AFSR).

The reference input $r(n)$ is filtered with the M-tap FIR filter, with coefficients $w_n(k)$. The filter output is given as

$$\hat{r}(n) = \sum_{k=0}^{M-1} w_n(k)\, r(n-k) \tag{4.1}$$

The output $\hat{r}(n)$ is subtracted from the delayed input $x_d(n)$ to get the error

$$e(n) = x(n-n_d) - \hat{r}(n) \tag{4.2}$$

For adaptation, we use the least mean square (LMS) algorithm, also known as the stochastic gradient algorithm (Widrow *et al.*, 1975; Haykin and Widrow, 2003; Haykin, 2005; Widrow and Stearns, 2005). It uses an instantaneous estimate of the gradient vector, based on sample values of the tap input vector and the error. The filter coefficients are updated using the equation

$$w_{n+1}(k) = w_n(k) + \mu\, e(n)\, r(n-k) \tag{4.3}$$

where μ is a step size selected to provide convergence of the LMS adaptive filter coefficients. This technique allows dynamic adaptation to adjust filter coefficients on sample-by-sample basis, such that the output has minimum artifact in a least-square sense.

4.3.2 Signal acquisition

Impedance cardiograph instrument developed at IIT Bombay (Venkatachalam, 2006; Pandey and Pandey, 2007; Pandey *et al.*, 2008), briefly described in Appendix B, was used for recording ICG and other related waveforms. In this instrument, ICG was sensed by injecting a high frequency (≈ 100 kHz) and low intensity (<5 mA) current into the thorax. Four-electrode configuration with disposable ECG spot electrodes was used. In the outer pair, one electrode was placed around abdomen at the lateral side of the lower ribs and the other around upper part of the neck. For the inner electrode pair, one electrode is placed around the thorax at the

level of joint between xiphoid and sternum and the other around the lower part of the neck (Witsoe *et al.*, 1969; Kubicek *et al*., 1974; Harley and Greenfield, 1969). These electrode positions do not interfere with the locations used for placing other sensors in cardiovascular diagnosis (Witsoe *et al.*, 1969). The respiratory signal was recorded to sense inhale and exhale phases by placing a thermistor based respiratory sensor close to the nostrils.

Waveforms of the ECG, basal impedance Z_o, thoracic impedance signal $z(t)$, ICG, and respiration were simultaneously acquired at a sampling frequency of 500 Hz with 12-bit quantization using a data acquisition unit (Keithley "KUSB 3102") interfaced to a PC through its USB port. Recordings were taken from a total of 52 volunteers (male, age: 23-40 years) with no known history of cardiovascular disorders. Four types of signals were recorded: (i) signals with normal breathing, (ii) signals with strong respiratory artifact and large beat-to-beat variation, (iii) signals with no breathing, , and (iv) signals with controlled periodic breathing. The first two types of signals were recorded from all the 52 volunteers. The signals without breathing and signals with controlled breathing were recorded from 23 volunteers. All the recordings were made with the volunteers resting in a quiet supine position without any nonventilatory movements to avoid motion artifacts.

Signals with normal respiration: These recordings were made with the volunteer breathing in a normal manner. Figure 4.2 shows ICG signal and other related waveforms during normal breathing.

Signals with strong respiratory artifact and large beat-to-beat variation: In order to introduce strong respiratory artifact and significant beat-to-beat variations, volunteers were asked to exercise for about 20 minute on an exercise bicycle. After exercise, signals were recorded with the subject in resting condition without any nonventilatory movement. The signals were recorded for 60 s duration at 5 minute intervals in the resting condition, while the respiration and heart beat returned to pre-exercise state. Figure 4.3 shows ICG signal and other related waveforms in post-exercise relaxation condition.

Signals with no breathing: The volunteer stopped breathing activity for these recordings. The recording duration varied with the volunteer's ability to hold the breath. These signals have no motion or respiratory artifacts. Figure 4.4 shows ICG signal and other related waveforms during no breathing.

Signals with controlled periodic respiration: These signals were acquired with the volunteer synchronizing the inhale and exhale phases with 0.4 Hz square wave displayed on an oscilloscope. Figure 4.5 shows ICG signal and other related waveforms with controlled periodic respiration.

A quantitative evaluation of the technique can be carried out by processing signals with known levels of artifacts which can be generated by a weighted sum of artifact-free ICG

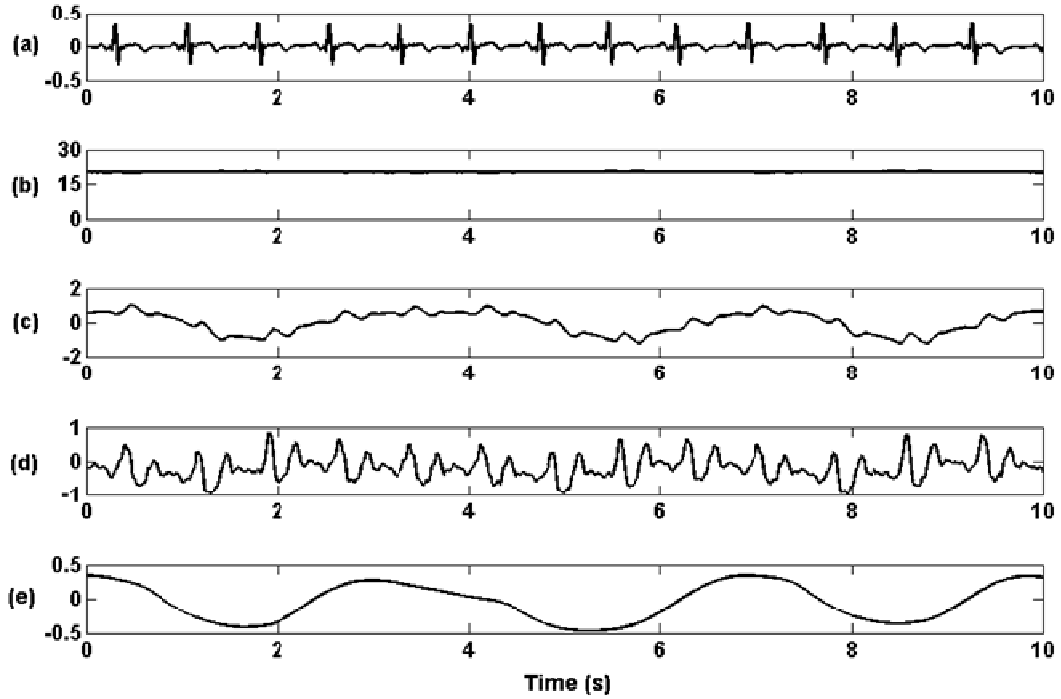

Fig. 4.2 Signals recorded during normal breathing (subject: 'MS'): **(a)** ECG (in arbitrary unit), **(b)** Z_o (in Ω) **(c)** $z(t)$ (in Ω), **(d)** ICG (in Ω/s), and **(e)** sensed airflow (in arbitrary units).

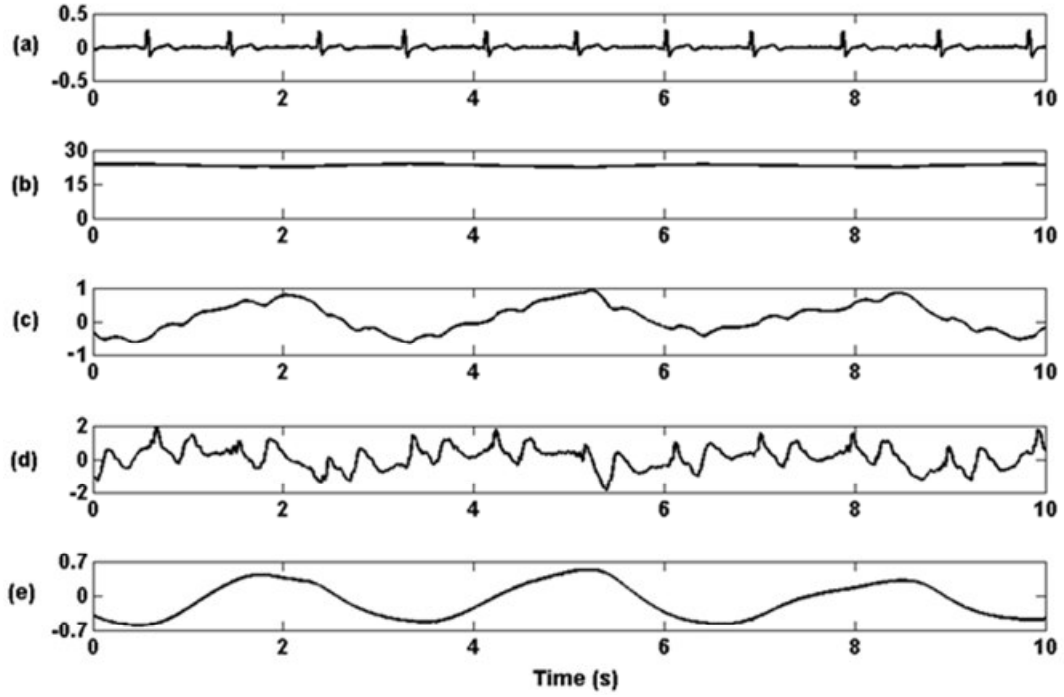

Fig. 4.3 Signals, with strong respiratory artifact, recorded during post-exercise relaxation (subject: 'MS'): **(a)** ECG (in arbitrary unit), **(b)** Z_o (in Ω) **(c)** $z(t)$ (in Ω), **(d)** ICG (in Ω/s), and **(e)** sensed airflow (in arbitrary units).

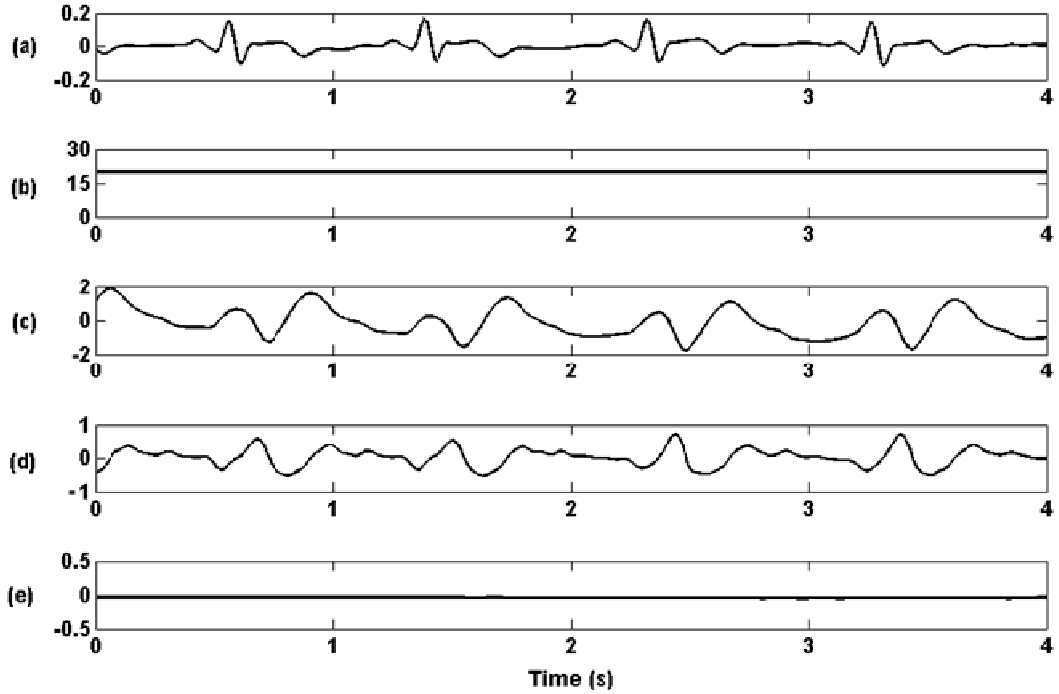

Fig. 4.4 Signals recorded during no breathing (subject: 'MS'): **(a)** ECG (in arbitrary unit), **(b)** Z_O (in Ω) **(c)** $z(t)$ (in Ω), **(d)** ICG (in Ω/s), and **(e)** sensed airflow (in arbitrary units).

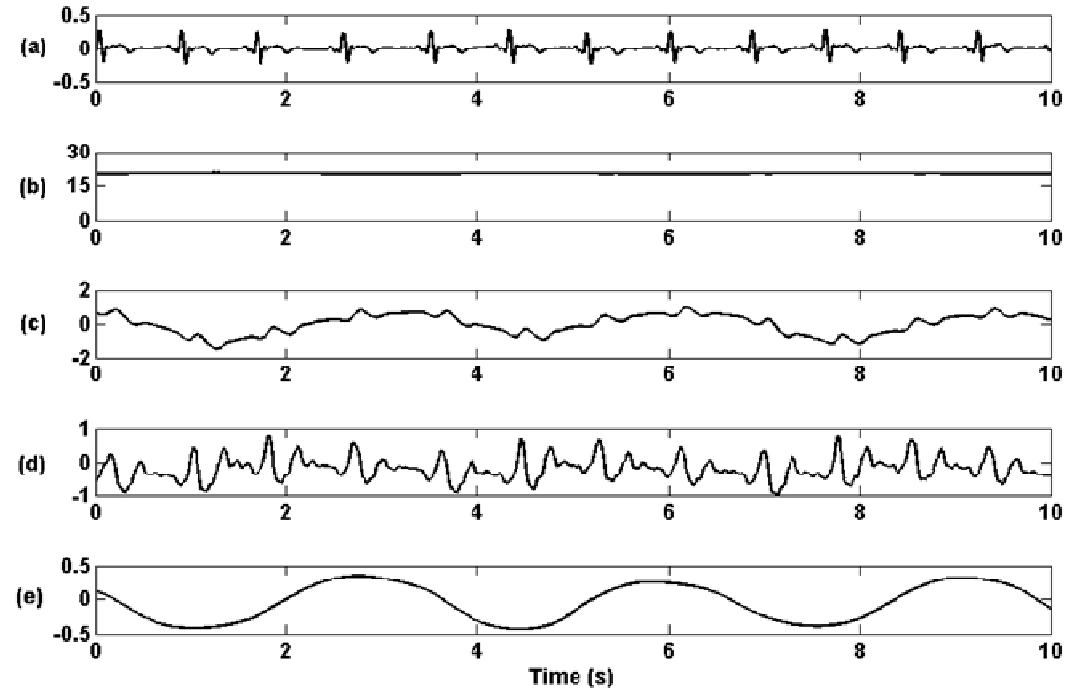

Fig. 4.5 Signals recorded with controlled periodic respiration (subject: 'MS'): **(a)** ECG (in arbitrary unit), **(b)** Z_O (in Ω) **(c)** $z(t)$ (in Ω), **(d)** ICG (in Ω/s), and **(e)** sensed airflow (in arbitrary units).

and ICG-free artifact. For this purpose, one cycle of the artifact-free ICG signal (acquired during no breathing) was repeatedly concatenated to simulate a periodic artifact-free ICG waveform. Sixty cycles of the ICG waveform acquired during controlled periodic breathing were ensemble averaged with respect to the respiratory cycle to estimate one cycle of respiratory artifact. It was repeatedly concatenated to simulate a periodic ICG-free respiratory artifact.

4.3.3 Processing of signals with simulated artifacts

For signals sampled at 500 Hz, the adaptive cancellation scheme of Fig. 4.1 was implemented for different combination of filter tap lengths and delays in the primary signal path. The step size μ in Eqn. 4.3 affects the convergence of the adaptive filter. Too small a value of μ results in slow conversion of filter coefficient, while too large a value may prevent the filter from converging. After empirical investigation, $\mu = 2.1\text{x}10^{-4}$ was selected. Most satisfactory results were obtained for tap length $M \approx 400$ and sample delay $n_d \approx 270$. Increasing filter tap length did not result in any significant increase in the output signal-to-artifact ratio (SAR). Changing the sample delay resulted in decreased SAR at the output. The filter coefficients were found to get stabilized in approximately 5 s. Signals with different levels of simulated artifacts were processed using the technique AFSR. The artifact-free ICG signal and the ICG-free artifact were scaled to have equal root mean square values. Amplitude of the artifact-free ICG was kept constant and the ICG-free respiratory artifact was added with different scaling factors to obtain contaminated ICG signals as

$$x(n) = s(n) + \alpha\, r_o\,(n) \tag{4.5}$$

where, $s(n)$ is the artifact-free input signal, and $r_o(n)$ is the ICG-free respiratory artifact. The input SAR for signal with simulated artifact $x(n)$ is given as

$$\begin{aligned} \text{SAR}_{\text{in}} &= 10\log\left(\sum_{i=1}^{N} s^2(n) / \sum_{i=1}^{N} \alpha^2\, r_o^2(n) \right) \\ &= -20\log\alpha \end{aligned} \tag{4.6}$$

where, N is the total number of samples in the signal. The signal $x(n)$ with different levels of simulated artifact was processed by the adaptive filter. The output SAR for the processed output $\hat{x}(n)$ was calculated as

$$\text{SAR}_{\text{out}} = 10\log\left(\sum_{i=1}^{N} s^2(n-n_d) / \sum_{i=1}^{N} |\hat{x}(n) - s(n-n_d)|^2 \right) \tag{4.7}$$

The output SAR was computed in a signal segment taken after the coefficients of the adaptive filter had settled.

Signals with simulated artifact with different SAR values were processed. Input signals were of 21 s duration. Filter coefficients settled in approximately 5 s. Output SAR values were computed during the last 6 s of the processed output. Figure 4.6 shows the result of processing of ICG with simulated artifact of 0 dB. ICG is contaminated by respiratory artifact, making it difficult to detect T_{lvet} and ICG peaks appear to change from beat-to-beat. The ICG obtained after filtering shows almost no effect of respiration, making it easy to detect the B and X points. Values of ICG peaks are found to be stable. Results for signals with simulated input SAR values of -9, -6, -3, 0, 3, 6, 9 dB are given in Appendix C. Figure 4.7 shows a plot for output SAR versus input SAR values in dB. We see a nearly linear relationship, with an SAR advantage of 18.5 dB for the input SAR range of -9 to 9 dB. This processing was repeated on signals with simulated artifact generated from the recordings taken from 23 volunteers. The relationship between the output SAR and the input SAR were almost similar to the plot in Fig. 4.7 and the SAR improvement ranged from 18.2 to 18.8 dB.

For assessing any error introduced by the adaptive filtering, the artifact-free signal without any artifact addition was processed. For signals from all the 23 volunteers, the signal-to-noise ratio in the output, calculated using Eqn. 4.7, was found to be 27 dB, indicating that the adaptive filtering did not introduce any significant error.

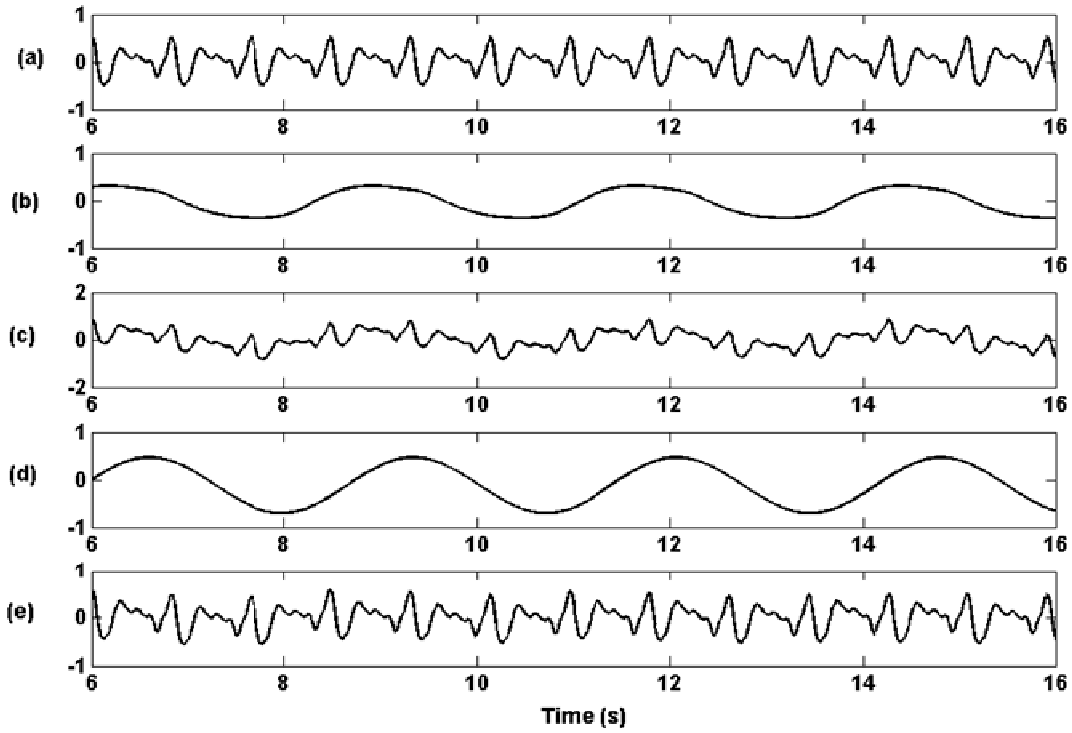

Fig. 4.6 Processing by AFSR of signal with simulated artifact: **(a)** artifact-free ICG, **(b)** ICG-free artifact, **(c)** ICG with simulated 0 dB artifact, **(d)** sensed respiration, and **(e)** processed output (all the waveforms are in arbitrary units).

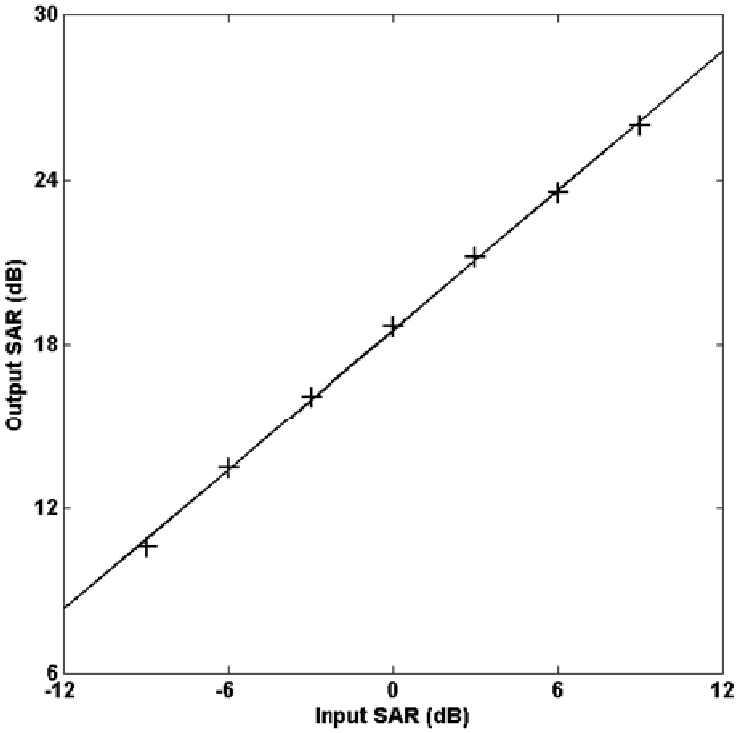

Fig. 4.7 Output SAR (in dB) versus input SAR (in dB) for the adaptive filtering technique AFSR (solid line: linear regression).

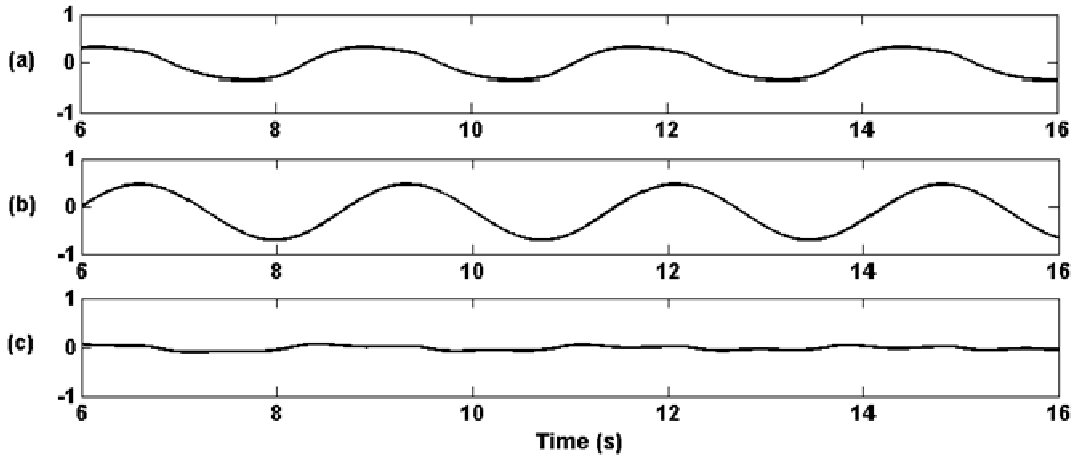

Fig. 4.8 Processing by AFSR of ICG-free artifact: **(a)** ICG-free artifact, **(b)** sensed respiration, and **(c)** processed output (all the waveforms are in arbitrary units).

In order to estimate limitation of the AFSR technique, it was applied on waveforms consisting of only the simulated artifacts. Figure 4.8 shows processed output when only ICG-free artifact is given to the artifact canceller. The attenuation of the artifact, for the recordings from the 23 volunteers, ranged over 27.1 to 27.5 dB. It is seen that the sensed respiration and the respiratory artifact are synchronized but their spectra differ, particularly in the high frequency region. As compared to the artifact, the sensed respiration is a smoothed waveform, deficient in higher frequencies. This limits the effectiveness of the adaptive filtering in

suppressing the higher frequencies of the respiratory artifacts. Adaptive filtering can be made more effective using a reference input which has a better representation of higher frequencies.

4.4 Adaptive filtering by using estimated respiration (AFER)

Processing of the artifact-free signal by the technique AFSR did not show introduction of any significant error. For signals with simulated artifacts in the SAR range of -9 to 9 dB, the technique resulted in attenuation of the artifacts by 18.2-18.8 dB and hence it may be considered as highly effective in suppressing the artifact. The output from the thermistor based respiration sensor is synchronously related to the respiratory artifact, but the sensed waveform is found to be low-pass filtered and using it as a reference did not help in reducing higher frequency components of the respiratory artifacts. Using a signal synchronous to the sensed respiration, but with a better representation of higher frequency components may improve the cancellation of the respiratory artifacts.

The variations in the impedance during the inspiration and expiration phases are different (Raza *et al*., 1992). Each phase of breathing is related to the underlying physiological events (Vander *et al*., 1980; Guyton, 1991). During inspiration, the inspiratory muscles contract, the diaphragm descends, and the rib cage rises. The thoracic cavity volume increases, stretching the lungs. The intrapulmonary volume increases, causing an increase in the intrapulmonary volume and a drop in the intrapulmonary pressure below the atmospheric pressure. Expiration is normally a passive phase, the thoracic cavity volume decreases, causing the lungs to recoil, resulting in an increase in the intrapulmonary pressure. The reference respiratory signal was analyzed to detect the inhale and exhale phases of the individual breathing cycle. A change in the slope of the respiratory waveform was taken as an indicator for a new respiration phase. We investigated the use of several reference waveforms obtained by fitting sinusoidal waveform, square waveform, triangular waveform, bipolar Gaussian pulses, and bipolar impulses over the inhale and exhale phases. The resulting new waveform was given as a reference input to the adaptive artifact canceller. Results related to these are presented in Appendix C. References based on the use of square and bipolar Gaussian pulse introduced distortion in the processed output. Sinusoidal waveform, as the reference signal, was unable to cancel the harmonics of the artifacts present in the recorded signal. Use of bipolar impulses as the reference failed to significantly cancel the fundamental frequency of the artifacts present in the recorded signal. On the basis of these observations, it was decided to estimate the respiration reference by using the sensed respiration and the ICG. Implementation of the technique and results from processing of the signals with simulated artifacts are presented in the following subsections.

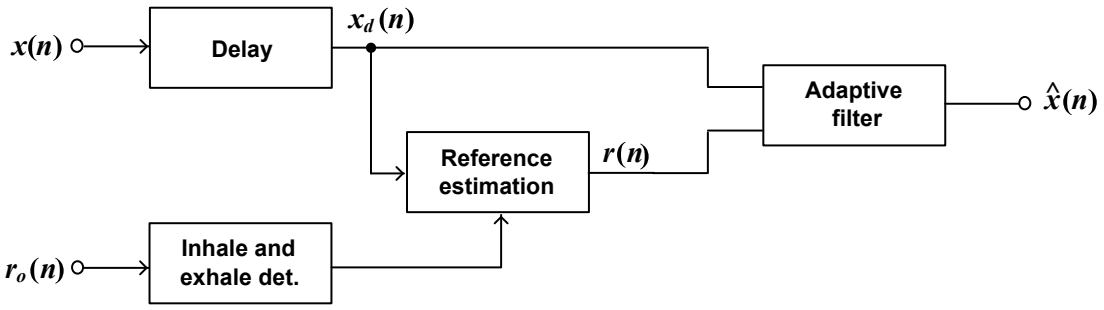

Fig. 4.9 Adaptive respiratory artifact canceller using estimated respiration reference (AFER).

4.4.1 Implementation of AFER

An examination of the ICG-free artifact waveform for a number of subjects showed the waveforms to be different during the inhale and exhale phases, and hence the reference input needs to be estimated in synchronism with the respiratory phases. From the sensed respiration, inspiration and expiration phases are detected. In each respiratory phase, a polynomial spline fitting on the contaminated signal is used for estimating the respiratory artifact. Polynomial spline fitting is carried out using the two end points of each phase as the two knots with equally spaced control points between the knots. Use of ten control points results in approximation of the artifact, with a small residual error, during both the phases. The resultant waveform thus obtained is used as the reference input for adaptive filtering. The advantage of the spline is that it has maximum number of continuous derivatives (De Boor, 1978; Kokkonis and Leute, 1996; Thijsse *et al.*, 1998; Solomon, 1999). Other techniques using the signals from the respiration sensor and the thoracic impedance sensor may also be used for estimating the respiratory artifact.

4.4.2 Processing of signal with simulated artifacts by the technique AFER

The block diagram of the technique is shown in Fig. 4.9. Signals with simulated artifact with different SAR values were processed by the technique AFER. Most satisfactory results were obtained by selecting filter tap length of 184, $\mu = 1.2 \times 10^{-4}$, and sample delay $n_d \approx 270$. Filter coefficients settled in approximately 2.7 s. As in the previous investigation with AFSR, the output SAR values were computed during the last 6 s of the processed output. Figure 4.10 shows the ICG with simulated artifact of 0 dB, the reference obtained by cubic spline fit on the contaminated ICG and the processed output. It is seen that the baseline is restored, facilitating the detection of the characteristic points in the waveform. Results from processing of the signal with the input SAR range of -9, -6, -3, 0, 3, 6, 9 dB are given in Appendix C. For

all the input SAR conditions, the respiratory artifact was found to be significantly attenuated in the output.

This method was found to be sensitive to the value of sample delay introduced in the primary signal path. In order to assess the error introduced by the adaptive filtering, the

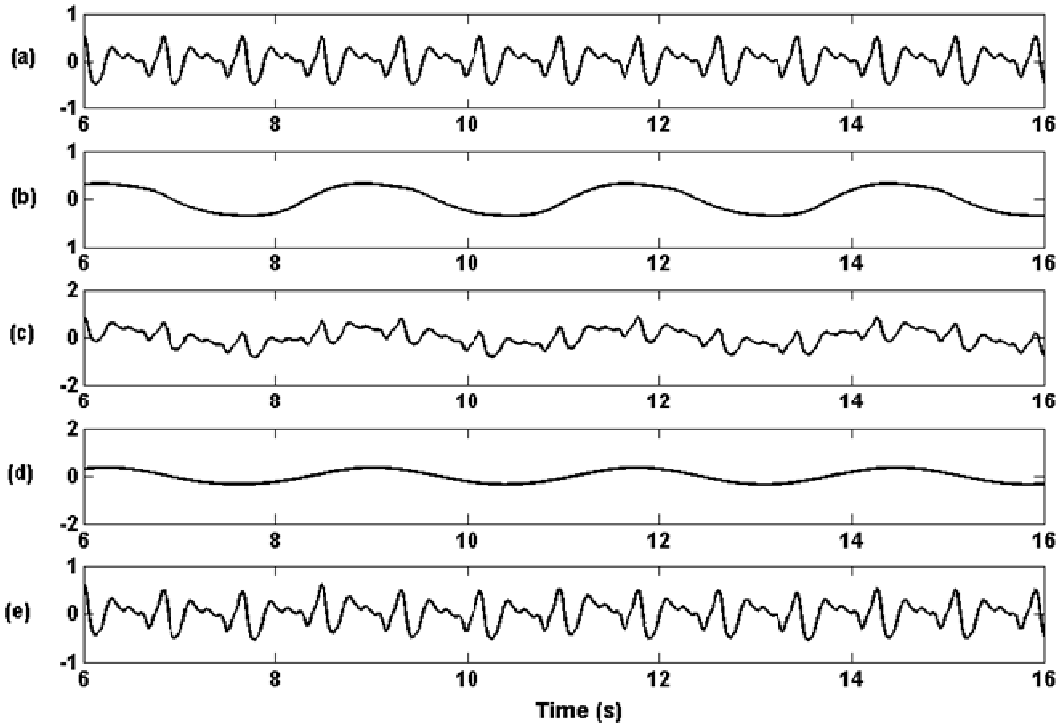

Fig. 4.10 Processing by AFER of signal with simulated artifact **(a)** artifact-free ICG, **(b)** ICG-free artifact, **(c)** ICG with simulated artifact of 0 dB, **(d)** fitted spline on the signal, and **(e)** processed output (all the waveforms are in arbitrary units).

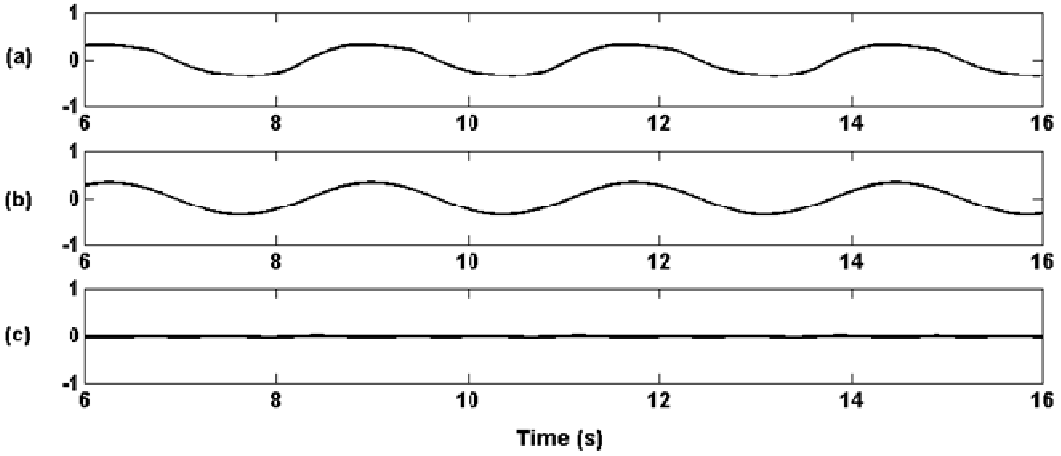

Fig. 4.11 Processing by AFER of ICG-free artifact: **(a)** ICG-free artifact, **(b)** fitted spline on the ICG-free artifact, and **(c)** processed output (all the waveforms are in arbitrary units).

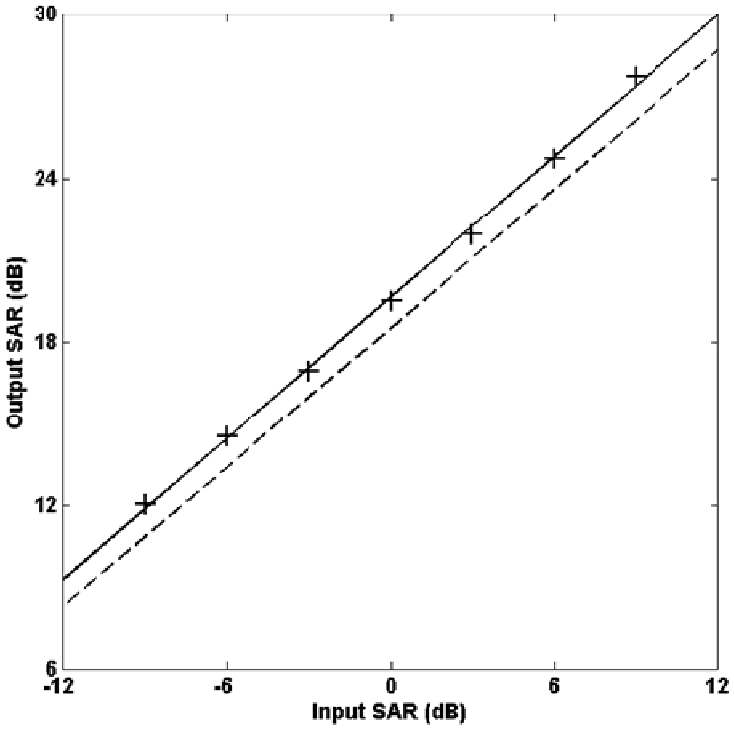

Fig. 4.12 Output SAR (in dB) versus input SAR (in dB) for the adaptive filtering technique AFER. Solid line: a linear regression, dotted line: linear regression for the technique AFSR in Fig. 4.4.

signals without any artifact addition were processed. For artifact-free signals from 23 volunteers, the signal-to-noise ratio in the processed output, as calculated by Eqn.4.7 was about 27.7 dB, indicating that the processing did not introduce significant error in the artifact free signal. The AFER technique was also applied on waveforms consisting of only the ICG-free simulated artifacts. As seen in Fig. 4.11, the simulated artifact was effectively suppressed.

A quantitative comparison of the magnitude spectra of the primary input signal, the reference signal, and the processed output showed that the estimated respiration improved the suppression of higher frequency components of the artifact.

A plot of output SAR versus input SAR values in dB for signals with simulated artifacts for one of the subjects are shown in Fig. 4.12. The relationship is nearly linear. Processing resulted in an SAR advantage of 19.6 dB. Plot of the output SAR versus input SAR for signals from the other 22 subjects was almost similar, with SAR advantage of 19.3 to 19.8 dB. As compared to the technique AFSR, the technique gave about 1 dB of additional improvement in the SAR at the output.

4.5 Enhancement of recorded signals

For quantification of the artifact suppression, the two adaptive filtering techniques AFSR and

AFER, were applied to signals with simulated artifact of different SAR's. The results presented in the two earlier sections show that both the techniques introduced negligible distortion in the artifact-free signals. For signals with simulated SAR in the -9 to 9 dB range, AFSR and AFER gave SAR improvement of 18.5 dB and 19.6 dB respectively. For seeing the effectiveness of these techniques on actual signals, they were applied on the signals acquired from 52 healthy volunteers as described in Section 4.3. These signals were recorded with the subject resting in a supine position in order to have negligible motion artifact. There were no restrictions on the breathing. Figure 4.13 shows the recorded ECG, Z_o, $z(t)$, ICG, and respiratory waveforms from a post-exercise signal recording on one of the volunteers. In the acquired waveform, $z(t)$ and ICG are contaminated by respiratory artifact, making it difficult to estimate T_{lvet} and ICG peaks. Figure 4.14 and Fig. 4.15 show processed output for ICG, by the technique AFSR and AFER, respectively. Similarly, Fig. 4.16 and Fig. 4.17 show processed output for $z(t)$, by the two techniques. Recordings from some of the volunteers and the processed outputs are given in Appendix C.

A visual examination of the waveforms showed that both the techniques effectively suppressed the respiratory artifacts from the recorded signals. For all the recordings, processed ICG output showed almost no effect of respiration, improving the detection of the B and X points. Values of ICG peaks are found to be stable. Both the techniques were found

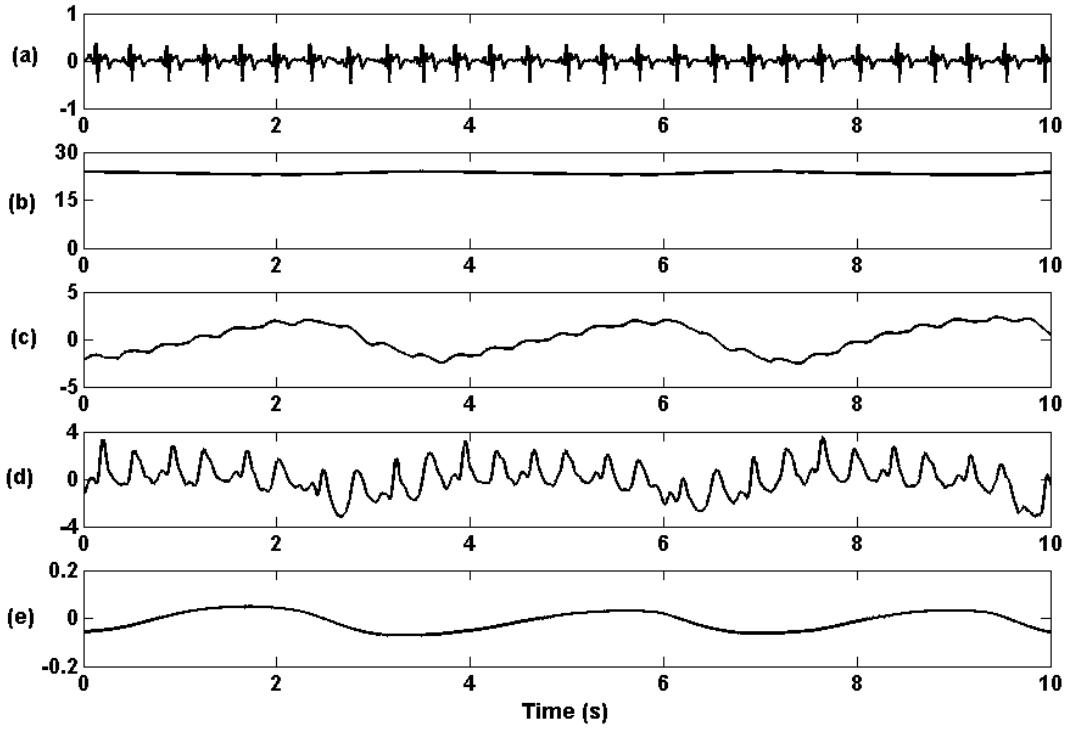

Fig. 4.13 Waveforms contaminated by strong respiratory artifact for processing: **(a)** ECG (in arbitrary units), **(b)** Z_o (in Ω), **(c)** $z(t)$ (in Ω), **(d)** ICG (in Ω/s), and **(e)** sensed airflow (in arbitrary units) from subject 'KI'.

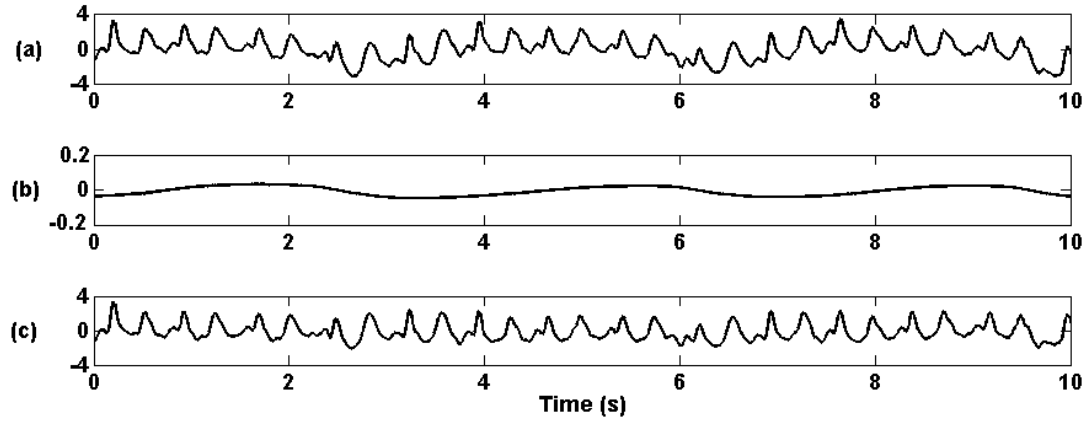

Fig. 4.14 Processing of ICG by AFSR: **(a)** recorded ICG (in Ω/s), **(b)** sensed airflow (in arbitrary units), and **(c)** processed ICG (in Ω/s) from subject 'KI'.

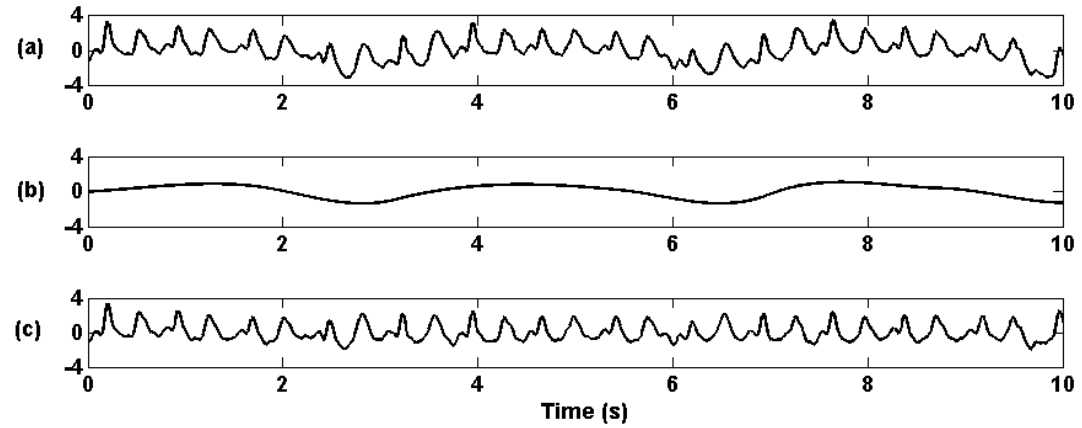

Fig. 4.15 Processing of ICG by AFER: **(a)** recorded ICG (in Ω/s), **(b)** fitted spline on recorded ICG (in arbitrary units), and **(c)** processed ICG (in Ω/s) from subject 'KI'.

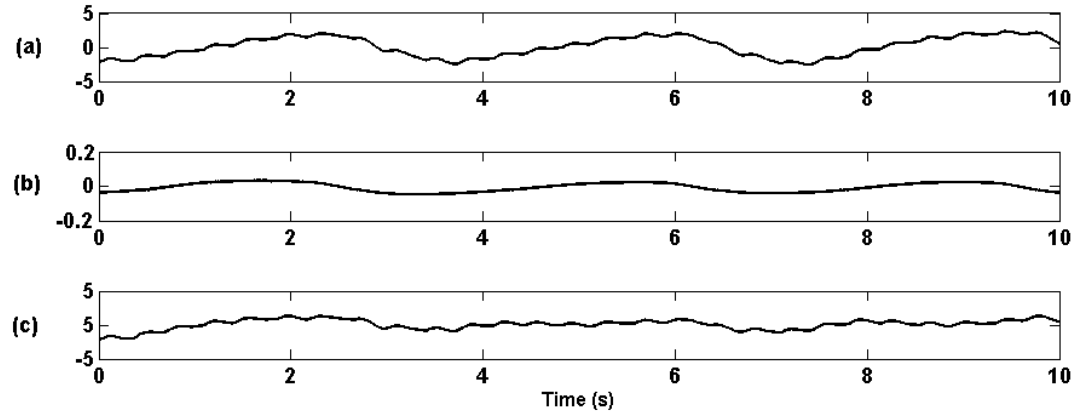

Fig. 4.16 Processing of impedance signal by AFSR: **(a)** recorded $z(t)$ (in Ω), **(b)** sensed airflow (in arbitrary units), and **(c)** processed $z(t)$ (in Ω) from subject 'KI'.

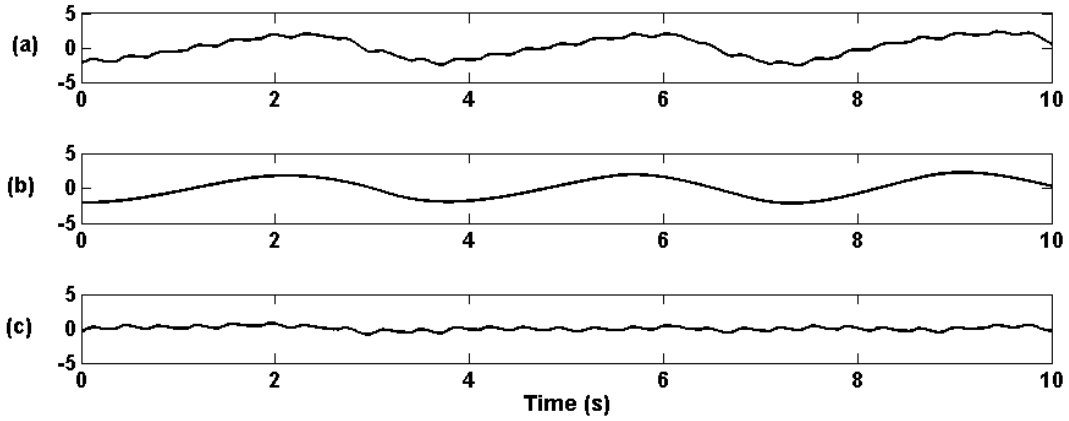

Fig. 4.17 Processing of impedance signal by AFER: **(a)** recorded $z(t)$ (in Ω), **(b)** fitted spline on recorded $z(t)$ (in arbitrary units), and **(c)** processed $z(t)$ (in Ω) from subject 'KI'.

to be effective in removing the artifacts from recorded $z(t)$ signals as well. A qualitative examination of the processed output for the recordings from the signals acquired from all the subjects showed that the artifact suppression remained effective even with a large heart rate variability in the post-exercise recordings, and the processing did not appear to affect the beat-to-beat variability in the characteristic points and the ICG peaks. As these waveforms show a significant heart rate variability and we do not have access to the artifact-free waveforms, a quantitative examination to the artifact suppression is not feasible.

4.6 Discussion

The two adaptive filtering based techniques were applied on signals with simulated respiratory artifact with input SAR in the range of -9 to 9 dB. Analysis of the results showed that the techniques were effective in attenuating the respiratory artifact without affecting the signal. For the technique AFSR, using respiration sensed by a thermistor based airflow sensor as the reference, the SAR advantage was approximately 18.5 dB. Detailed analysis showed that this technique is not efficient in suppressing the higher frequency components of the artifacts present in the sensed signal. The technique AFER was developed to provide a better approximation of the respiratory artifact. It uses respiratory reference estimated by cubic spline fitting on the ICG signal with reference to the inhale and exhale phases of the respiration. This technique showed an SAR advantage of approximately 19.6 dB. Although it appears to be giving only 1 dB additional attenuation of the artifact, the technique is very effective in suppressing higher frequency components of the artifact which can severely affect the detection of point B, C, and X in the ICG waveform. It may be noted that this SAR advantage is close to what would be achieved by ensemble averaging over 100 frames, in the absence of any cycle-to-cycle variability in the ICG signal. When the techniques were applied on artifact-free signals, the signal-to-noise ratio in the processed output was about 27.0 and

27.7 dB for AFSR and AFER respectively, indicating that both the techniques did not introduce any significant distortion in the signal. The effectiveness of the techniques in reducing the simulated artifacts in the thoracic impedance signal was the same as for the ICG signals. The filter tap lengths for the techniques AFSR and AFER were 400 and 184 respectively and the settling times were 5 s and 2.7 s respectively. The reduction in the tap length and the settling time in AFER may be attributed to the better approximation of the artifact.

Both the techniques were used for processing of the signals acquired from 52 volunteers with normal health and no known cardiovascular history. These signals showed a large beat-to-beat variation and large respiratory artifacts. A visual examination of the processed outputs showed that the respiratory artifacts were suppressed and the beat-to-beat variations were not affected. The technique AFER was more effective in suppressing the artifact because the estimated reference waveform was a better approximation of the respiratory artifact. There are limitations in applying these techniques for removal of motion artifact, because of practical limitations in obtaining and combining reference signals related to the various motions that may cause variation in the thoracic impedance.

The effectiveness of the artifact suppression by the two techniques has been assessed quantitatively using simulated artifacts on signal from 23 volunteers and qualitatively on pre-exercise and post-exercise signals from 52 volunteers. Both the techniques need to be further validated on signals acquired from several subjects with normal health and subjects with different cardiovascular disorders, under a clinical setting, by comparing the estimated values of the stroke volume and the other indices as obtained from a clinically established method. These recording and the results from processing are presented later in Chapter 6.

Chapter 5

WAVELET BASED DENOISING FOR SUPPRESSION OF ARTIFACTS

5.1 Introduction

This chapter presents investigations on a wavelet based denoising (WBD) technique for suppression of the respiratory and motion artifacts in the thoracic impedance signals, without using a reference signal. In this technique, no control of the respiration is required. An FIR based Meyer wavelet (Daubechies, 1992; Sidney *et al*. 1998; Addison, 2002) has been used for decomposition of the contaminated signal and to obtain a denoised signal. The artifact suppression is carried out to permit beat-to-beat estimation of ICG related indices.

The chapter begins with a review of wavelet based denoising techniques for removal of respiratory and motion artifacts from several biosignals. This is followed by a brief description of wavelet based signal decomposition. Next WBD technique is presented. A quantitative estimate of the artifact suppression is carried out by processing the signals with simulated artifacts with different signal-to-artifact ratios (SAR). This technique is applied on several signal recordings obtained from the volunteers and the results are qualitatively examined. Next, this technique is applied on signals acquired from several subjects with normal health and subjects with different cardiovascular disorders, under a clinical setting, and the result from the processing are presented later in Chapter 6.

5.2 Wavelet based denoising of biosignals

Wavelet analysis has been applied for denoising of several biosignals (Lim *et al*., 1995; Unser and Aldroubi, 1996; Addison, 2002). Lim *et al*. (1995) have reported good results with wavelet based linear denoising of respiratory related evoked potentials. The evoked potential signals, acquired as 2 kHz, were decomposed to seven scales and reconstructed from the last four scales.

As compared to ensemble averaging, the essential characteristics of the evoked potential signal could be obtained in a much smaller number of trials.

Cherkassky and Kilts (2001) compared several wavelet denoising techniques for removing electromyopotential (EMG) noise from the ECG signal. Visual shrink (VisuShrink), Stein's Unbiased Risk Estimate (SURE), and soft threshold were tested and a new thresholding, based on Vapnik-Chervonenkis learning theory, was proposed. Symlet wavelet was used for the analysis and mean square error and visual identification of P, R, and T waves in the ECG signals showed that Vapnik-Chervonenkis based thresholding was better than the other investigated techniques. Von Borris *et al.* (2005) used wavelet technique for removal of slow baseline drift in ECG. The ECG was decomposed up to six scales with a biorthogonal wavelet. Hard thresholding was applied by setting the coefficients of the low frequency components to zero. The technique was applied on artifact-free signals added with simulated drifts. Visual inspection of the processed ECG showed that the technique was effective in removing low frequency drift from the signal without any significant distortion in the signal. Tinati and Mozaffary (2006) used wavelet denoising to remove the baseline wandering in ECG, assuming that the baseline drift and the ECG are independent. Wavelet packet decomposition of the ECG was carried out using Daubechies wavelet. Hard thresholding, based on energy levels of the scales, was used to denoise the ECG signal. The technique was applied on simulated signals and signals recorded from healthy subjects. For simulated signals, power spectrum and R-R intervals of artifact-free signal were compared with those obtained from the denoised signal. The technique was found to be effective in removing the artifacts without distorting features of the ECG waveform. Kania *et al.* (2007) applied wavelet technique for removal of EMG and electrode-to-skin contact noise from ECG signals, recorded from patients with arrhythmia. From a visual inspection of the input signals and denoised signals, it was found that Daubechies (order 1) and Symlet (order 3) wavelets were effective in noise reduction.

Zhou and Gotman (2004) used a combination of wavelet denoising and independent component analysis (ICA, a method to separate independent components, based on the principle of statistical independence), for removing EMG and ECG from EEG signals. The technique was applied on the signal recorded from subjects. Visual inspection of the input and the denoised signals showed that integration of wavelet denoising and ICA techniques efficiently removed the EMG noise and ECG artifact in the EEG. Xu *et al.* (2005) used a wavelet-based cascaded adaptive filter for detecting and removing baseline drift from arterial pulse waveforms. The pulse signal was decomposed to 6 scales and baseline drift level was estimated by computing energy ratio of the first and the sixth scales of decomposition. If the energy ratio was less than 50 dB, the

pulse was filtered by a discrete Meyer wavelet filter followed by cubic spline estimation. Otherwise, the pulse was filtered using only the cubic spline estimation. This technique was applied on 50 simulated and 500 actual pulse signals and it was found that the wavelet based cascaded adaptive filter gave better results than the same obtained by morphology and FIR filters.

For removing ECG artifacts from EMG signal, Zhou *et al.* (2005) investigated the performance of high pass filtering, spike clipping, template subtracting, wavelet thresholding, and adaptive filtering. Processing of simulated signals showed that high pass filtering (with optimal cutoff frequency and filter order) was faster and effective in removing ECG artifacts from EMG. Jiang and Kuo (2007) used second order of Daubechies wavelet for removal of motor unit action potential from EMG. The ratio of power of approximation and detail at scale one was used for performance evaluation. Results from processing of the simulated signals showed better performance for soft thresholding.

Ouyang *et al.* (1998) reported techniques based on continuous wavelet transform (CWT) and discrete wavelet transform (DWT) for cancellation of respiratory artifact from ICG. For DWT, Coiflets wavelet (order 5) was used to decompose ICG upto 7 scales and soft thresholding was applied for denoising of signals with simulated artifact. On the basis of output SAR values and correlation between artifact-free ICG and processed output, it was concluded that the DWT based denoising was more effective in reducing the respiratory artifact from thoracic impedance signal. In this technique, breath holding for about 8 s was needed to construct the auto-regressive (AR) model of the artifact-free ICG signal. Shyu *et al.* (2004) used a wavelet based technique for detecting various cardiac events in impedance cardiography, during rest and cardiovascular activation evoked by Valsalva maneuver (a maneuver in which a person tries to exhale forcibly with a closed glottis so that no air exits through the mouth or nose). A quadratic spline wavelet was used for 7 scales of decomposition. Left ventricular pressure and left ventricular volume curve, simultaneously recorded by a conductance catheter, were used for validation of T_{lvet} and stroke volume on beat-to-beat basis. The result showed that the local minimum in the 6^{th} scale was the best indicator for detection of point B. The first zero crossing in the 5^{th} scale was the best indicator for detection of point X. Nine ward referral patients (5 male, 4 female) participated in this study and the wavelet technique demonstrated good accuracy for estimating T_{lvet}. However, stroke volumes estimated by impedance cardiography and those measured by the conductance catheter were poorly correlated.

5.3 Wavelet based signal decomposition

The wavelet transform provides a time-frequency decomposition with an optimal resolution in the time and the frequency domains (Mallat, 1989; Daubechies, 1992; Aldroubi and Unser, 1996; Rao *et al.*, 1998; Sidney *et al.*, 1998; Akansu and Haddad, 2001; Addison, 2002). The basis functions for the wavelet transform are formed by dilation and translation of a prototype function $\psi(t)$, known as the mother wavelet. The discrete wavelet transform (DWT) of a continuous signal $x(t)$ is given as

$$W(m,n) = \int_{-\infty}^{\infty} x(t)\, \Psi^{*}_{m,n}(t)\, dt \tag{5.1}$$

where $\Psi_{m,n}(t)$ is a dilated and shifted version of the mother wavelet $\Psi(t)$ and is given as

$$\Psi_{m,n}(t) = a_0^{-m/2} \Psi(a_0^{-m} t - n b_0) \tag{5.2}$$

Usually in DWT, we take $a_0 = 2$ and $b_0 = 1$. Values of $W(m, n)$ for a given m are known as the wavelet detail coefficients at scale m. The signal detail at scale m is defined as

$$d_m(t) = \sum_{n=-\infty}^{\infty} W(m,n) \Psi_{m,n}(t) \tag{5.3}$$

The signal approximation at scale m is defined as

$$a_m(t) = x(t) - d_m(t) \tag{5.4}$$

The signal can be obtained from the details up to scale m_o as

$$x(t) = \sum_{m=-\infty}^{m_o} d_m(t) + a_{m_o}(t) \tag{5.5}$$

From Eqn. 5.5, we see that the approximation at a scale is given as the sum of the detail and approximation at the next higher scale

$$a_m(t) = d_{m+1}(t) + a_{m+1}(t) \tag{5.6}$$

Thus the DWT decomposes a signal into a set of detail coefficients and an approximation. The approximation is subsequently decomposed to give the set of detail coefficients and the approximation at the next scale. This is carried out iteratively, by decomposing the signal into many lower-resolution components. In wavelet denoising, a threshold is applied at each scale of DWT and the coefficients larger than the threshold are retained. Denoised signal is reconstructed, by applying inverse wavelet transform, from the resulting detail coefficients and the approximation. Hard thresholding and soft thresholding are commonly used in wavelet denoising. Hard thresholding sets to zero all the coefficients with an absolute value below a certain threshold. In soft thresholding, coefficients with an absolute value

below a certain threshold are set to zero while the threshold is subtracted from the remaining coefficients (Donoho, 1995). It has been reported that soft thresholding, under certain statistical assumptions, may result in a slightly better noise reduction and may reduce the accompanying signal distortion. Several other types of thresholding, including SURE, VisuShrunk, Vapnik-Chervonenkis, hybrid, and minimax threshold, have been reported for wavelet based denoising (Donoho, 1995; Donoho *et al*., 1995; Donoho and Johnstone, 1998; Rao *et al*., 1998; Cherkassky and Kilts, 2001). In wavelet based linear denoising or scale dependent thresholding (Lim *et al*., 1995; Addison, 2002), the DWT is applied on the signal for a number of scales of decomposition, and each scale is reconstructed into the details and the approximation, to visualize the signal and artifact component at each scale. If the signal and noise are consistently represented on different scales, the signal can be reconstructed from the appropriate scales.

5.4 Artifact suppression

We investigated the application of wavelet based linear denoising or scale dependent thresholding (Lim *et al*., 1995; Addison, 2002) for suppression of respiratory and motion artifacts in the ICG signal. The DWT is applied on the signal for a number of scales of decomposition, and each scale is reconstructed into the details and the approximation, to visualize the signal and artifact component at each scale. For selection of the mother-wavelet and the number of scales in the decomposition, we studied several types of wavelets: Daubechies, Coiflets, Symlets, and FIR Meyer for the signal acquired at sampling frequency of 500 Hz. These wavelet functions and results from decompositions of the artifact-free signal and signal-free artifact are given in Appendix D. The FIR based Meyer wavelet (Daubechies, 1992; Sidney *et al*. 1998; Addison, 2002) captured the ICG in its first few scales and the artifacts in the other scales for a wide variation in the heart rate, respiration rate, and motion artifacts. It was found that decomposing the signal up to 10 scales gave sufficient resolution to separate the signal and the artifact. This resulted in 10 details and 1 approximation. Increasing the number of scales beyond 10 gave very low frequency DC-like details at the higher scales and did not provide any useful information for denoising.

The decomposed signals are classified into a low band (lower scales, with higher temporal resolution) where only signal components are present, a high band (higher scales, with lower temporal resolution) where only the artifacts are present, and an intermediate band with very small contribution from either. For thresholding, detail and approximation at each scale were examined. Artifact-free ICG signals and ICG-free artifacts were acquired by the method described earlier in Section 4.3.2. Figure 5.1 shows the details and approximation of an artifact-

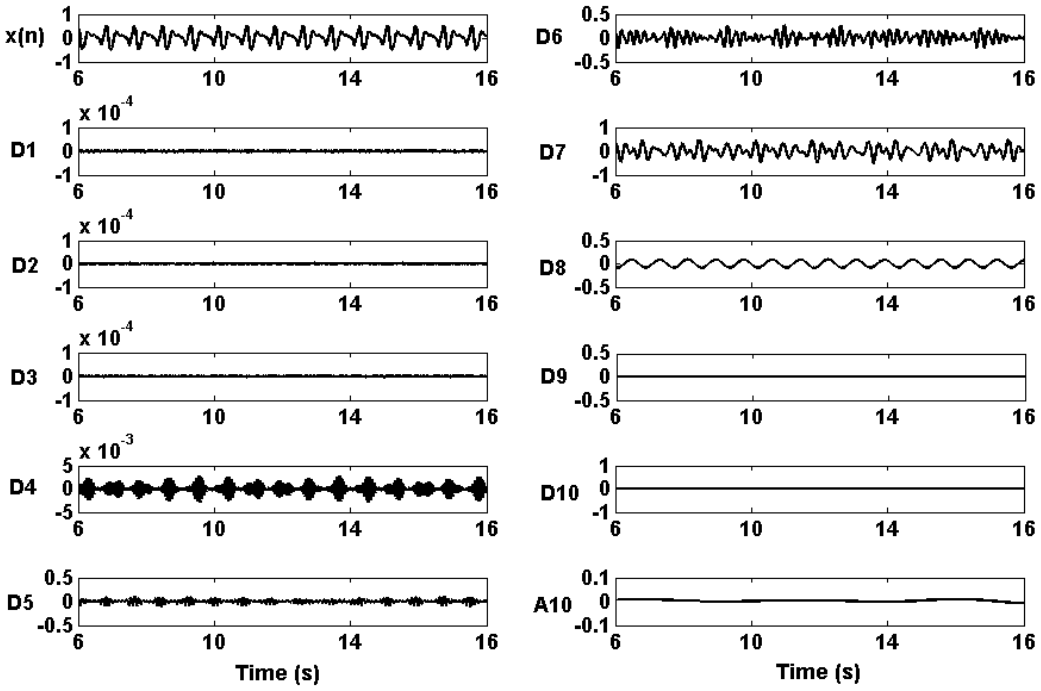

Fig. 5.1 Details D1-D10 and approximation A10 of artifact-free ICG $x(n)$, using discrete Meyer wavelet (all the waveforms are in arbitrary units).

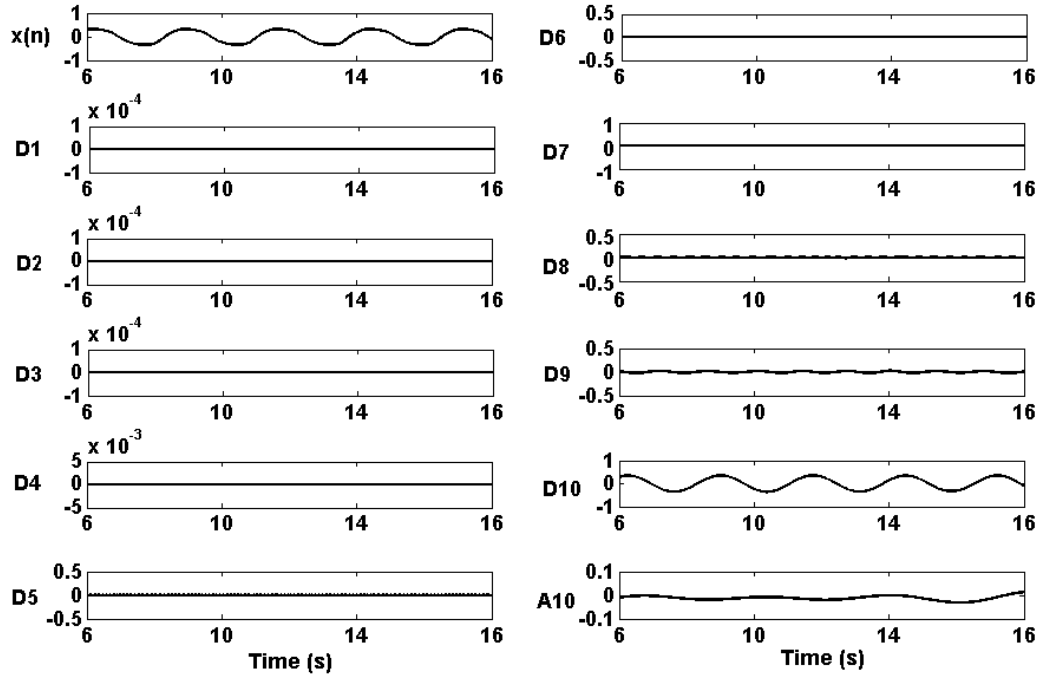

Fig. 5.2 Details D1-D10 and approximation A10 of ICG-free artifacts $x(n)$, using discrete Meyer wavelet (all the waveforms are in arbitrary units).

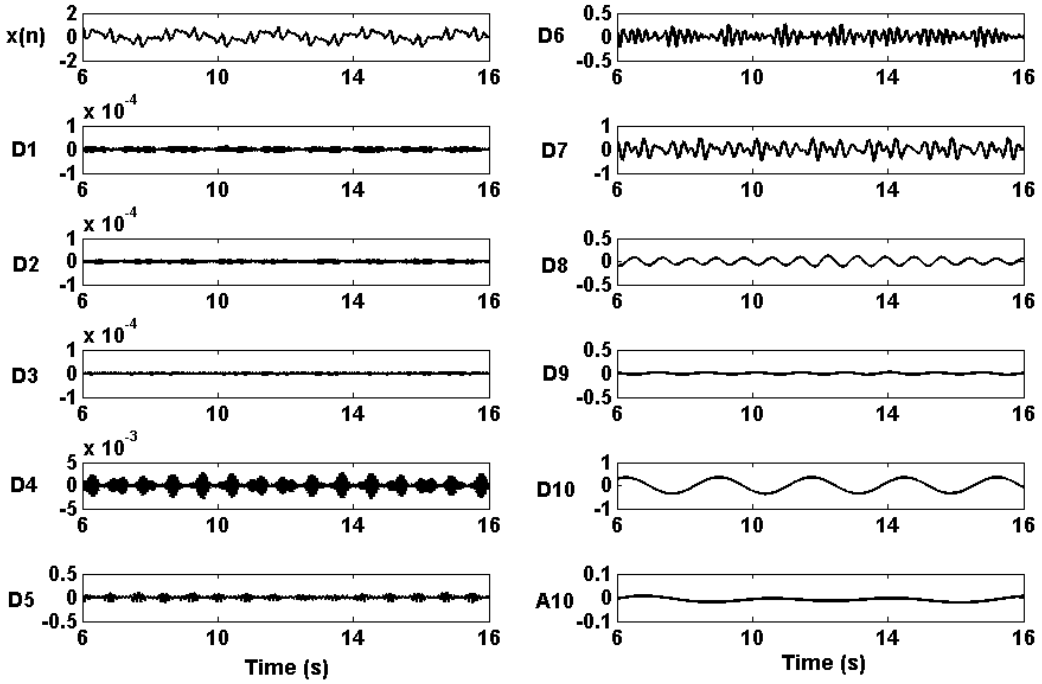

Fig. 5.3 Details D1-D10 and approximation A10 of ICG $x(n)$ with simulated artifact 0 dB SAR using discrete Meyer wavelet (all the waveforms are in arbitrary units).

free ICG signal. Figure 5.2 shows the details and approximation at each scales of an ICG-free artifact due to controlled breathing at 0.4 Hz. In this example, artifact-free ICG signal is captured within first eight details while ICG-free artifact related components are captured at higher scales. An analysis of the signals recorded from 23 volunteers showed that mostly the signal components are captured in details D1-D8 while the artifact related component were found in details D9-D10, and approximation A10. Figure 5.3 show the detail and approximation at each scale of decomposition of a simulated contamination of ICG with input SAR of 0 dB. As shown in the figure, the signal components are captured in details D1-D8 while the respiratory artifact related components are captured in details D9-D10 and approximation A10.

5.4.1 Processing of signals with simulated artifacts

For estimating the effectiveness of the WBD technique in removing the respiratory artifacts, signals with simulated artifacts with different SAR values were generated, as described earlier in Section 4.3.3 of the previous chapter. For input SAR = ∞ dB (*i.e.*, zero artifact), signal is decomposed to details D1-D8. Figure 5.4 shows ICG with input SAR of 0 dB and processed output. The denoised signal was reconstructed by adding the details D1-D8. In the processed

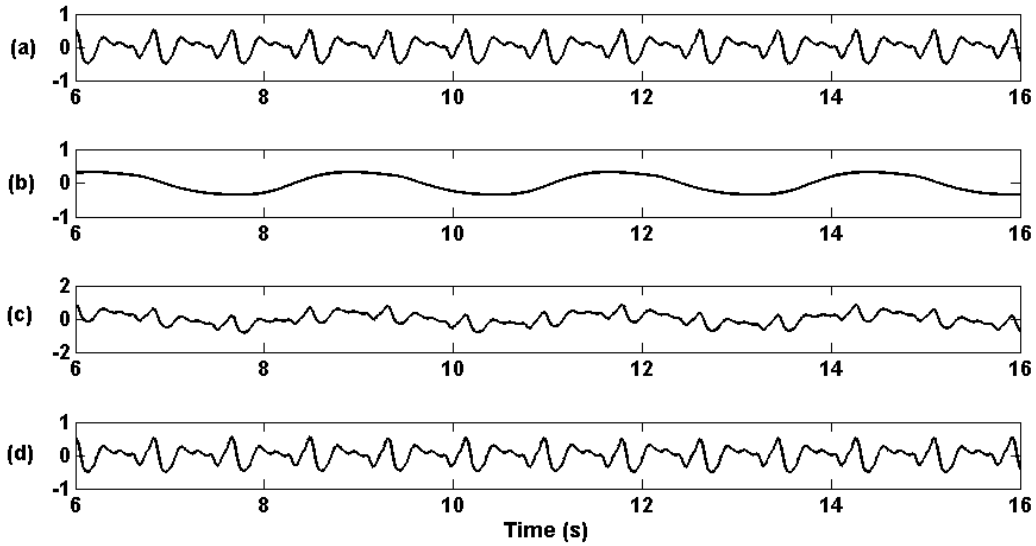

Fig. 5.4 Processing by WBD of signal with simulated artifact: **(a)** artifact-free ICG (in arbitrary unit), **(b)** ICG-free artifact (in arbitrary unit), **(c)** ICG with simulated 0 dB artifact (in arbitrary unit), and **(d)** processed output (in arbitrary unit).

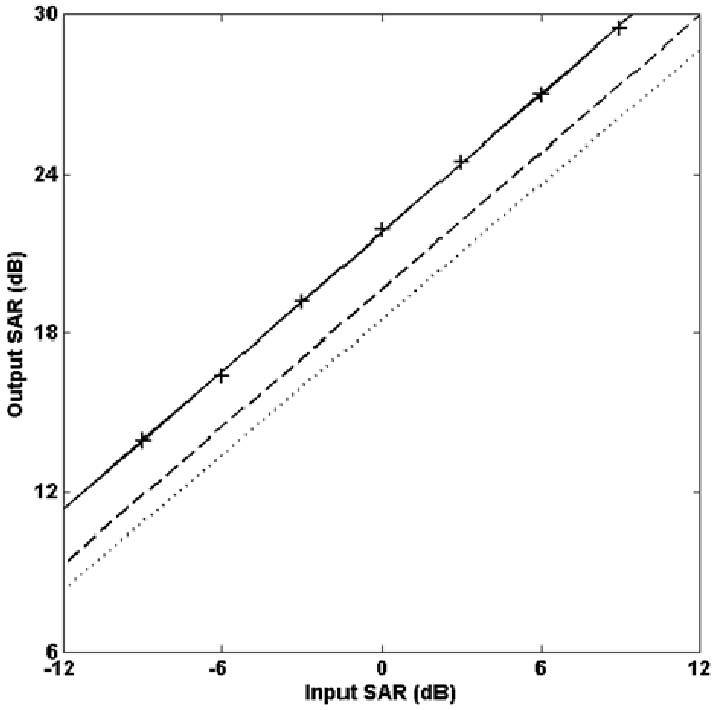

Fig. 5.5 Output SAR (in dB) versus input SAR (in dB) for the wavelet based technique (WBD). Solid line: a linear regression, dotted line: linear regression for the technique AFSR in Fig. 4.4, dashed line: linear regression for the technique AFER in Fig. 4.12.

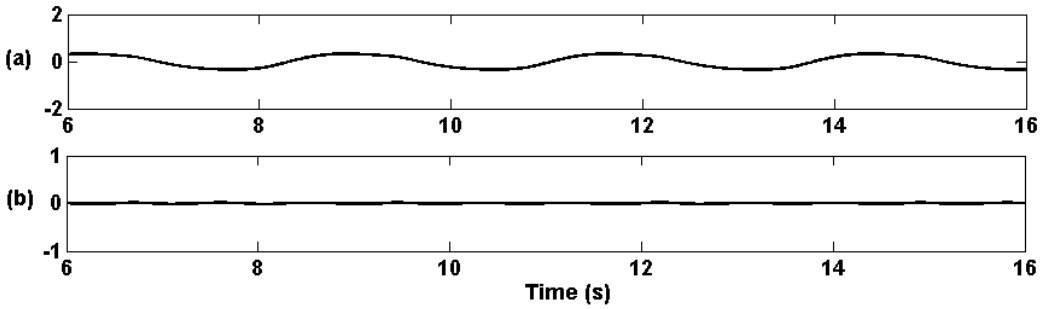

Fig. 5.6 Processing by WBD of ICG-free artifact: **(a)** ICG-free artifact, and **(b)** processed output (all in arbitrary unit).

output, artifacts are suppressed and baseline has been restored, facilitating the detection of characteristic points and estimation of the parameters required for calculating the stroke volume. Results from processing of the signal with SAR values of -9, -6, -3, 0, 3, 6, 9 dB are presented in Appendix D. Output SAR values were computed by using Eqn. 4.6. Figure 5.5 shows a plot of output SAR values for different input SAR values in dB. Relationship between output SAR and input SAR is nearly linear and we see that the processing has resulted in an SAR improvement of 21.8 dB. The signal-to-noise ratio in the output after applying this technique on artifact-free signal was found to be 33.2 dB, indicating that the technique produced very little distortion in the processed output, and approximately 6 dB lower than the two adaptive filtering techniques. Figure 5.6 shows processed output when only artifact is given as the input. As shown in the figure, this technique effectively suppresses the artifacts with very little error after denoising.

For the simulated artifacts, the technique WBD has shown better signal enhancement as compared to the two adaptive filtering based techniques, presented in the previous chapter. The processing was applied on signals with simulated artifact generated from the recordings taken from 23 volunteers. The relationship between the output SAR and the input SAR were almost similar to the plot in Fig. 5.5 with SAR improvement ranging from 21.5 to 21.9 dB.

5.4.2 Enhancement of recorded signal

For assessing the effectiveness of the technique on the actual signals, it was applied on signals acquired from 52 healthy volunteers, as in Section 4.3. These signals were recorded with the subject resting in a supine position in order to have negligible motion artifact. Figure 5.7 shows the recorded ECG, Z_o, $z(t)$, ICG, and respiratory waveform from a subject in post-exercise relaxation. The signals $z(t)$ and ICG show strong presence of respiratory artifact and minimum motion artifacts. Baseline is not stable making it difficult to estimate the parameters (peak height and T_{lvet}). Figures 5.8 and 5.9 show the processed output of the ICG and $z(t)$ signal. Processed

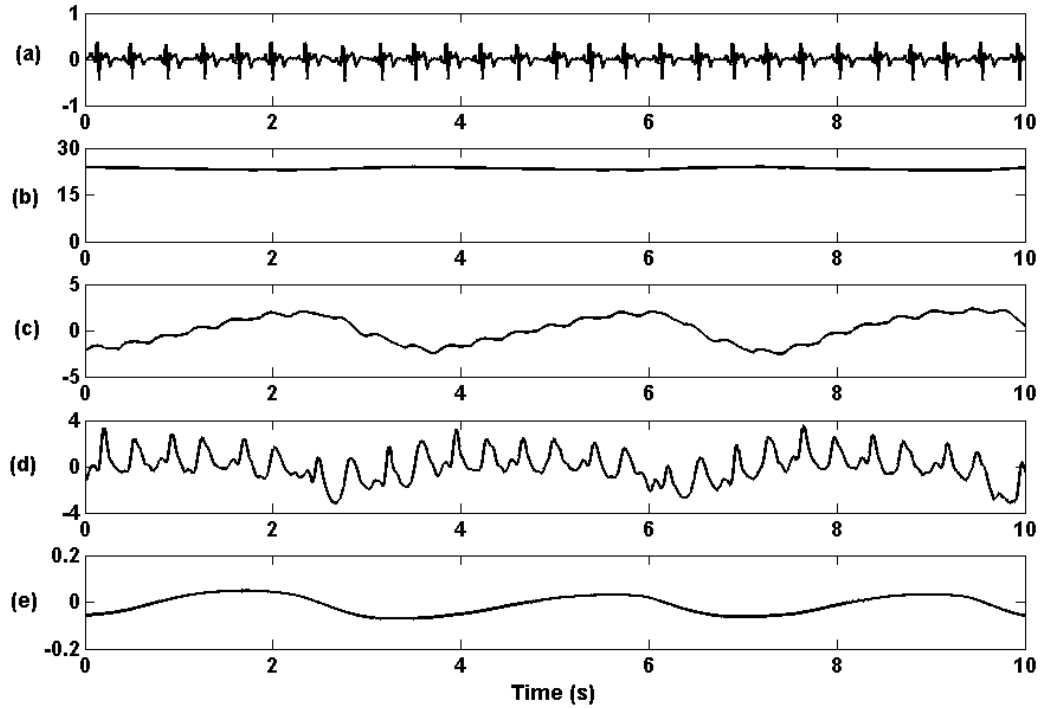

Fig. 5.7 Waveforms contaminated by strong respiratory artifact for processing: **(a)** ECG (in arbitrary units), **(b)** Z_o (in Ω), **(c)** $z(t)$ (in Ω), **(d)** ICG (in Ω/s), and **(e)** sensed airflow (in arbitrary units) from subject 'KI'.

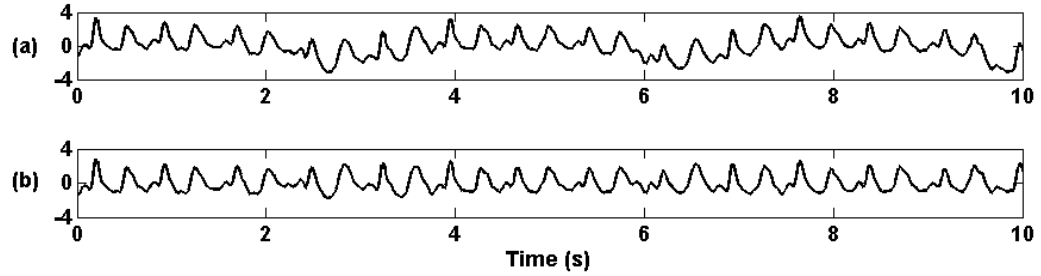

Fig. 5.8 Processing of ICG by WBD: **(a)** recorded ICG (in Ω/s), and **(b)** processed ICG (in Ω/s), from subject 'KI'.

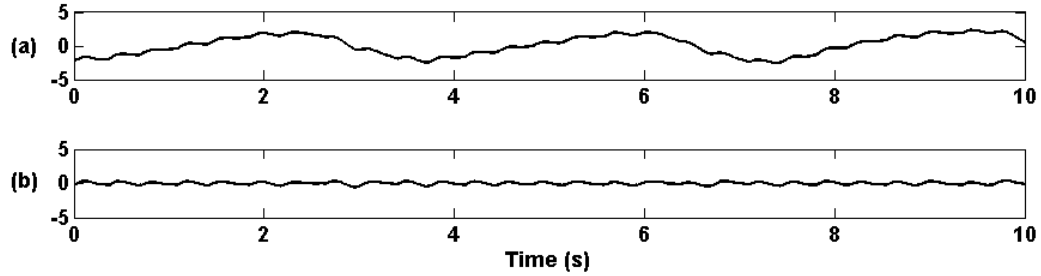

Fig. 5.9 Processing of impedance signal by WBD: **(a)** recorded $z(t)$ (in Ω), and **(b)** processed $z(t)$ (in Ω), from subject 'KI'.

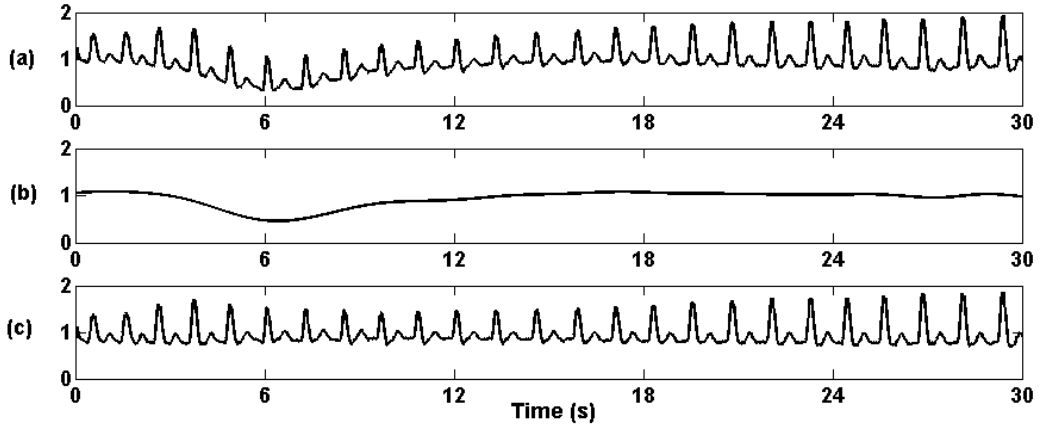

Fig. 5.10 Processing of ICG by WBD with motion artifact: **(a)** recorded ICG (in Ω/s), **(b)** estimated artifact (in arbitrary units), and **(c)** processed ICG (in Ω/s), from subject 'JJ'.

output shows almost no effect of the artifacts, improving the detection of the B and X points. The peaks in the waveform are found to be stable. Recordings from some of the volunteers and the processed outputs are given in Appendix D. A visual examination of these waveforms showed that both the techniques effectively suppressed the respiratory artifacts from the recorded signals.

The effectiveness of the technique in removing the motion artifact was investigated by processing the signals corrupted by motion artifacts but free from respiratory artifacts. Figure 5.10 shows a signal from a volunteer 'JJ' (a professional swimmer) who could comfortably hold the breath for a relatively long period. Recordings were taken with the breath holding for 32 s and left hand movement. In the waveform shown in Fig. 5.10 (a), the ICG is contaminated by only the motion artifact. After applying the wavelet based denoising, the motion artifact is suppressed and a stable baseline is achieved, as seen in Fig. 5.10 (c). This technique was applied on the signals contaminated from motion artifact with minimum respiratory artifact as well as on the signals contaminated by motion as well as the respiratory artifacts, obtained from seven volunteers. The signals and processed outputs for some of them are presented in Appendix D. For all the recordings, a visual examination showed that the technique has been effective in removing the artifacts without any visible degradation in the ICG signal.

5.5 Discussion

From the analysis of details and approximation of simulated respiratory artifacts, it was seen that the WBD helps in attenuating the respiratory artifact. Applying the technique on artifact-free signals did not introduce distortion in the signal. The technique was applied for processing the thoracic impedance signals with simulated artifact generated from the recordings taken from the

23 volunteers. For the input SNR range of -9 dB to 9 dB, the relationship between the output SAR and the input SAR was almost linear, with SAR improvement of approximately 21.8 dB which is about 3 dB more than the two adaptive filtering based techniques.

This technique was applied on several signal recordings, severely contaminated from respiratory artifacts with minimum motion artifacts, obtained from 52 volunteers in resting and post-exercise relaxation condition. A visual examination showed that the baseline was restored and the technique did not affect the beat-to-beat variability of the characteristics point in the waveforms. Applying the technique on signals contaminated by both the respiratory and motion artifacts showed that the technique was very effective in suppressing the respiratory and motion artifacts. The processed outputs showed a very stable baseline, permitting beat-to-beat estimation of stroke volume and other cardiac indices. As this technique does not require any reference related to the respiratory and motion artifacts, it can be used for suppressing the artifacts during exercise or stress test.

The results presented here involved a quantitative assessment of the suppression of the simulated respiratory artifact and a qualitative assessment of the suppression of the respiratory and motion artifacts in actual signals. Results from the investigation for validation of the technique under a clinical setting are presented in the following chapter.

Chapter 6

EVALUATION OF ARTIFACT SUPRESSION

6.1 Introduction

Artifact suppression techniques based on adaptive filtering (AFSR and AFER) and wavelet based denoising (WBD) have been presented in Chapter 4 and Chapter 5, respectively. Application of the techniques on signals with simulated artifacts and actual signals resulted in suppression of the artifacts, permitting beat-by-beat estimation of the stroke volume and other cardiac indices. The values estimated by impedance cardiography need to be compared with those obtained using an established technique, for subjects with normal health and subjects with cardiovascular disorders under a clinical setting. Doppler echocardiography is an established noninvasive technique for estimating stroke volume and several other cardiac indices, and it can be used for monitoring beat-to-beat variations. The purpose of this investigation is to examine the agreement between the results obtained using impedance cardiography and Doppler echocardiography, and to examine the effectiveness of the artifact suppression techniques in improving the agreement.

This chapter begins with a review of Doppler echocardiography. Estimation of the stroke volume and T_{lvet} using impedance cardiography and Doppler echocardiography are presented in the next section. The experimental method and the results obtained are presented and discussed in the subsequent sections.

6.2 Doppler echocardiography

The standard techniques for estimating the stroke volume, such as Fick's dilution, thermo dye dilution, and electromagnetic flow-meter techniques, are invasive and their use for healthy subjects is generally precluded. Further, these techniques provide only an average estimate. Variability in the stroke volume and the other cardiac indices may provide additional diagnostic information on the cardiovascular dynamics. Doppler echocardiography has been lately used for estimating the stroke volume and some cardiac indices. It is a noninvasive technique and one of its main features is that it can be used for estimation on a beat-to-beat

basis. In this technique, velocity time integral (VTI) is computed by computing the area of the envelope of the blood flow profile over the systole. The stroke volume is estimated as the product of the VTI across a certain location and the cross-sectional area (CSA) of the location. The locations commonly used for determining the stroke volume are: (i) aortic annulus, (ii) mitral annulus, and (iii) pulmonary annulus (Quiñones e*t al.*, 2002). The aortic annulus is the most widely used location for estimating the stroke volume (Lewis *et al.*, 1984).

Kiwoski *et al.* (1981) compared the cardiac output estimates from left ventricular echocardiograms and Fick's dye dilution in 10 healthy volunteers, with increase and decrease in stroke volume caused by intravenous administration of isoproterenol and propranolol, respectively. During the rest, cardiac outputs estimated by the two techniques were reproducible for up to 40% increase in the stroke volume. Decrease in the cardiac outputs as estimated by the two techniques was also comparable. Fisher *et al.* (1983) measured left heart flows, in 54 open-chest dogs, by Doppler echocardiography at the mitral valve orifice and found that the estimated volumetric flow correlated well with the values obtained from electromagnetic flow meter. Huntsman *et al.* (1983) compared the cardiac output by Doppler echocardiography and thermodilution on 54 patients in the intensive care unit. Echocardiography could estimate the cardiac output reliably in most patients. Christie *et al.* (1987) estimated cardiac output by simultaneous application of Doppler echocardiography, two-dimensional echocardiography, thermodilution, and Fick oximetry during graded upright maximal exercise in 10 male subjects. It was reported that the stroke volume estimated by both the echocardiography techniques were very close. The agreement of Doppler echocardiography with the other two techniques varied with the method used for estimating aortic cross-sectional area and the agreement was high for the areas calculated from diameters measured at the insertion of the aortic valve leaflets.

Northridge *et al.* (1990) compared cardiac output estimated by Doppler echocardiography and impedance cardiography with that obtained by thermodilution in 24 patients with myocardial infarction. Stroke volumes were simultaneously measured by impedance cardiography and thermodilution. Doppler echocardiograms were recorded either before or after the two techniques. The agreement between the estimates was examined by correlation and Bland-Altman test. The 95% limits of agreement (mean bias ± 2 s.d.) for the echocardiography and impedance cardiography were -1.23 to 1.32 L/ minute and -1.43 to 1.11 L/ minute, respectively, with both the techniques showing a good agreement with thermodilution technique for most of the patients. Arora *et al.* (2007) compared the cardiac outputs measured by a continuous Doppler echocardiograph instrument (USCOM) and bolus thermodilution technique during postoperative period in 30 patients of coronary artery bypass

surgery. The 95% limits of agreement were –0.86 and 0.59 L/ minute. They concluded that echocardiography could reliably estimate the cardiac output.

As these and several other studies have established a good correspondence between stroke volume or cardiac output estimated from Doppler echocardiography and the other standard techniques, we have used Doppler echocardiography as a reference for comparing stroke volume estimates from impedance cardiography on beat-to-beat basis.

6.3 Estimation of T_{lvet} and stroke volume

The thoracic impedance signals acquired in the pre-exercise and the post-exercise relaxation conditions were contaminated by respiratory artifacts. The adaptive filtering techniques AFSR and AFER (described in Chapter 4), and the wavelet based denoising technique WBD (described in Chapter 5), were applied on these signals. The unprocessed waveforms and the waveforms processed by the application of the three techniques were used for estimation of the left ventricular ejection time and the stroke volume, for comparison with the values estimated using Doppler echocardiography.

The Kubicek's modified formula for the estimation of the stroke volume, as described in Chapter 2, requires two parameters estimated from the ICG waveform: (i) the left ventricular ejection time and (ii) the peak height $(-dz/dt)_{max}$. The left ventricle ejection time (T_{lvet}) is the time difference between point B (the opening of the aortic valve) and point X (the closing of the aortic valve) in the ICG waveform. Estimation of T_{lvet} requires a stable baseline. Usually $(-dz/dt)_{max}$ is measured as the peak height from the point B or from the point of zero crossover. It is generally not easy to get a clear point B or a stable baseline in the waveform. We visually examined the signals, acquired during breath hold in the pre-exercise and post-exercise conditions, from 23 volunteers with no known cardiovascular history (the signals acquired for the investigation are presented in the previous two chapters). It was found that $(-dz/dt)_{max}$ measured as the peak from the zero crossover point was approximately 0.72 times peak-to-peak height of $-dz/dt$. Hence, $(-dz/dt)_{max}$ was estimated by multiplying peak-peak height of $-dz/dt$ with 0.72 in each cardiac cycle. Point B was taken as the baseline crossover point and the point X was taken as the most negative point in the cycle. The recorded ICG signals and the signals processed by the technique AFSR showed, in some of the signals, a baseline drift. Hence, peak-to-peak height of $-dz/dt$, point B, and point X were identified manually and they were used for estimation of T_{lvet} and $(-dz/dt)_{max}$. For signals processed by the technique AFER and WBD, $(-dz/dt)_{max}$ was estimated automatically by measuring peak-to-peak height of $-dz/dt$ and point B as the baseline crossover point.

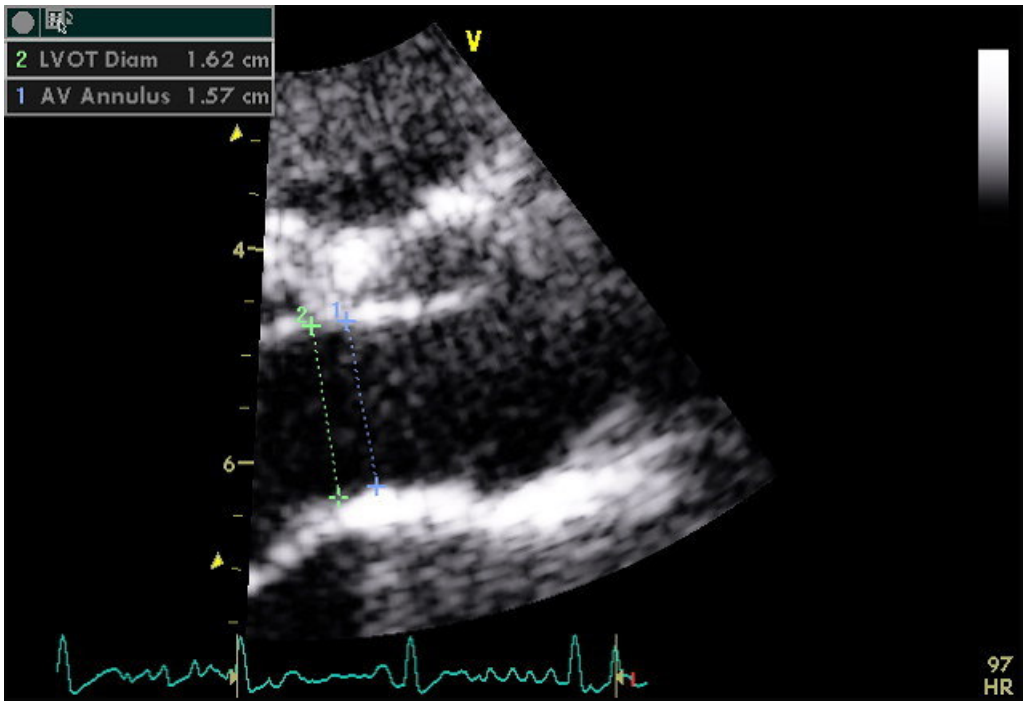

Fig. 6.1 Estimation of aortic diameter (from inner wall to inner wall) from the Doppler echocardiogram, for the subject "VM', measured at aortic valve annulus. The lower trace: ECG using the same machine.

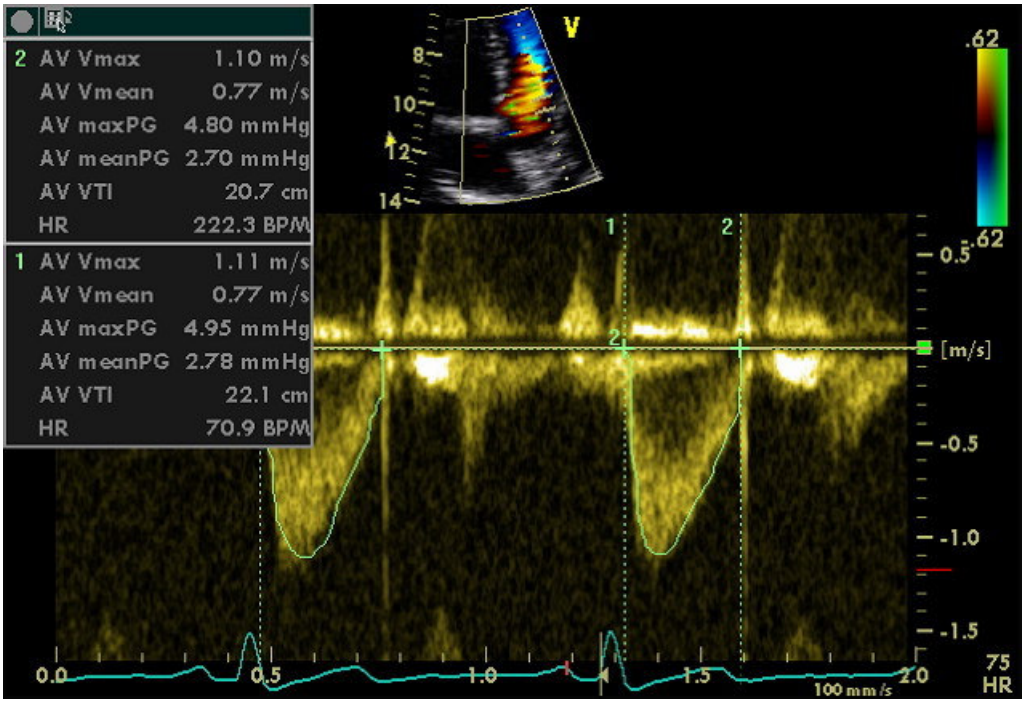

Fig. 6.2 Continuous wave Doppler echocardiogram of the selected segment at the level of the aortic valve for a healthy subject 'VM' (velocity is shown in the form of a spectral display per unit time in m/s and VTI is displayed in cm). The lower trace: ECG using the same machine.

In Doppler echocardiography, continuous wave (CW) Doppler signal is used to obtain an instantaneous blood velocity profile at the ascending aorta or pulmonary artery. The area of the envelope of the velocity profile over the systole was taken as the velocity time integral (VTI). The stroke volume was calculated by multiplying the VTI and the cross sectional area (CSA) of the aortic annulus (the insertion point of the aortic valve leaflets). The cross section of the aortic annulus was taken to be circular and its area was calculated from the annulus diameter, manually measured in the parasternal long axis view. Aortic diameter, by M-mode echocardiography, was measured at mid-systole and end-diastole at the aortic valve annulus. Figure 6.1 shows the aortic diameter (from inner wall) measured at mid-systole and end-diastole at the level of the aortic valve annulus. Doppler flow velocity of the aorta was recorded from the suprasternal notch. A good quality CW Doppler signal was denoted by a sharp, well defined waveform seen on the monitor and by a crisp sound. The values of peak velocity, mean velocity, and the VTI were measured manually by zooming each cycle and identifying the envelope of the blood flow profile with the help of a track-ball. Figure 6.2 shows the envelope of the velocity profile marked over two systoles for calculating VTI at the ascending aorta for a healthy subject. Stroke volumes were estimated as the product of the VTI and the CSA obtained at the aortic annulus in each cardiac cycle. The lower trace in both the images is the ECG signal from the limb electrodes.

6.4 Experimental method

Signals from the impedance cardiography and Doppler echocardiography were simultaneously acquired and the recordings were used for estimating the values of the left ventricular ejection time (T_{lvet}) and the stroke volume. An exercise protocol was used to introduce strong respiratory artifact and significant beat-to-beat variations. The relationship between the values as estimated by the techniques was examined. The recordings were carried out during 27th May 2007 to 29th July 2007 at the Asian Heart Institute and Research Center, Mumbai. The investigation protocol was reviewed and approved by the hospital's research committee. All the participating subjects read and signed an informed consent for participating in the investigation (on a form as given in Appendix F). The recording setup used in the investigation, the subjects and the exercise protocol, and comparison methods used for estimating the agreement between impedance cardiography and Doppler echocardiography are described in the following section.

6.4.1 Recording setup

Thoracic impedance related waveforms were recorded by using the instrument as described earlier in Chapter 4. The respiratory signal was recorded by placing a thermistor based airflow

sensor close to the nostrils. Simultaneously, Doppler echocardiograms were recorded by a radiologist, using ultrasonograph "GE Vivid 7 Dimension". A 2.5 MHz phased-array transducer was placed in the left parasternal long axis view of the aortic valve and left ventricle and an M-mode echocardiogram of the aortic valve and at the cardiac apex to record a four-chamber view. Ultrasound gel "Aquasonic" was used for a good contact of the transducer with the chest skin. The aortic flow curve was recorded from the apex and from the suprasternal notch. Still frames of the cross sectional images (derived from M mode tracings) and Doppler velocity outputs were recorded and saved on the hard disk of the instrument for 25 s (18-40 separate cardiac cycles, depending on the heart rate). Doppler gain, Wall filter (the threshold below which low frequency signals due to heart movements are removed from the display), and the scale factor (the range for the display) were adjusted to optimize the quality of the Doppler recordings. Poor quality Doppler images were ignored. The ECG amplifier of the echocardiography machine was connected to the three limb electrodes. The machine displayed the ECG signal as a trace below the echocardiogram and provided a pulse output corresponding to the R-wave of the ECG. This pulse output was acquired simultaneously along with the ICG waveform and was used for synchronization of the ICG and Doppler echocardiogram cycles.

6.4.2 Subjects and exercise protocol

Investigations were carried out on two groups of subjects. The first group consisted of volunteers with normal health from among the persons undergoing cardiovascular diagnostic tests at the hospital. All the subjects were non-smokers, and in good health. None of the subjects had cardiovascular symptoms or had taken medication within a week before this investigation. Each subject was examined by a cardiologist and the results from physical examination, maximal treadmill exercise tests, 12-lead ECG, M-mode echocardiogram, two-dimensional echocardiogram, and Doppler echocardiogram were found to be normal. A total of nine male subjects, aged 22-56 years formed this group. Second group consisted of subjects with cardiovascular disorders. Screening by Doppler echocardiography was used to exclude subjects with significant heart valve disease, pacemaker, myocardial infarction, intracardiac shunts, extremely low stroke volume, or difficulty in obtaining an acceptable echocardiogram. Five male subjects, aged 36-57 years, participated in this study: one with hypertension and severe chest pain, one subject with severe obesity and mild chest pain (ward referral, suspected for cardiac disease), and three post operated subjects of coronary heart disease. All the recordings were carried out between 8 A.M. and 2 P.M.

Motion artifact causes inaccuracy in estimating various cardiovascular parameters from the Doppler echocardiogram. Hence, the pre-exercise and the post-exercise signal recordings were carried out with the subject lying in the left lateral position: (i) after resting

for 15 minutes in the left lateral position, and (ii) after an exercise of approximately 10 minutes. All subjects performed a jogging of moderate intensity to increase the heart rate. Exercise was started at a slower warm-up speed. Further, the jogging speed was increased as the heart rate was continuously monitored using three lead ECG from the limb electrodes on the echocardiograph's screen. Subjects with normal health were asked to exercise until their heart rate reached up to 100 beats per minute. However, the subjects with cardiac disorders were asked to stop the exercise if feeling breathless. Ward referral subject was excluded from the exercise protocol. Signals ECG, Z_o, $z(t)$, ICG, respiration, and synchronization pulses were acquired along with the Doppler echocardiogram from all the subjects.

6.4.3 Comparison of results

The values of the left ventricular ejection time (T_{lvet}) and the stroke volume (SV) estimated using ICG were compared with those obtained by Doppler echocardiogram, and the effectiveness of the artifact suppression techniques in improving the beat-to-beat agreement was examined. A scatter plot of values estimated by ICG versus the corresponding values obtained by the echocardiography was used for visual examination of the relationship. It may be noted that several data points may get represented as a single point in these plots. Correlation and linear regression analyses were also used to examine the correspondence between the values estimated from the two techniques. The agreement between the values estimated by the two methods was also assessed by calculating the mean bias, the standard deviation (s.d.) of the difference, and the 95% confidence limits of agreement (mean bias ± 2 s.d.), as described by Bland and Altman (1983). In this test, the difference of the values estimated by the two methods being compared is plotted against the average of values. The relationship between the difference and the average of the parameter values has been widely used to examine any systematic bias and to identify possible outliers (Northridge *et al*., 1990; Woltjer, *et al*., 1996; Schmidt *et al*., 2005; Cotter *et al*., 2006; Leonard *et al*., 2006).

6.5 Results from subjects with normal health

In the following description of the results, the parameter values obtained from Doppler echocardiography are indicated by the term "echo" in parentheses after the parameters: T_{lvet}(echo) and SV(echo). The values estimated from the unprocessed ICG waveforms are indicated by "UP": T_{lvet}(UP) and SV(UP). The values estimated from ICG waveforms after the artifact suppression are indicated by "AFSR", "AFER", or "WBD", depending on the artifact suppression technique used. For all the comparisons, the values estimated from the echocardiography were used as the reference. We first examine the results for one of the

subjects for agreement between the values estimated by ICG and echocardiography on beat-to-beat basis for the pre-exercise and post-exercise conditions. This is followed by the results for all the subjects, analyzed by three statistical analyses: (i) correlation, (ii) linear regression, and (iii) Bland-Altman test. These statistical tests were applied on signal recordings from each subject in pre-exercise and post-exercise conditions. After examining the agreement of the results on beat-to-beat basis, we also examine the agreement of the results obtained by ensemble averaging.

6.5.1 Results for a subject

Figure 6.3 shows a segment of the simultaneously recorded ECG, Z_o, $z(t)$, ICG, respiration, and synchronization pulse waveform from a healthy subject 'DM' (age: 33 years, weight: 74 kg) in pre-exercise resting condition. Simultaneously acquired Doppler echocardiogram is shown in Fig. 6.4. Pulse output from the Doppler echocardiograph, produced corresponding to the R-wave of ECG is used here for synchronizing cycles of Doppler echocardiogram and ICG. Waveforms ICG and $z(t)$ are contaminated by respiratory artifact, making it difficult to estimate cardiac parameters from the waveform. Figure 6.5 shows a segment of the processed ICG signal, after the stabilization of the adaptive filter weights, by the three artifact suppression techniques. Cleaned ICG after applying the technique AFSR shows a small presence of the artifacts in the signal. Processing by the techniques AFER and WBD showed a more stable baseline, with almost no effect of the respiratory artifact.

Figure 6.6 shows the waveforms for the same subject, in post-exercise condition. As compared to the pre-exercise signal, the post-exercise signal has a much stronger artifact. Figure 6.7 shows the simultaneously acquired Doppler echocardiogram. Processed output for the segment of the ICG recording of Fig. 6.6 is shown in Fig. 6.8. It is seen from the figure that the signal output after applying the artifact suppression techniques have much smaller artifacts and the beat-to-beat detection of the characteristic points B, C, and X has become easier. By visual examination of these waveforms, we can say that AFER and WBD have been more effective than AFSR in reducing the artifact.

For the subject 'DM' in pre-exercise condition, correlation coefficients between the values of SV as estimated by the echocardiography and impedance cardiography were 0.61, 0.85, 0.91, 0.92 for UP, AFSR, AFER, WBD, respectively. Figure 6.9 gives a scatter plot between SV values from the ICG and the echocardiogram. We see that the processing has resulted in a reduction in the scatter and a decrease in the slope error in linear regression. Plots of observed difference versus the mean of the values are given in Fig. 6.10. The mean

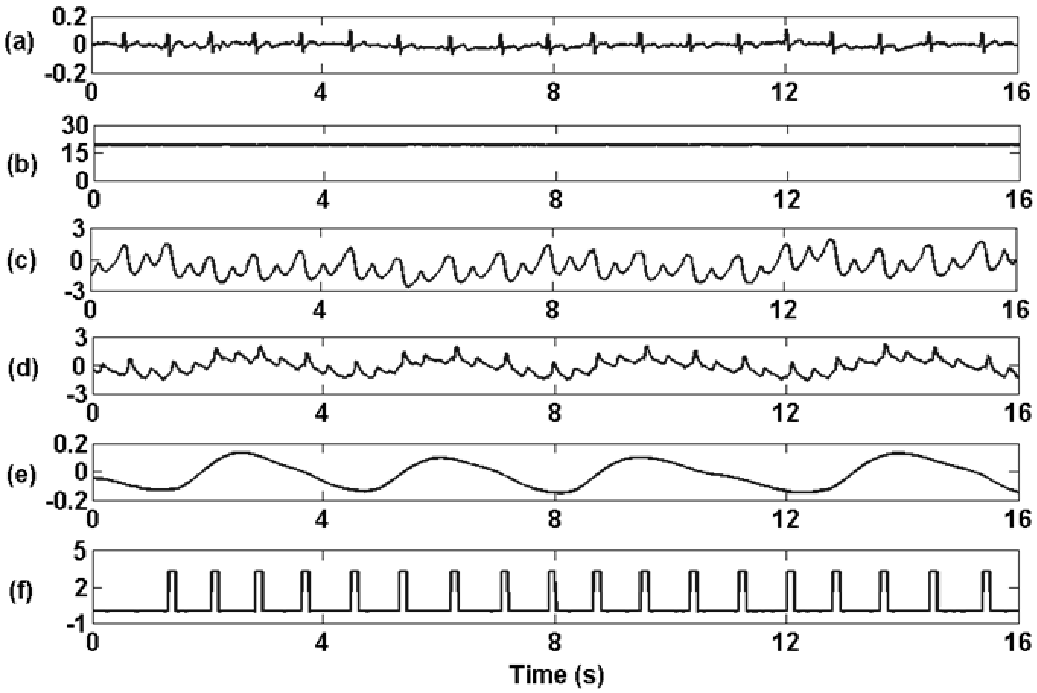

Fig. 6.3 Segment of waveforms for the subject 'DM' in resting condition: **(a)** ECG (in arbitrary units), **(b)** Z_o (in Ω), **(c)** $z(t)$ (in Ω), **(d)** ICG (in Ω/s), **(e)** sensed airflow (in arbitrary units), and **(f)** synchronization pulse from Doppler echocardiograph (in V).

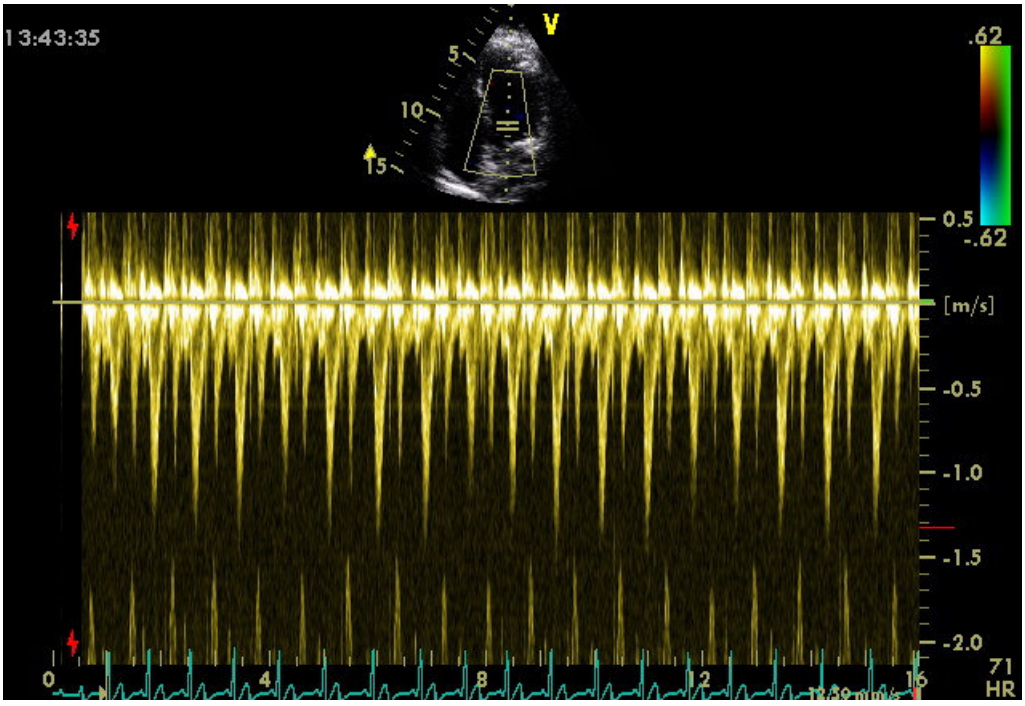

Fig. 6.4 Continuous wave Doppler echocardiogram for the subject "DM' in resting condition. X-axis- time (s). The lower trace: ECG using the same machine.

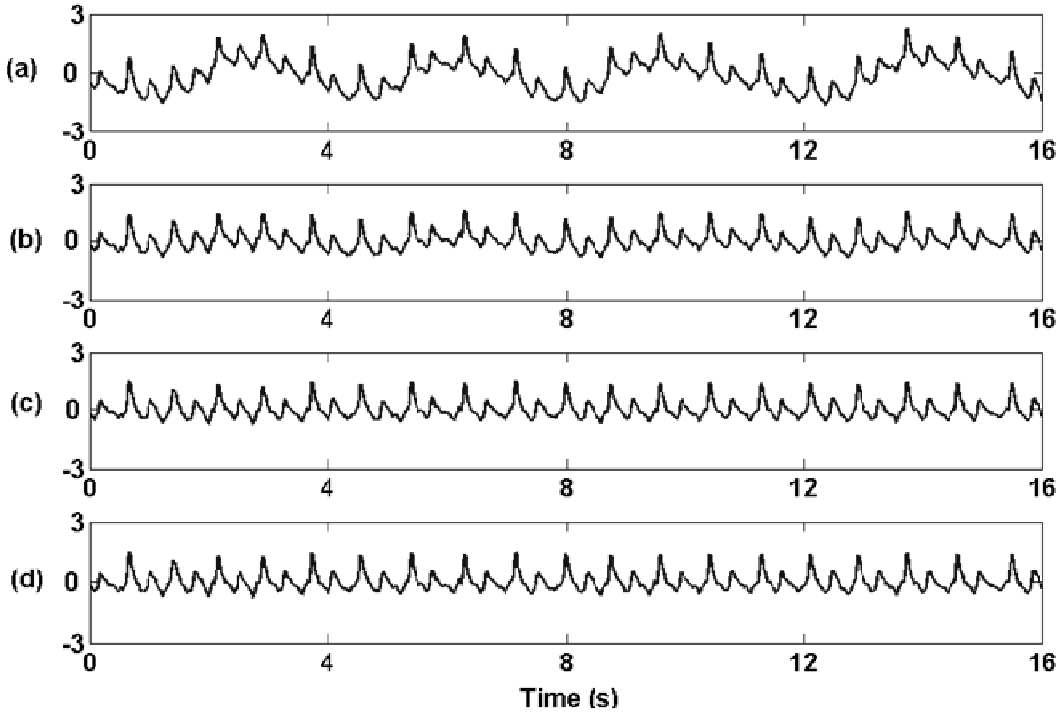

Fig. 6.5 Processing segment of output for the ICG in Fig 6.3: **(a)** Recorded ICG (in Ω/s), **(b)** ICG (in Ω/s) processed by the technique AFSR, **(c)** ICG (in Ω/s) processed by the technique AFER, and **(d)** ICG (in Ω/s) processed by the technique WBD.

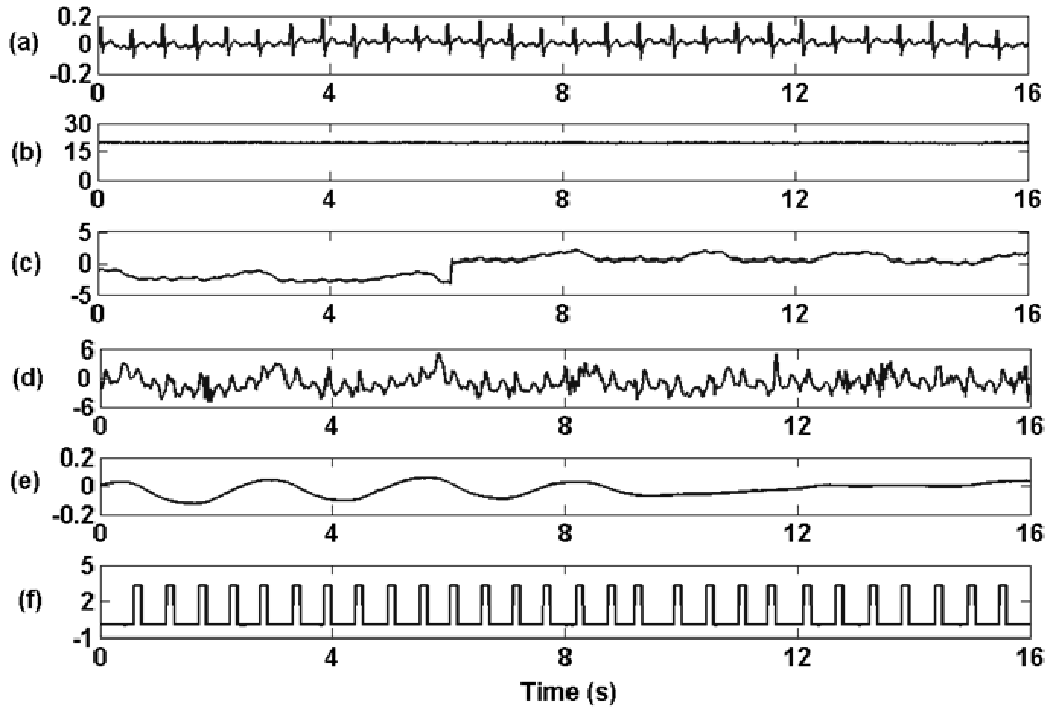

Fig. 6.6 Segment of waveforms for the subject 'DM' in post-exercise relaxation: **(a)** ECG (in arbitrary units), **(b)** Z_o (in Ω), **(c)** $z(t)$ (in Ω), **(d)** ICG (in Ω/s), **(e)** sensed airflow (in arbitrary units), and **(f)** synchronization pulse from Doppler echocardiograph (in V).

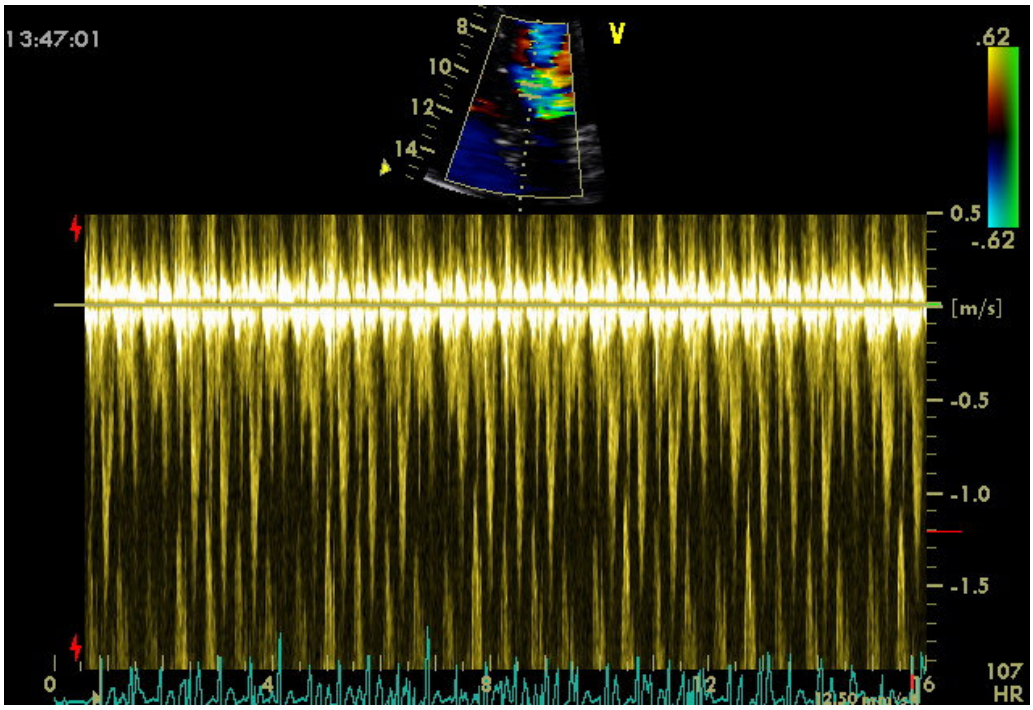

Fig. 6.7 Continuous wave Doppler echocardiogram for the subject "DM' in post-exercise relaxation. The lower trace: ECG using the same machine.

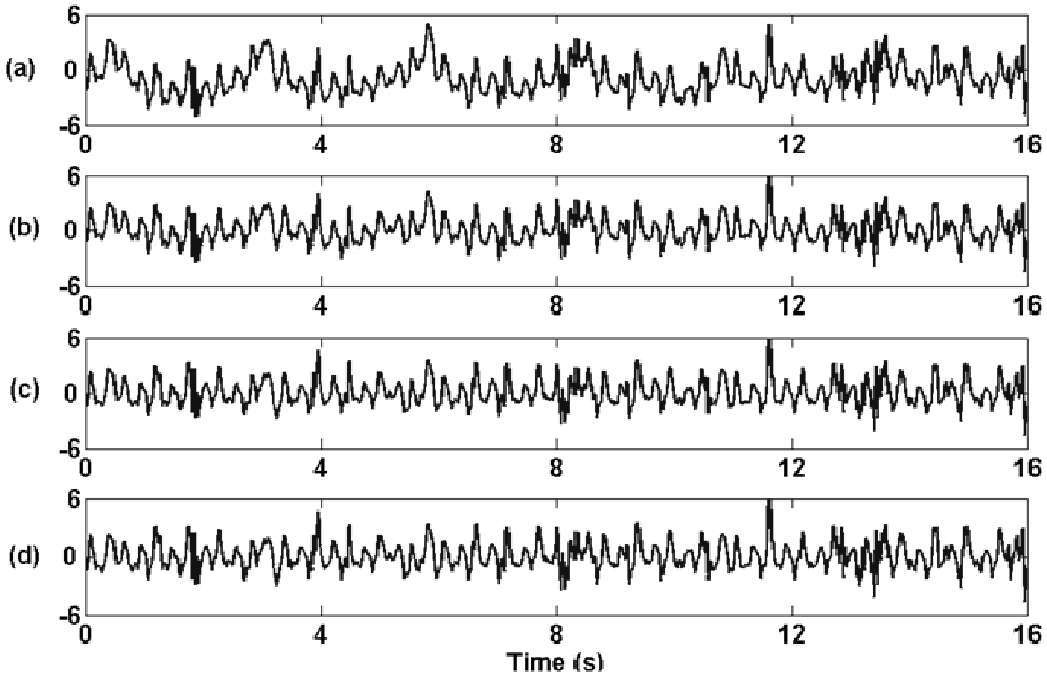

Fig. 6.8 Processing segment of output for the ICG (in Ω/s) in Fig 6.6: **(a)** Recorded ICG (in Ω/s), **(b)** ICG (in Ω/s) processed by the technique AFSR, **(c)** ICG (in Ω/s) processed by the technique AFER, and **(d)** ICG (in Ω/s) processed by the technique WBD.

biases are 21.1, 2,1, -1.2, -3.0 mL for UP, AFSR, AFER, WBD, respectively. The corresponding standard deviations of the differences are 12.9, 3.0, 2.4, 2.3 mL.

For the post-exercise recordings from the same subject, correlation coefficients for SV values were 0.80, 0.97, 0.97, 0.97 for UP, AFSR, AFER, WBD, respectively. It can be observed that the correlation increased after processing the ICG waveform. Figure 6.11 gives a scatter plot between SV values from ICG and the echocardiogram. We see that all the three artifact suppression techniques have resulted in a reduction in the scatter and a decrease in the slope error in linear regression. Figure 6.12 gives the Bland-Altman plot of the difference versus the mean values. It is seen that the mean bias was 46.5 mL for unprocessed ICG. After processing by the techniques AFSR, AFER, and WBD it decreases to -7.7, -11.1, and -14.3 mL, respectively. The standard deviations of the differences were 32.0, 8.8, 8.3, 7.8 mL for UP, AFSR, AFER, WBD, respectively.

An examination of the results across the subjects showed a similar pattern of improvements due to the three artifact suppression techniques.

6.5.2 Correlation coefficients

Correlation coefficients for T_{lvet} and SV from the echocardiogram and ICG for all the nine subjects with normal health are given in Table 6.1. It is seen that for the unprocessed ICG, the correlation coefficients for T_{lvet} values are not very high, particularly in the post-exercise condition and are not statistically significant for many of the subjects. After processing, the correlation coefficients are found to be very high, and are statistically significant at $p <$ 0.0001 for all the subjects in both pre-exercise and the post-exercise conditions. Among the three techniques, the correlation coefficients are highest for WBD.

Similarly, processing based on artifact suppression techniques resulted in an increase in correlation coefficients for stroke volumes also. Correlation coefficients for SV(UP) varied over 0.15 – 0.67 for pre-exercise and 0.35 – 0.80 for post-exercise. After processing, the correlation coefficients are found to vary over 0.72 – 0.93, 0.78 – 0.95, 0.76 – 0.95 in the pre-exercise and 0.80 – 0.97, 0.84 – 0.97, 0.87 – 0.98 for the post-exercise condition for AFSR, AFER, WBD, respectively.

6.5.3 Linear regression

Scatter plots for the all the subjects with normal health are given in Appendix E. Across the subjects, the processing resulted in a decrease in the scatter from the best fit line. Results from the linear regression analysis are given in Table 6.2. For both the pre-exercise and post-exercise recordings, processing by the three techniques resulted in the best fit lines with slopes close to one. We see that for SV(UP), the rms error from the best fit line ranges over

29.0 – 80.0 mL for the pre-exercise and 36.7 – 171.2 mL for the post-exercise condition. After processing, the rms errors from the best bit straight line are found to be much smaller and range over 6.0 – 22.3, 5.8 – 18.3, 5.1 – 16.1 mL for the pre-exercise condition for AFSR, AFER, WBD techniques, respectively. The corresponding values for the post-exercise recordings are 13.6 – 44.0, 11.6 – 42.8, 7.9 – 40.8 mL.

6.5.4 Bland-Altman test

Table 6.3 gives the values of T_{lvet} as obtained from the echocardiography and the results from Bland-Altman test for the estimates using impedance cardiography. It is seen that all the artifact suppression techniques resulted in a reduction in the mean bias and standard deviations, for both the pre-exercise and post-exercise recordings. Table 6.4 gives the results for the Bland-Altman test for SV values. As seen in the table, all the artifact suppression techniques resulted in a large reduction in the mean bias and standard deviations of the differences. As estimated by echocardiography, the SV for the nine healthy subjects varied over 42.7 – 74.5 mL for pre-exercise condition and 48.0 – 133.7 mL for post-exercise condition. The standard deviation of the beat-to-beat estimates ranged over 2.4 – 6.7 mL for pre-exercise condition and 3.6 – 32.8 mL for post-exercise condition. Taking echocardiography estimates as the reference, the range for standard deviation of the differences across the subjects are 5.1 – 15.8, 1.7 – 4.5, 1.5 – 3.6, 1.4 – 3.2 mL for the pre-exercise condition and 6.0 – 32.0, 2.3 – 8.8, 1.9 – 8.3, 1.3 – 7.8 mL for post-exercise condition for UP, AFSR, AFER, WBD, respectively. Thus we see that the processing has reduced the standard deviations of differences to values generally comparable to the beat-to-beat variation in the stroke volume under pre-exercise condition and to values generally much smaller than the beat-to-beat variation in the post-exercise condition.

6.5.5 Estimation by ensemble averaging

In the earlier subsections, we looked at agreement between the SV values estimated by echocardiography and ICG on beat-to-beat basis. For checking the agreement of the average values, the statistical analyses were carried out across the subjects. In addition to the mean of the estimated values, an estimate was obtained after ensemble averaging of the ICG signal, with respect to the ECG R-peaks, as described by Kubicek *et al.* (1966). The R-peak detection was carried using the algorithm by Hamilton and Tompkins (1986). With the average R-R interval given as $T_{R\text{-}R}$, the ensemble averaging of the *dz/dt* signal was carried out over 0.75 $T_{R\text{-}R}$ segment of the waveform starting from 0.25 $T_{R\text{-}R}$ prior to the R-peak in each heart beat, as this segment contains all the characteristic points. The means of beat-to-beat values as well as the values estimated from the ensemble averaged waveform are given in Table 6.5.

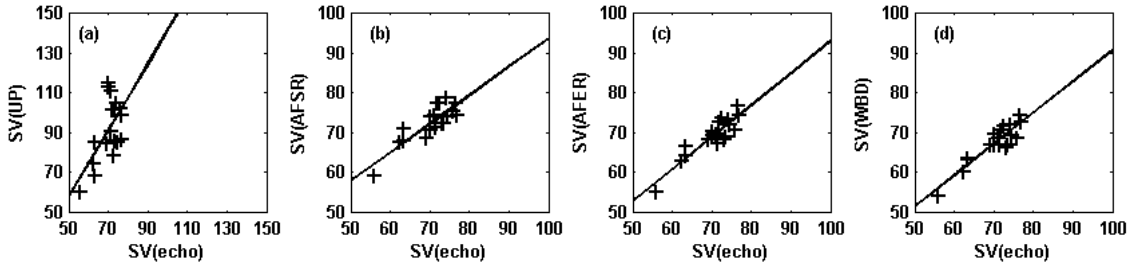

Fig. 6.9 Scatter plot and linear regression for SV (in mL) estimated for subject 'DM' in resting condition: **(a)** UP, **(b)** AFSR, **(c)** AFER, and **(d)** WBD.

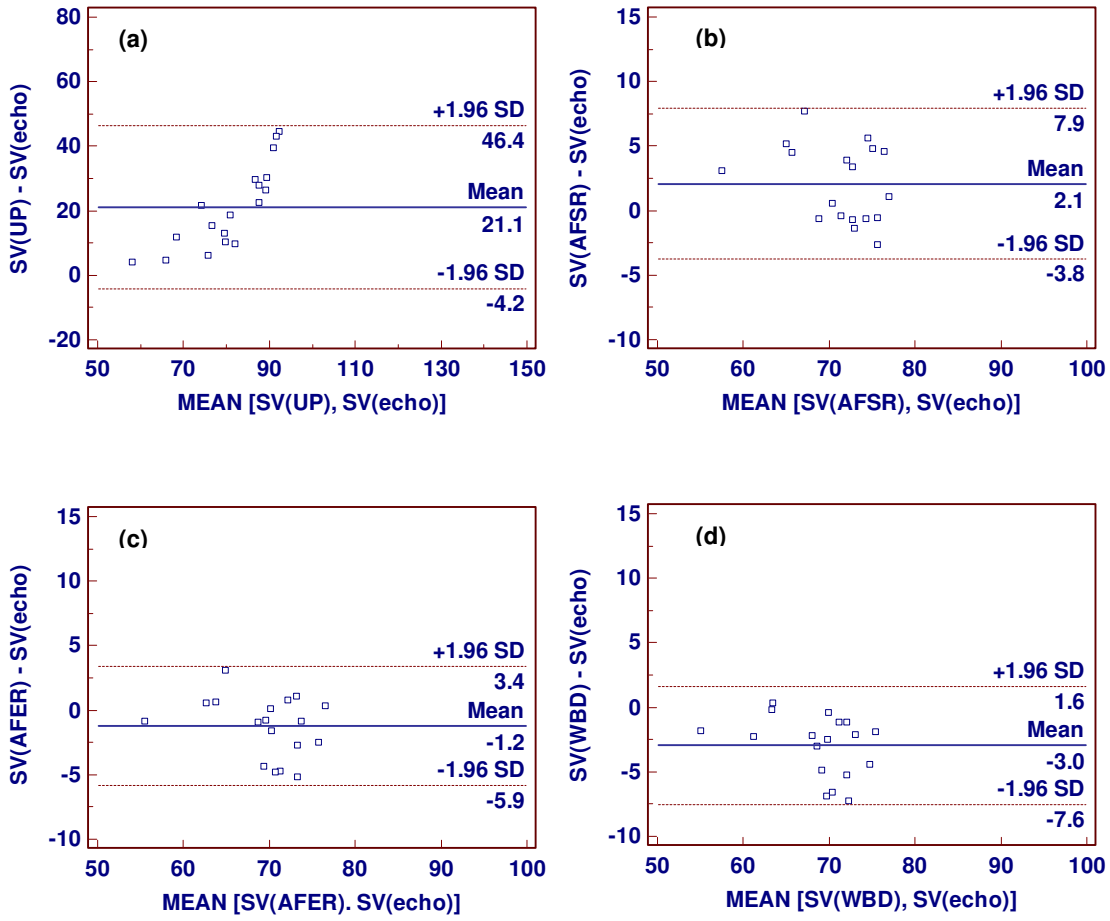

Fig. 6.10 Bland-Altman plot for SV (in mL) estimated for subject 'DM' in resting condition: **(a)** UP, **(b)** AFSR, **(c)** AFER, and **(d)** WBD.

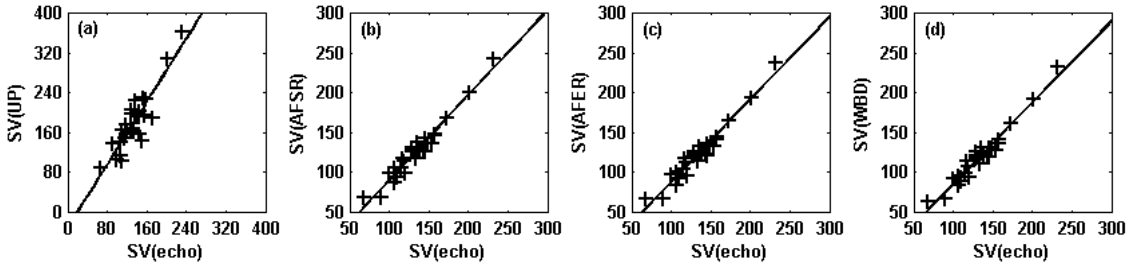

Fig. 6.11 Scatter plot and linear regression for SV (in mL) estimated for subject 'DM' in post-exercise condition: **(a)** UP, **(b)** AFSR, **(c)** AFER, and **(d)** WBD.

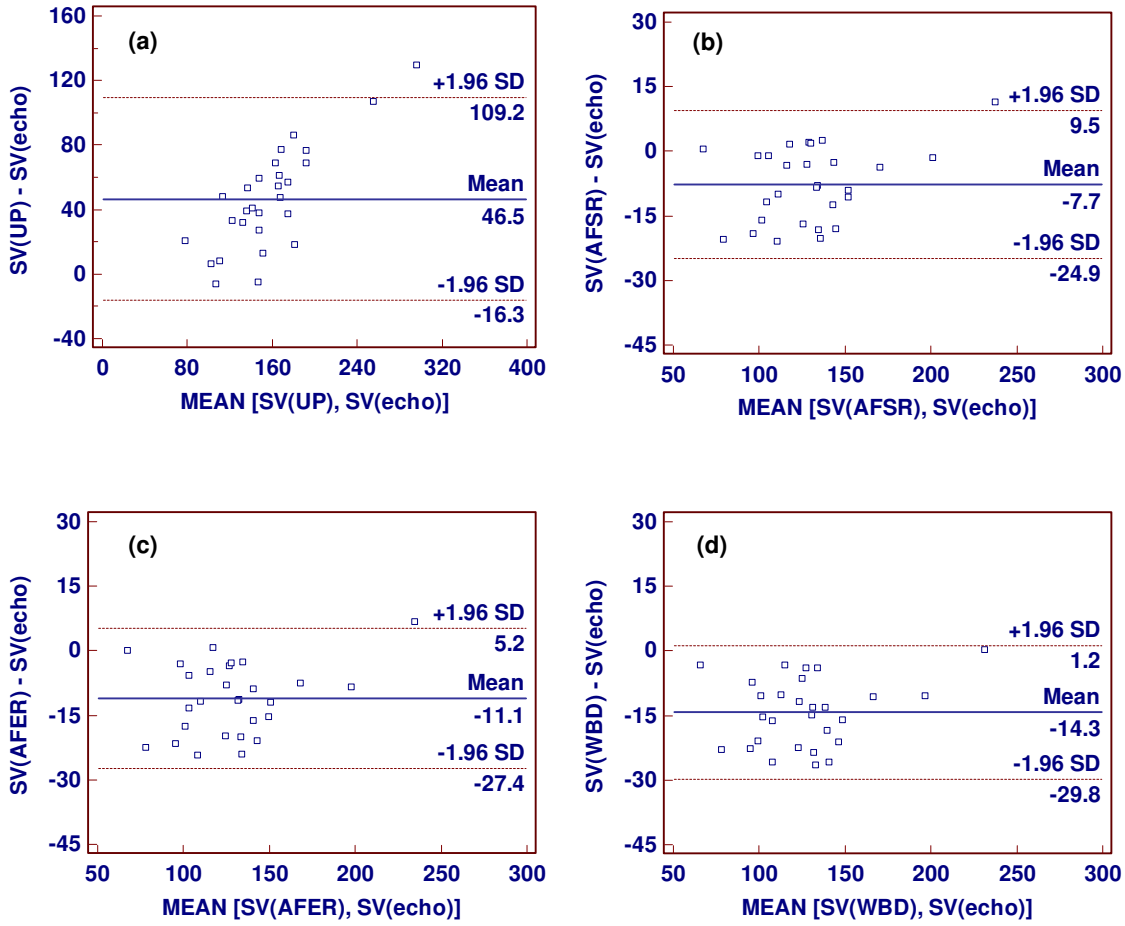

Fig. 6.12 Bland-Altman plot for SV (in mL) estimated for subject 'DM' in post-exercise condition: **(a)** UP, **(b)** AFSR, **(c)** AFER, and **(d)** WBD.

Table 6.1 Correlation coefficients, for the subjects with normal health, for T_{lvet} (ms) and SV (mL).

Subject (age)	Condition	Corr. coeff.							
		T_{lvet}				SV			
		UP	AFSR	AFER	WBD	UP	AFSR	AFER	WBD
DM (33)	Pre-ex.	0.55	0.95†	0.97†	0.99†	0.61	0.85†	0.91†	0.92†
	Post-ex.	0.37	0.97†	0.97†	1.00†	0.80†	0.97†	0.97†	0.97†
ML (22)	Pre-ex.	0.36	0.95†	0.96†	1.00†	0.18*	0.85†	0.91†	0.92†
	Post-ex.	0.31	0.97†	0.98†	1.00†	0.75†	0.97†	0.97†	0.98†
MR (41)	Pre-ex.	0.46	0.98†	0.98†	1.00†	0.46	0.87†	0.89†	0.90†
	Post-ex.	0.40	0.99†	0.99†	1.00†	0.53*	0.94†	0.94†	0.94†
P0 (56)	Pre-ex.	0.90†	0.99†	1.00†	1.00†	0.34	0.81†	0.84†	0.89†
	Post-ex.	0.80†	0.99†	0.99†	0.99†	0.69†	0.96	0.97†	0.98†
P1 (48)	Pre-ex.	0.67†	0.98†	0.98†	0.99†	0.53*	0.72†	0.78†	0.76†
	Post-ex.	0.19	0.99†	0.99†	1.00†	0.35	0.89†	0.91†	0.92†
PK (51)	Pre-ex.	0.37	0.92†	0.99†	0.99†	0.15	0.76*	0.83*	0.77*
	Post-ex.	0.72†	0.98†	0.99†	1.00†	0.56*	0.92†	0.94†	0.95†
RK (24)	Pre-ex.	0.30	0.92†	0.92†	0.93†	0.66†	0.91†	0.95†	0.95†
	Post-ex.	0.46*	0.89†	0.90†	0.90†	0.65†	0.87†	0.90†	0.90†
UT (29)	Pre-ex.	0.48	0.87†	0.89†	0.93†	0.58*	0.93†	0.93†	0.94†
	Post-ex.	0.38*	0.94†	0.95†	0.97†	0.49*	0.80†	0.84†	0.94†
VM (26)	Pre-ex.	0.45*	0.99†	0.99†	1.00†	0.67†	0.87†	0.87†	0.89†
	Post-ex.	0.46*	0.99†	0.99†	1.00†	0.52*	0.88†	0.86†	0.87†
Min.	Pre-ex.	0.30	0.87	0.89	0.93	0.15	0.72	0.78	0.76
	Post-ex.	0.19	0.89	0.90	0.90	0.35	0.80	0.84	0.87
Max.	Pre-ex.	0.90	0.99	1.00	1.00	0.67	0.93	0.95	0.95
	Post-ex.	0.80	0.99	0.99	1.00	0.80	0.97	0.97	0.98
Mean	Pre-ex.	0.50	0.95	0.96	0.98	0.46	0.84	0.88	0.88
	Post-ex.	0.45	0.97	0.97	0.98	0.59	0.91	0.92	0.94
s.d.	Pre-ex.	0.19	0.04	0.04	0.03	0.20	0.07	0.05	0.07
	Post-ex.	0.19	0.03	0.03	0.03	0.14	0.06	0.05	0.04

* $p < 0.01$, † $p < 0.0001$

Table 6.2 Linear regression for SV (in mL) estimation, for the subjects with normal health: c = intercepts, m = slope, ε = root mean square (rms) error for linear regression.

Subject (age)	Condition	Linear regression											
		UP			AFSR			AFER			WBD		
		c	m	ε	c	m	ε	c	m	ε	c	m	ε
DM	Pre-ex.	-25.8	1.7	50.9	22.3	0.7	10.3	12.7	0.8	8.5	12.2	0.8	8.2
(33)	Post-ex.	-31.1	1.6	133.9	-16.8	1.1	44.0	-16.1	1.0	42.8	-7.5	1.0	40.8
ML	Pre-ex.	40.1	0.5	32.1	8.9	0.9	6.0	-8.5	1.1	5.8	-5.9	1.1	5.1
(22)	Post-ex.	0.2	1.3	84.5	-1.6	1.0	17.4	-2.4	1.0	16.4	-4.2	1.0	14.5
MR	Pre-ex.	26.6	1.2	80.0	-0.4	1.2	22.3	3.0	1.1	18.3	5.1	1.0	16.1
(41)	Post-ex.	39.0	1.3	171.2	6.2	1.1	34.2	4.8	1.1	33.6	4.5	1.1	31.7
P0	Pre-ex.	28.0	0.8	42.4	-0.4	1.1	15.3	-1.6	1.1	13.5	1.2	1.0	10.0
(56)	Post-ex.	16.3	1.0	53.5	6.6	1.0	17.7	7.0	1.0	16.4	4.1	1.0	12.1
P1	Pre-ex.	-27.0	1.9	47.9	3.1	1.1	16.7	9.9	0.9	14.0	12.0	0.9	14.5
(48)	Post-ex.	32.9	1.0	88.4	2.6	1.1	18.5	1.2	1.1	16.1	1.7	1.1	14.9
PK	Pre-ex.	35.5	0.7	35.3	-13.8	1.4	10.2	0.3	1.1	5.8	14.4	0.8	5.1
(51)	Post-ex.	-8.0	1.6	79.4	2.6	1.1	14.9	3.8	1.0	11.6	6.9	0.9	8.2
RK	Pre-ex.	-7.5	1.4	43.6	-1.8	1.1	13.4	0.8	1.0	9.4	0.4	1.0	9.3
(24)	Post-ex.	-6.9	1.5	53.2	12.3	0.8	14.5	6.9	0.9	13.9	6.8	0.9	13.4
UT	Pre-ex.	18.4	0.9	29.0	3.2	1.1	9.6	6.1	1.0	8.8	3.6	1.0	8.0
(29)	Post-ex.	18.1	1.0	36.7	14.3	0.8	13.6	8.7	0.9	12.9	-1.9	1.1	7.9
VM	Pre-ex.	-10.5	1.6	43.5	-0.3	1.1	15.9	-0.7	1.1	14.0	-0.2	1.1	13.5
(26)	Post-ex.	20.8	1.1	64.6	2.5	1.1	22.1	4.0	1.1	22.7	2.6	1.1	21.7
Min.	Pre-ex.	-27.0	0.5	29.0	-13.8	0.7	6.0	-8.5	0.8	5.8	-5.9	0.8	5.1
	Post-ex.	-31.1	1.0	36.7	-16.8	0.8	13.6	-16.1	0.9	11.6	-4.2	0.9	7.9
Max.	Pre-ex.	40.1	1.9	80.0	22.3	1.4	22.3	12.7	1.1	18.3	14.4	1.1	16.1
	Post-ex.	39.0	1.6	171.2	14.3	1.1	44.0	8.7	1.1	42.8	6.9	1.1	40.8
Mean	Pre-ex.	8.6	1.2	45.0	2.3	1.1	13.3	2.4	1.0	10.9	4.3	1.0	10.0
	Post-ex.	9.0	1.3	85.0	3.2	1.0	21.9	2.0	1.0	20.7	2.0	1.0	18.4
s.d.	Pre-ex.	26.4	0.5	15.0	9.6	0.2	4.9	6.4	0.1	4.3	7.0	0.1	4.0
	Post-ex.	21.2	0.5	48.5	8.6	0.3	12.0	7.2	0.3	12.0	3.6	0.3	12.0

Table 6.3 Results for Bland-Altman test, for the subjects with normal health, for T_{lvet} (ms).

Sub-ject (age)	Condi-tion	T_{lvet}(echo)		Mean bias				s.d. of difference			
		Mean	s.d.	UP	AFSR	AFER	WBD	UP	AFSR	AFER	WBD
DM	Pre-ex.	266.5	10.3	48.4	8.6	6.8	1.8	24.6	3.3	2.8	1.4
(33)	Post-ex.	216.2	11.6	86.8	9.5	7.2	2.1	47.4	3.0	3.2	1.2
ML	Pre-ex.	278.7	10.0	36.5	8.5	6.6	2.0	24.4	3.1	2.9	0.9
(22)	Post-ex.	239.8	13.7	74.1	9.5	7.4	2.2	43.0	3.3	2.9	1.2
MR	Pre-ex.	312.1	19.2	74.3	8.7	6.9	2.6	10.4	1.1	1.1	0.6
(41)	Post-ex.	285.4	24.3	101.0	9.7	7.7	3.0	16.0	1.2	1.0	0.6
P0	Pre-ex.	326.5	21.2	19.4	6.6	5.2	3.6	3.0	0.8	0.7	0.6
(56)	Post-ex.	209.2	15.1	20.7	6.2	4.6	3.1	4.8	1.2	1.2	0.9
P1	Pre-ex.	297.6	14.1	51.5	9.9	7.9	2.8	8.4	1.1	1.0	0.5
(48)	Post-ex.	277.1	15.6	63.6	9.6	8.0	2.7	12.9	1.0	0.9	0.5
PK	Pre-ex.	380.9	21.8	54.6	16.5	9.9	6.0	7.1	2.2	0.9	0.8
(51)	Post-ex.	335.0	32.2	53.2	14.4	9.0	4.9	7.7	2.1	1.2	0.8
RK	Pre-ex.	344.7	15.4	45.1	16.9	15.1	10.0	6.9	1.8	1.8	1.7
(24)	Post-ex.	313.7	13.2	52.7	16.1	14.1	10.1	8.2	2.0	1.9	1.9
UT	Pre-ex.	307.1	12.1	49.8	16.0	13.1	7.4	6.9	2.2	2.2	1.6
(29)	Post-ex.	291.2	12.8	55.2	14.6	11.6	4.9	7.6	1.5	1.5	1.0
VM	Pre-ex.	270.8	18.0	48.2	9.2	7.3	2.5	31.8	3.3	3.2	1.6
(26)	Post-ex.	324.8	27.1	64.7	9.4	7.4	2.2	39.5	3.0	1.0	0.5
Min.	Pre-ex.	266.5	10.0	19.4	6.6	5.2	1.8	3.0	0.8	0.7	0.5
	Post-ex.	209.2	11.6	20.7	6.2	4.6	2.1	4.8	1.0	0.9	0.5
Max.	Pre-ex.	380.9	21.8	74.3	16.9	15.1	10.0	31.8	3.3	3.2	1.7
	Post-ex.	335.0	32.2	101.0	16.1	14.1	10.1	47.4	3.3	3.2	1.9
Mean	Pre-ex.	309.4	15.8	47.5	11.2	8.8	4.3	13.7	2.1	1.8	1.1
	Post-ex.	276.9	18.4	63.6	11.0	8.6	3.9	20.8	2.0	1.6	1.0
s.d.	Pre-ex.	37.2	4.5	14.6	4.0	3.3	2.9	10.3	1.0	1.0	0.5
	Post-ex.	97.7	9.1	29.5	4.6	3.8	2.7	17.6	1.1	1.0	0.5

Table 6.4 Results for Bland-Altman test, for the subjects with normal health, for SV (in mL).

Subject (age)	Condition	SV(echo)		Mean bias				s.d. of difference			
		Mean	s.d.	UP	AFSR	AFER	WBD	UP	AFSR	AFER	WBD
DM	Pre-ex.	70.3	5.6	21.1	2.1	-1.2	-3.0	12.9	3.0	2.4	2.3
(33)	Post-ex.	133.7	32.8	46.5	-7.7	-11.1	-14.3	32.0	8.8	8.3	7.8
ML	Pre-ex.	49.4	3.0	14.8	2.3	1.4	2.8	8.7	1.7	1.6	1.4
(22)	Post-ex.	96.9	15.3	31.8	2.5	5.5	7.9	18.3	3.6	3.4	3.1
MR	Pre-ex.	70.6	6.7	41.8	10.1	6.6	4.8	15.8	4.5	3.6	3.2
(41)	Post-ex.	84.1	13.9	59.8	14.7	11.2	9.1	28.0	5.7	5.5	5.2
P0	Pre-ex.	74.5	3.1	13.1	6.4	4.9	2.3	6.9	2.5	2.2	1.6
(56)	Post-ex.	60.6	8.4	13.9	6.3	4.7	2.2	7.0	2.7	2.1	1.6
P1	Pre-ex.	52.1	2.8	21.9	8.4	5.9	4.5	8.9	3.0	2.5	2.6
(48)	Post-ex.	70.9	5.5	33.4	10.2	7.7	5.8	15.2	3.2	2.8	2.6
PK	Pre-ex.	47.4	2.4	19.1	7.1	3.3	2.5	10.2	3.1	1.7	1.6
(51)	Post-ex.	66.0	5.7	28.2	6.5	3.5	2.4	13.5	2.5	1.9	1.4
RK	Pre-ex.	56.9	4.7	14.8	2.2	0.5	0.1	7.6	2.3	1.6	1.6
(24)	Post-ex.	48.0	4.9	15.6	4.8	3.0	2.1	8.7	2.4	2.2	2.2
UT	Pre-ex.	52.4	3.9	13.8	6.5	4.5	3.2	5.1	1.7	1.5	1.4
(29)	Post-ex.	52.8	3.6	15.8	5.8	4.8	2.8	6.0	2.3	2.1	1.3
VM	Pre-ex.	42.7	4.0	15.9	4.1	2.7	1.7	7.5	2.6	2.3	2.2
(26)	Post-ex.	49.8	6.0	24.9	8.6	6.8	5.6	10.8	3.8	3.8	3.6
Min.	Pre-ex.	42.7	2.4	13.1	2.1	-1.2	-3.0	5.1	1.7	1.5	1.4
	Post-ex.	48.0	3.6	13.9	-7.7	-11.1	-14.3	6.0	2.3	1.9	1.3
Max.	Pre-ex.	74.5	6.7	41.8	10.1	6.6	4.8	15.8	4.5	3.6	3.2
	Post-ex.	133.7	32.8	59.8	14.7	11.2	9.1	32.0	8.8	8.3	7.8
Mean	Pre-ex.	57.4	4.0	19.6	5.5	3.2	2.1	9.3	2.7	2.2	2.0
	Post-ex.	73.6	10.7	30.0	5.7	4.0	2.6	15.5	3.9	3.6	3.2
s.d.	Pre-ex.	11.5	1.4	8.9	2.9	2.6	2.4	3.3	0.9	0.7	0.6
	Post-ex.	35.0	9.3	17.3	6.1	6.0	6.5	9.9	2.3	2.3	2.2

Table 6.5 SV (in mL) estimated from echocardiography and ICG, with and without ensemble averaging, for subjects with normal health (m.b.: mean bias, s.d.d.: standard deviation of the differences, across the subjects).

Subject (age)	Condition	SV(echo)	SV(ICG–mean)				SV(ICG–ensemble avg.)			
		Mean	UP	AFSR	AFER	WBD	UP	AFSR	AFER	WBD
DM (33)	Pre-ex.	70.3	91.4	72.4	69.1	67.3	67.4	67.2	67.1	67.3
	Post-ex.	133.7	180.2	126.0	122.7	119.4	111.0	115.9	119.7	121.8
ML (22)	Pre-ex.	49.4	64.2	51.7	48.0	46.6	48.0	48.3	47.8	47.6
	Post-ex.	96.9	128.7	94.4	91.4	89.0	87.5	86.7	87.4	88.0
MR (41)	Pre-ex.	70.6	112.4	80.7	77.2	75.5	78.3	77.9	77.2	78.5
	Post-ex.	84.1	143.9	98.8	95.3	93.1	90.2	91.0	91.0	90.7
P0 (56)	Pre-ex.	74.5	87.6	80.8	79.4	76.8	73.2	73.5	72.9	73.8
	Post-ex.	60.6	74.4	66.9	65.3	62.8	61.7	62.0	61.0	61.4
P1 (48)	Pre-ex.	52.1	74.0	60.4	58.0	56.6	44.3	44.6	44.5	45.0
	Post-ex.	70.9	104.3	81.0	78.5	76.7	60.9	61.2	61.1	61.8
PK (51)	Pre-ex.	47.4	66.5	54.5	50.7	49.8	50.1	50.7	50.0	50.7
	Post-ex.	66.0	94.2	72.5	69.5	68.4	62.2	62.5	62.0	62.5
RK (24)	Pre-ex.	56.9	71.8	59.1	57.5	57.0	59.3	59.4	58.7	59.7
	Post-ex.	48.0	63.6	52.9	51.0	50.1	45.4	45.7	45.0	46.0
UT (29)	Pre-ex.	52.4	66.2	58.9	56.9	55.6	48.1	48.3	47.4	48.1
	Post-ex.	52.8	68.6	58.5	57.5	55.6	57.2	57.4	56.7	57.4
VM (26)	Pre-ex.	42.7	58.6	46.8	45.5	44.4	44.1	44.4	44.0	44.1
	Post-ex.	49.8	74.7	58.3	56.5	55.4	55.1	54.9	55.4	55.4
c	Pre-ex.		2.5	3.2	0.8	1.5	-4.0	-2.9	-3.5	-4.1
	Post-ex.		1.9	16.8	16.1	15.9	16.0	13.4	10.3	9.9
	Pooled		-1.9	12.7	11.3	11.3	11.9	10.1	7.4	7.1
m	Pre-ex.		1.3	1.0	1.0	1.0	1.1	1.1	1.1	1.1
	Post-ex.		1.4	0.8	0.8	0.8	0.7	0.8	0.8	0.8
	Pooled		1.4	0.9	0.9	0.9	0.8	0.8	0.9	0.9
ε	Pre-ex.		23.2	8.1	8.3	8.1	12.7	12.5	12.1	12.6
	Post-ex.		31.3	14.1	13.2	13.1	16.4	16.0	15.9	14.9
	Pooled		40.0	17.7	17.5	11.3	22.9	21.9	21.1	20.7
m.b.	Pre-ex.		19.2	-0.2	2.9	1.5	-0.4	2.9	-0.7	-0.2
	Post-ex.		30.0	5.2	2.8	0.9	-3.5	-2.8	-2.6	-2.0
	Pooled		24.8	5.3	2.8	1.2	-1.9	-1.5	-1.7	-1.1
s.d.d.	Pre-ex.		8.9	4.4	3.0	2.9	4.5	3.0	4.3	4.5
	Post-ex.		15.3	6.7	6.9	7.3	9.4	8.3	7.4	6.9
	Pooled		13.3	5.0	5.1	5.1	7.3	6.6	6.0	5.7

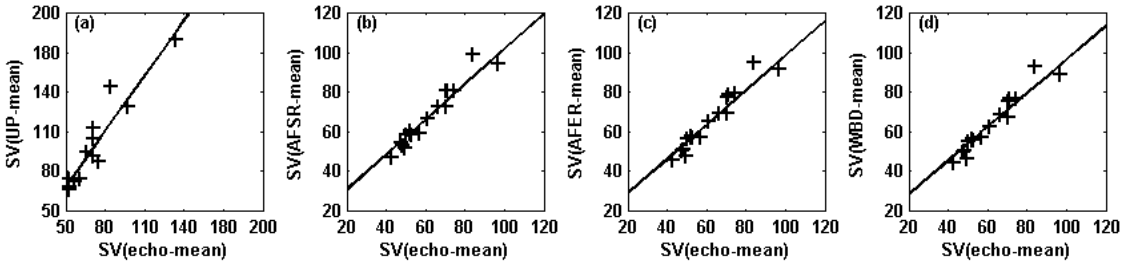

Fig. 6.13 Scatter plot and linear regression for mean of beat-to-beat SV (in mL) across subjects with normal health: **(a)** UP, **(b)** AFSR, **(c)** AFER, and **(d)** WBD.

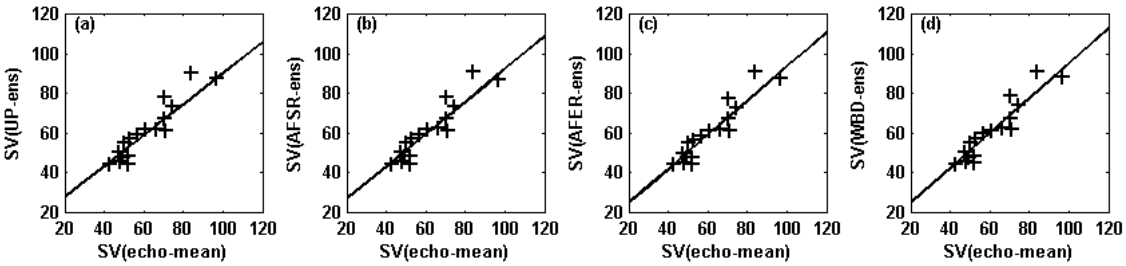

Fig. 6.14 Scatter plot and linear regression for SV (in mL) from ensemble averaged ICG across subjects with normal health: **(a)** UP, **(b)** AFSR, **(c)** AFER, and **(d)** WBD.

The mean bias and standard deviation for the differences are given for the pre-exercise and post-exercise condition as well as the estimates from the two pooled together. The standard deviation of differences for mean values of SV(UP) are 8.9, 15.3, 13.3 mL for pre-exercise, post-exercise condition, and pooled values, respectively. We see that these values for SV(WBD) have been reduced to 2.9, 7.3, 5.1 mL, respectively. The corresponding values for the other two processing techniques are almost similar. Figure 6.13 and Fig. 6.14 show scatter plots across subjects for mean of the beat-to-beat SV values from ICG and SV values from ensemble averaged ICG, for both the pre-exercise and post-exercise conditions, respectively, with the echocardiography as the reference. A quantitative examination of these plots, as well as the values of the slope and error for linear regression in Table 6.5, shows a high agreement between the mean of the beat-to-beat values and echocardiography, and results are somewhat better than that for ensemble averaging.

We see that ensemble averaging applied on the unprocessed waveform has resulted in standard deviation of differences as 4.5, 9.4, 7.3 mL, for the pre-exercise, post-exercise, and the two pooled together, respectively. Thus we see that ensemble averaging has reduced the standard deviation of the differences. However, the mean of the beat-to-beat values estimated after artifact suppression results in even smaller standard deviations. It is also seen that ensemble averaging after artifact suppression does not result in any further improvement in the estimates.

6.6 Results from subjects with cardiovascular disorders

We will first examine the results for the five individual subjects with cardiovascular disorders, and then the statistical analyses.

6.6.1 Results for individual subjects

Figure 6.15 shows a segment of the simultaneously recorded ECG, Z_o, $z(t)$, ICG, respiration, and synchronization pulse waveform recorded from subject 'AB' (age: 49 years, weight: 73 kg, hypertension and sever chest pain) in the pre-exercise resting condition. The impedance waveform is contaminated by the artifact, making it difficult to detect the B and X points. There is a very large apparent beat-to-beat variation in ICG peaks. Simultaneously acquired Doppler echocardiogram is shown in Fig. 6.16. Figure 6.17 shows a segment of the ICG signal processed by the three artifact suppression techniques. The ICG obtained after applying the artifact suppression techniques shows almost no effect of respiration, making it easy to detect the characteristic points from the waveform.

Figures 6.18 and 6.19 show the recorded ECG, Z_o, $z(t)$, ICG, respiration, and synchronizing signal and simultaneously acquired Doppler echocardiogram, respectively, from the same subject in post-exercise condition. Figure 6.20 shows processed output for the signal recording of Fig. 6.18. The ICG outputs, processed by all the three techniques, show almost no effect of the artifact, improving the detection of the B and X points. Values of ICG peaks are found to be stable.

For this subject in resting condition, correlation coefficients between the SV values were 0.34, 0.69, 0.89, 0.92 for UP, AFSR, AFER, WBD, respectively. Figure 6.21 gives a scatter plot between SV values from the ICG and the echocardiogram. Processing resulted in a reduction in the scatter and a decrease in the slope error in linear regression. Plots of observed difference versus the mean of the values are given in Fig. 6.22. The standard deviations of the differences were 9.1, 1.6, 1.0, 0.8 mL for UP, AFSR, AFER, WBD, respectively. For the post-exercise recordings for the same subject, the correlation coefficients for the values of SV were 0.64, 0.88, 0.88, 0.87 for UP, AFSR, AFER, WBD, respectively. It can be observed that the correlation increased after processing the ICG waveform. Figure 6.23 gives a scatter plot between SV values from ICG and the echocardiogram. We see that all the three artifact suppression techniques have resulted in a reduction in the scatter and a decrease in the slope error in linear regression. Figure 6.24 gives the Bland-Altman plot of the difference versus the mean values. It is seen that the mean bias was 29.0 mL for unprocessed ICG. After processing by the techniques AFSR, AFER, and WBD, it decreases to 8.5, 6.6, and 5.6 mL, respectively. The standard deviations of the differences were 11.6, 3.7, 3.6, 3.6

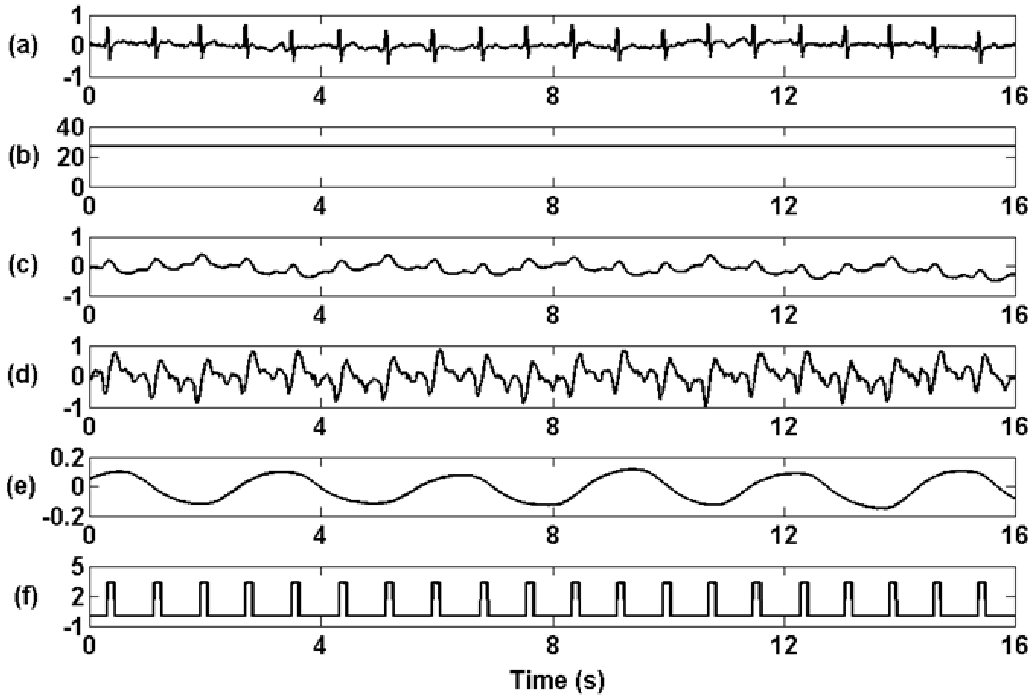

Fig. 6.15 Segment of waveforms for the subject 'AB' in post-exercise relaxation: **(a)** ECG (in arbitrary units), **(b)** Z_o (in Ω), **(c)** $z(t)$ (in Ω), **(d)** ICG (in Ω/s), **(e)** sensed airflow (in arbitrary units), and **(f)** synchronization pulse from Doppler echocardiograph (in V).

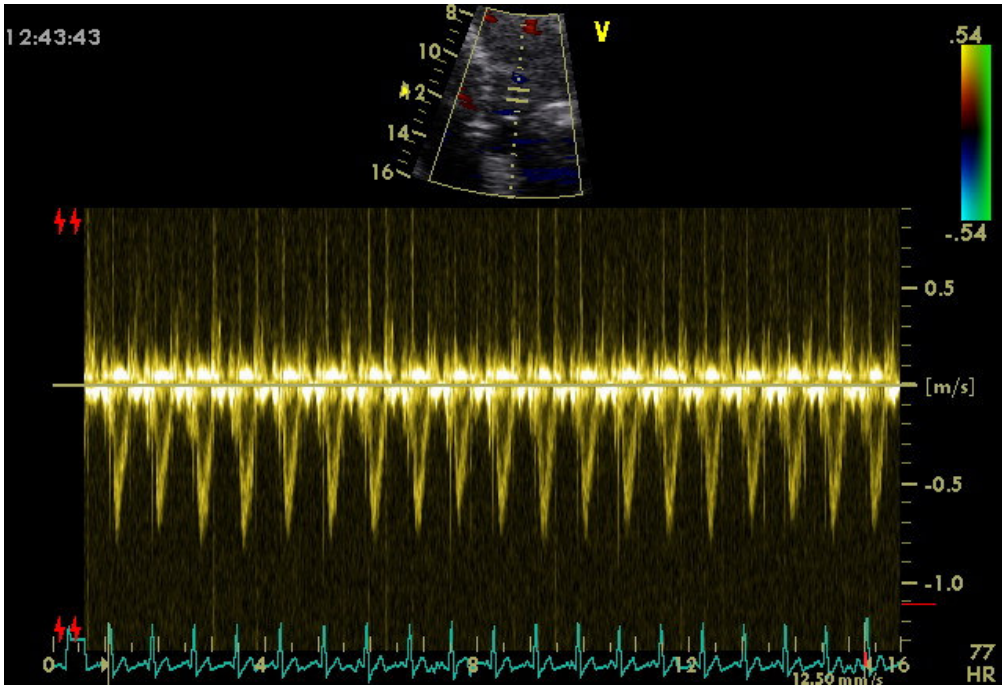

Fig. 6.16 Continuous wave Doppler echocardiogram for the subject "AB' in resting condition. X-axis- time (s). The lower trace: ECG using the same machine.

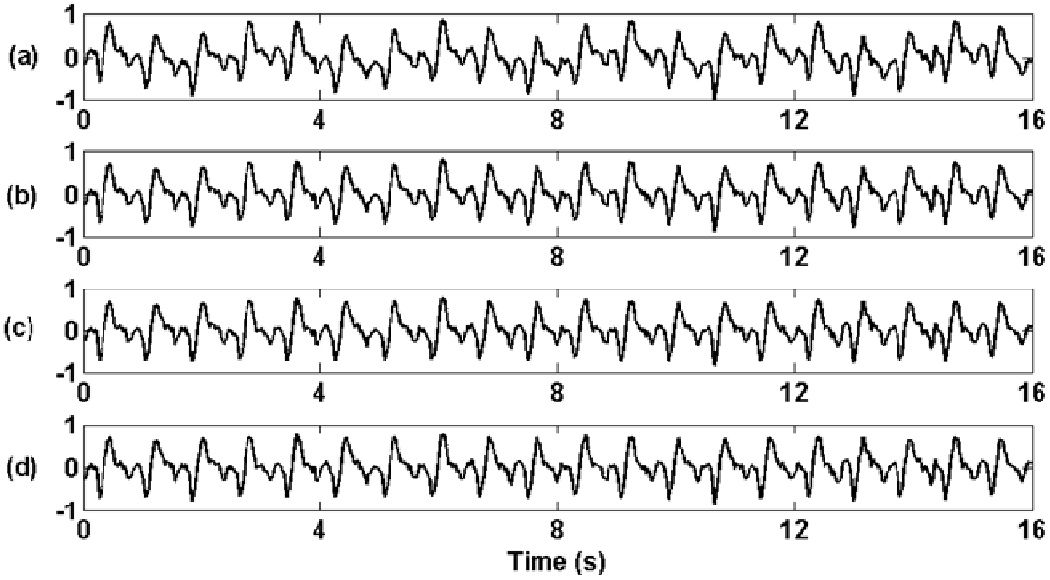

Fig. 6.17 Processing segment of output for the ICG (in Ω/s) in Fig 6.15: **(a)** Recorded ICG (in Ω/s), **(b)** ICG (in Ω/s) processed by the technique AFSR, **(c)** ICG (in Ω/s) processed by the technique AFER, and **(d)** ICG (in Ω/s) processed by the technique WBD.

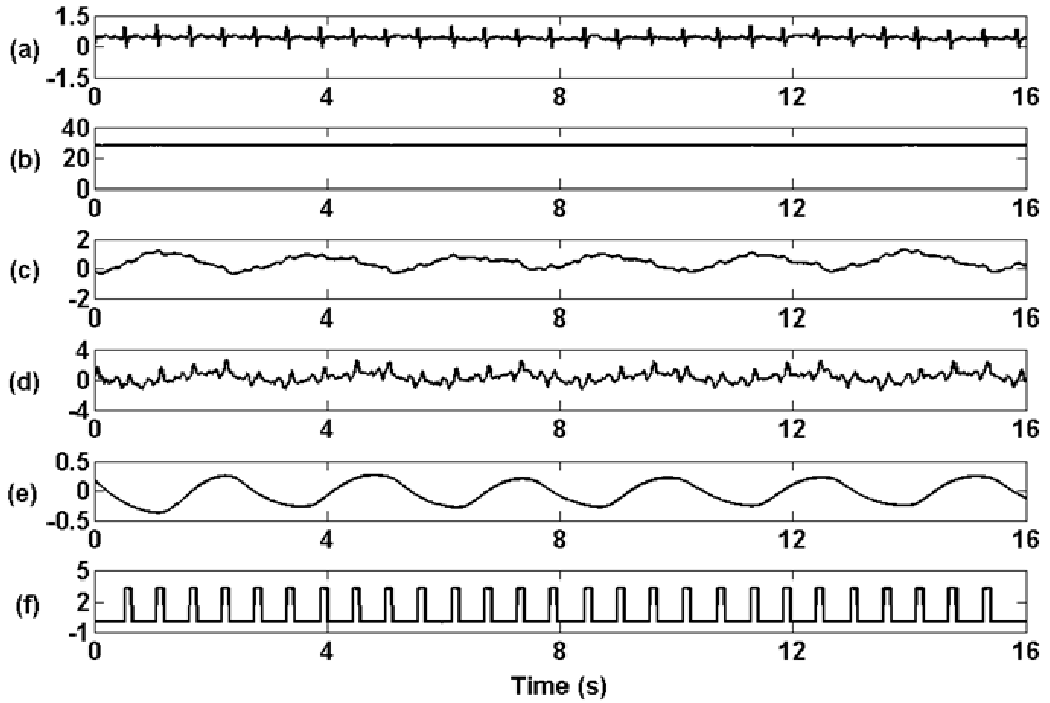

Fig. 6.18 Segment of waveforms for the subject 'AB' in post-exercise relaxation: **(a)** ECG (in arbitrary units), **(b)** Z_o (in Ω), **(c)** $z(t)$ (in Ω), **(d)** ICG (in Ω/s), **(e)** sensed airflow (in arbitrary units), and **(f)** synchronization pulse from Doppler echocardiograph (in V).

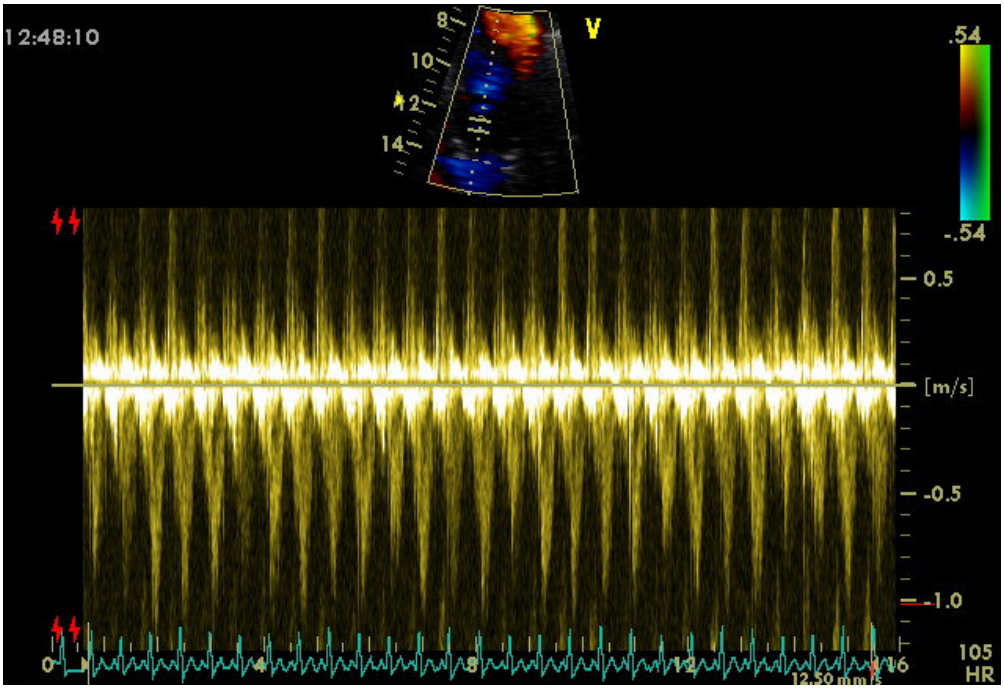

Fig. 6.19 Continuous wave Doppler echocardiogram for the subject "AB' in post-exercise relaxation. The lower trace: ECG using the same machine.

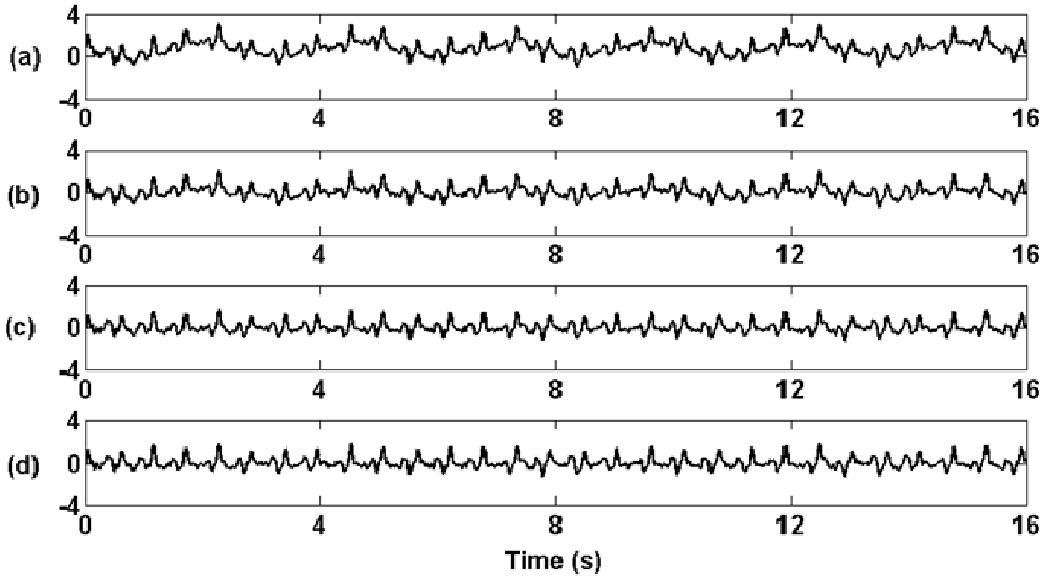

Fig. 6.20 Processing segment of output for the ICG (in Ω/s) in Fig 6.16: **(a)** Recorded ICG (in Ω/s), **(b)** ICG (in Ω/s) processed by the technique AFSR, **(c)** ICG (in Ω/s) processed by the technique AFER, and **(d)** ICG (in Ω/s) processed by the technique WBD.

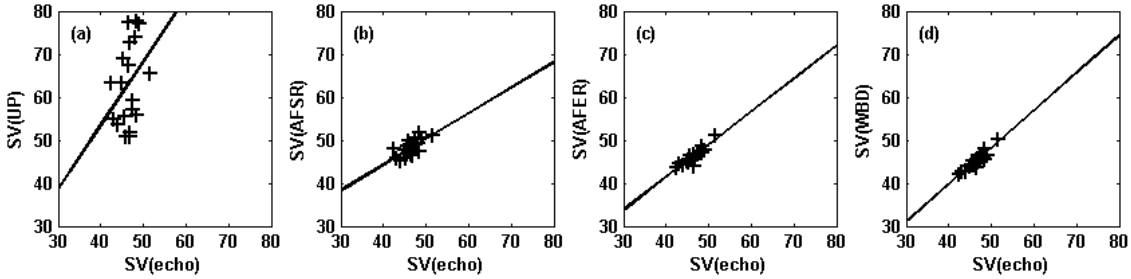

Fig. 6.21 Scatter plot and linear regression SV (in mL) estimated for subject 'AB' in resting condition: **(a)** UP, **(b)** AFSR, **(c)** AFER, and **(d)** WBD.

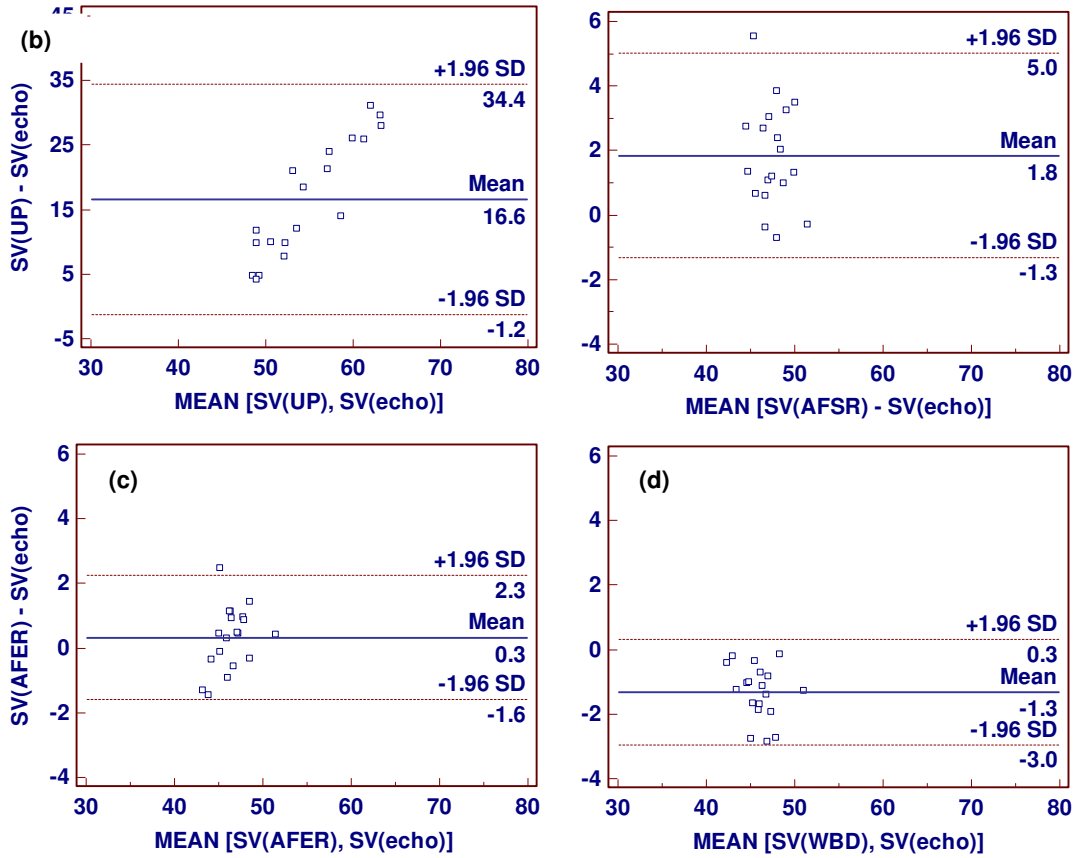

Fig. 6.22 Bland-Altman plot for SV (in mL) estimated for subject 'AB' in resting condition: **(a)** UP, **(b)** AFSR, **(c)** AFER, and **(d)** WBD.

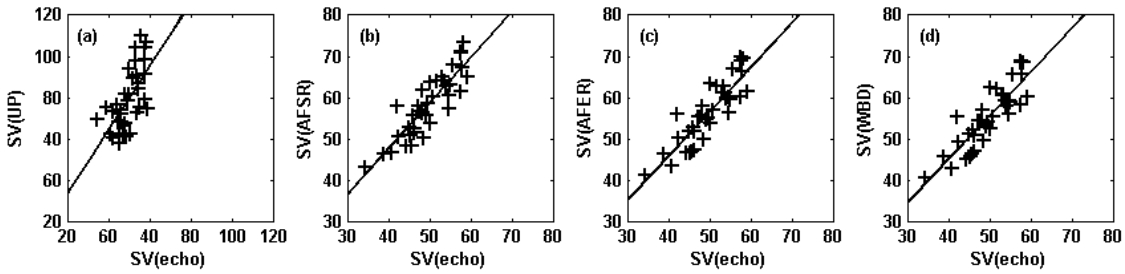

Fig. 6.23 Scatter plot and linear regression for SV (in mL) estimated for subject 'AB' in post-exercise condition: **(a)** UP, **(b)** AFSR, **(c)** AFER, and **(d)** WBD.

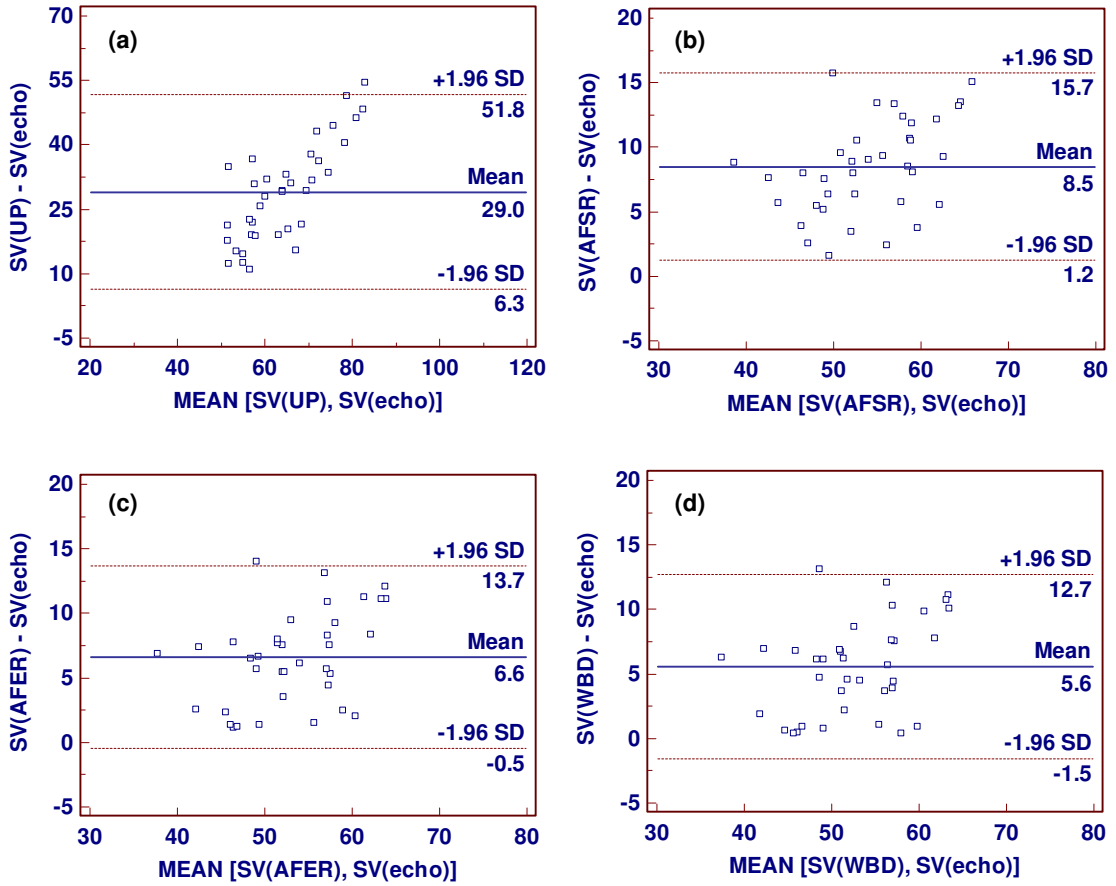

Fig. 6.24 Bland-Altman plot for SV (in mL) estimated for subject 'AB' in post-exercise condition: **(a)** UP, **(b)** AFSR, **(c)** AFER, and **(d)** WBD.

Table 6.6 Correlation coefficients, for the subjects with cardiovascular disorders, for T_{lvet} (ms) and SV values.

Subject (age)	Condition	Corr. coeff.							
		T_{lvet}				SV			
		UP	AFSR	AFER	WBD	UP	AFSR	AFER	WBD
AB (49)	Pre-ex.	0.49	0.91†	0.94†	0.99†	0.34	0.69*	0.89†	0.92†
	Post-ex.	0.51	0.98†	0.97†	1.00†	0.64	0.88†	0.88†	0.87†
DD (36)	Pre-ex.	0.46	0.99†	0.99†	1.00†	0.22	0.72*	0.88†	0.88†
	Post-ex.	0.57	0.98†	0.98†	1.00†	0.35	0.78†	0.87†	0.89†
IK (41)	Pre-ex.	0.48	0.97†	0.97†	0.99†	0.38	0.70†	0.71†	0.71†
	Post-ex.	-	-	-	-	-	-	-	-
LR (43)	Pre-ex.	0.44	0.97†	0.98†	0.99†	0.57	0.80†	0.82†	0.84†
	Post-ex.	-	-	-	-	-	-	-	-
ML (57)	Pre-ex.	0.39	0.99†	0.99†	1.00†	0.20	0.76†	0.84†	0.85†
	Post-ex.	0.54	0.98†	0.98†	1.00†	0.35	0.82†	0.86†	0.84†
Min.	Pre-ex.	0.39	0.91	0.94	0.99	0.20	0.69	0.71	0.71
	Post-ex.	0.51	0.98	0.97	1.00	0.35	0.78	0.86	0.84
Max.	Pre-ex.	0.49	0.99	0.99	1.00	0.57	0.80	0.89	0.92
	Post-ex.	0.57	0.98	0.98	1.00	0.64	0.88	0.88	0.89
Mean	Pre-ex.	0.45	0.97	0.97	0.99	0.34	0.73	0.83	0.84
	Post-ex.	0.54	0.98	0.98	1.00	0.45	0.83	0.87	0.87
s.d.	Pre-ex.	0.04	0.03	0.02	0.01	0.15	0.05	0.07	0.08
	Post-ex.	0.03	0.00	0.01	0.00	0.17	0.05	0.01	0.03

* $p < 0.01$, † $p < 0.0001$

mL for UP, AFSR, AFER, WBD, respectively.

Subject ‘IK’ had severe obesity and mild chest pain (ward referral, suspected for cardiac disease), and subjects ‘DD’, ‘LR’, and ‘ML’ were post operated cases of coronary heart disease. Subjects ‘IK’ and ‘LR’ had difficulty in performing exercise and hence they were excluded from the exercise protocol. For subject ‘IK’, the correlation coefficients for SV were relatively low (0.38, 0.70, 0.71, 0.71 for UP, AFSR, AFER, WBD, respectively) as compared with the values for other subjects. Basal impedance and change in the impedance of the subject ‘IK’ were 39.0 Ω and 0.8 Ω, respectively. High basal impedance may have masked the changes in the impedance. For other subjects, basal impedance and change in impedance varied over 17.0 – 28.5 Ω and 0.6 – 1.7 Ω, respectively.

Table 6.7 Linear regression for SV (in mL) estimation, for the subjects with cardiovascular disorders: c = intercepts, m = slope, ε = root mean square (rms) error for linear regression.

Subject (age)	Condition	Linear regression											
		UP			AFSR			AFER			WBD		
		c	m	ε	c	m	ε	c	m	ε	c	m	ε
AB (49)	Pre-ex.	-6.5	1.5	38.3	20.3	0.6	5.8	11.5	0.8	3.5	6.6	0.8	3.2
	Post-ex.	1.7	1.6	66.8	3.1	1.1	21.8	3.1	1.1	21.8	2.6	1.1	21.7
DD (36)	Pre-ex.	-6.2	1.8	146.3	-4.7	1.2	21.4	0.0	1.0	14.2	-0.2	1.0	12.4
	Post-ex.	35.4	1.1	97.5	10.9	1.0	26.7	4.0	1.0	19.6	4.2	1.0	18.5
IK (41)	Pre-ex.	15.6	1.4	76.4	6.3	1.1	23.0	6.8	1.0	23.0	5.1	1.0	22.4
	Post-ex.	-	-	-	-	-	-	-	-	-	-	-	-
LR (43)	Pre-ex.	-13.5	1.9	39.9	2.4	1.3	14.5	-6.3	1.4	14.1	-4.9	1.3	13.5
	Post-ex.	-	-	-	-	-	-	-	-	-	-	-	-
ML (57)	Pre-ex.	67.5	0.6	106.5	26.7	0.8	22.6	15.3	0.9	19.0	14.6	0.9	18.2
	Post-ex.	17.1	1.5	116.8	4.1	1.1	22.9	5.4	1.0	18.4	6.2	1.0	18.9
Min.	Pre-ex.	-13.5	0.6	38.3	-4.7	0.6	5.8	-6.3	0.8	3.5	-4.9	0.8	3.2
	Post-ex.	1.7	1.1	66.8	3.1	1.0	21.8	3.1	1.0	18.4	2.6	1.0	18.5
Max.	Pre-ex.	67.5	1.9	146.3	26.7	1.3	23.0	15.3	1.4	23.0	14.6	1.3	22.4
	Post-ex.	35.4	1.6	116.8	10.9	1.1	26.7	5.4	1.1	21.8	6.2	1.1	21.7
Mean	Pre-ex.	11.4	1.4	81.5	10.2	1.0	17.5	5.5	1.0	14.8	4.2	1.0	13.9
	Post-ex.	13.6	1.1	70.3	4.5	0.8	17.9	3.1	0.8	15.0	3.3	0.8	14.8
s.d.	Pre-ex.	33.2	0.5	46.0	13.0	0.3	7.4	8.7	0.2	7.3	7.4	0.2	7.2
	Post-ex.	16.5	0.7	51.2	4.6	0.5	12.1	2.3	0.5	10.1	2.6	0.5	10.0

Scatter plots for all the subjects with cardiovascular disorders are given in Appendix E. It is observed that processing resulted in a considerable decrease in scatter from linear regression for all the subjects in both pre-exercise and post-exercise conditions.

6.6.2 Correlation coefficients

Correlation coefficients for T_{lvet} and SV for all the subjects with cardiovascular disorders are given in Table 6.6. After processing, the correlation coefficients for T_{lvet} are found to be very high in both pre-exercise and post-exercise conditions, indicating a good agreement between the values of T_{lvet} from the echocardiogram and processed ICG on beat-to-beat basis.

Correlation coefficients for SV(UP) varied over 0.20 - 0.57 for pre-exercise and 0.35 - 0.64 for post-exercise recordings. After processing, the correlation coefficients are found to vary over 0.69 - 0.80, 0.71 - 0.89, 0.71 - 0.92 for pre-exercise and 0.78 - 0.88, 0.86 - 0.88, 0.84 - 0.89 for AFSR, AFER, WBD, respectively.

Table 6.8 Results for Bland-Altman test, for the subjects with cardiovascular disorders, for T_{lvet} (in ms)

Subject (age)	Condition	T_{lvet}(echo)		Mean bias				s.d. of difference			
		Mean	s.d.	UP	AFSR	AFER	WBD	UP	AFSR	AFER	WBD
AB	Pre-ex.	284.7	8.5	15.7	8.2	6.5	1.9	28.5	3.8	3.1	1.3
(49)	Post-ex.	266.6	18.5	81.9	9.1	7.2	1.8	41.6	3.4	3.1	1.3
DD	Pre-ex.	301.9	23.4	67.2	8.7	6.7	2.6	47.6	3.4	3.2	1.6
(36)	Post-ex.	313.6	17.2	-84.0	9.2	7.2	2.5	38.9	3.6	3.3	1.6
IK	Pre-ex.	202.1	12.7	50.7	9.1	7.5	2.4	28.9	3.2	3.1	1.5
(41)	Post-ex.	-	-	-	-	-	-	-	-	-	-
LR	Pre-ex.	239.1	12.3	47.4	8.9	7.0	2.6	24.3	3.0	2.5	1.6
(43)	Post-ex.	-	-	-	-	-	-	-	-	-	-
ML	Pre-ex.	302.1	22.8	71.0	10.2	8.2	2.8	40.9	3.6	3.6	1.5
(57)	Post-ex.	281.7	17.8	79.2	9.3	7.3	2.4	38.4	3.3	3.5	1.5
Min.	Pre-ex.	202.1	8.5	15.7	8.2	6.5	1.9	24.3	3.0	2.5	1.3
	Post-ex.	266.6	17.2	-84.0	9.1	7.2	1.8	38.4	3.3	3.1	1.3
Max.	Pre-ex.	302.1	23.4	71.0	10.2	8.2	2.8	47.6	3.8	3.6	1.6
	Post-ex.	313.6	18.5	81.9	9.3	7.3	2.5	41.6	3.6	3.5	1.6
Mean	Pre-ex.	221.7	13.3	42.0	7.5	6.0	2.1	34.0	3.4	3.1	1.5
	Post-ex.	287.3	17.8	25.7	9.2	7.2	2.2	29.7	2.6	2.5	1.1
s.d.	Pre-ex.	115.5	8.9	28.4	3.7	3.0	1.1	9.8	0.3	0.4	0.1
	Post-ex.	24.0	0.6	95.0	0.1	0.1	0.4	19.9	1.7	1.7	0.7

6.6.3 Linear regression

Results from the linear regression analysis are given in Table 6.7. We see that for SV(UP), the slope varies from 0.6 to 1.9 and the rms error about the regression line being from 38.3 to 146.3 mL. After processing, the slope varies in a small range about 1. The rms errors have also considerably reduced to 5.8 – 23.0, 3.5 – 23.0, 3.2 – 22.4 mL for pre-exercise conditions for AFSR, AFER, WBD, respectively. The corresponding values for post-exercise condition are 21.8 – 26.7, 18.4 – 21.8, 18.5 – 21.7 mL.

Table 6.9 Results for Bland-Altman test, for the subjects with cardiovascular disorders, for SV (in mL).

Sub-Ject (age)	Condi-tion	SV(echo)		Mean bias				s.d. of difference			
		Mean	s.d.	UP	AFSR	AFER	WBD	UP	AFSR	AFER	WBD
AB	Pre-ex.	46.6	2.1	16.6	1.8	0.3	-1.3	9.1	1.6	1.0	0.8
(49)	Post-ex.	49.8	6.0	29.0	8.5	6.6	5.6	11.6	3.7	3.6	3.6
DD	Pre-ex.	63.0	3.1	42.2	6.4	2.0	-0.4	23.9	3.5	2.3	2.0
(36)	Post-ex.	69.6	5.4	41.3	8.8	4.6	2.8	15.4	4.3	3.1	2.9
IK	Pre-ex.	37.5	3.6	31.3	10.5	7.8	6.2	12.2	3.7	3.6	3.5
(41)	Post-ex.	-	-	-	-	-	-	-	-	-	-
LR	Pre-ex.	46.7	2.7	27.1	12.5	10.9	9.7	7.5	2.8	2.7	2.6
(43)	Post-ex.	-	-	-	-	-	-	-	-	-	-
ML	Pre-ex.	63.5	5.8	44.6	11.6	7.2	5.3	18.1	4.1	3.3	3.2
(57)	Post-ex.	59.6	4.6	44.3	9.5	5.8	4.0	19.9	3.5	2.8	2.9
Min.	Pre-ex.	37.5	2.1	16.6	1.8	0.3	-1.3	7.5	1.6	1.0	0.8
	Post-ex.	49.8	4.6	29.0	8.5	4.6	2.8	11.6	3.5	2.8	2.9
Max.	Pre-ex.	63.5	5.8	44.6	12.5	10.9	9.7	23.9	4.1	3.6	3.5
	Post-ex.	69.6	6.0	44.3	9.5	6.6	5.6	19.9	4.3	3.6	3.6
Mean	Pre-ex.	51.5	3.5	32.4	8.6	5.6	3.9	14.2	3.1	2.6	2.4
	Post-ex.	44.8	4.0	28.7	6.7	4.3	3.1	11.7	2.9	2.4	2.4
s.d.	Pre-ex.	11.4	1.4	11.4	4.4	4.4	4.6	6.8	1.0	1.0	1.1
	Post-ex.	30.9	2.7	20.2	4.5	3.0	2.4	8.5	1.9	1.6	1.6

6.6.4 Bland-Altman test

Table 6.8 gives results for Bland-Altman test for T_{lvet}. As seen in the table, all the artifact suppression techniques resulted in a large reduction in mean bias and standard deviations of the differences, for both the pre-exercise and post-exercise recordings. Table 6.9 gives results for Bland-Altman test for SV values. The values of SV(echo) for the five subjects with cardiovascular disorders ranged from 37.5 to 63.5 mL for pre-exercise condition and increased to 49.8 to 69.6 mL for post-exercise condition. Taking echocardiography estimates as the reference, the range for standard deviation of the differences across the subjects are 7.5 – 23.9, 1.6 – 4.1, 1.0 – 3.6, 0.8 – 3.5 mL for the pre-exercise condition and 11.6 – 19.9, 3.5 – 4.3, 2.8 – 3.6, 2.9 – 3.6 mL for post-exercise condition for UP, AFSR, AFER, WBD, respectively. We see a good agreement between the values obtained from the reference technique and processed ICG in the pre-exercise condition as well as in the post-exercise condition.

Table 6.10 SV (in mL) estimated from echocardiography and ICG, with and without ensemble averaging, for the subjects with cardiovascular disorders (m.b.: mean bias, s.d.d.: standard deviation of the differences, across the subjects).

Sub-ject (age)	Condi-tion	SV(echo)	SV(ICG–mean)				SV(ICG–ensemble avg.)			
		Mean	UP	AFSR	AFER	WBD	UP	AFSR	AFER	WBD
AB	Pre-ex.	46.6	63.2	48.4	46.2	45.3	41.2	41.1	40.3	40.3
(49)	Post-ex.	49.8	78.8	58.3	56.4	55.4	67.3	64.9	67	67.3
DD	Pre-ex.	63.0	105.2	69.4	65.0	63.4	53.4	58.3	56.6	57.6
(36)	Post-ex.	69.6	110.8	78.3	74.1	72.4	75.3	74.9	74.7	74.9
IK	Pre-ex.	37.5	78.8	28.0	25.3	23.7	35.7	30.9	30.6	30.6
(41)	Post-ex.	-	-	-	-	-	-	-	-	-
LR	Pre-ex.	46.7	73.9	59.2	57.6	56.4	49.9	53.8	52.1	53.6
(43)	Post-ex.	-	-	-	-	-	-	-	-	-
ML	Pre-ex.	63.5	108.1	75.1	70.7	68.8	69.3	66.6	68.6	60.6
(57)	Post-ex.	59.6	103.9	69.1	65.4	63.6	69.2	66.7	68.8	69.6
c	Pre-ex.		10.8	-23.1	-21.4	-15.6	-1.1	-8.1	-10.7	2.6
	Post-ex.		1.4	8.1	11.7	12.5	46.5	38.6	46.9	47.7
	Pooled		8.9	-16.3	-14.6	-15.0	-1.5	-6.0	-7.5	-3.5
m	Pre-ex.		1.5	1.5	1.4	1.3	1.0	1.1	1.2	1.0
	Post-ex.		1.6	1.0	0.9	0.9	0.4	0.5	0.4	0.4
	Pooled		1.5	1.4	1.3	1.3	1.1	1.2	1.2	1.1
ε	Pre-ex.		21.8	13.1	14.5	12.7	12.4	11.7	12.2	11.3
	Post-ex.		7.5	0.7	0.0	0.0	1.7	2.6	1.6	1.2
	Pooled		23.1	14.6	16.1	16.5	22.7	19.7	22.3	23.6
m.b.	Pre-ex.		34.4	4.6	0.5	0.3	-1.6	-1.3	-1.8	-2.9
	Post-ex.		38.2	8.0	5.0	4.0	11.0	9.2	10.5	11.0
	Pooled		35.8	6.2	3.1	1.6	3.1	2.6	2.8	2.3
s.d.d.	Pre-ex.		12.1	9.0	8.8	7.3	6.2	6.0	6.4	5.7
	Post-ex.		22.3	0.4	1.0	1.4	6.0	5.2	6.1	6.1
	Pooled		10.3	7.1	7.0	7.1	8.6	7.6	8.6	8.8

6.6.5 Estimation by ensemble averaging

Table 6.10 gives SV estimated from echocardiography and ICG, with and without ensemble averaging. The mean bias and standard deviation for the differences are given for pre-exercise and post-exercise condition as well as the estimates from the two pooled together. The standard deviation of differences, across the subjects, for mean values of SV(UP) are 12.1, 22.3, 10.3 mL for pre-exercise, post-exercise condition, and pooled values. We see that these values for SV(AFSR) have been reduced to 9.0, 0.4, 7.1 mL, respectively. The corresponding values for the other two processing techniques are almost similar. Standard deviations of differences are higher in case of ensemble averaging. Figure 6.25 and Fig. 6.26 show scatter

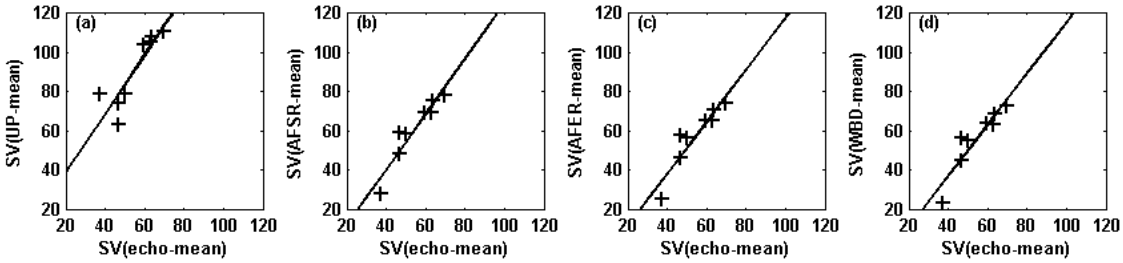

Fig. 6.25 Scatter plot and linear regression for mean of beat-to-beat SV (in mL) across subjects with cardiovascular disease: **(a)** UP, **(b)** AFSR, **(c)** AFER, and **(d)** WBD.

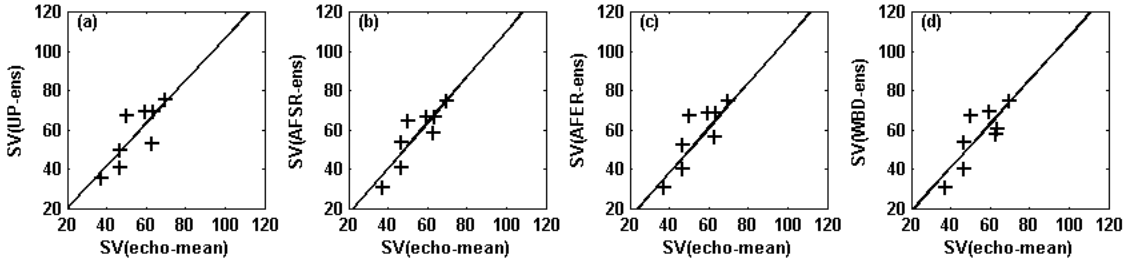

Fig. 6.26 Scatter plot and linear regression for SV (in mL) from ensemble averaged ICG across subjects with cardiovascular disease: **(a)** UP, **(b)** AFSR, **(c)** AFER, and **(d)** WBD.

plots across subjects for mean of the beat-to-beat SV values from ICG and SV values from ensemble averaged ICG with the echocardiography as the reference. The values of the slope and error for linear regression show a high agreement between the mean of the beat-to-beat values and echocardiography, and better than that for ensemble averaging.

6.7 Discussion

The investigations were carried out for examining the effectiveness of the artifact suppression techniques in improving the agreement between the values obtained using impedance cardiography and Doppler echocardiography under a clinical setting, for subjects with normal health and subjects with cardiovascular disorders. A total of nine subjects with normal health and five subjects with cardiovascular disorders participated in this investigation. Doppler echocardiograms were recorded simultaneously with the impedance related waveforms in the pre-exercise and post-exercise conditions.

The artifact suppression techniques AFSR, AFER, and WBD attenuated the artifacts and restored the baseline, facilitating a consistent detection of the characteristic points in the ICG waveform. The values of T_{lvet}, $(-dz/dt)_{max}$, and SV were estimated from each cycle of ICG waveform. The parameter $(-dz/dt)_{max}$, measured as the peak from the zero crossover point, was approximately 0.72 times peak-to-peak height of $-dz/dt$. The characteristic points in the unprocessed waveforms and those processed by AFSR had to be manually located, while

automated detection could be done in case of the waveforms processed by AFER and WBD. The values of $(-dz/dt)_{max}$ and T_{lvet} were used for calculation of SV. The values T_{lvet} and SV from Doppler echocardiogram were measured graphically by zooming each cycle and identifying the envelope of the blood flow waveform with the help of a track-ball. The agreement between the values from echocardiography and the values obtained from the ICG were examined by correlation, linear regression, and Bland-Altman test.

It was observed that the beat-to-beat variations of the T_{lvet} and SV, from nine subjects with normal health and five subjects with cardiovascular disorders, estimated from the processed ICG are highly correlated with those estimated from Doppler echocardiography, for all the subjects, except for a subject with severe obesity and relatively higher basal impedance. Linear regression analyses showed that the artifact suppression techniques resulted in reduced rms errors from the best bit straight line and in smaller slope errors, for both pre-exercise and post-exercise recordings. All the artifact suppression techniques resulted in a large reduction in mean bias and standard deviations of the differences, indicating an increased agreement between the values estimated from the ICG and Doppler echocardiogram. It is also seen that the processing has reduced the standard deviations of differences to values generally comparable to the standard deviation of stroke volume estimated on beat-to-beat basis by echocardiography under pre-exercise condition and to generally much smaller values in the post-exercise condition, for both groups of subjects.

Apart from looking at agreement between the SV values estimated on beat-to-beat basis, the statistical analyses were carried out, across the subjects, on the means of beat-to-beat values as well as the values estimated from the ensemble averaged waveform. Ensemble averaging reduced the standard deviation of the differences but the mean of the beat-to-beat values estimated after artifact suppression resulted in even smaller standard deviations. Ensemble averaging after artifact suppression did not result in any further significant reduction in the standard deviations. Hence we can say that the values estimated using impedance cardiography after artifact suppression have good agreement with those estimated from Doppler echocardiography, for mean values as well as for beat-to-beat variations. Among the three techniques, AFER and WBD are definitely superior to AFSR as they permit automated estimation of T_{lvet} and SV. The results obtained by AFER and WBD are almost similar, but WBD may be considered as the preferable technique because it does not require a reference signal.

By visual examination of the waveforms, as described in Section 5.4, it has been qualitatively verified that the technique WBD is effective in removing the respiratory as well as the motion artifacts. However, as our reference technique Doppler echocardiogram could

not be used with the subjects in motion, an evaluation of the WBD for suppression of the motion artifact in the clinical study could not be carried out.

Chapter 7

SUMMARY AND CONCLUSIONS

7.1 Introduction

Impedance cardiography is a noninvasive technique for monitoring stroke volume and other cardiac indices. This technique is based on sensing the changes in the electrical impedance of the thorax $z(t)$, caused by variation in blood volume during the cardiac cycle. Negative of the time derivative of the thoracic impedance is known as the impedance cardiogram (ICG). The parameters required for estimating the stroke volume, using Kubicek, Bernstein, or Sramek formulas are left ventricular ejection time (T_{lvet}) and the ICG peak ($(-dz/dt)_{max}$). Left ventricular ejection time (T_{lvet}) is defined as the time difference between point B (opening of the aortic valve) and point X (closure of the aortic valve) in ICG waveform. Sensing of the variation in thoracic impedance due to blood flow is influenced by respiratory and motion artifacts. Spectra of the respiratory and motion artifacts partly overlap with that of the ICG waveform. These artifacts have much larger amplitudes and cause a large drift in the baseline of the signal. Presence of these artifacts in the signal restricts proper use of the input dynamic range of analog-to-digital (A/D) converter and severely affects the estimation of the various cardiovascular indices, particularly during stress test.

Ensemble averaging is generally employed for suppressing the artifacts, but it also suppresses beat-to-beat variations and it tends to smear the peak in the ICG and blur or suppress the less distinctive characteristic points in the waveform and may result in error in their detection. Due to a partial overlap between the spectra of ICG and respiratory artifacts, non-adaptive digital filters are not effective in removing the artifacts. Adaptive filtering may be used for canceling the artifacts but sensing the reference signal, related to the artifacts, and combining them is a serious problem.

The research objective was to investigate techniques for removal of the artifacts from ICG, for estimation of stroke volume and other cardiovascular indices on beat-to-beat basis. In order to make effective use of the input dynamic range of the signal acquisition setup, a baseline restoration circuit was implemented, as part of an impedance cardiography

instrument, to partly remove the drift before A/D conversion. Signal processing techniques, based on adaptive filtering and wavelet based denoising, were investigated for suppression of the artifacts in the acquired signals. The signal processing techniques were validated on the signals recorded from several subjects with normal health and subjects with cardiovascular disorders, under a clinical setting. Implementation details and analysis results related to these investigations have been presented in the previous chapters.

The summary of investigations, conclusion drawn on the basis of the results, and some suggestions for further studies are given in the following sections.

7.2 Summary of the investigations

Investigations carried out can be summarized as the following.

1) Baseline restoration circuit: A baseline restoration circuit was developed as part of an impedance cardiography instrument for effective use of the input dynamic range of the signal acquisition setup (as described in Chapter 3). It is based on the amplitude tracking technique for fast estimation and partial removal of the baseline drift. In this technique, tracking of the baseline is initiated by the output going out of the defined range. An estimate of the baseline drift is subtracted from the signal and the baseline is restored in one clock cycle.

2) Adaptive filtering for suppression of respiratory artifact: Two techniques were developed and investigated for removing the respiratory artifact from the sensed signal (as presented in Chapter 4). In the adaptive filtering with sensed respiration (AFSR) technique, the output from a thermistor based airflow sensor was taken as the reference input for respiration. The contaminated ICG was taken as the primary input and the difference between the primary input and filtered reference was taken as the processed output. The sensed reference signal had a delay with respect to the artifact and this was partly compensated by introducing a delay in the path of the primary signal. For quantifying the noise suppression, the technique was applied on the thoracic impedance signal with simulated respiratory artifact with different values of signal-to-artifact ratio (SAR), generated using recordings from 23 volunteers with normal health. A detailed analysis showed that the effectiveness of the technique in suppressing the higher frequency components of the respiratory artifacts was limited because the sensed respiration waveform was deficient in higher frequency components. In the adaptive filtering based on estimated respiration (AFER), the respiratory reference estimated by cubic spline fitting on the ICG signal provided a better approximation of the artifact. This technique was very effective in suppressing higher frequency components of the respiratory artifact. Both the techniques were applied on several signal recordings, severely contaminated from respiratory artifacts with minimum motion artifacts, obtained

from 52 volunteers in the resting and post-exercise relaxation and the results were qualitatively examined.

3) Wavelet based denoising (*WBD*) *technique for suppression of artifacts*: In this technique (as described in Chapter 5), discrete wavelet transform (DWT) was applied on the signal for a number of scales of decomposition, and each scale was reconstructed to visualize the signal and the artifact component at each scale. From examination of decomposition with several wavelets, it was observed that a dyadic wavelet decomposition using an FIR based Meyer wavelet captured signal in first few scales and artifacts in next scales, permitting the use of scale-dependent thresholding for denoising. A limited number of scales were used to obtain a denoised signal. This technique does not involve a reference signal, and can be used for suppression of both the respiratory and motion artifacts. The technique was applied for processing the thoracic impedance signals with simulated artifact generated from the recordings taken from the 23 volunteers. A qualitative examination was carried out by applying the technique on several signal recordings, contaminated by respiratory artifact, obtained from 52 volunteers in the pre-exercise and post-exercise relaxation. The effectiveness of the WBD technique in removing the motion artifact was also examined by applying it on the signals corrupted by motion artifacts but free from the respiratory artifacts and signals with both types of artifacts.

4) Validation under a clinical setting: Application of the artifact suppression techniques on signals with simulated artifacts and signals acquired from volunteers enhanced the signal by suppressing the artifacts, facilitating a beat-to-beat estimation of the stroke volume and other cardiovascular indices. A clinical validation of the techniques, as presented in Chapter 6, was carried out using Doppler echocardiography, an established noninvasive technique for stroke volume estimation, as a reference. The values of left ventricular ejection time (T_{lvet}) and stroke volume (SV) from the unprocessed and processed ICG were estimated on beat-to-beat basis, and compared with those obtained from simultaneously acquired Doppler echocardiogram, under a clinical setting. Signal recordings were carried out from nine subjects with normal health and five subjects with cardiovascular disorders, in the pre-exercise and post-exercise conditions. Correlation, linear regression, and Bland-Altman test were used to examine the agreement between values estimated from the ICG waveform and those obtained from Doppler echocardiography. These statistical tests were applied on the signal recordings from each subject in the pre-exercise and post-exercise conditions. In addition to examining the agreement of the results on the beat-to-beat basis, the agreement of the average values was also examined. As the Doppler echocardiography could be used only for subjects resting in the supine position, the evaluation was restricted for respiratory artifact and could not be carried out for motion artifact.

7.3 Conclusions

The tracking based baseline restoration circuit, developed for fast restoration of baseline, was extensively tested on several biosignals and it was found that the drift removal remained effective for different types of the baseline drifts. The circuit has been used in our impedance cardiograph instrument and used for recording of the signals from subjects under pre-exercise and post-exercise conditions. This circuit can also be used for acquisition of other bio signals with large drift or abrupt baseline shift.

Signal processing techniques, based on adaptive filtering and wavelet based denoising, were applied on the signals with simulated artifacts generated from the recordings taken from 23 volunteers. Processing the signals by the technique AFSR, AFER, and WBD resulted in a SAR advantage of 18.5, 19.6, and 21.8 dB, respectively. Detailed analysis of the amplitude spectrum of the primary input, the sensed respiratory reference, the estimated reference signal, and the processed output signals showed that the improved effectiveness of AFER was because of better suppression of higher frequency components of the artifact, and it improved detection of the point B, C, and X in the ICG waveform. Compared to the technique AFSR, the technique AFER required a lower order filter tap length. The technique WBD offered SAR improvement about 3 dB more than the technique AFSR. Applying the three artifact suppression techniques on artifact-free signals showed that none of the techniques introduced any significant errors.

For examining the effectiveness of these techniques on actual signals, they were applied on the signals acquired from 52 healthy volunteers. These signals were recorded with the subject resting in a supine position in order to have negligible motion artifact. All the three techniques effectively suppressed the respiratory artifacts from the recorded signals and showed almost no effect of respiration, hence improving the detection of the B and X points. A visual examination of the processed output for the recordings from the signals acquired from all the subjects showed that the artifact suppression remained effective even with a large heart rate variability in the post-exercise recordings, and the processing did not appear to affect the beat-to-beat variability in the characteristic points and the ICG peaks. Processing the signals, contaminated by motion artifacts with negligible respiratory artifact as well those contaminated by a combination of both types of the artifacts, by the technique WBD was effective in reducing motion artifact and resulted in a stable baseline.

Validation of the techniques under a clinical setting was carried out by applying them on signals acquired from nine subjects with normal health and five subjects with different cardiovascular disorders and examining the agreement with values estimated from Doppler echocardiography. It may be noted that as the Doppler echocardiography can be used only on subjects resting in supine position, the evaluation in the clinical setting could be carried out only for the suppression of the respiratory artifacts, and not for the motion artifact.

Correlation coefficients, for subjects with normal health, between the stroke volumes estimated from the unprocessed ICG and the Doppler echocardiogram varied from 0.15 to 0.67 for the pre-exercise recordings and 0.35 to 0.80 for the post-exercise recordings. After processing, the correlation coefficients were found to vary over 0.72 - 0.93, 0.78 - 0.95, 0.76 - 0.95 for the pre-exercise and 0.80 - 0.97, 0.84 - 0.97, 0.87 - 0.98 for the post-exercise recordings, for AFSR, AFER, WBD, respectively. The slope of the regression line was not significantly different from unity and the rms error from the best fit straight line was significantly reduced. Results from Bland-Altman test showed that all the artifact suppression techniques resulted in a large reduction in mean bias and standard deviations of the differences. The correlation coefficients, for subjects with cardiac disorders, are found to vary over 0.20 - 0.57, 0.69 - 0.80, 0.71 - 0.89, 0.71 - 0.92 for the pre-exercise and 0.35 – 0.64, 0.78 - 0.88, 0.86 - 0.88, 0.84 - 0.89 for the post-exercise recordings, for UP, AFSR, AFER, WBD, respectively. Processed outputs showed a reduction in the scatter and a decrease in the slope error in linear regression. After processing, the slope of the linear regression was found to be close to one. Processing the signals with all the artifact suppression techniques reduced the mean bias and the standard deviation of differences with Doppler echocardiogram as the reference. These results show a good agreement between the stroke volume estimated from Doppler echocardiography and impedance cardiography after artifact suppression. Among the three techniques, AFER and WBD permitted automated estimation of T_{lvet} and SV. The technique WBD may be considered as the preferable technique because it does not require a reference signal.

Analysis of the means of beat-to-beat values and the values estimated from the ensemble averaged waveform showed that ensemble averaging reduced the standard deviation of the differences but the mean of the beat-to-beat values estimated after artifact suppression resulted in even smaller standard deviations. Ensemble averaging after the artifact suppression did not result in any further improvement in the estimates. Hence we may conclude that the artifact suppression techniques were more effective than ensemble averaging in suppression of the respiratory artifacts, and they can be used for monitoring beat-to-beat variations in various cardiovascular parameters.

Doppler echocardiography is noninvasive and can be used for estimation of the stroke volume and some other cardiovascular indices on beat-to-beat basis. The technique needs a radiologist or a skilled operator, there are difficulties in getting Doppler images in ambulatory conditions, and it can not be used for monitoring the indices over extended periods. Impedance cardiography with the artifact suppression techniques may be useful for continuous monitoring of beat-to-beat variations in the stroke volume and some other cardiovascular parameters.

In summary, the initial contribution in the thesis is a tracking based baseline restoration circuit, developed as a part of impedance cardiogram instrument, for fast restoration of baseline and removal of the different types of the baseline drift. Major contribution of the thesis is investigation of artifact suppression techniques, based on adaptive filtering and wavelet based denoising without introducing distortion in the signal. These techniques facilitated estimation of stroke volume and other cardiovascular indices on beat-to-beat basis. The values estimated using impedance cardiography after suppression of the respiratory artifact had a very good agreement with those estimated from Doppler echocardiography, for the mean values as well as for the beat-to-beat variations. Hence, it may be concluded that the artifact suppression techniques can be used with impedance cardiography instrument for continuous monitoring of the stroke volume and other cardiovascular parameters for the mean values as well as for the beat-to-beat variations.

7.4 Suggestions for future work

Further validation of the techniques on recordings from a larger number of patients with different age groups and different types of cardiovascular disorders needs to be carried out. Other processing techniques, *e.g.* Kalman filtering (Mneimneh *et al*. 2006; Sayadi and Shamsollahi, 2008), need to be investigated for further enhancement of the signal. As discussed in the thesis, the Kubicek's formula and its variants are based on the assumption that the aortic blood flow is a square wave pulse lasting until the end of the systole. Actual aortic blood flow profile significantly differs from a square pulse and varies across individuals. Artifact-free ICG signals will be helpful in the research for developing modified model for precise and accurate estimation of the stroke volume and other indices for cardiovascular diagnosis. Further, the morphology of artifact-free ICG signal waveshape may help in the diagnosis of cardiovascular disorders. Use of wearable instruments can be used for extended ambulatory recordings and for studying the beat-to-beat variations in stroke volume and other cardiovascular indices, particularly the respiratory modulation of these parameters.

Appendix A

COMMERCIALLY AVAILABLE IMPEDANCE CARDIOGRAPHS

Some of the commercially available instruments for impedance cardiography are

1) HIC-2000/ 3000 (Bio-Impedance Technology, Chapel Hill, NC, USA) [http://www.microtronics-nc.com/BIT/HICProductInfo.html]
2) HIC-4000 (Microtronics Corp. of Chapel Hill, NC, USA) [http://www.microtronics-nc.com/BIT/PDF%20files/HIC4000prodsheet.pdf]
3) NCCOM3 (BoMed Medical Manufacturing Ltd., Irvine, CA, USA)
4) BioZ (CardioDynamics, San Diego, CA, USA) [http://www.cdic.com/cdprod10.html]
5) Niccomo (Medizinische Messtechnik GmbH, Germany) [http://www.niccomo.com/en/index.html]
6) CircMon (J R Medical, Estonia) [http://www.online.ee/~medical/]
7) TEBCO (Hemo Sapinens Inc., Sedona, AZ, USA) [http://www.hemosapiens.com/tebco.html]
8) THRIM (UFI, Morro Bay, CA, USA) [http://www.ufiservingscience.com/DSThrim1.html]
9) LifeGard (Peabody, MA, USA) [http://analogic.com/lifegard/special/sub_pages/life_icg_hemo_stat.html]
10) Philips Impedance Cardiograph (Philips Medical Systems, Andover, MA, USA) [http://www.medical.philips.com/main/products/patient_monitoring/products/icg/]

For some of the research applications, we need to simultaneously acquire impedance cardiogram and signals from some other instruments. This can be easily carried out by applying the analog outputs from the impedance cardiograph and other instruments as inputs to a multi-channel signal acquisition set-up. Hence, for such applications we need impedance cardiograph with analog outputs. The key features of the above instruments are briefly described here including the availability of analog outputs.

The HIC-2000/HIC-3000 (Hutcheson Impedance Cardiograph) provides basal impedance (Z_o), ICG (dz/dt), Δz, ECG, and phonocardiogram (PCG) as analog outputs. It uses excitation frequency of 100 kHz and can be used for thoracic impedance in the range of 5-80 Ω. HIC-4000 is an impedance cardiograph instrument which acquires and displays basal impedance (Z_o), ICG (dz/dt), Δz, ECG, PCG, and respiration (with the help of a separate respiration transducer). It uses excitation frequency of 95 kHz and can be used for thoracic impedance in the range of 5-100 Ω. This instrument can also be used for monitoring of pulmonary congestion, pulmonary edema, pleural effusion, and numerous indices related to cardiac dynamics. This instrument provides analog output for Z_o, ICG (dz/dt), Δz, ECG, PCG, and respiration. HIC series instruments use external medical-grade power supply. COP-WIN software (optional for HIC series instruments) may be used for acquisition and ensemble averaging of the ICG waveform.

BioZ uses proprietary DISQ (digital impedance signal quantifier) technology and Z-MARC algorithm for processing and calculation of cardiac output, systemic vascular resistance, contractility, thoracic fluid status. It uses excitation frequency of 60 kHz and current amplitude of 4.0 mA.

Niccomo monitors cardiac output and systemic vascular resistance. This instrument combined with blood pressure measurement enables the therapy optimization of patients with hypertension. Niccomo pacemaker software, provided with the instrument, enables homodynamic monitoring during cardiac pacing. Also, this instrument offers a diagnostic screen to evaluate ICG curve shape characteristics which could be used for identifying some of the cardiac diseases.

CircMon can be used for continuous monitoring of cardiac output, systemic vascular resistance, and extracellular water.

TEBCO (Thoracic Electrical Bioimpedance Cardiac Output) measures cardiac index (CI) and nine other cardiodynamic parameters (stroke index, heart rate, respiratory rate, ventricular ejection time, pre-ejection period, ejection phase contractility index, inotropic state index, estimate of ejection fraction, and end-diastolic index). TEBCO can be interfaced to a PC either via serial RS232 or via USB.

THRIM (Tetra-polar High Resolution Impedance Meter) provides complex impedance (R_o and X_c) as well as pulsatile (ΔR and dR/dt) signal outputs. This instrument can be configured for up-to four channels of impedance measurement. This instrument provides four analog outputs R_o, X_c, ΔR, and dR/dt.

LifeGard is an impedance cardiograph instrument with an option of signal quality indicator. Integrated printer is provided with this instrument for instant documentation.

Philips Impedance Cardiograph can display ICG parameters along with other physiological measurements, including heart rate, blood pressure, pulse oximetry, cardiac output, and system vascular resistance.

Appendix B

IMPEDANCE CARDIOGRAPH DEVELOPED AT IIT BOMBAY

B.1 Introduction

In this appendix, an impedance cardiogram and respiration sensing instrument "ICRS06" developed in our lab (Pandey and Pandey, 2007; Venkatachalam, 2006; Naidu, 2005; Pandey *et al.*, 2005; Manigandan, 2004; Pandey *et al.*, 2004; Kuriakose, 2000; Patwardhan, 1997; Joshi and Pandey, 1994; Joshi, 1993) is described. The instrument is basically based on the circuit reported earlier by Qu *et al.* (1986), with the baseline restoration circuit as reported in Chapter 3. A prototype instrument has been developed and extensively tested. It has been used for the recordings for the research reported in this thesis.

B.2 Impedance cardiograph instrument developed at IIT Bombay

Basic blocks of the prototype of the ICG hardware are: excitation circuit, demodulator, and baseline restoration circuit, as shown in Fig. B.1. The excitation circuit generates a sinusoidal voltage of frequency 100 kHz and amplitude < 5 mA. For generating a stable high frequency sinusoidal wave, modified Wein bridge oscillator has been used. The oscillator output is given as input to the voltage-to-current converter. The current is injected into the thorax using a ferrite core transformer and a pair of electrodes I1 and I2. The amplitude modulated voltage developed is picked up by another pair of electrodes E1 and E2.

The front end of the sensing circuit is an instrumentation amplifier followed by a high pass filter with cutoff frequency of 16 kHz. This high pass filter suppresses ECG signal and power line interference. The output of the instrumentation amplifier is an amplitude modulated wave with modulation proportional to varying thoracic impedance. A full-wave precision rectifier followed by a low pass filter is used for demodulation. The resulting output is sum of the basal impedance Z_o, time varying component of the impedance $z(t)$, and respiratory and other artifacts. The respiratory component amplitude may be much higher than signal range and it is partly suppressed by baseline restoration circuit. The output of the demodulator is fed to a low pass filter for getting basal impedance Z_o, to baseline circuit to get $z(t)$ waveform and to the differentiator to get the dz/dt signal. In the baseline restoration circuit, discussed in Chapter 3, two comparators are used to set threshold and whenever the ICG signal crosses the threshold range, signal is pulled in the threshold range, hence restoring the baseline. Differentiator acts as high pass filter and hence further suppresses the lower frequency component, related to respiration and motion artifacts present in the waveform.

Another instrumentation amplifier is used for picking-up the ECG signal. This, simultaneously acquired ECG is used for heart rate calculation and ensemble averaging of ICG waveform. This ECG is helpful in identifying various cardiac phases, particularly during high contamination of ICG.

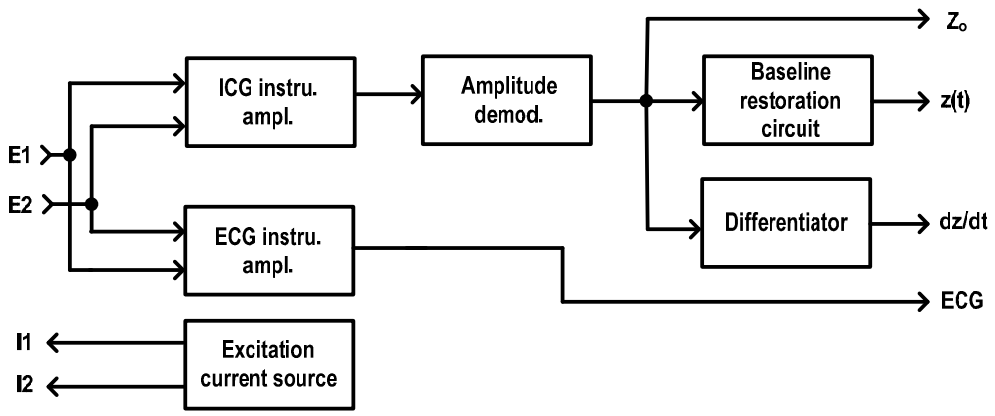

Fig. B.1 Block diagram of impedance cardiograph developed at IIT Bombay.

Circuit diagram of ICG unit is shown in Fig. B.2. The baseline restoration circuit is separately shown in Fig. B.3.

For testing and calibration of the impedance cardiograph, an impedance simulator is developed by using a microcontroller and analog switches. It can be used for measuring sensitivity and frequency response of the instrument, and for studying the effect of various electrode configurations and common mode interference caused by bioelectric sources and external pickups. The simulator has facility for varying beat rate, magnitude of common and differential mode ECG, multiple basal impedances and fixed percentage in change in impedance (Pandey *et al.*, 2008).

B.2 Respiration sensing

The respiratory signal was recorded using a thermistor based airflow sensor (Pamtrons, Mumbai, India) placed inside a plastic mask, located beneath one nostril. Thermistor based airflow sensor monitors the variation in its temperature caused by airflow in different respiratory phases. The measured airflow is related to change the intra-thoracic pressure, which causes change in the air into the lungs and venous return to the thorax. Output of the sensor is amplified, filtered, and given as an analog output. The measured airflow is referred here as the respiration signal and it is used in the adaptive filtering based techniques. It may be noted that the sensed respiration signal and the respiratory artifact may be different in shape. This instrument has an option to detect breathing rate. Also, this instrument offers a threshold adjustment to detect the breathing rate and a screen to display respiratory rate.

B.3 Data acquisition

The analog outputs of the impedance cardiograph instrument are ECG, Z_o, $z(t)$, and dz/dt. The estimation of cardiac output requires value of heart rate and stroke volume, which can be obtained by processing the signals ECG, Z_o, $z(t)$, and dz/dt. In order to obtain stroke volume and other cardiac indices, these waveforms need to be digitized and processed. In order to have a low noise system, it was decided to use a USB based signal acquisition unit. We have used data acquisition unit (DAQ) KUSB-3102, manufactured by Keithley Instruments Inc. (Cleveland, Ohio, USA). This unit has 16 single-ended or 8 differential 12-bit A/D inputs and 2 D/A outputs.

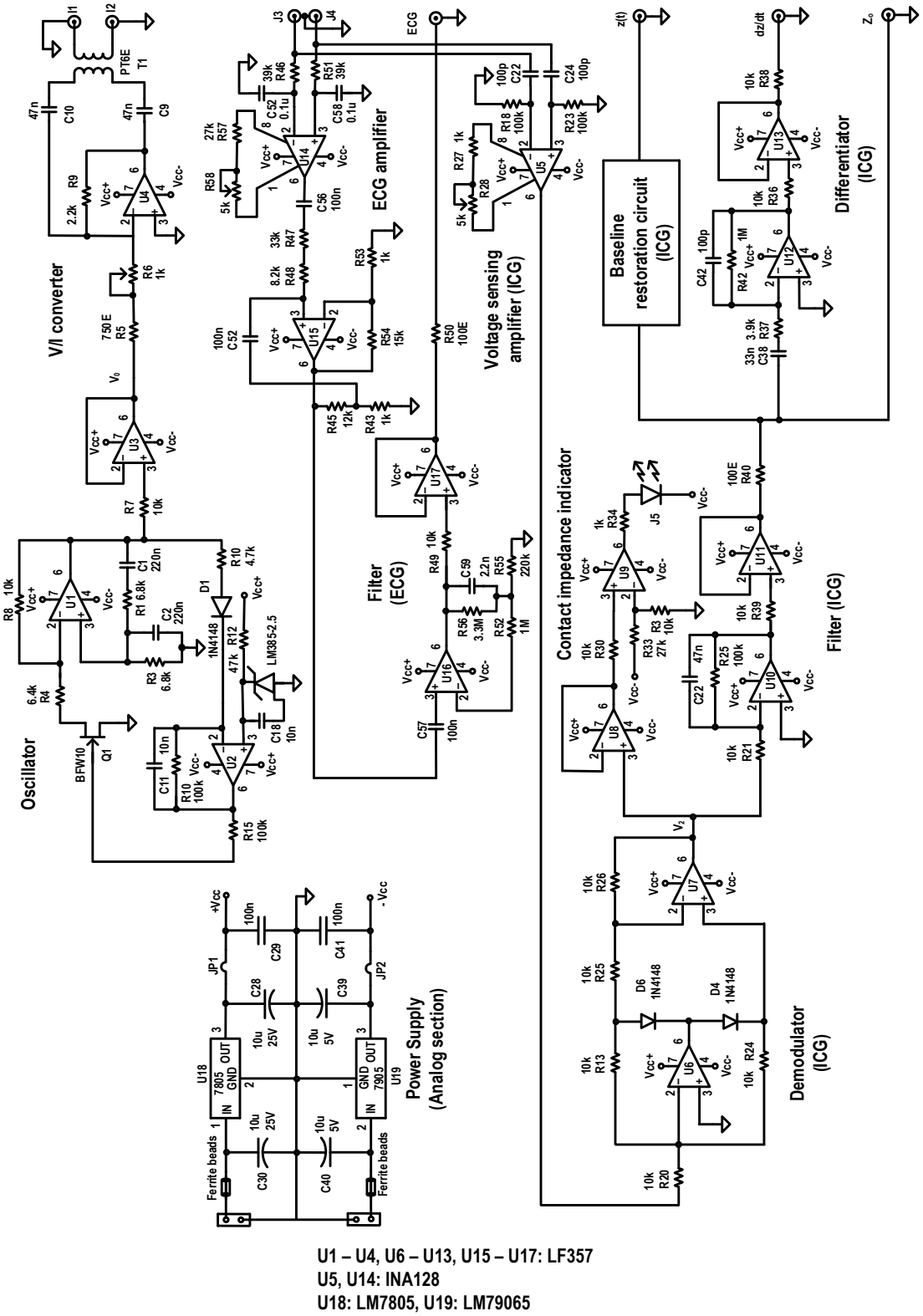

Fig. B.2 Complete circuit diagram of ICG hardware.

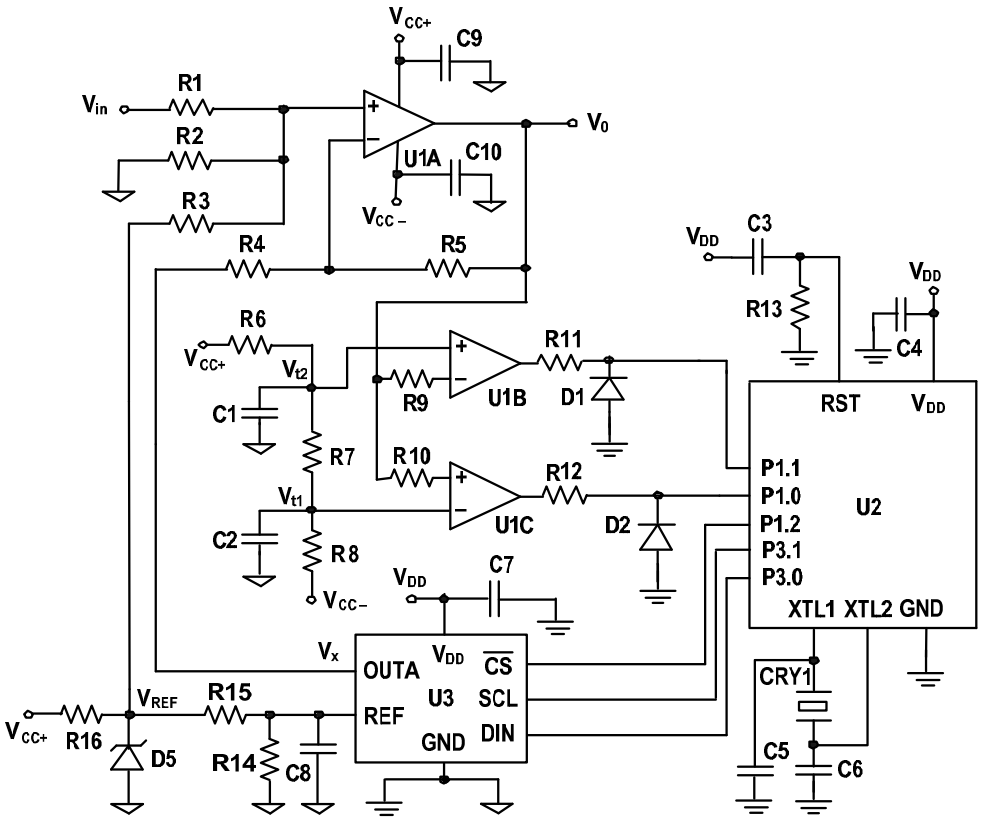

Fig. B.3 Baseline restoration circuit.

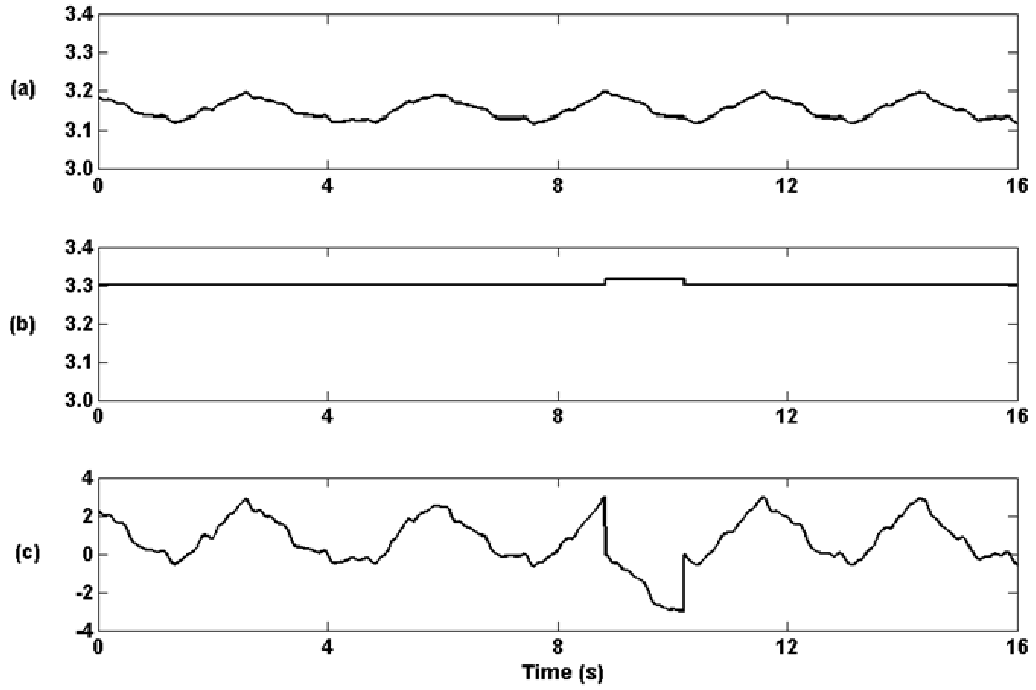

Fig. B.4 Output of the baseline restoration circuit for the thoracic impedance signal $z(t)$, from a subject, with large baseline shifts **(a)** input (in V), **(b)** correction voltage (in V), **(c)** output (in V).

Some of the important features of the unit are

- Up-to 100 kSa/s continuous A/D sampling
- 500 V isolation barrier for protecting the computer and module from voltage spikes, ESD, and surges
- Programmable input range (bipolar: ± 10 V, ± 5 V, ± 2.5 V, ± 1.25 V; unipolar: 0–10 V, 5 V, 2.5 V, 1.25 V)
- Programmable Gain (1, 2, 4, 8)
- 17 Digital I/O Channels
- Two general purpose timer/counters (8254) with programmable interface

The inter-channel cross-talk for this DAQ was found to be less than -70 dB at 1 kHz.

A program 'DATAQ' for signal acquisition was developed using A/D driver routines in Visual Basic 6 as well as in Matlab 7. The Visual Basic code can be used to generate a standalone Windows executable program. However, the Matlab code needs an installed version of the software. The specified input channels are sampled at specified sampling rate for the specified number of samples and the data are stored on the computer's hard disk. The specifications of the final hardware-software set-up are

- Sampling frequency: 1 Hz to 100 kHz
- Acquisition length: 5 s to 30 min
- Channels: upto 6 channel simultaneously
- Output format: binary/ascii

B.4 Recordings from impedance cardiograph

Figure B.4 shows the output obtained when baseline restoration circuit has been used in the impedance cardiograph instrument for recording the signals from a subject. The input signal is the variation in the thoracic impedance $z(t)$ superimposed on a slowly varying baseline drift due to respiration, superimposed on the basal impedance Z_o. The output waveform shows that the baseline is restored when the signal after amplification crosses the threshold range in either direction. In this example, two corrections happened between 8 s and 12 s. The baseline correction introduces a discontinuity and hence the correction during the cardiac cycle makes the output waveform during that cycle unsuitable for estimation of the parameters.

Figure B.5 shows ICG waveform, acquired from a volunteer, using the instrument developed in our lab and the commercial impedance cardiograph instrument 'HIC2000' respectively. Figure B.7 shows ICG waveform acquired from another volunteer by using the two impedance cardiograph instruments. For recordings from both the instruments, spot electrodes were used. Location of injection and sensing electrodes were also same for the two instruments. All these recordings were made with the subjects in the resting state. It may be noted that the recordings from the two instruments were made one after the other, and not simultaneously. Several signal recordings from 14 male subjects, using both the instruments, were carried out and it was found that the ICG waveforms acquired from both the instruments were nearly the same and they exhibited similar artifacts.

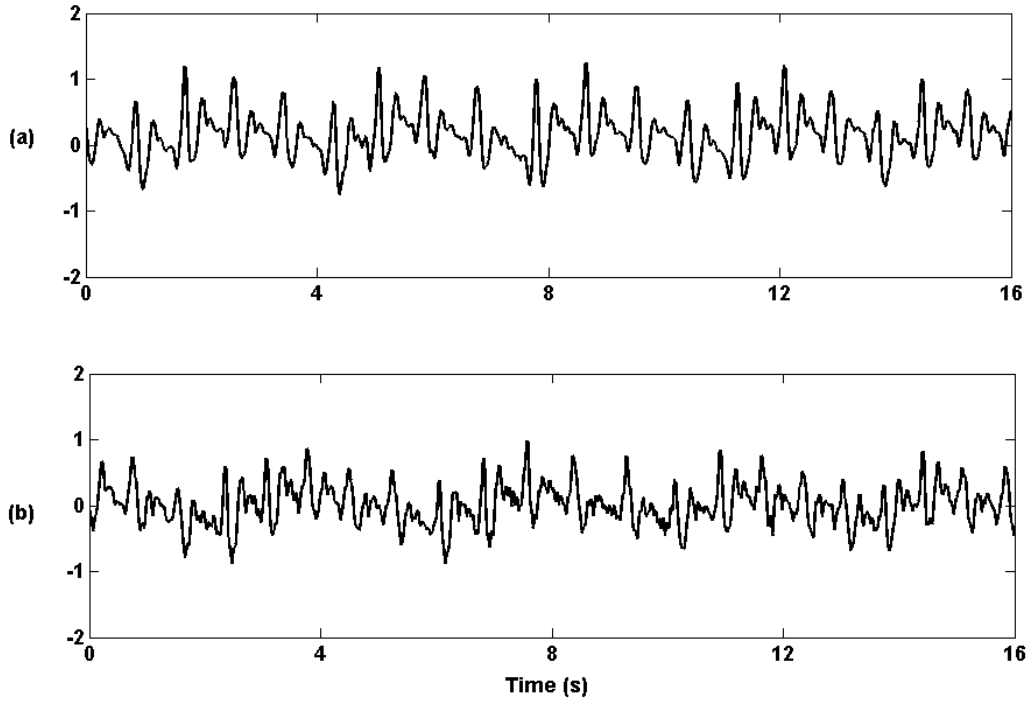

Fig. B.5 Signal ICG (in Ω/s): **(a)** using impedance cardiograph "ICRS06" developed in our lab and **(b)** using commercial impedance cardiograph 'HIC2000' from subject 'LV'.

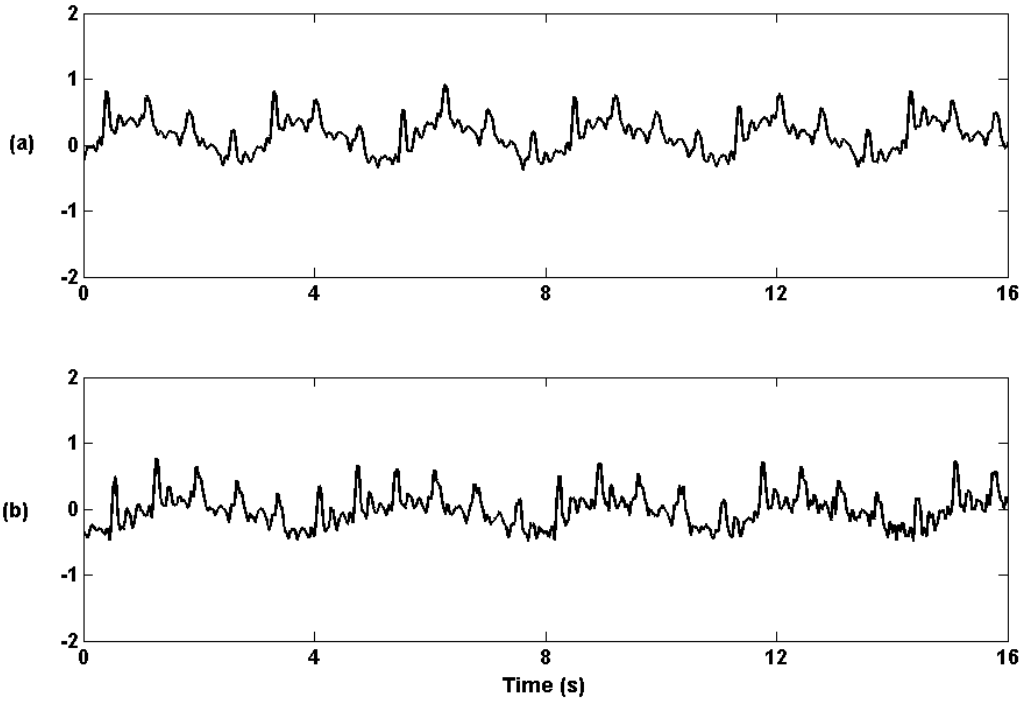

Fig. B.6 Signal ICG (in Ω/s): **(a)** using impedance cardiograph "ICRS06" developed in our lab and **(b)** using commercial impedance cardiograph 'HIC2000' from subject 'MS'.

Appendix C

RESULTS FROM ADAPTIVE FILTERING

C.1 Introduction

To assess the performance of the two adaptive filtering techniques, they were applied on signal, from 23 volunteers, with different levels of simulated artifacts. Improvement in the signal-to-artifact ratio (SAR) was used as the performance index. Results for input SAR for the range of -9 to 9 dB are presented in this appendix. Both the techniques were applied on the signals acquired from 52 volunteers with normal health and no known cardiovascular history. Results for 4 volunteers are presented here.

C.2 Adaptive filtering by sensing respiration (AFSR)

The technique AFSR is based on LMS based adaptive filtering. In this technique, the airflow signal acquired from a respiratory sensor, simultaneously along with the ICG and $z(t)$ signals, is taken as the reference input and sensed contaminated impedance signal is used as the primary input to the filter. This technique permits beat-by-beat stroke volume (SV) estimation, even in the presence of large respiratory artifacts.

Signals with different levels of simulated artifacts were processed using the technique AFSR. Figure C.1 shows waveforms: (a) artifact-free ICG, (b) ICG-free artifact, (c) sensed respiration, (d) ICG with simulated -9 dB artifact, (e) ICG with simulated -6 dB artifact, (f) ICG with simulated -3 dB artifact, (g) ICG with simulated 0 dB artifact, (h) ICG with simulated 3 dB artifact, (i) ICG with simulated 6 dB artifact, and (j) ICG with simulated 9 dB artifact. The processed outputs, by the technique AFSR, for the inputs given in Fig. C.1, are presented in Fig. C.2.

C.3 Adaptive filtering by using estimated respiration (AFER)

An analysis of the results obtained using the AFSR technique showed that that the sensed respiration did not approximate the higher frequencies in the respiratory artifact. Hence, investigations were carried out for a better approximation of the respiratory artifact using the sensed respiration. In the recordings with controlled respiration it was observed that change in the slope of the sensed respiration corresponded to the beginning of the inhale and exhale phases. Hence, for approximation of respiratory artifact we experimented with fitting different waveforms through the points of beginning of inhale and exhale phases.

For sinusoidal wave fitting, estimated reference signal had constant amplitude with frequency equal to that of the respiration cycle. For square wave fitting, estimated reference signal had constant amplitude with polarity change at the change of respiration phases. Reference signal as triangular wave was generated by inverting the slope of a straight line at the change of

respiration phases. For bipolar Gaussian pulse, estimated reference signal had Gaussian pulse of constant amplitude with polarity change at the change of respiration phases. Similarly, for bipolar impulses, estimated reference signal had bipolar impulse of constant amplitude with polarity change at the change of respiration phases. Sinusoidal waveform, as the reference signal, was unable to cancel the harmonics of the artifacts present in the recorded signal. References based on the use of square and bipolar Gaussian pulse introduced distortion in the processed output. Use of bipolar impulses as the reference failed to significantly cancel the lower frequency components of the artifacts present in the recorded signal.

On the basis of the observation, it was decided to estimate the respiration reference by using the sensed respiration and the ICG. For this purpose, a polynomial spline fitting on contaminated ICG was used for estimating the respiratory artifact. A separate spline was fitted on each respiratory phase by using two knots and 10 control points equally spaced between knots. The waveform thus obtained can be used as the reference input for adaptive filtering. The estimated reference inputs (sinusoidal, square, triangular, bipolar Gaussian pulse, bipolar impulses, and spline fit on the signal) and corresponding processed outputs for signal ICG with simulated 0 dB artifact are shown in Fig. C.3 and Fig. C.4, respectively. Figure C.5 shows estimated reference input for AFER by fitting spline on the signal with different levels of simulated artifact. Processed outputs by AFER for the primary input signal of Fig. C.1, using the reference of Fig. C.5, are shown in Fig. C.6.

C.4 Results for recorded signal

The recorded $z(t)$, ICG, and other related waveforms and their processed outputs, by technique AFSR and AFER, for 4 subjects in post-exercise relaxation, are presented in Figs. C.7 to C.26. It can be observed that point B, point X, and ICG peaks are not stable in contaminated ICG signal and hence parameters estimation from contaminated ICG results in large error in the estimated stroke volume. In processed output, points B, point X, and ICG peaks are found to be stable and hence suited for estimation of stroke volume and other cardiac indices.

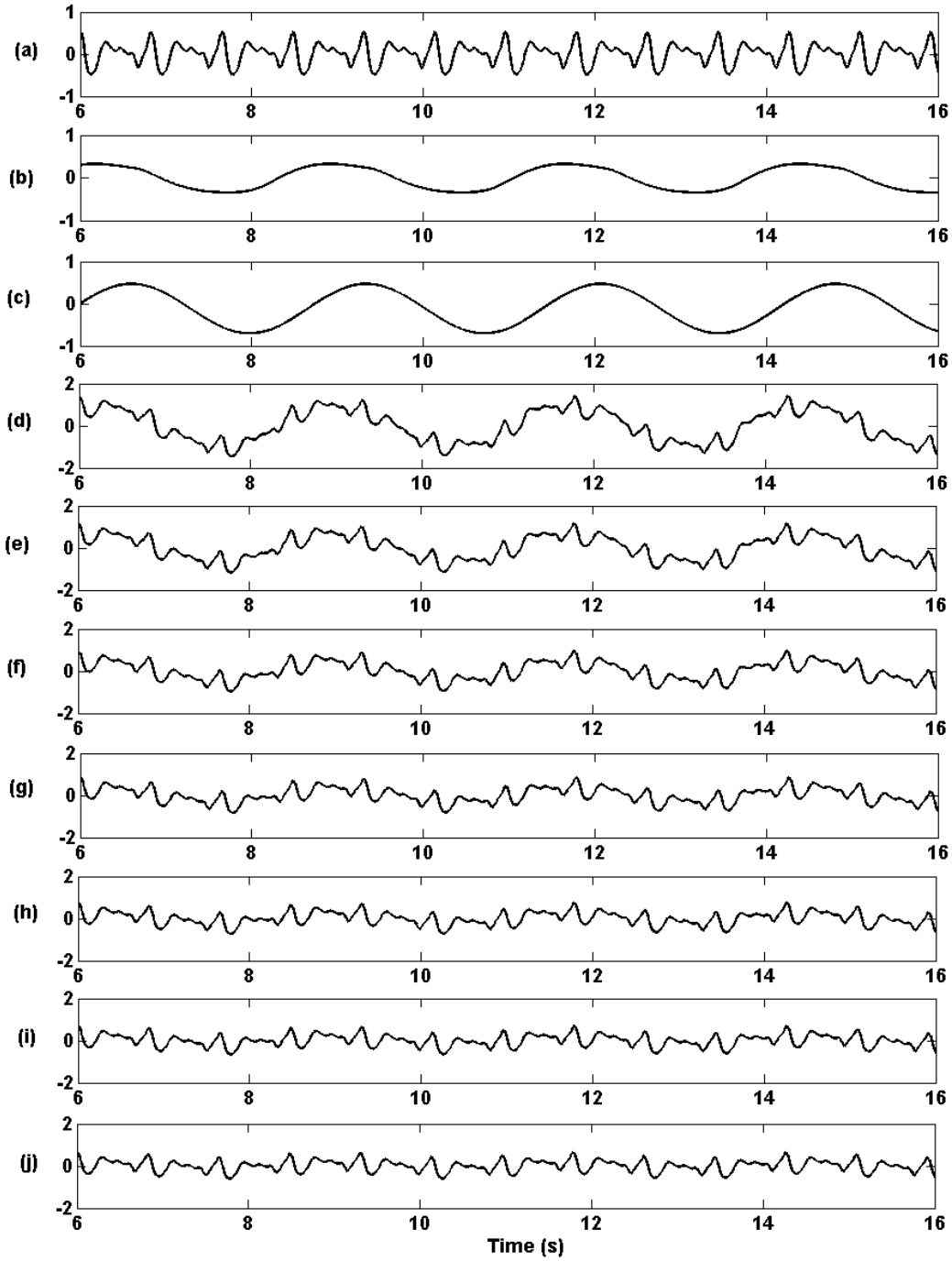

Fig. C.1 Waveforms: **(a)** artifact-free ICG, **(b)** ICG-free artifact, **(c)** sensed respiration, **(d)** ICG with simulated **-9** dB artifact, **(e)** ICG with simulated **-6** dB artifact, **(f)** ICG with simulated **-3** dB artifact, **(g)** ICG with simulated **0** dB artifact, **(h)** ICG with simulated 3 dB artifact, **(i)** ICG with simulated **6** dB artifact, and **(j)** ICG with simulated **9** dB artifact (all the waveforms are in arbitrary units).

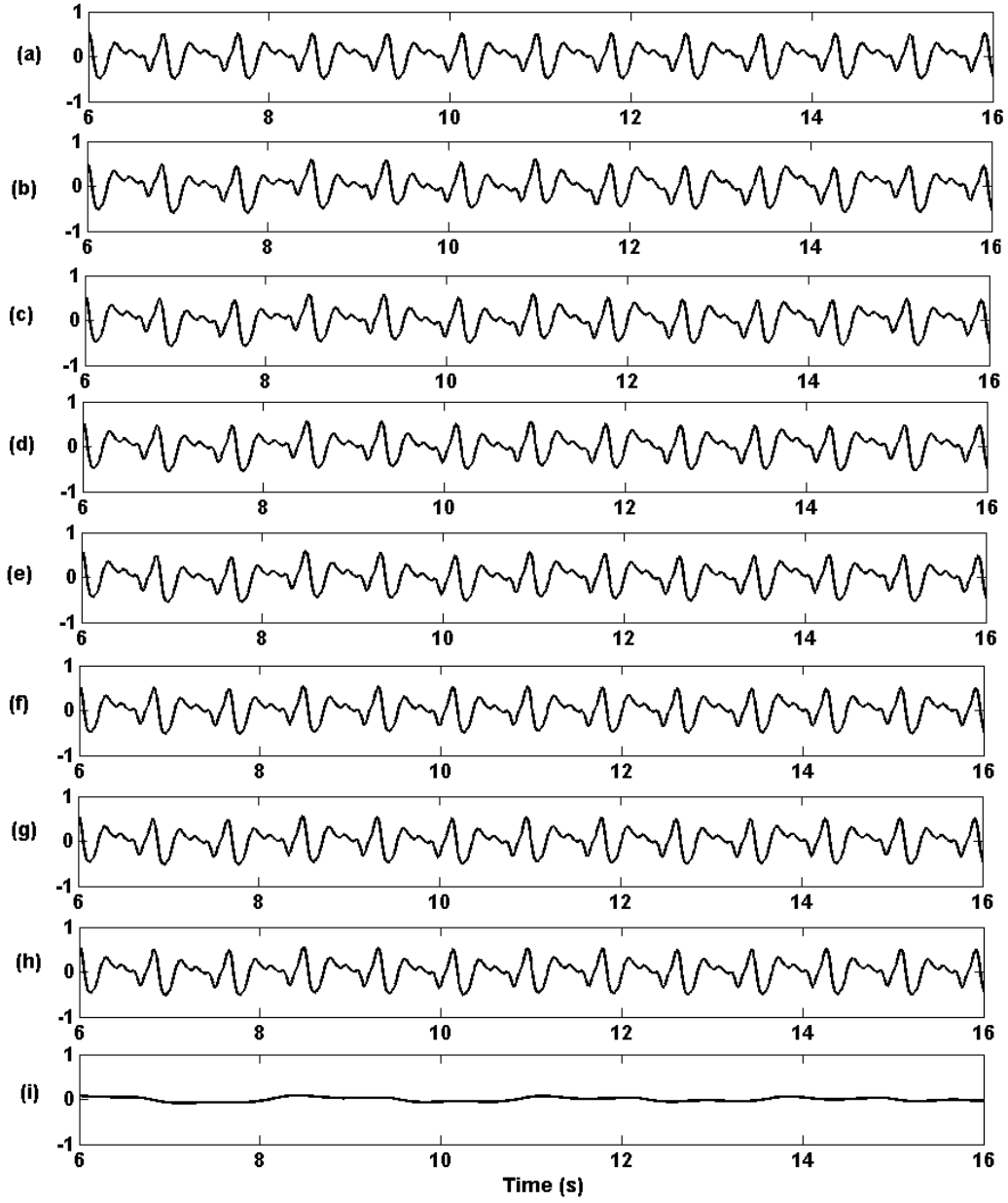

Fig. C.3 Processed output by AFSR of signal: **(a)** artifact-free ICG, **(b)** ICG with simulated -9 dB artifact, **(c)** ICG with simulated **-6** dB artifact, **(d)** ICG with simulated **-3** dB artifact, **(e)** ICG with simulated **0** dB artifact, **(f)** ICG with simulated **3** dB artifact, **(g)** ICG with simulated **6** dB artifact, **(h)** ICG with simulated **9** dB artifact, and **(i)** ICG-free artifact (all the waveforms are in arbitrary units).

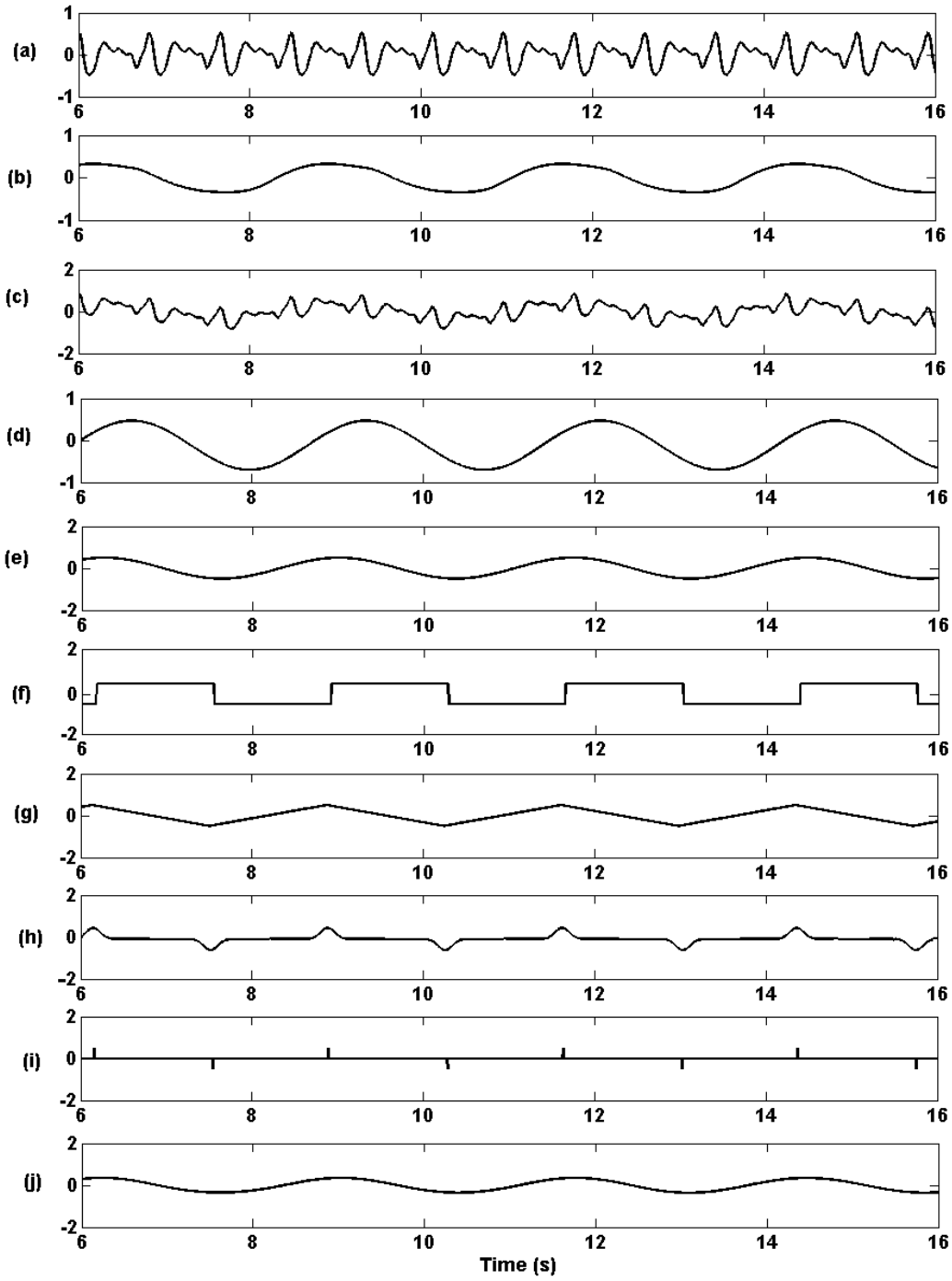

Fig. C.3 Waveforms related to estimation of respiratory reference in AFER: **(a)** artifact-free ICG, **(b)** ICG-free artifact, **(c)**, ICG with simulated **0** dB artifact **(d)** sensed respiration, **(e)** estimated reference by sinusoidal fitting, **(f)** estimated reference by square wave fitting, **(g)** estimated reference by triangular wave fitting, **(h)** bipolar Gaussian pulses, **(i)** bipolar impulses, and **(j)** estimated reference by spline fitting on the signal (all the waveforms are in arbitrary units).

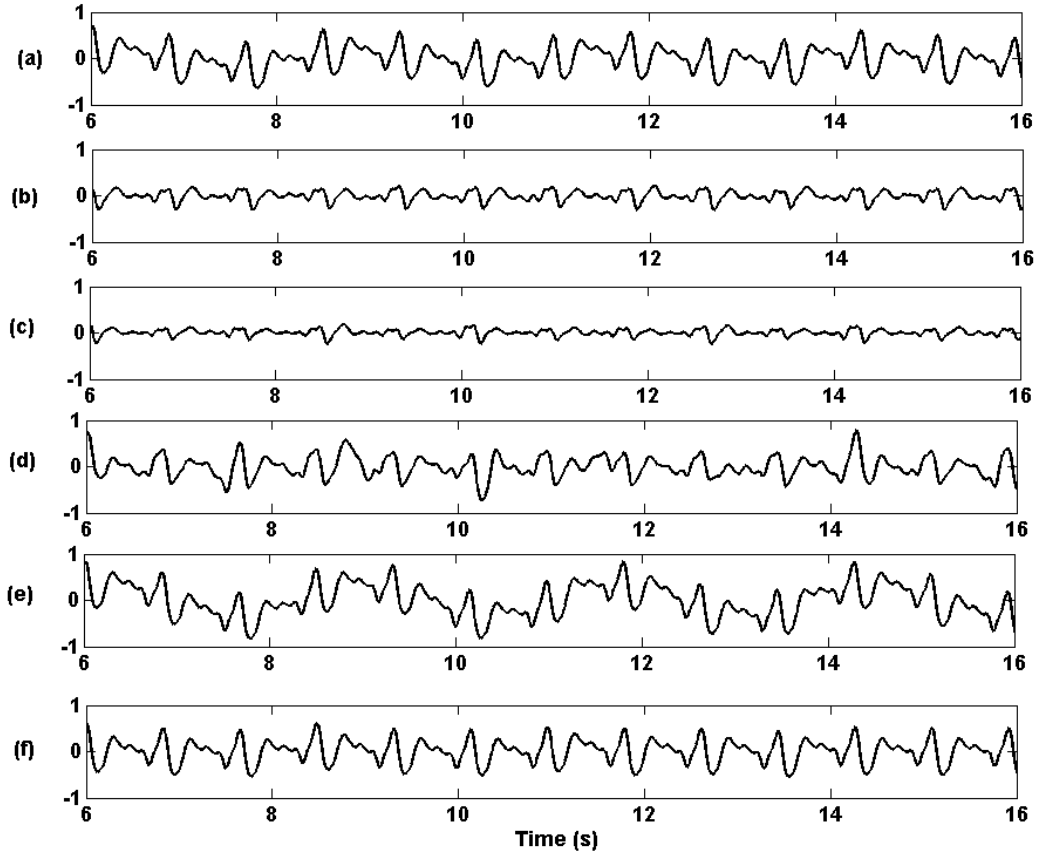

Fig. C.4 Processed output for signal ICG with simulated **0** dB artifact by AFER using estimated reference input: **(a)** sinusoidal **(b)** square, **(c)** triangular, **(d)** bipolar Gaussian pulses, **(e)** bipolar impulses, and **(f)** spline fit on the signal (all the waveforms are in arbitrary units).

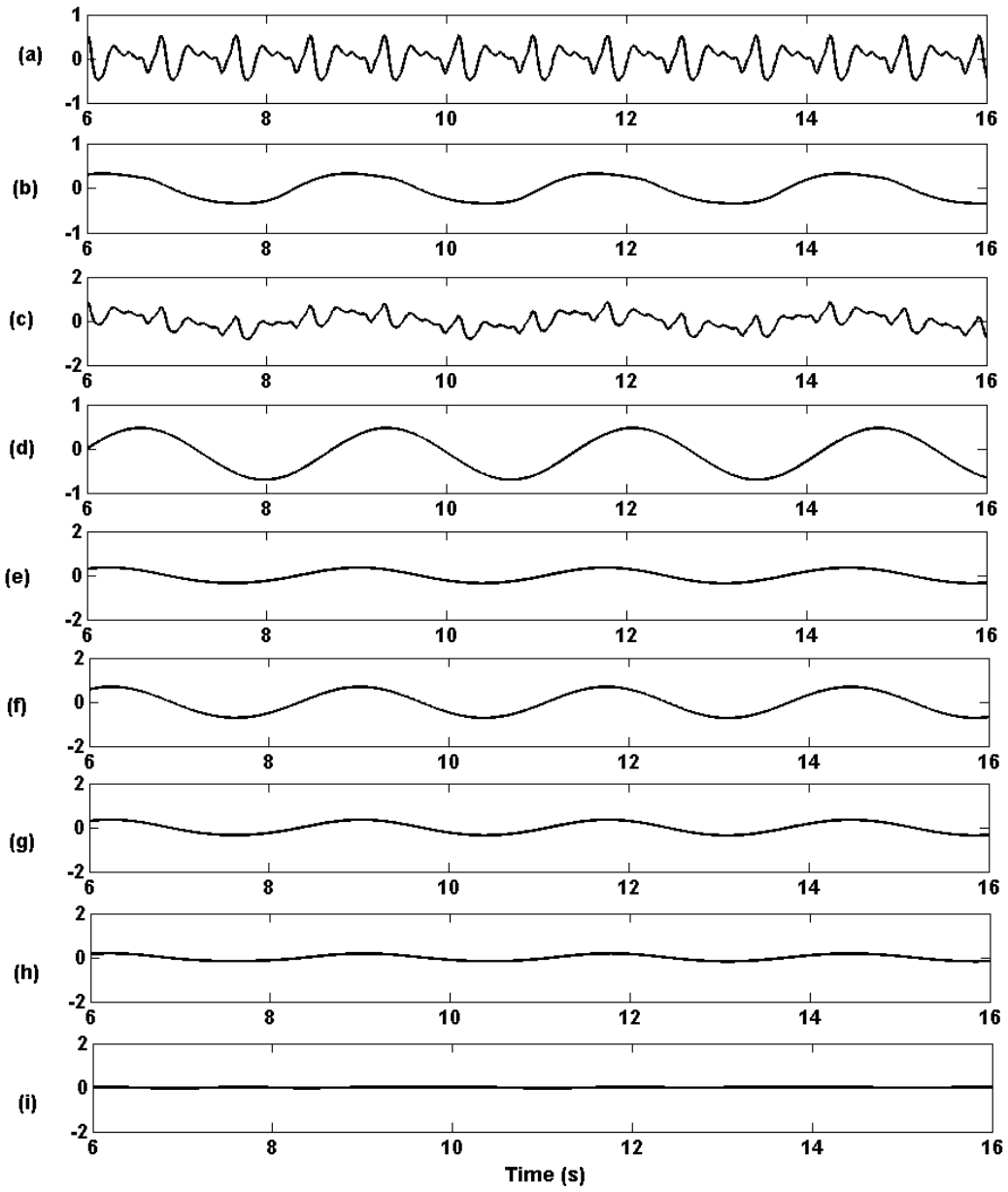

Fig. C.5 Waveforms related to reference input for AFER by spling fitting on the signal: **(a)** artifact-free ICG, **(b)** ICG-free artifact, **(c)**, ICG with simulated **0** dB artifact **(d)** sensed respiration, reference input for AFER by fitting spline on the signal: **(e)** ICG-free artifact, **(f)** ICG with simulated -6 dB artifact, **(g)** ICG with simulated **0** dB artifact, **(h)** ICG with simulated **6** dB artifact, **and (i)** artifact-free ICG (all the waveforms are in arbitrary units).

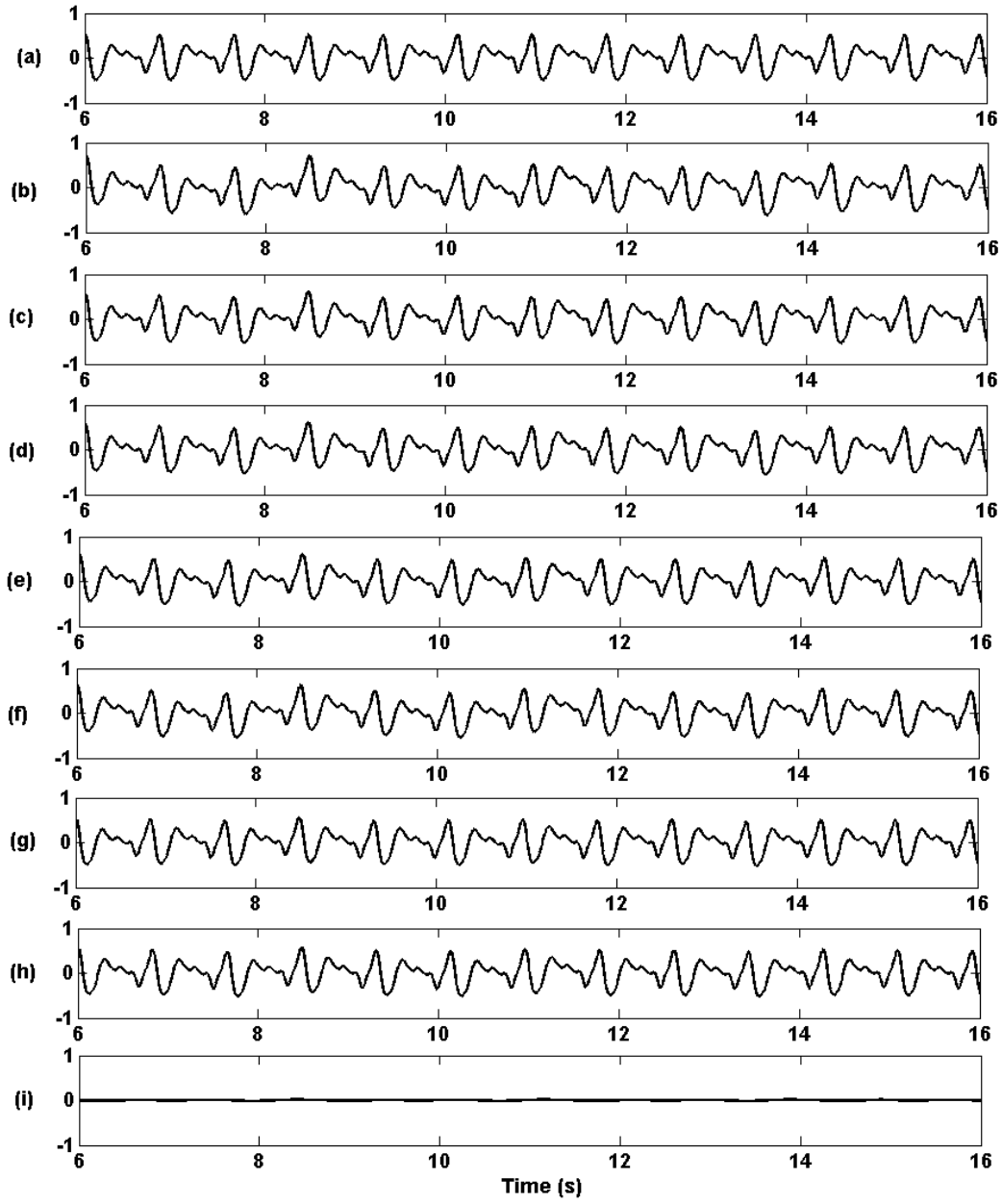

Fig. C.6 Processed output, using reference obtained by fitting spline on the signal, by AFER of signal: **(a)** artifact-free ICG, **(b)** ICG with simulated -9 dB artifact, **(c)** ICG with simulated **-6** dB artifact, **(d)** ICG with simulated **-3** dB artifact, **(e)** ICG with simulated **0** dB artifact, **(f)** ICG with simulated **3** dB artifact, **(g)** ICG with simulated **6** dB artifact, and **(h)** ICG with simulated **9** dB artifact, and **(i)** ICG-free artifact (all the waveforms are in arbitrary units).

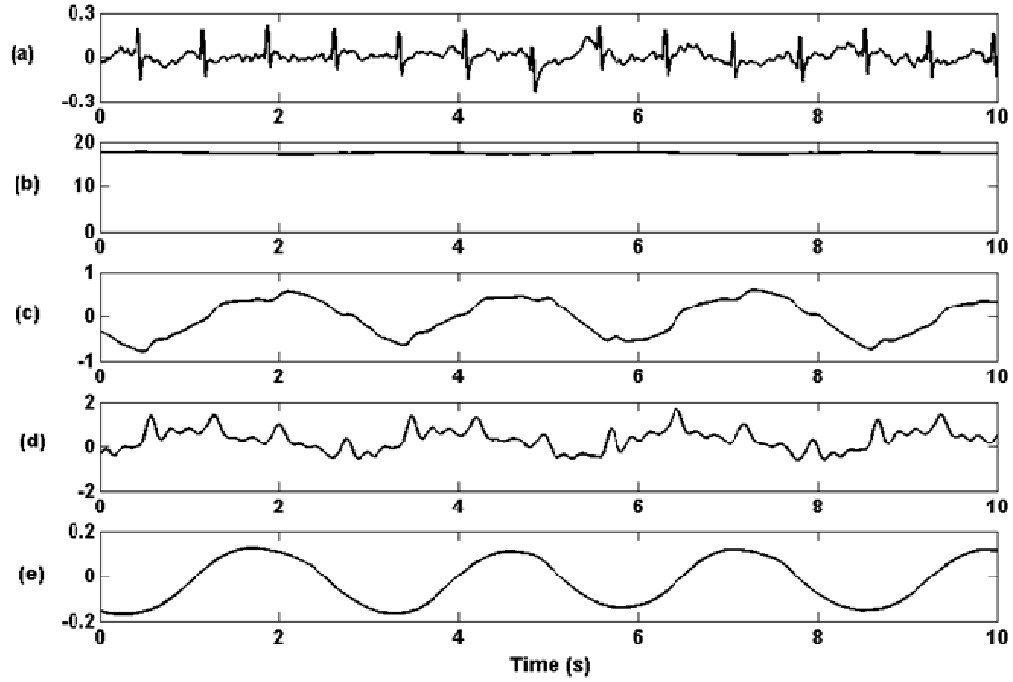

Fig. C.7 Waveforms for processing: **(a)** ECG (in arbitrary units), **(b)** Z_o (in Ω), **(c)** $z(t)$ (in Ω), **(d)** ICG (in Ω/s), and **(e)** sensed airflow (in arbitrary units) from subject 'MS'.

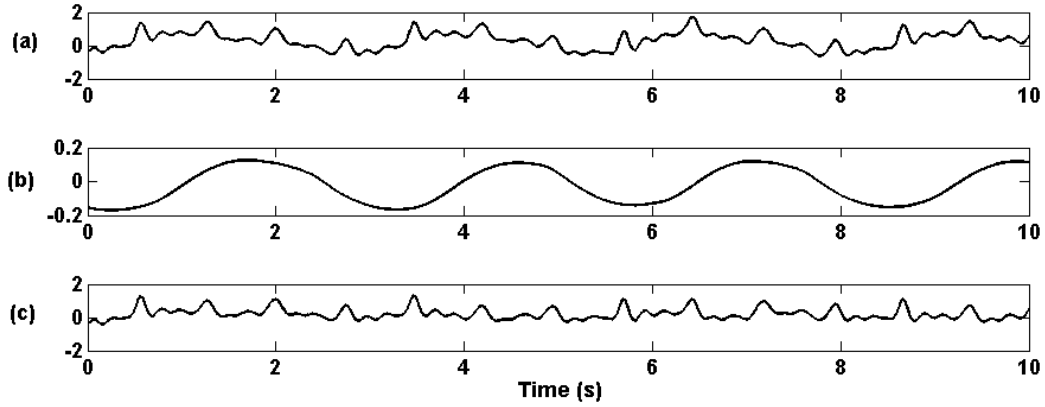

Fig. C.8 Processing of ICG by AFSR: **(a)** recorded ICG (in Ω/s), **(b)** sensed airflow (in arbitrary units), and **(c)** processed ICG (in Ω/s) from subject 'MS'.

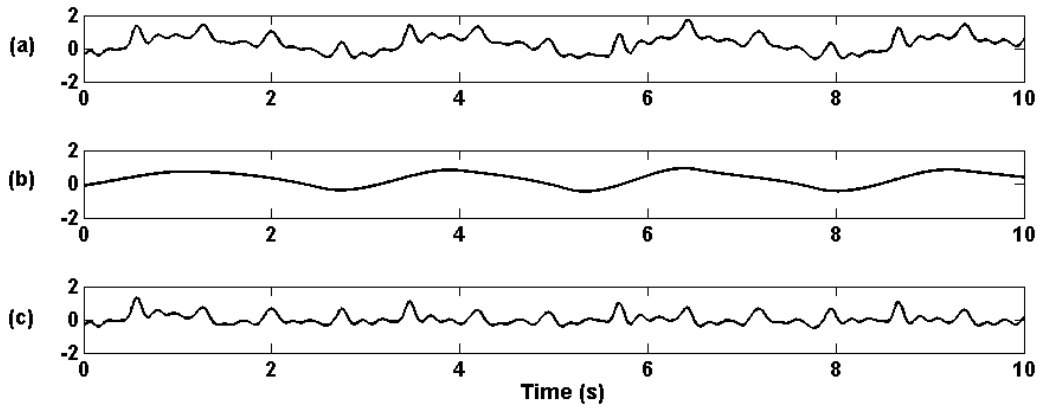

Fig. C.9 Processing of ICG by AFER: **(a)** recorded ICG (in Ω/s), **(b)** fitted spline on recorded ICG (in arbitrary units), and **(c)** processed ICG (in Ω/s) from subject 'MS'.

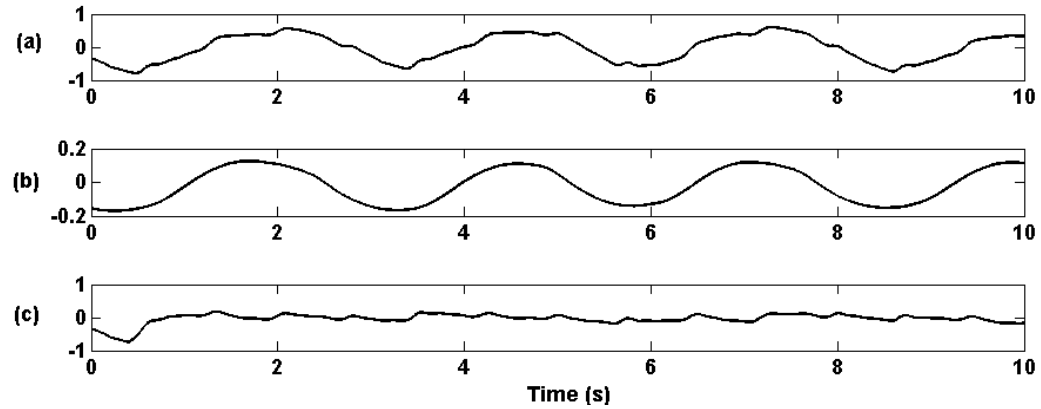

Fig. C.10 Processing of impedance signal by AFSR: **(a)** recorded $z(t)$ (in Ω), **(b)** sensed airflow (in arbitrary units), and **(c)** processed $z(t)$ (in Ω) from subject 'MS'.

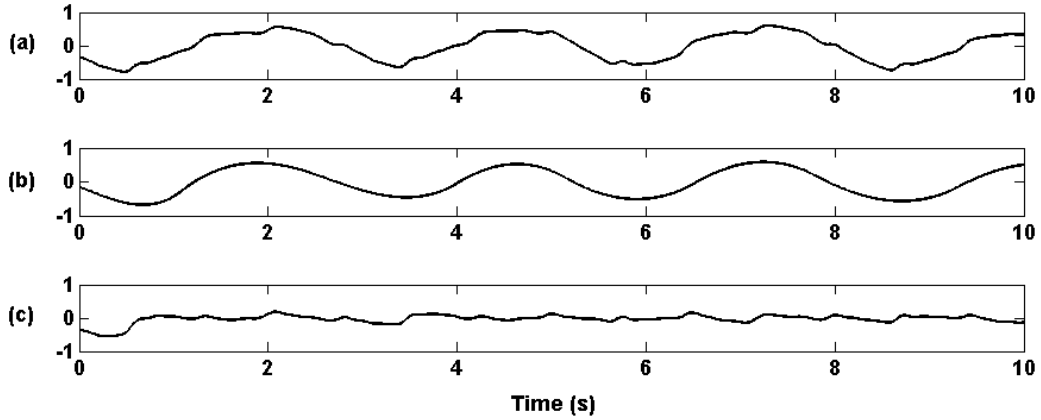

Fig. C.11 Processing of impedance signal by AFER: **(a)** recorded $z(t)$ (in Ω), **(b)** fitted spline on recorded $z(t)$ (in arbitrary units), and **(c)** processed $z(t)$ (in Ω) from subject 'MS'.

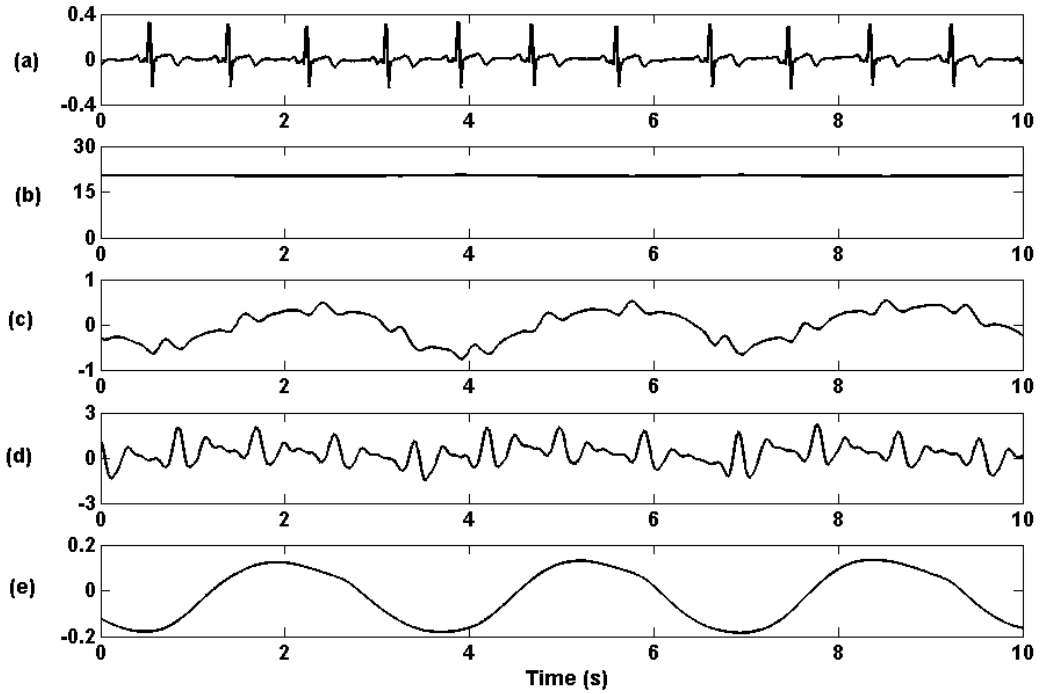

Fig. C.12 Waveforms for processing: **(a)** ECG (in arbitrary units), **(b)** Z_o (in Ω), **(c)** $z(t)$ (in Ω), **(d)** ICG (in Ω/s), and **(e)** sensed airflow (in arbitrary units) from subject 'PP'.

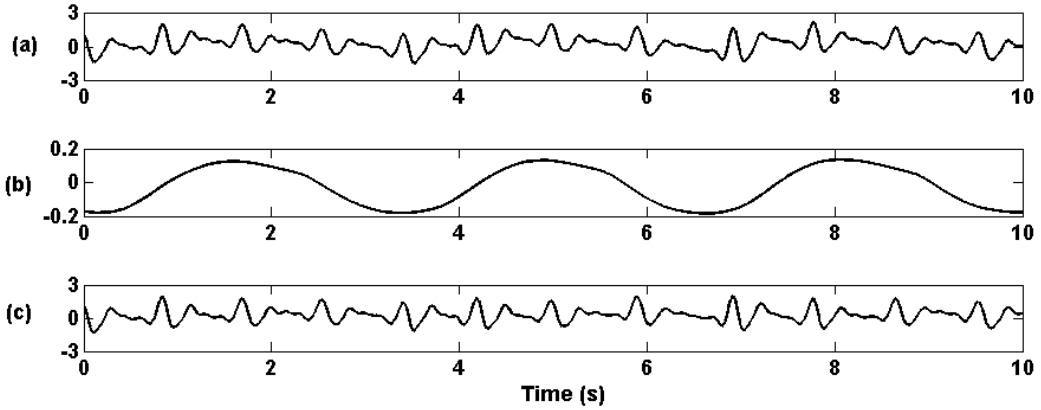

Fig. C.13 Processing of ICG by AFSR: **(a)** recorded ICG (in Ω/s), **(b)** sensed airflow (in arbitrary units), and **(c)** processed ICG (in Ω/s) from subject 'PP'.

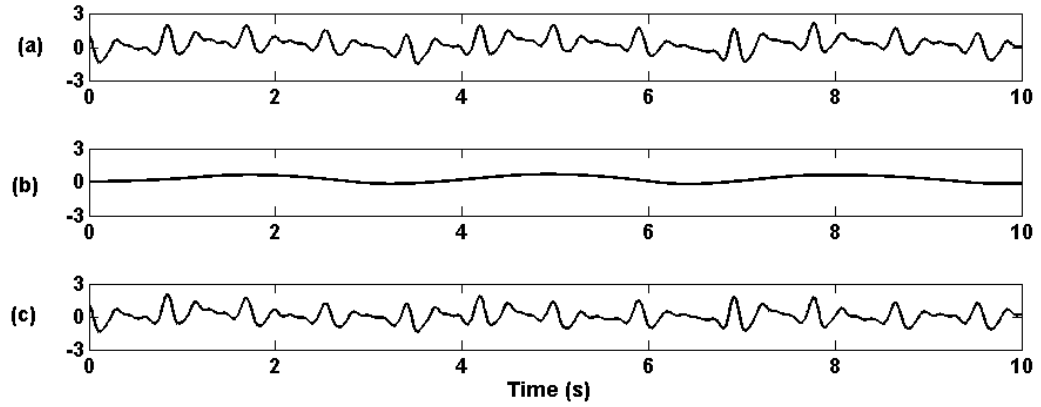

Fig. C.14 Processing of ICG by AFER: **(a)** recorded ICG (in Ω/s), **(b)** fitted spline on recorded ICG (in arbitrary units), and **(c)** processed ICG (in Ω/s) from subject 'PP'.

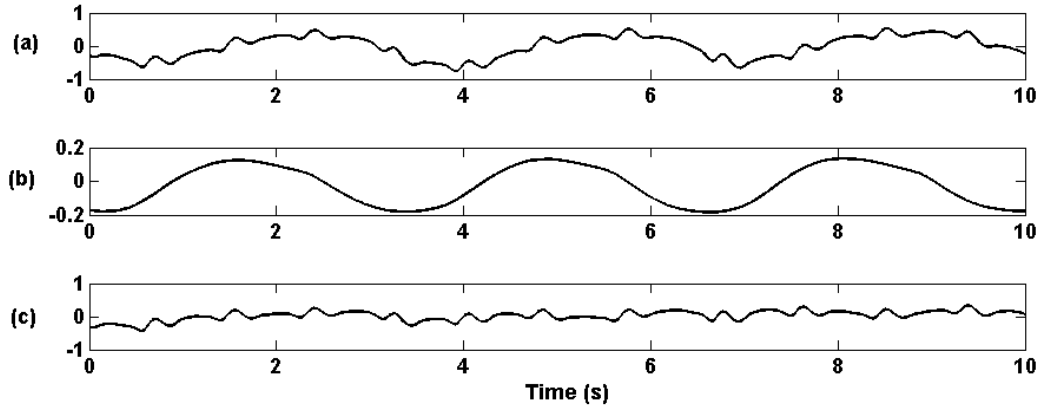

Fig. C.15 Processing of impedance signal by AFSR: **(a)** recorded $z(t)$ (in Ω), **(b)** sensed airflow (in arbitrary units), and **(c)** processed $z(t)$ (in Ω) from subject 'PP'.

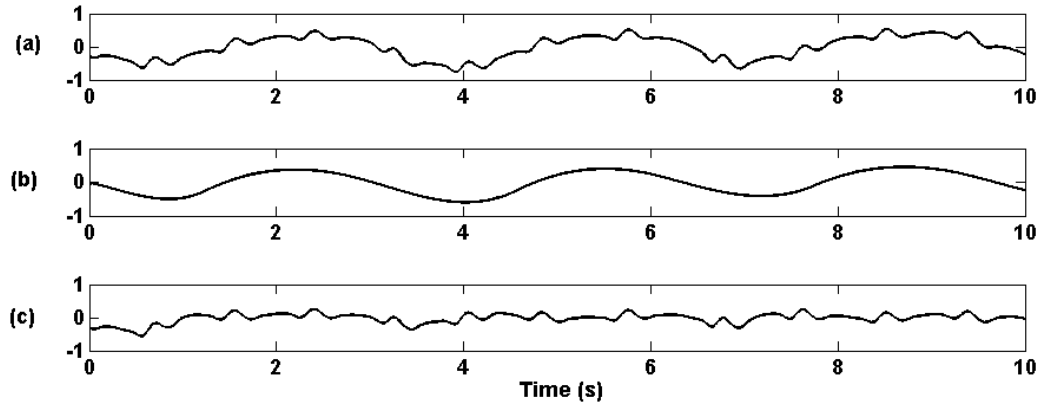

Fig. C.16 Processing of impedance signal by AFER: **(a)** recorded $z(t)$ (in Ω), **(b)** fitted spline on recorded $z(t)$ (in arbitrary units), and **(c)** processed $z(t)$ (in Ω) from subject 'PP'.

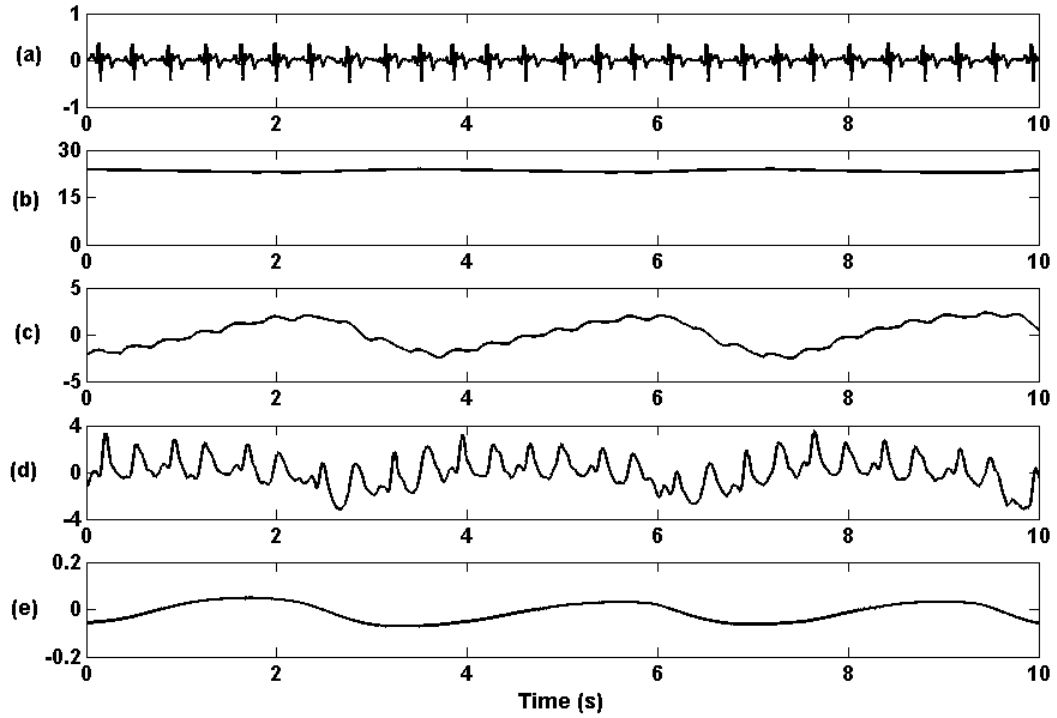

Fig. C.17 Waveforms for processing: **(a)** ECG (in arbitrary units), **(b)** Z_o (in Ω), **(c)** $z(t)$ (in Ω), **(d)** ICG (in Ω/s), and **(e)** sensed airflow (in arbitrary units) from subject 'KI'.

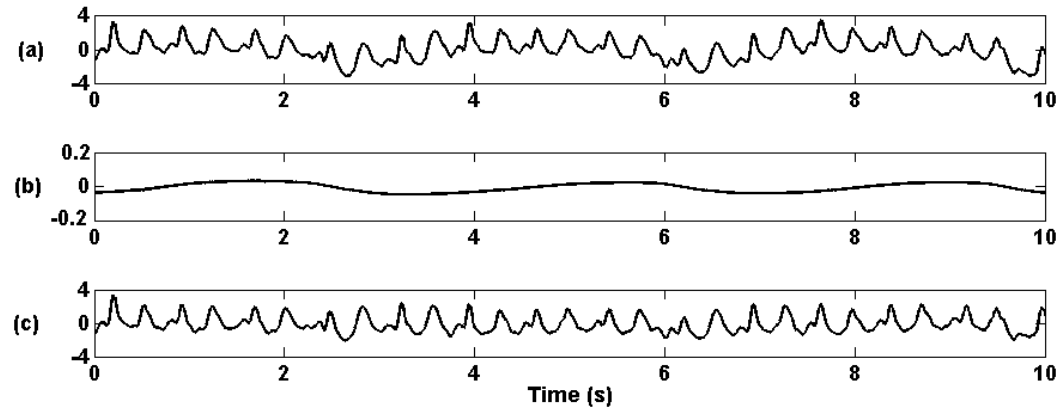

Fig. C.18 Processing of ICG by AFSR: **(a)** recorded ICG (in Ω/s), **(b)** sensed airflow (in arbitrary units), and **(c)** processed ICG (in Ω/s) from subject 'KI'.

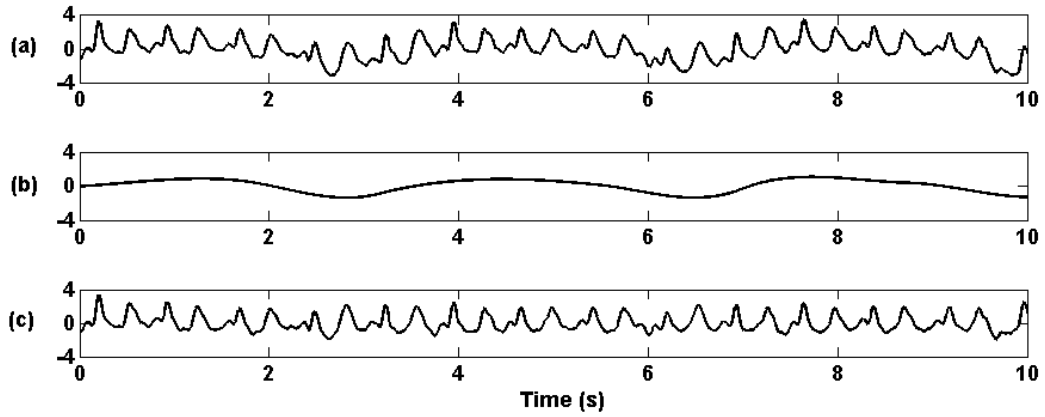

Fig. C.19 Processing of ICG by AFER: **(a)** recorded ICG (in Ω/s), **(b)** fitted spline on recorded ICG (in arbitrary units), and **(c)** processed ICG (in Ω/s) from subject 'KI'.

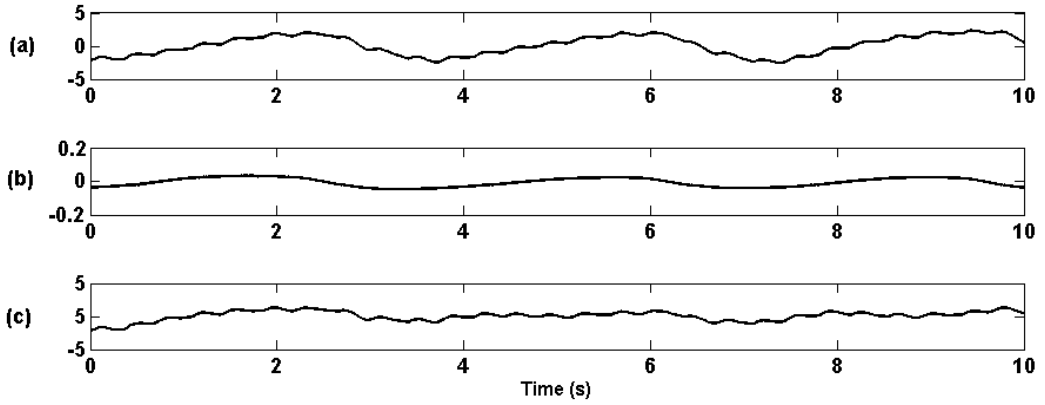

Fig. C.20 Processing of impedance signal by AFSR: **(a)** recorded $z(t)$ (in Ω), **(b)** sensed airflow (in arbitrary units), and **(c)** processed $z(t)$ (in Ω) from subject 'KI'.

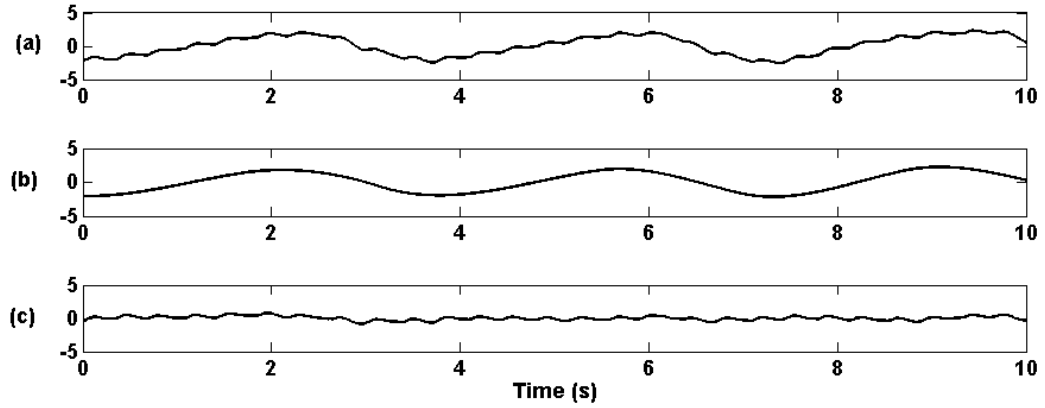

Fig. C.21 Processing of impedance signal by AFER: **(a)** recorded $z(t)$ (in Ω), **(b)** fitted spline on recorded $z(t)$ (in arbitrary units), and **(c)** processed $z(t)$ (in Ω) from subject 'KI'.

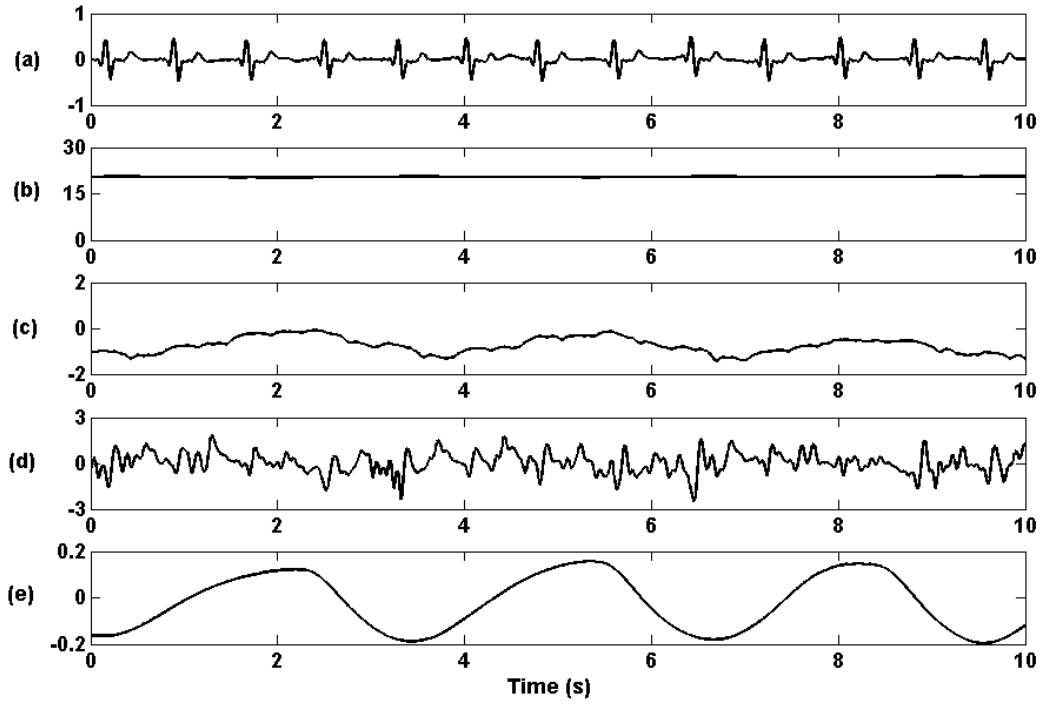

Fig. C.22 Waveforms for processing: **(a)** ECG (in arbitrary units), **(b)** Z_o (in Ω), **(c)** $z(t)$ (in Ω), **(d)** ICG (in Ω/s), and **(e)** sensed airflow (in arbitrary units) from subject 'AJ'.

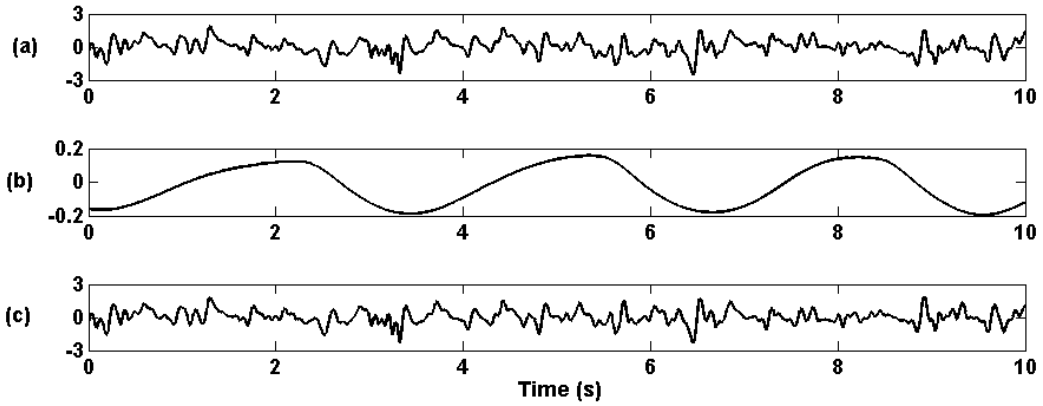

Fig. C.23 Processing of ICG by AFSR: **(a)** recorded ICG (in Ω/s), **(b)** sensed airflow (in arbitrary units), and **(c)** processed ICG (in Ω/s) from subject 'AJ'.

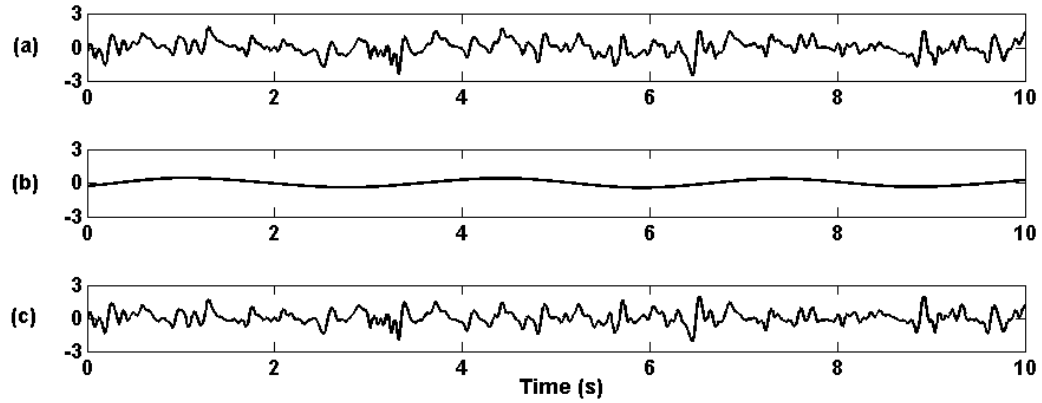

Fig. C.24 Processing of ICG by AFER: **(a)** recorded ICG (in Ω/s), **(b)** fitted spline on recorded ICG (in arbitrary units), and **(c)** processed ICG (in Ω/s) from subject 'AJ'.

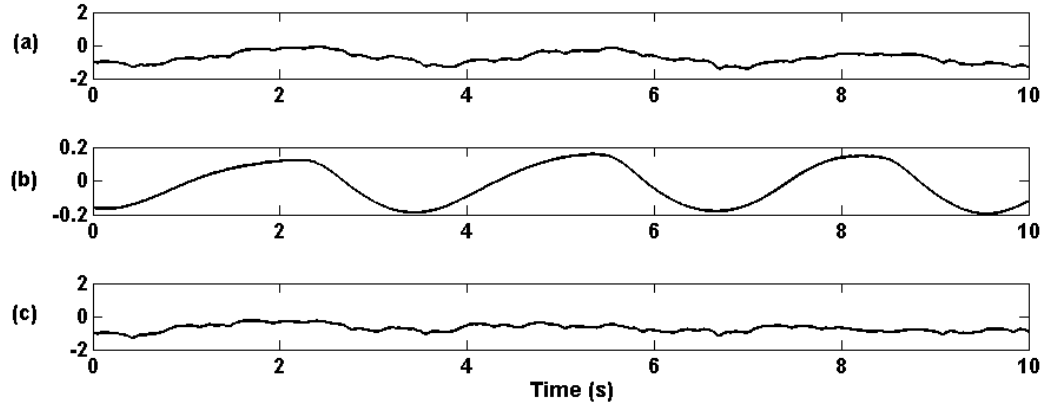

Fig. C.25 Processing of impedance signal by AFSR: **(a)** recorded $z(t)$ (in Ω), **(b)** sensed airflow (in arbitrary units), and **(c)** processed $z(t)$ (in Ω) from subject 'AJ'.

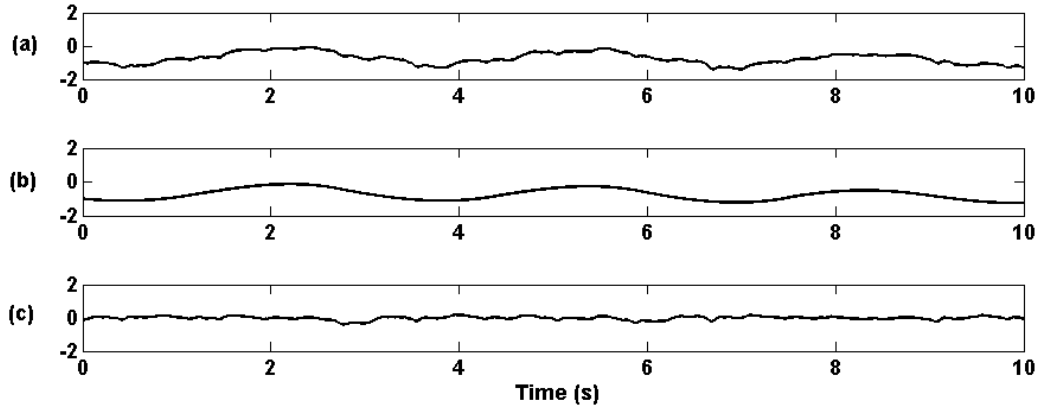

Fig. C.26 Processing of impedance signal by AFER: **(a)** recorded $z(t)$ (in Ω), **(b)** fitted spline on recorded $z(t)$ (in arbitrary units), and **(c)** processed $z(t)$ (in Ω) from subject 'AJ'.

Appendix D

RESULTS FROM WAVELET BASED DENOISING

D.1 Introduction

In this appendix, supplementary results of wavelet based denoising (WBD) technique are given. In the technique, FIR based Meyer wavelet has been used for decomposition of the signal, and the first 8 details have been used to reconstruct the signal.

D.2 Results for simulated contamination of ICG

In this technique, we have used linear denoising, also known as scale-dependent thresholding, for artifact suppression. Selection of the mother-wavelet and the number of scales in the decomposition is an important issue. For decomposition, we studied several types of wavelet families: Daubechies, coiflets, symlets, and discrete Meyer. For the signal acquired at sampling frequency of 500 Hz, the wavelet function and the scaling function along with their magnitude spectra are shown in Fig. D.1 for discrete Meyer wavelet. Similar plots for coiflets (order 5) and Daubechies (order 6) wavelet are given in Fig. D.2 and D.3, respectively. As seen in the figure, scaling function acts as a lowpass filter and corresponding wavelet acts as highpass filter. The lowpass filter coefficients for discrete Meyer, Coiflets (order 5) and Daubechies (order 6) are given in Table D.1.Figures D.4 and D.5 show the details and approximation at each scales of an ICG-free artifact and an artifact-free ICG signal using discrete Meyer wavelet. As shown in the figure, artifact-free ICG signal is captured within first eight details while ICG-free artifact related components are captured at higher scales. Figures D.6 to Fig. D9 show the details and approximation at each scales of an ICG-free artifact and an artifact-free ICG signal using Coiflets (order 5) and Daubechies (order 6) wavelet. It is seen that the signal component at different scales for artifact-free ICG signal and ICG-free artifact are overlapping and hence difficult to separate them. Discrete Meyer wavelet is able to separate the signal and artifact component at different scales, hence we have used discrete Meyer wavelet in the technique WBD.

Signals with different levels of simulated artifacts were processed using the technique WBD. Figure D.10 shows waveforms: (a) artifact-free ICG, (b) ICG-free artifact, (c) sensed respiration, (d) ICG with simulated -9 dB artifact, (e) ICG with simulated -6 dB artifact, (f) ICG with simulated -3 dB artifact, (g) ICG with simulated 0 dB artifact, (h) ICG with simulated 3 dB artifact, (i) ICG with simulated 6 dB artifact, and (j) ICG with simulated 9 dB artifact. The processed outputs, by the technique WBD, for the inputs given in Fig. D.10, are presented in Fig. D.11.

D.3 Results for recorded signal

The recorded $z(t)$, ICG, and other related waveforms and their processed outputs, by the technique WBD, for 4 subjects in post-exercise relaxation, are presented in Figs. D.12 to D.23.

D.3 Tabulation of SAR improvement

The SAR improvement (output SAR – input SAR) by the three techniques are given in Table D.2. Plots of output SAR versus input SAR with simulated input in the range of -9 to 9 dB for recordings from different subjects sowed a nearly straight line relationship, similar to the plot in Fig. 5.5. We see that the mean of the SAR improvements were 18.5, 19.6, and 21.7 dB for the technique AFSR, AFER, and WBD, respectively, with a very small (< 0.2 dB) standard deviation across the subjects.

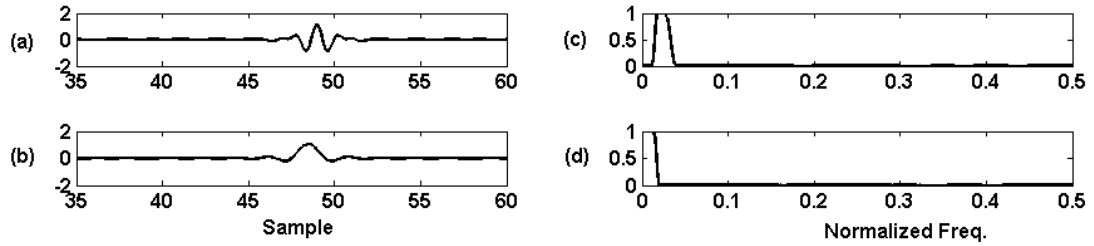

Fig. D.1 Discrete Meyer wavelet: **(a)** wavelet function, **(b)** scaling function, **(c)** magnitude spectrum of the wavelet function, **(d)** magnitude spectrum of the scaling function.

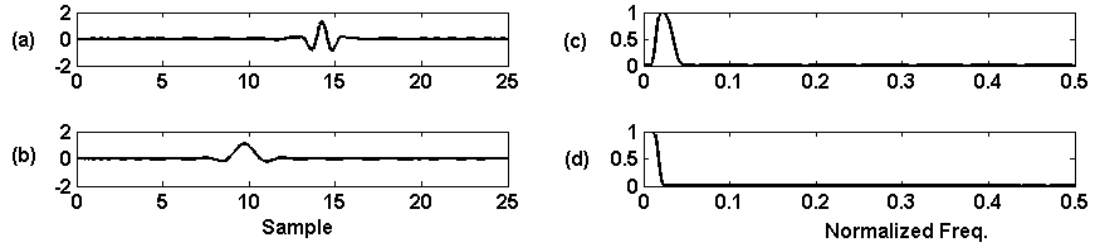

Fig. D.2 Coiflets (order 5) wavelet: **(a)** wavelet function, **(b)** scaling function, **(c)** magnitude spectrum of the wavelet function, **(d)** magnitude spectrum of the scaling function.

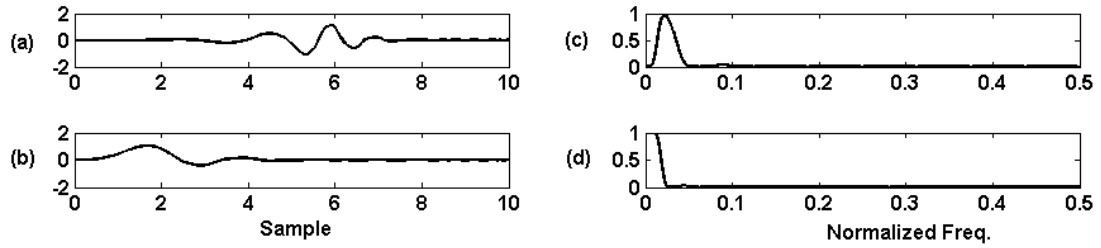

Fig. D.3 Daubechies (order 6) wavelet: **(a)** wavelet function, **(b)** scaling function, **(c)** magnitude spectrum of the wavelet function, **(d)** magnitude spectrum of the scaling function.

Table D.1 The lowpass filter coefficients (*hn*) for discrete Meyer, Coiflets (order 5) and Daubechies (order 6) wavelets.

Discrete Meyer			Coiflets	Daubechies
*h*1- *h*40	*h*41- *h*80	*h*81- *h*101	*h*1- *h*30	*h*1- *h*12
0.0000	-0.0064	0.0000	0.0000	-0.0011
0.0000	-0.0110	0.0000	0.0000	0.0048
0.0000	0.0153	0.0000	0.0000	0.0006
0.0000	0.0174	0.0000	0.0000	-0.0316
0.0000	-0.0321	0.0000	0.0000	0.0275
0.0000	-0.0243	0.0000	0.0000	0.0975
0.0000	0.0637	0.0000	0.0001	-0.1298
0.0000	0.0306	0.0000	0.0003	-0.2263
0.0000	-0.1327	0.0000	-0.0006	0.3153
0.0000	-0.0350	0.0000	-0.0017	0.7511
0.0000	0.4441	0.0000	0.0024	0.4946
0.0000	0.7438	0.0000	0.0068	0.1115
0.0000	0.4441	0.0000	-0.0092	
0.0000	-0.0350	0.0000	-0.0198	
0.0000	-0.1327	0.0000	0.0327	
0.0000	0.0306	0.0000	0.0413	
0.0000	0.0637	0.0000	-0.1056	
0.0000	-0.0243	0.0000	-0.0620	
0.0000	-0.0321	0.0000	0.4380	
0.0000	0.0174	0.0000	0.7743	
0.0000	0.0153	0.0000	0.4216	
0.0000	-0.0110		-0.0520	
0.0000	-0.0064		-0.0919	
0.0000	0.0060		0.0282	
0.0000	0.0022		0.0234	
0.0000	-0.0027		-0.0101	
0.0000	-0.0006		-0.0042	
0.0000	0.0009		0.0022	
-0.0001	0.0002		0.0004	
0.0000	-0.0001		-0.0002	
0.0001	-0.0001			
-0.0001	-0.0001			
-0.0001	0.0001			
-0.0001	0.0000			
0.0002	-0.0001			
0.0009	0.0000			
-0.0006	0.0000			
-0.0027	0.0000			
0.0022	0.0000			
0.0060	0.0000			

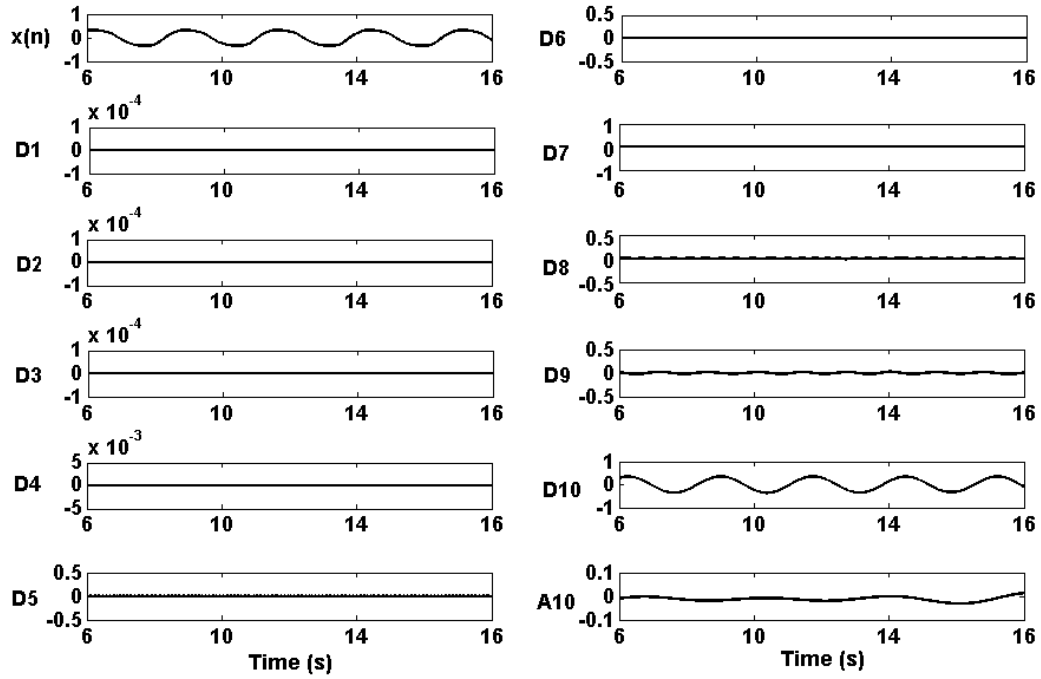

Fig. D.4 Details D1-D10 and approximation A10 of ICG-free artifacts $x(n)$, using discrete Meyer wavelet (all the waveforms are in arbitrary units).

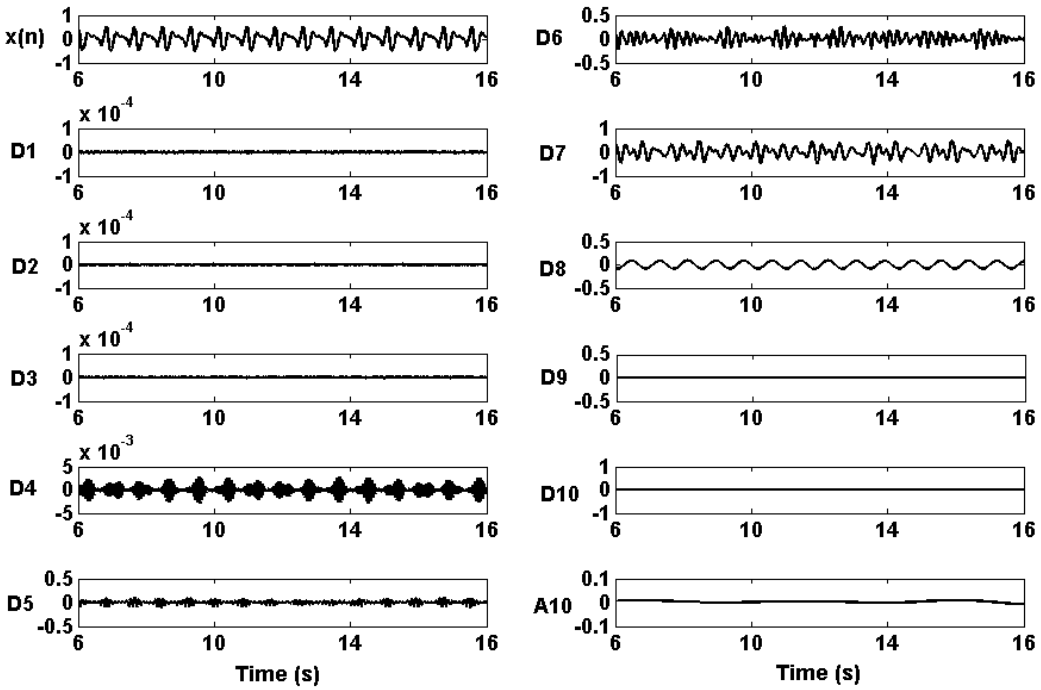

Fig. D.5 Details D1-D10 and approximation A10 of artifact-free ICG $x(n)$, using discrete Meyer wavelet (all the waveforms are in arbitrary units).

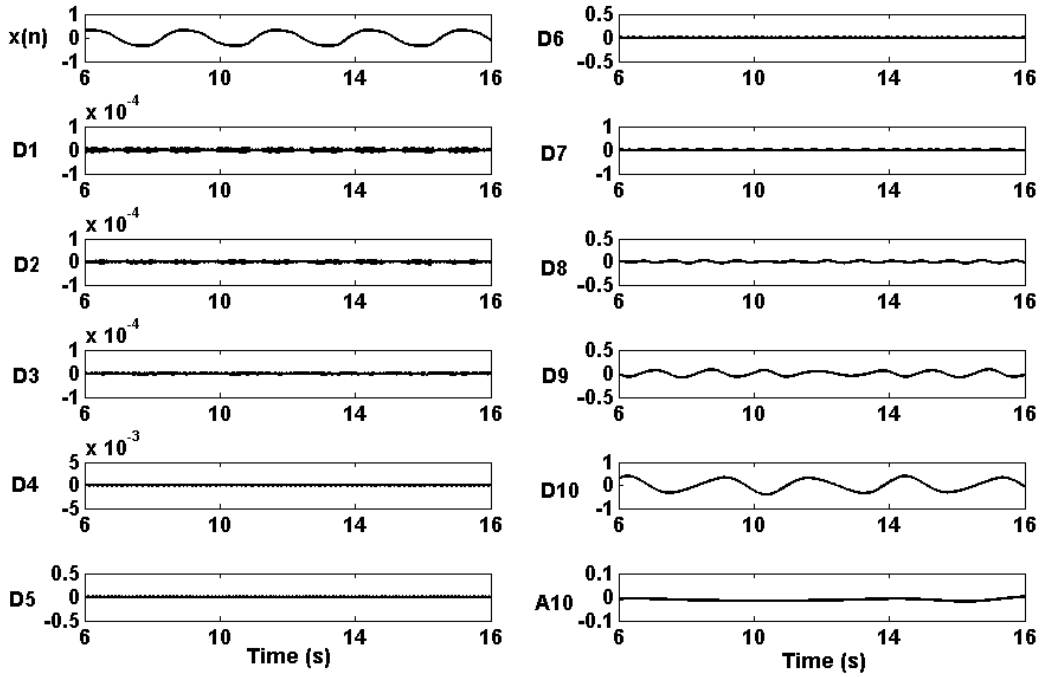

Fig. D.6 Details D1-D10 and approximation A10 of ICG-free artifacts $x(n)$, using Coiflets (order 5) wavelet (all the waveforms are in arbitrary units).

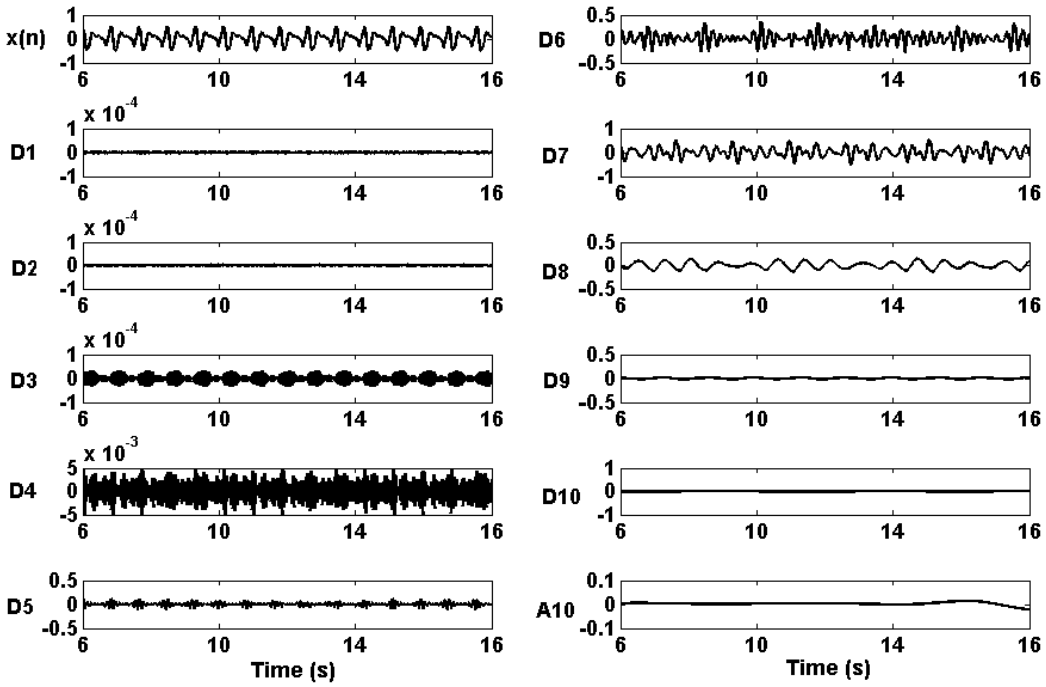

Fig. D.7 Details D1-D10 and approximation A10 of artifact-free ICG $x(n)$, using Coiflets (order 5) wavelet (all the waveforms are in arbitrary units).

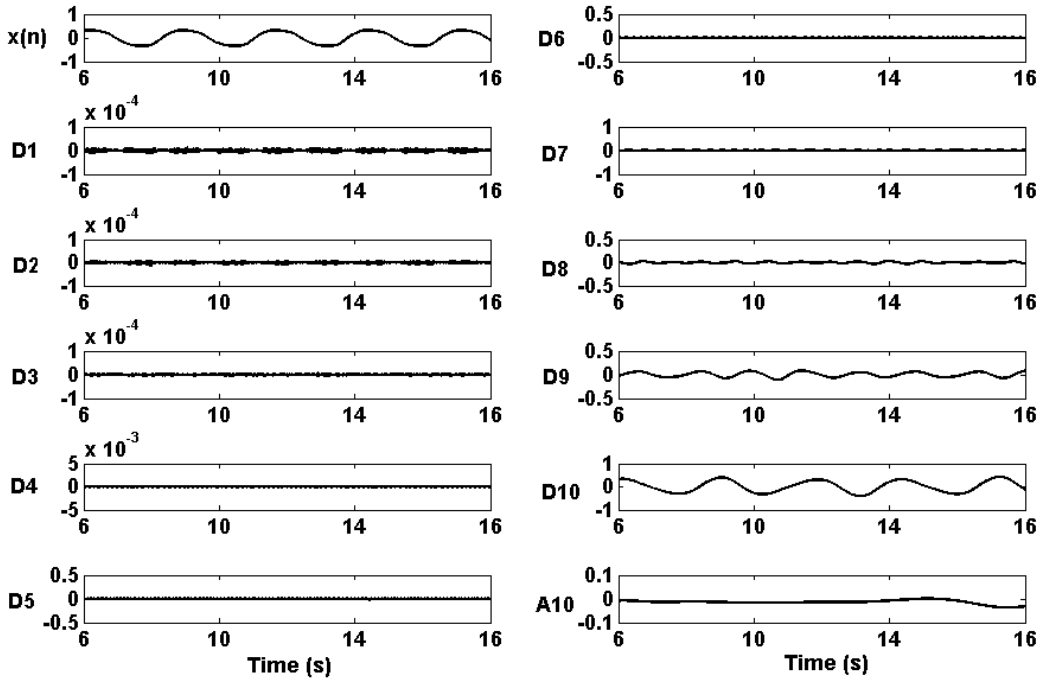

Fig. D.8 Details D1-D10 and approximation A10 of ICG-free artifacts $x(n)$, using Daubechies (order 6) wavelet (all the waveforms are in arbitrary units).

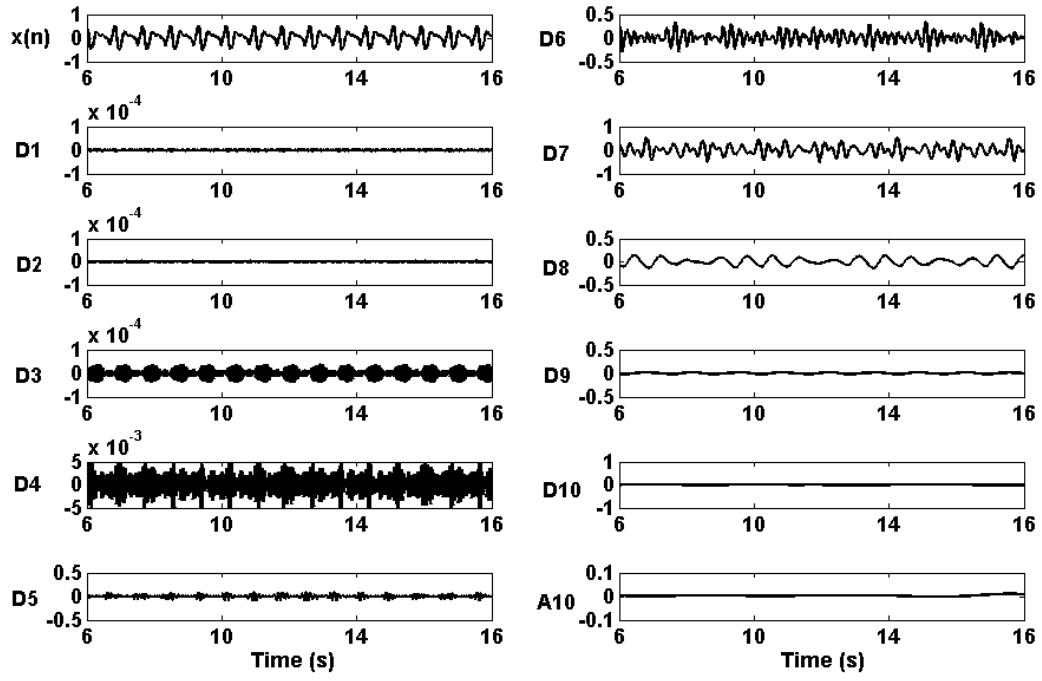

Fig. D.9 Details D1-D10 and approximation A10 of artifact-free ICG $x(n)$, using Daubechies (order 6) wavelet (all the waveforms are in arbitrary units).

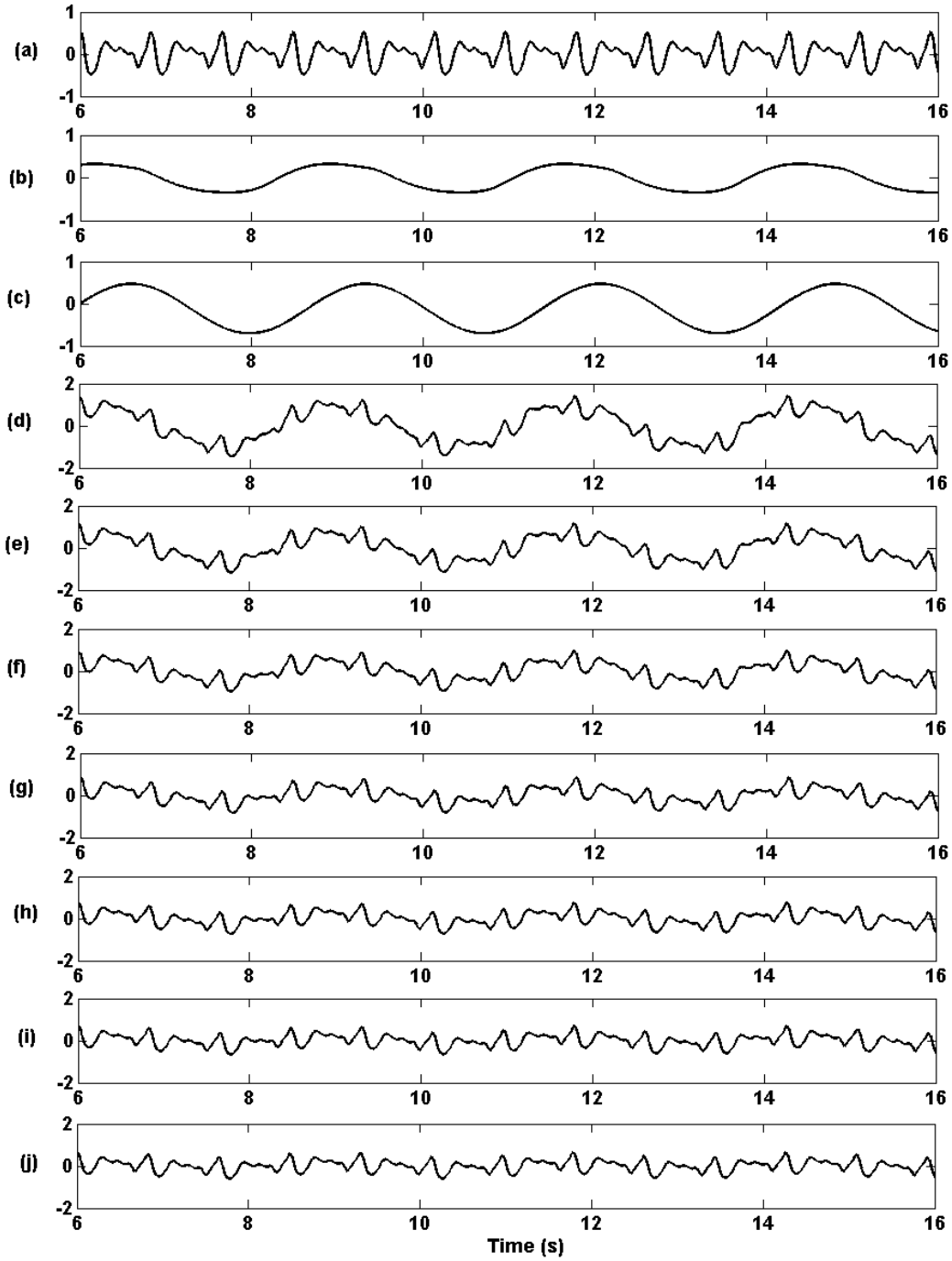

Fig. D.10 Waveforms: **(a)** artifact-free ICG, **(b)** ICG-free artifact, **(c)** sensed respiration, **(d)** ICG with simulated **-9** dB artifact, **(e)** ICG with simulated **-6** dB artifact, **(f)** ICG with simulated **-3** dB artifact, **(g)** ICG with simulated **0** dB artifact, **(h)** ICG with simulated 3 dB artifact, **(i)** ICG with simulated **6** dB artifact, and **(j)** ICG with simulated **9** dB artifact (all the waveforms are in arbitrary units).

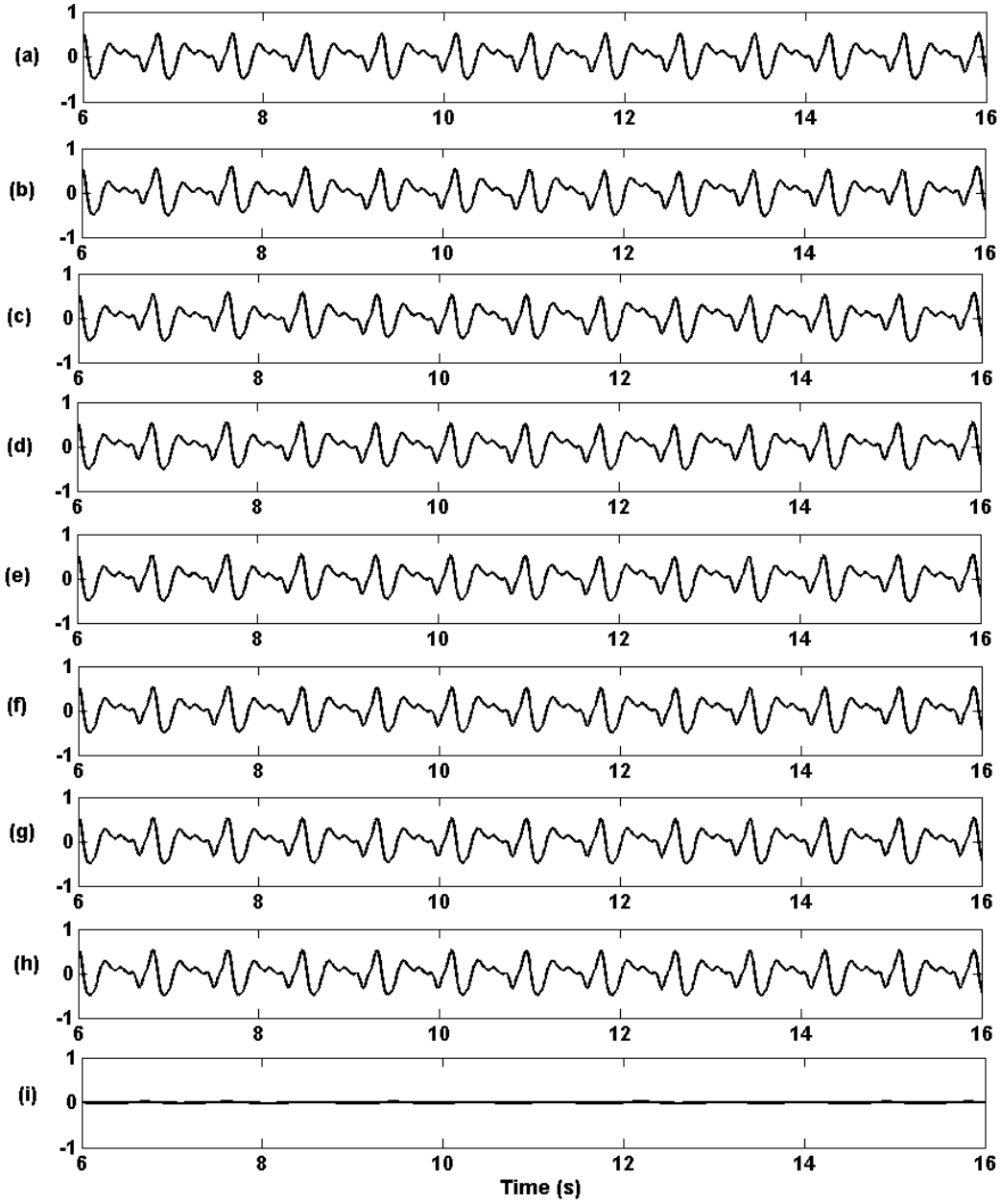

Fig. D.11 Processed output by WBD of signal: **(a)** artifact-free ICG, **(b)** ICG with simulated -9 dB artifact, **(c)** ICG with simulated **-6** dB artifact, **(d)** ICG with simulated **-3** dB artifact, **(e)** ICG with simulated **0** dB artifact, **(f)** ICG with simulated **3** dB artifact, **(g)** ICG with simulated **6** dB artifact, and **(h)** ICG with simulated **9** dB artifact, and **(i)** ICG-free artifact (all the waveforms are in arbitrary units).

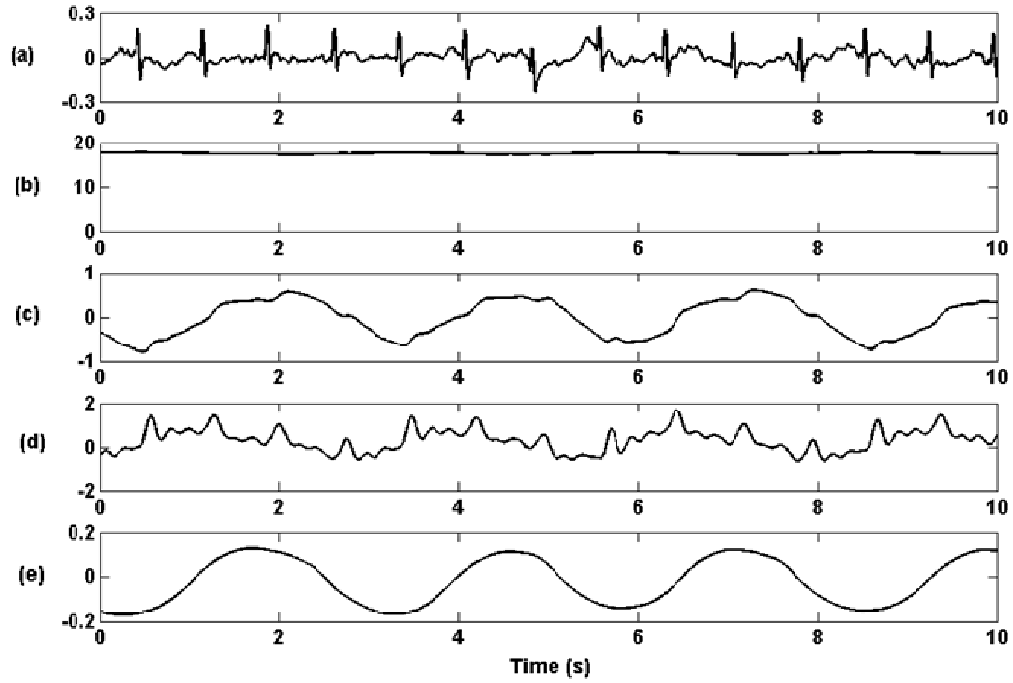

Fig. D.12 Waveforms contaminated by strong respiratory artifacts for processing: **(a)** ECG (in arbitrary units), **(b)** Z_o (in Ω), **(c)** $z(t)$ (in Ω), **(d)** ICG (in Ω/s), and **(e)** sensed airflow (in arbitrary units) from subject 'MS'.

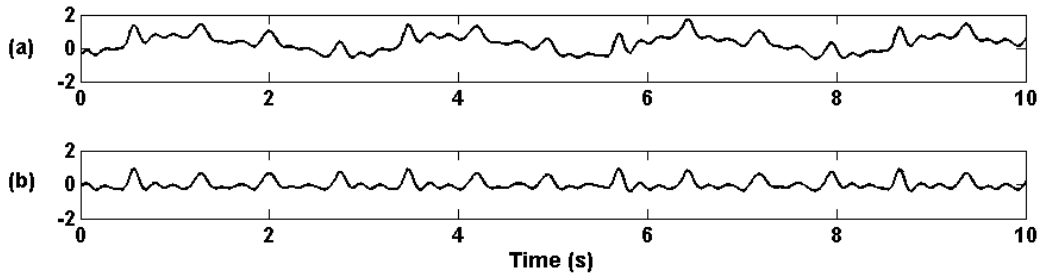

Fig. D.13 Processing of ICG by WBD: **(a)** recorded ICG (in Ω/s), and **(b)** processed ICG (in Ω/s), subject 'MS'.

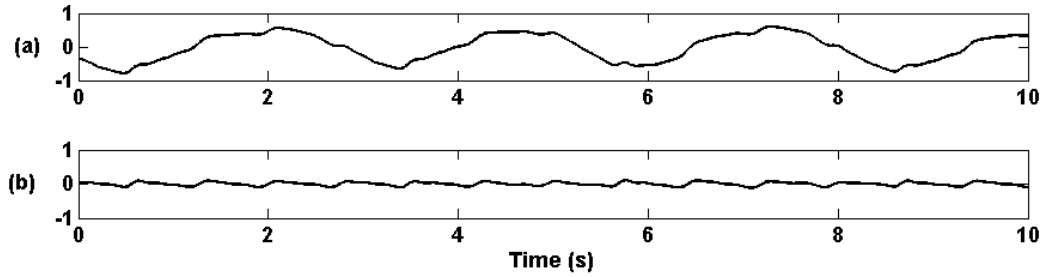

Fig. D.14 Processing of impedance signal by WBD: **(a)** recorded $z(t)$ (in Ω), and **(b)** processed $z(t)$ (in Ω), subject 'MS'.

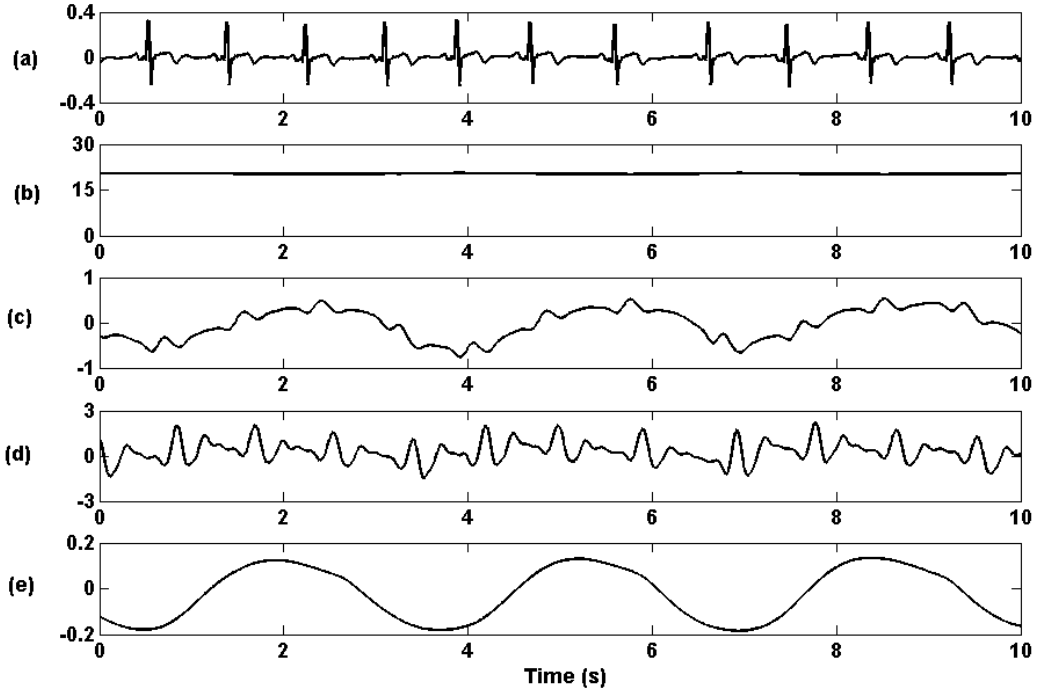

Fig. D.15 Waveforms contaminated by strong respiratory artifacts for processing: **(a)** ECG (in arbitrary units), **(b)** Z_o (in Ω), **(c)** $z(t)$ (in Ω), **(d)** ICG (in Ω/s), and **(e)** sensed airflow (in arbitrary units) from subject 'PP'.

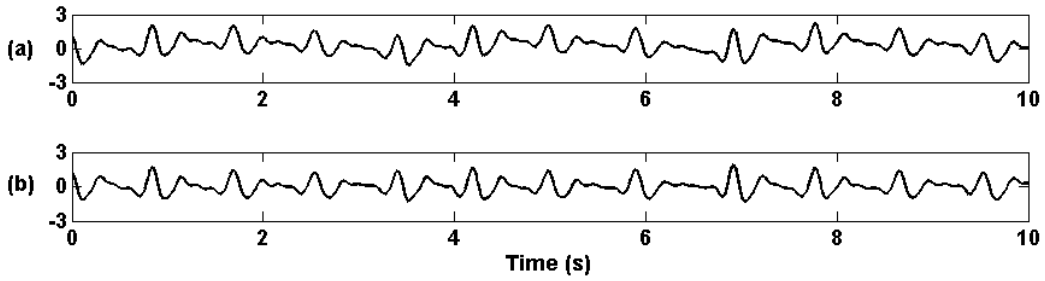

Fig. D.16 Processing of ICG by WBD: **(a)** recorded ICG (in Ω/s), and **(b)** processed ICG (in Ω/s), from subject 'PP'.

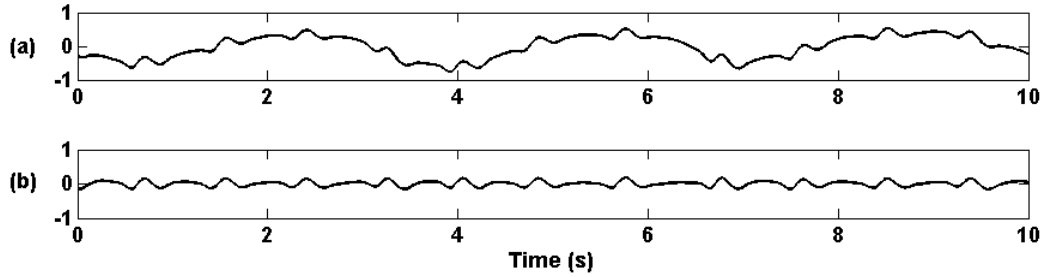

Fig. D.17 Processing of impedance signal by WBD: **(a)** recorded $z(t)$ (in Ω), and **(b)** processed $z(t)$ (in Ω), from subject 'PP'.

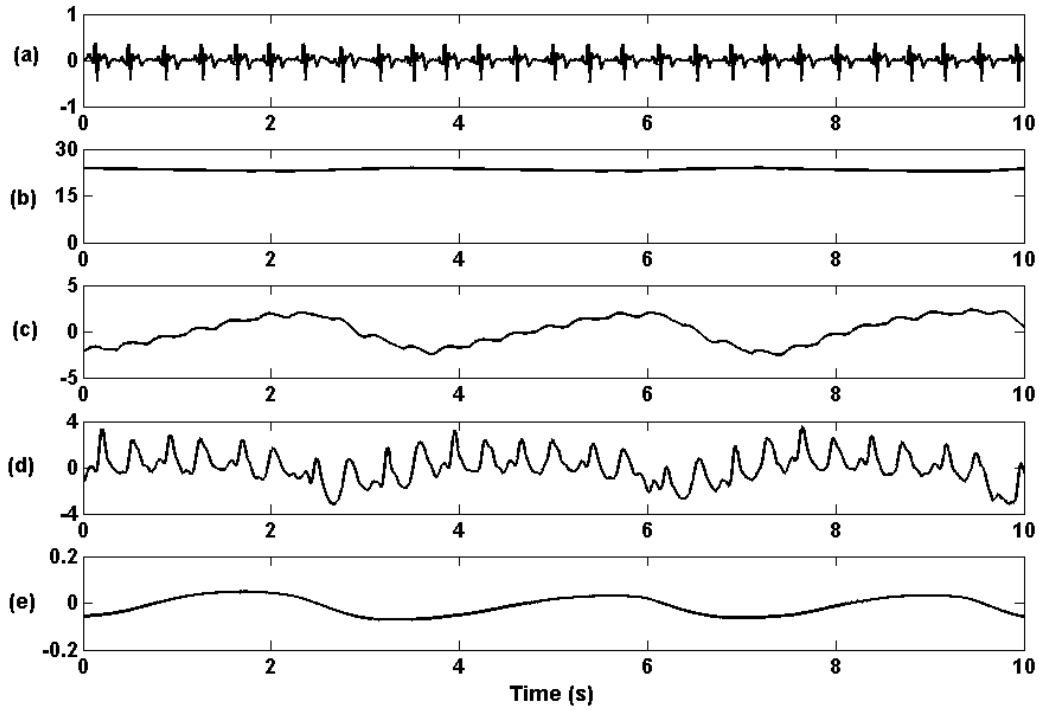

Fig. D.18 Waveforms contaminated by strong respiratory artifacts for processing: **(a)** ECG (in arbitrary units), **(b)** Z_o (in Ω), **(c)** $z(t)$ (in Ω), **(d)** ICG (in Ω/s), and **(e)** sensed airflow (in arbitrary units) from subject 'KI'.

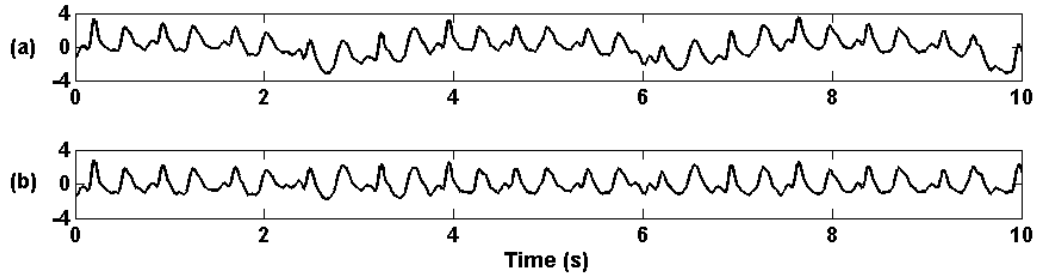

Fig. D.19 Processing of ICG by WBD: **(a)** recorded ICG (in Ω/s), and **(b)** processed ICG (in Ω/s), from subject 'KI'.

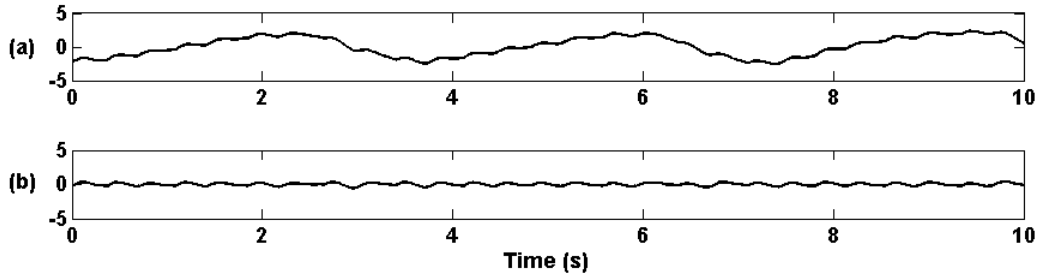

Fig. D.20 Processing of impedance signal by WBD: **(a)** recorded $z(t)$ (in Ω), and **(b)** processed $z(t)$ (in Ω), from subject 'KI'.

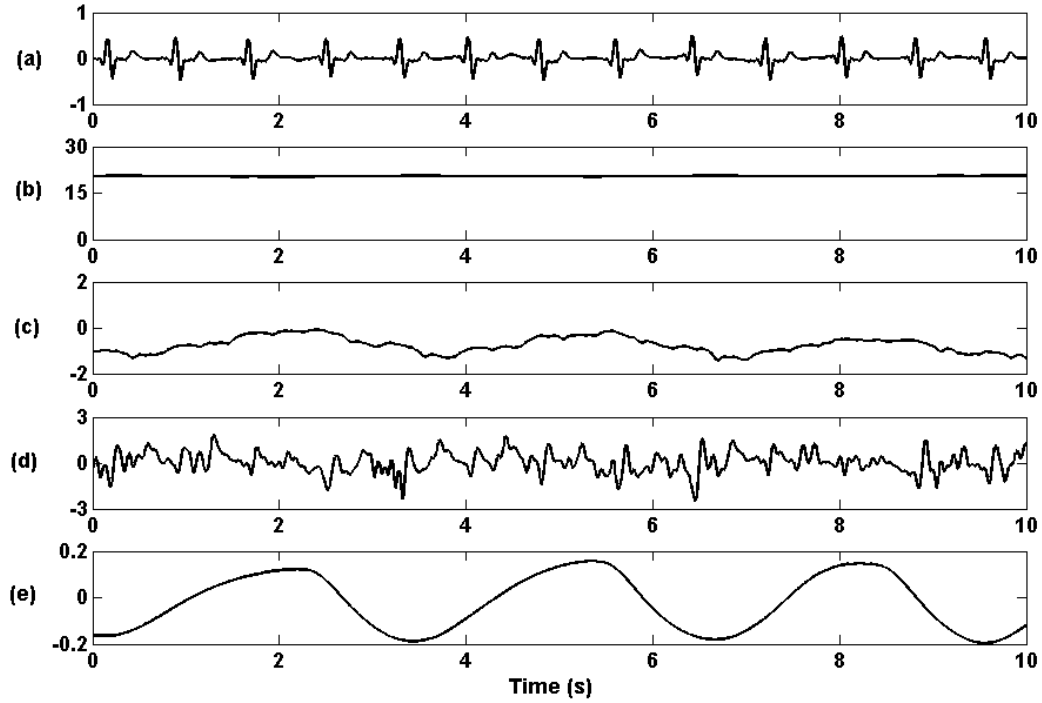

Fig. D.21 Waveforms contaminated by strong respiratory artifacts for processing: **(a)** ECG (in arbitrary units), **(b)** Z_o (in Ω), **(c)** $z(t)$ (in Ω), **(d)** ICG (in Ω/s), and **(e)** sensed airflow (in arbitrary units) from subject 'AJ'.

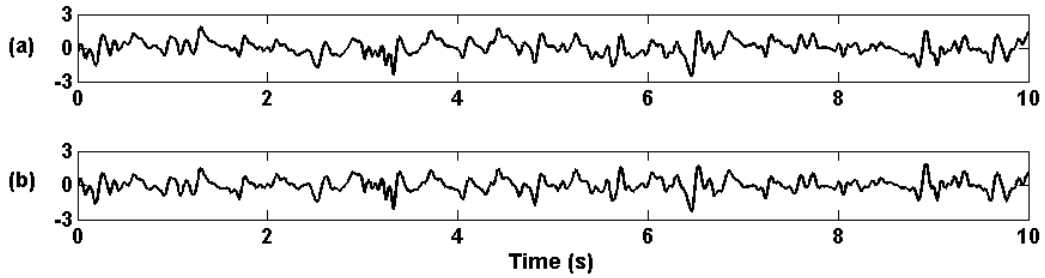

Fig. D.22 Processing of ICG by WBD: **(a)** recorded ICG (in Ω/s), and **(b)** processed ICG (in Ω/s), from subject 'AJ'.

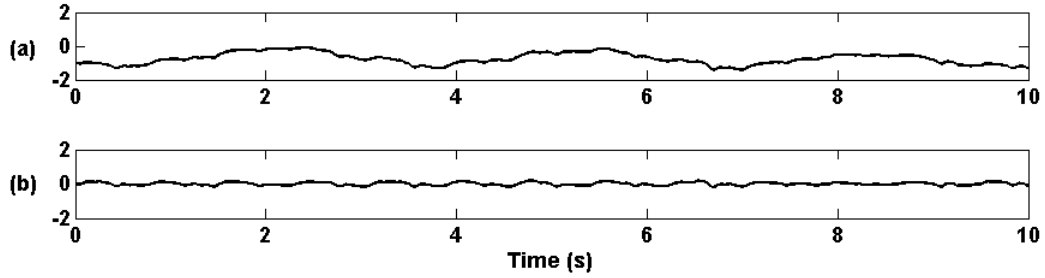

Fig. D.23 Processing of impedance signal by WBD: **(a)** recorded $z(t)$ (in Ω), and **(b)** processed $z(t)$ (in Ω), from subject 'AJ'.

Table D.2 SAR improvement in dB, for simulated input SAR in the –9 to 9 dB range for recordings from different subjects.

Subject	SAR improvement (dB)		
	AFSR	AFER	WBD
AS	18.4	19.4	21.9
AT	18.5	19.6	21.9
BT	18.8	19.7	21.5
CT	18.5	19.7	21.6
DC	18.5	19.5	21.5
DV	18.8	19.3	21.8
GR	18.8	19.7	21.8
GS	18.6	19.8	21.5
LN	18.2	19.7	21.5
LV	18.7	19.7	21.5
MN	18.7	19.3	21.6
MP	18.7	19.3	21.7
MS	18.5	19.6	21.8
PK	18.6	19.4	21.7
PM	18.8	19.8	21.5
RN	18.6	19.7	21.6
RY	18.3	19.8	21.8
SK	18.2	19.5	21.5
SN	18.5	19.6	21.7
SY	18.6	19.5	21.6
VK	18.5	19.4	21.9
UK	18.4	19.5	21.7
VP	18.3	19.5	21.8
Min	18.2	19.3	21.5
Max	18.8	19.8	21.9
Mean	18.5	19.6	21.7
s.d.	0.2	0.2	0.1

Appendix E

RESULTS FROM EVALUATION IN A CLINICAL SETTING

In Chapter 6, the values of the left ventricular ejection time (T_{lvet}) and the stroke volume (SV) estimated using ICG are compared with those obtained by Doppler echocardiogram, and the effectiveness of the artifact suppression techniques in improving the beat-to-beat agreement is examined. Correlation coefficient, regression, and Bland-Altman test have been used to compare the values from impedance cardiography and Doppler echocardiography. This appendix includes scatter plots for signal recordings from the all the subjects with normal health and subjects with cardiovascular disorders. Figures E.1-E18 give scatter plots between SV values from the ICG and the echocardiogram for all the subjects with normal health. Scatter plots between SV values for all the subjects with cardiovascular disorders are given in Figs. E19-E26. It is observed that processing resulted in a considerable decrease in scatter from linear regression for all the subjects in both pre-exercise and post-exercise conditions.

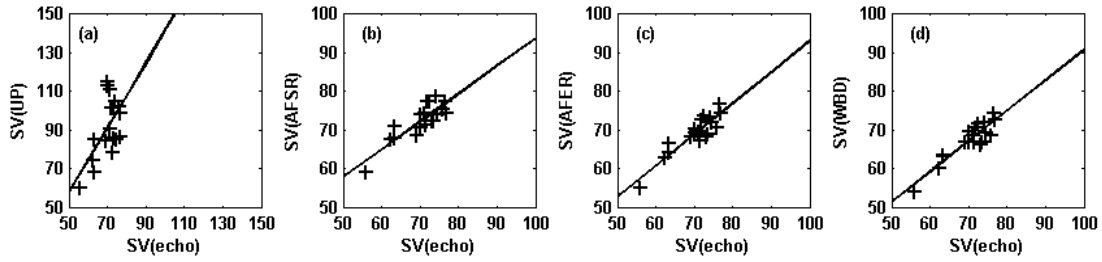

Fig. E.1 Scatter plot and linear regression for SV (in mL) estimated for subject 'DM' in resting condition: **(a)** UP, **(b)** AFSR, **(c)** AFER, and **(d)** WBD.

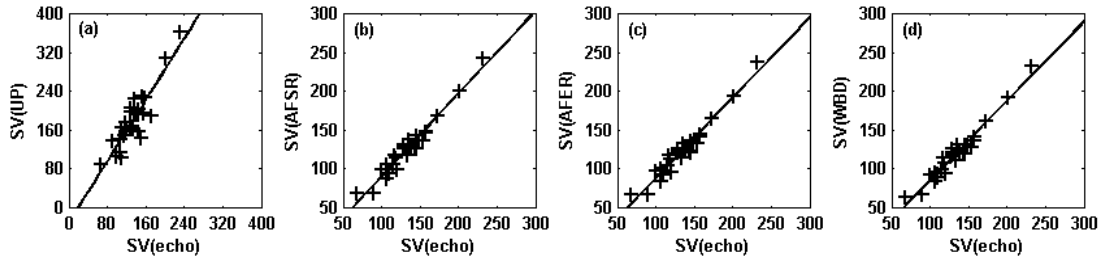

Fig. E.2 Scatter plot and linear regression for SV (in mL) estimated for subject 'DM' in post-exercise condition: **(a)** UP, **(b)** AFSR, **(c)** AFER, and **(d)** WBD.

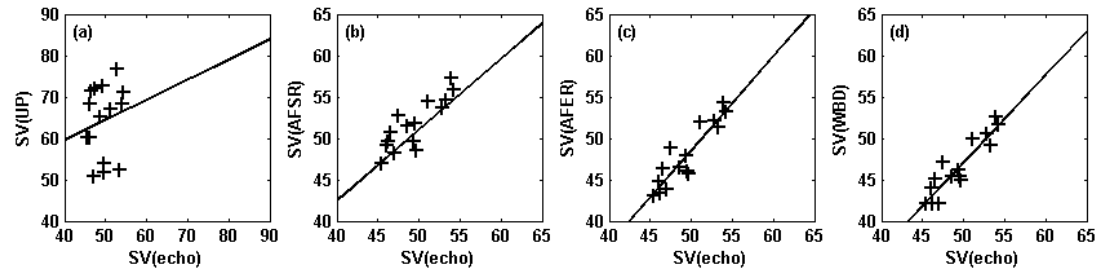

Fig. E.3 Scatter plot and linear regression for SV (in mL) estimated for subject 'ML' in resting condition: **(a)** UP, **(b)** AFSR, **(c)** AFER, and **(d)** WBD.

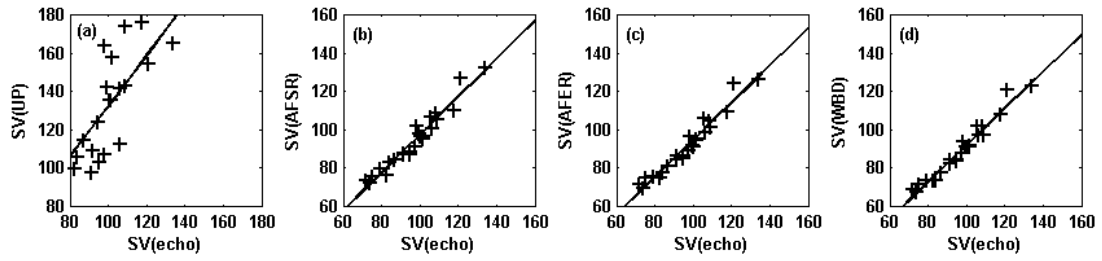

Fig. E.4 Scatter plot and linear regression for SV (in mL) estimated for subject 'ML' in post-exercise condition: **(a)** UP, **(b)** AFSR, **(c)** AFER, and **(d)** WBD.

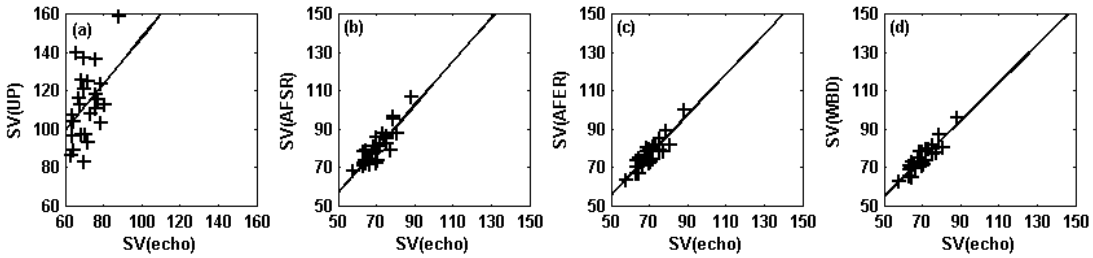

Fig. E.5 Scatter plot and linear regression for SV (in mL) estimated for subject 'MR' in resting condition: **(a)** UP, **(b)** AFSR, **(c)** AFER, and **(d)** WBD.

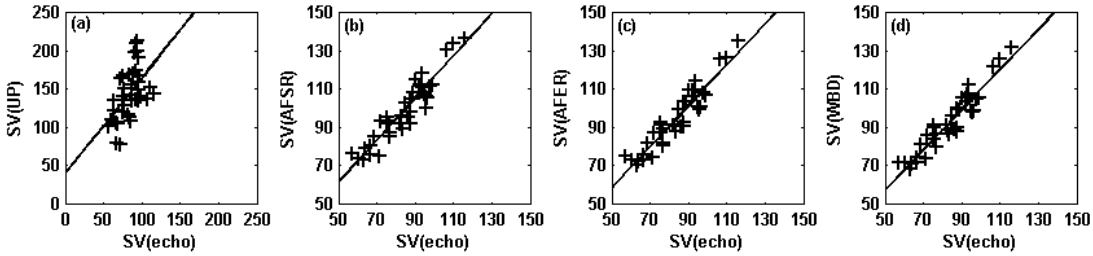

Fig. E.6 Scatter plot and linear regression for SV (in mL) estimated for subject 'MR' in post-exercise condition: **(a)** UP, **(b)** AFSR, **(c)** AFER, and **(d)** WBD.

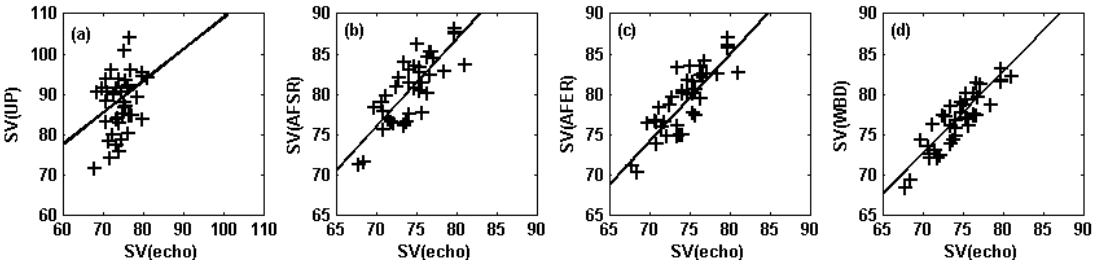

Fig. E.7 Scatter plot and linear regression for SV (in mL) estimated for subject 'P0' in resting condition: **(a)** UP, **(b)** AFSR, **(c)** AFER, and **(d)** WBD.

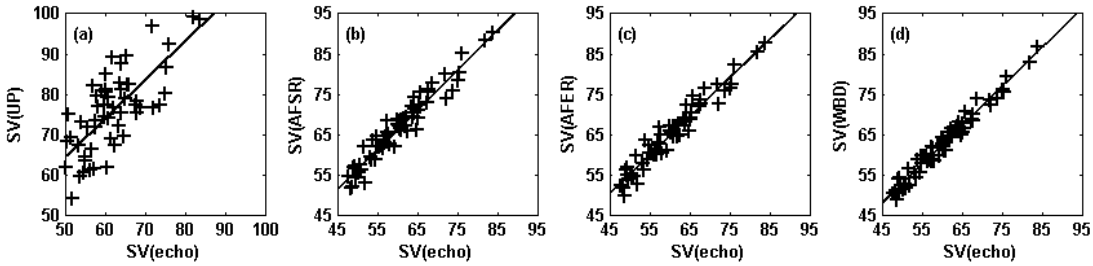

Fig. E.8 Scatter plot and linear regression for SV (in mL) estimated for subject 'P0' in post-exercise condition: **(a)** UP, **(b)** AFSR, **(c)** AFER, and **(d)** WBD.

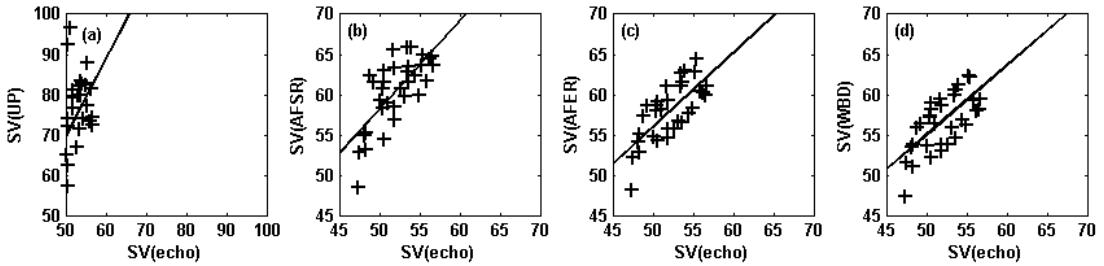

Fig. E.9 Scatter plot and linear regression for SV (in mL) estimated for subject 'P1' in resting condition: **(a)** UP, **(b)** AFSR, **(c)** AFER, and **(d)** WBD.

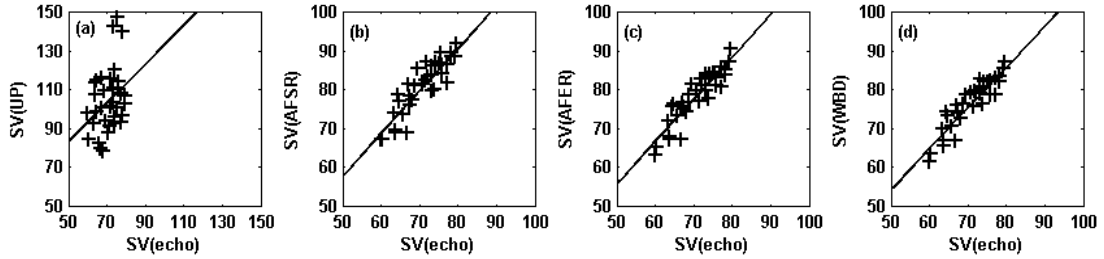

Fig. E.10 Scatter plot and linear regression for SV (in mL) estimated for subject 'P1' in post-exercise condition: **(a)** UP, **(b)** AFSR, **(c)** AFER, and **(d)** WBD.

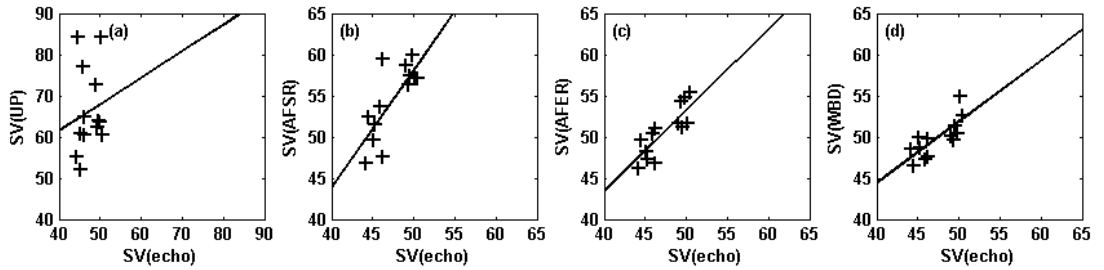

Fig. E.11 Scatter plot and linear regression for SV (in mL) estimated for subject 'PK' in resting condition: **(a)** UP, **(b)** AFSR, **(c)** AFER, and **(d)** WBD.

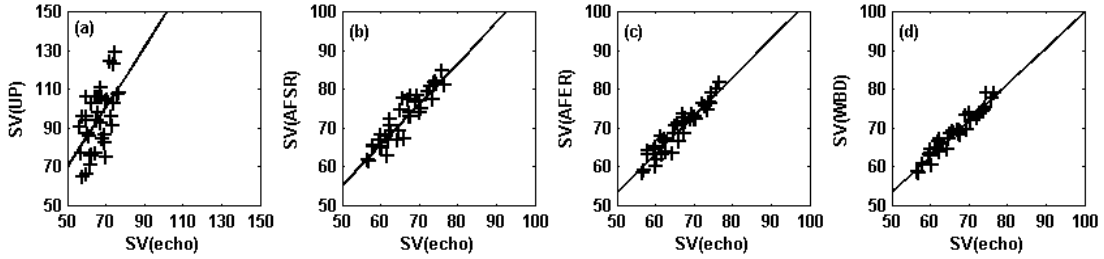

Fig. E.12 Scatter plot and linear regression for SV (in mL) estimated for subject 'PK' in post-exercise condition: **(a)** UP, **(b)** AFSR, **(c)** AFER, and **(d)** WBD.

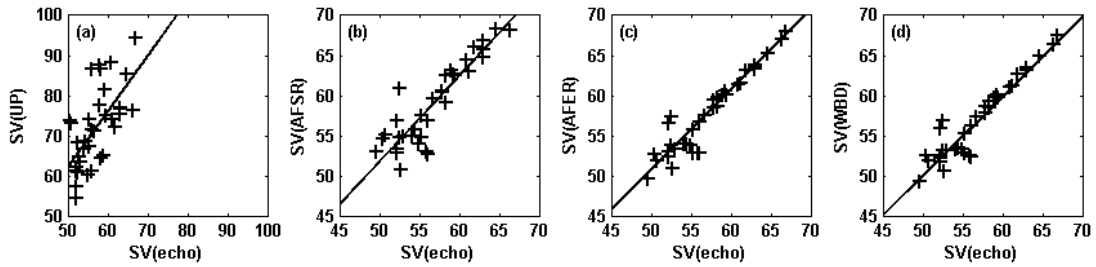

Fig. E.13 Scatter plot and linear regression for SV (in mL) estimated for subject 'RK' in resting condition: **(a)** UP, **(b)** AFSR, **(c)** AFER, and **(d)** WBD.

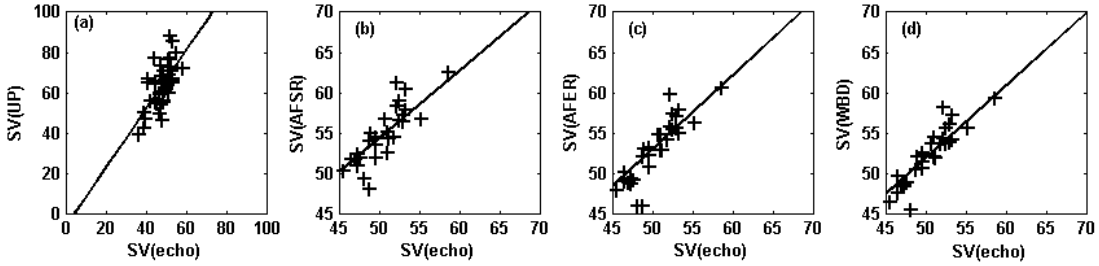

Fig. E.14 Scatter plot and linear regression for SV (in mL) estimated for subject 'RK' in post-exercise condition: **(a)** UP, **(b)** AFSR, **(c)** AFER, and **(d)** WBD.

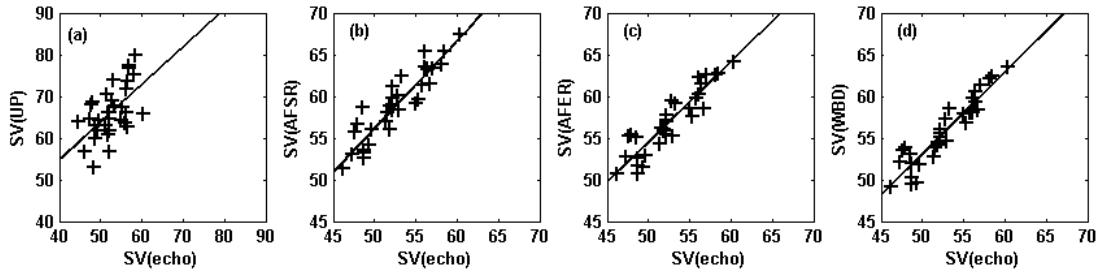

Fig. E.15 Scatter plot and linear regression for SV (in mL) estimated for subject 'UT' in resting condition: **(a)** UP, **(b)** AFSR, **(c)** AFER, and **(d)** WBD.

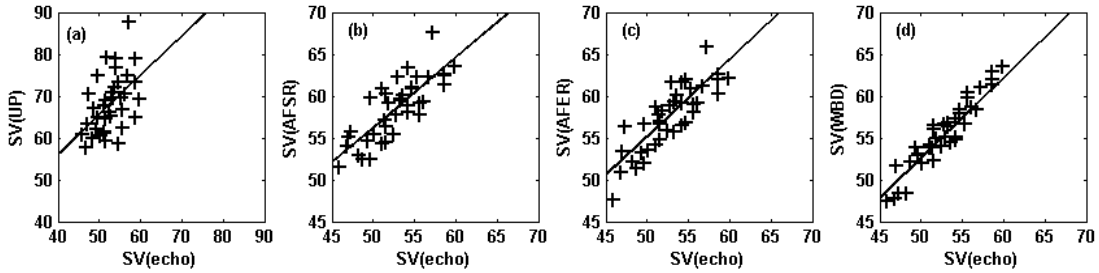

Fig. E.16 Scatter plot and linear regression for SV (in mL) estimated for subject 'UT' in post-exercise condition: **(a)** UP, **(b)** AFSR, **(c)** AFER, and **(d)** WBD.

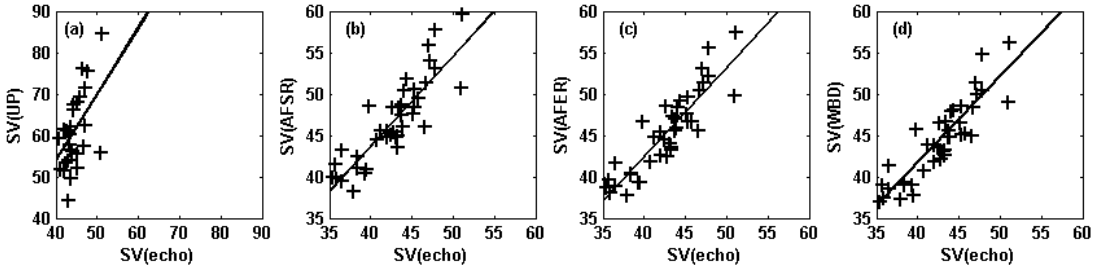

Fig. E.17 Scatter plot and linear regression for SV (in mL) estimated for subject 'VM' in resting condition: **(a)** UP, **(b)** AFSR, **(c)** AFER, and **(d)** WBD.

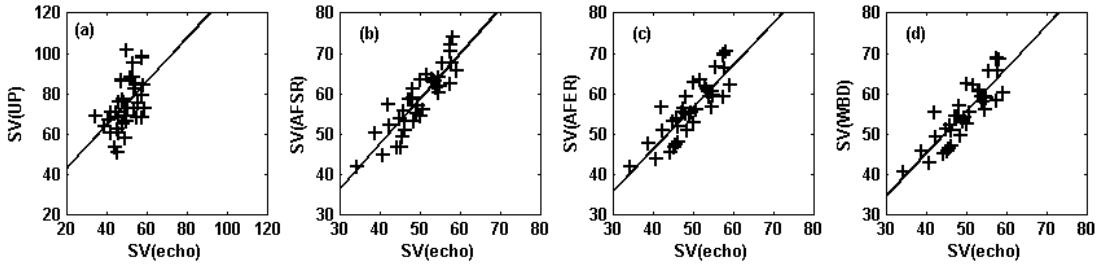

Fig. E.18 Scatter plot and linear regression for SV (in mL) estimated for subject 'VM' in post-exercise condition: **(a)** UP, **(b)** AFSR, **(c)** AFER, and **(d)** WBD.

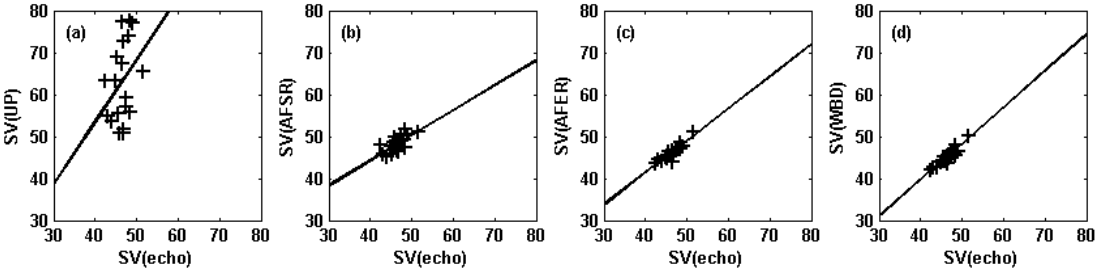

Fig. E.19 Scatter plot and linear regression for SV (in mL) estimated for subject 'AB' in resting condition: **(a)** UP, **(b)** AFSR, **(c)** AFER, and **(d)** WBD.

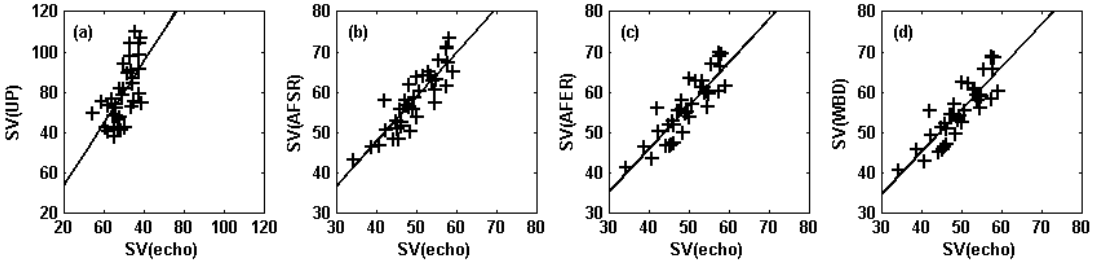

Fig. E.20 Scatter plot and linear regression for SV (in mL) estimated for subject 'AB' in post-exercise condition: **(a)** UP, **(b)** AFSR, **(c)** AFER, and **(d)** WBD.

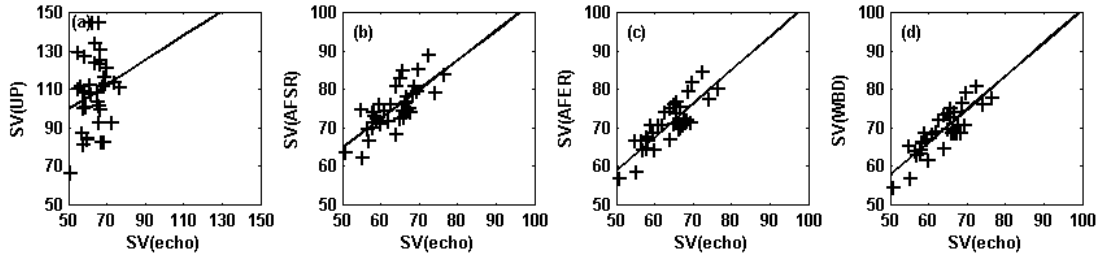

Fig. E.21 Scatter plot and linear regression for SV (in mL) estimated for subject 'ML' in resting condition: **(a)** UP, **(b)** AFSR, **(c)** AFER, and **(d)** WBD.

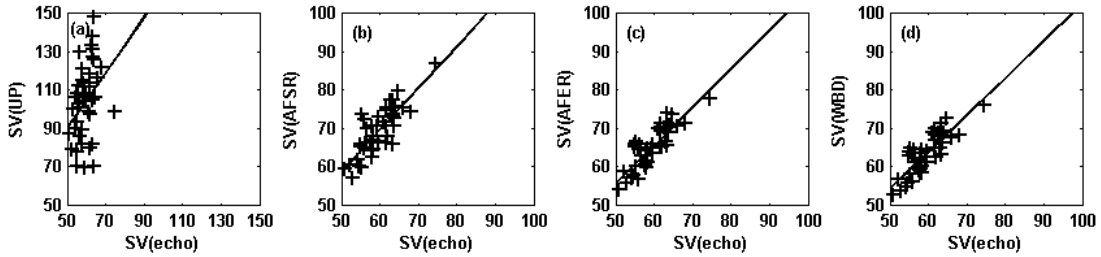

Fig. E.22 Scatter plot and linear regression for SV (in mL) estimated for subject 'ML' in post-exercise condition: **(a)** UP, **(b)** AFSR, **(c)** AFER, and **(d)** WBD.

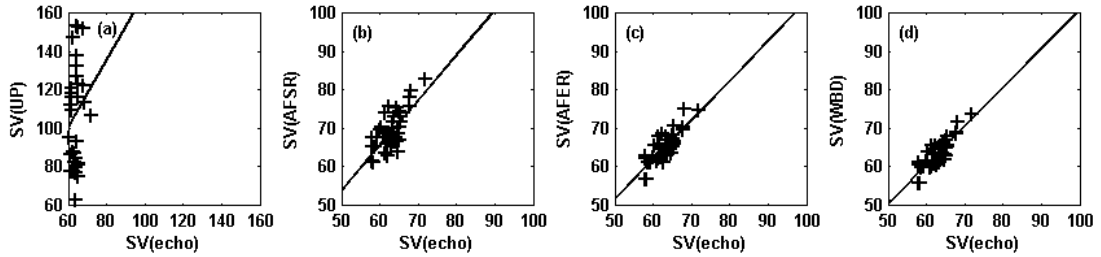

Fig. E.23 Scatter plot and linear regression for SV (in mL) estimated for subject 'DD' in resting condition: **(a)** UP, **(b)** AFSR, **(c)** AFER, and **(d)** WBD.

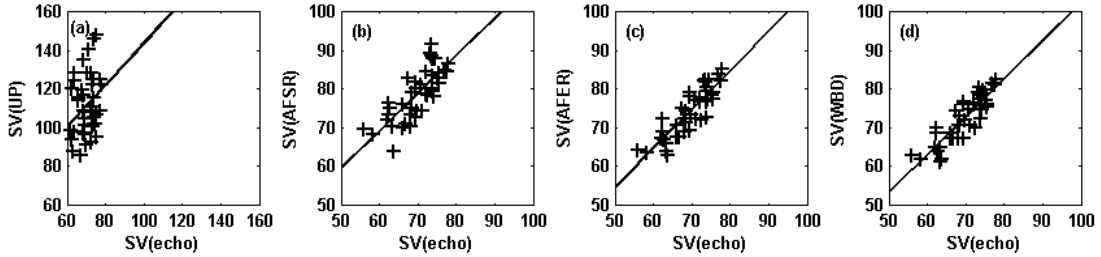

Fig. E.24 Scatter plot and linear regression for SV (in mL) estimated for subject 'DD' in post-exercise condition: **(a)** UP, **(b)** AFSR, **(c)** AFER, and **(d)** WBD.

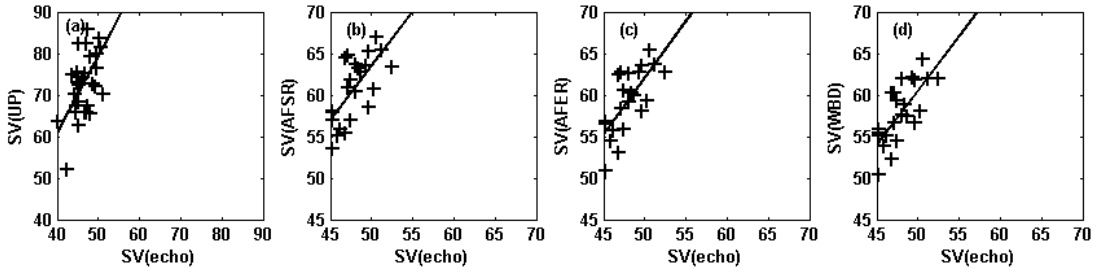

Fig. E.25 Scatter plot and linear regression for SV (in mL) estimated for subject 'LR' in resting condition: **(a)** UP, **(b)** AFSR, **(c)** AFER, and **(d)** WBD.

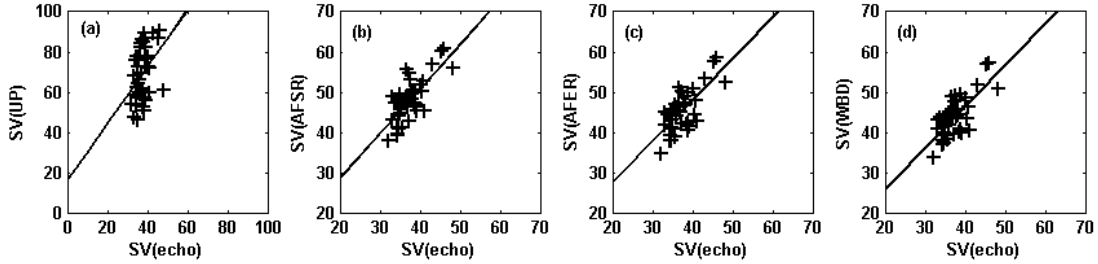

Fig. E.26 Scatter plot and linear regression for SV (in mL) estimated for subject 'IK' in resting condition: **(a)** UP, **(b)** AFSR, **(c)** AFER, and **(d)** WBD.

Appendix F

FORMS FOR BACKGROUND INFORMATION AND SUBJECT'S INFORMED CONSENT

F.1 Form for recording background information of the participating subjects

SUBJECT'S BACKGROUND INFORMATION

Date __/__/ 2007

Name: _____ Code: _____

Address: _____

_____

Phone: ( ) _____Extension: _____

Sex: _____ Age: _____

Occupation: _____

Place of birth: _____

First language: _____

Problem diagnosed: _____

Cardiac history: _____

_____

History of other medical problems: _____

Other remarks: _____

_____

F.2 Form for subject's informed consent to participate in the investigation

CONSENT FOR PARTICIPATION

Investigation: Evaluation of signal processing techniques for impedance cardiography

Investigators
V. K. Pandey, Prof. P. C. Pandey, and Prof. L. R. Subramanyan, IIT Bombay
Dr. N. Burkule, Asian Heart Institute and Research Centre, Bandra-Kurla Complex, Mumbai

Information
This investigation involves non-invasive recordings related to cardiovascular functioning with an Impedance Cardiograph and Doppler Echocardiograph. If you agree to participate in this investigation, recordings will be taken by using surface electrodes connected to an impedance cardiograph attached to signal acquisition interface unit. Four ECG disposable pre-gelled electrodes and one nostril sensor will be placed for a duration of approximately 10 minutes. During these recordings, Doppler echocardiogram will also be acquired in the left lateral position. At the end of the recordings, the nostril sensor and electrodes will be removed. Investigation may involve several recordings before and after mild levels of exercise. The risks of participating in this investigation are almost zero.

Participation
Your participation in this investigation is voluntary and you may decline to participate in this investigation at any time. If you withdraw from the investigation before recordings are completed, your data will be destroyed at your request.

Benefits
There are no direct benefits to you for participating in this investigation. No diagnostic information or inference based on these recordings will be made available to you. Knowledge gained from this research may help in developing better instruments for diagnosis of cardiovascular diseases in the future.

Confidentiality
The information in the investigation will be kept confidential. Data will be stored in files referenced by a number that is not linked to your identity. No reference will be made in oral or written reports which could link you to the investigation.

Compensation
No compensation will be given to you for your participation.

Consent
I have read and understood the above information. I have received a copy of this form. I agree to participate in this investigation with the understanding that I may withdraw at any time.

Participant's Signature: _____
Participant's Name: _____
Date: _____ Place: Mumbai

REFERENCES

Addison, P. S. **(2002).** *The Illustrated Wavelet Transform Handbook: Applications in Science, Engineering, Medicine and Finance* (Taylor & Francis, New York).

Akansu, A. N., and Haddad, R. A. **(2001)**. *Multiresolution Signal Decomposition* (Academic, San Diego).

Akkiraju, P., and Reddy, D. C. **(1992).** "Adaptive cancellation technique in processing myoelectric activity of respiratory muscles," IEEE Trans. Biomed. Engg. **6**, 652-655.

Aldroubi, A., and Unser, M. **(1996)**. *Wavelets in Medicine and Biology* (CRC, Boca Raton).

Andersen, K., and H., Vik-Mo **(1984)**. "Effects of spontaneous respiration on left ventricular function assessed by echocardiography," Circulation **69**, 874–879.

Appel, P. L., Kram, H. B., Mackabee, J., Fleming, A. W., and Shoemaker, W. C. **(1986).** "Comparison of measurements of cardiac output by bioimpedance and thermodilution in severely ill surgical patients," Crit. Care Med. **14(11),** 933-935.

Arora, D., Chand, R., Mehta, Y., and Trehan, N. **(2007).** "Cardiac output estimation after off-pump coronary artery bypass: A comparison of two different techniques," Annals of Cardiac Anaesthesia **10**, 132-136.

Aust, P. E., Belz, G. G., Belz, G., and Koch, W. **(1982).** "Comparison of impedance cardiography and echocardiography for measurement of stroke volume," Eur. J. Clin. Pharmacol. **23(6)**, 475-477.

Baker, L. E. **(1989)**. "Principles of the impedance cardiography technique," IEEE Engg. Med. Biol. Mag., 11-15.

Barde, P. B., Jindal, G. D., Singh, R., and Deepak, K. K. **(2006).** "New method of electrode placement for determination of cardiac output using impedance cardiography," Indian J. Physiology & Pharmacology **50(3)**, 234-240.

Barrows, A. K., Yoshizawa, M., and Yasuda, Y. **(1995)**. "Filtering noncorrelated noise in impedance cardiography," IEEE Trans. Biomed. Engg. **42(3)**, 324-327.

Bellerdinelli, R., Ciampani, N., Castantini, C., Blandini, A., and Purcaso, A. **(1996)**. "Comparison of impedance cardiography with thermodilution and direct Fick methods for noninvasive measurements of stroke volume and cardiac output during incremental exercise in patient with ischemic cardiomyopathy," Am. J. Cardiol. **77**, 1293-1301.

Bernstein, D. P. **(1986)**. "A new stroke volume equation for thoracic electrical bioimpedance: theory and rationale," Crit. Care Med. **14**, 904-909.

Bernstein, D. P., and Lemmens, H. J. M. **(2005)**. "Stroke volume equation for impedance cardiography," Med. Biol. Engg. Comp. **43***,* 443-449.

Bhuta, A. C., Babu, J. P., Jindal, G. D., and Parulkar, G. B. **(1990).** "Technical aspects of impedance plethysmography," J. Postgraduate Medicine **36**, 64-70.

Bland, J. M., and Altman, D. G. **(1986).** "Statistical methods for assessing agreement between two methods of clinical measurement," Lancet **1**, 307-310.

Bland, M. J., and Altman, D. G. **(1983).** "Measurement in medicine: the analysis of method comparison studies," Statistician **32**, 307-317.

Boer, P., Roos, J. C., Geyskes, G. G., and Mees, E. J. **(1979).** "Measurement of cardiac output by impedance cardiography under various conditions," Am. J. Physiol. **237(4)**, 491-496.

Boll, S. F. **(1979).** "Suppression of acoustic noise in speech using spectral subtraction," IEEE Trans. Acoust., Speech, Signal Process. **27**, pp. 113-120.

Bonjer, F. H., Van Den Berg, J., and Dirken M.N. **(1952).** "The origin of the variations of body impedance occurring during the cardiac cycle," Circulation **6(3)**, 415-420.

Boomsma, D. I., de Vries, J., and Orlebeke, J. F. **(1989).** "Comparison of spot and band impedance cardiogram electrodes across different tasks," Psychophysiology **26(6)**, 695-699.

Brown, B. H., Barber, D. C., Morica, A. H., and Leathard, A. D. **(1994**). "Cardiac and respiratory related electric impedance changes in the human thorax," IEEE Trans. Biomed. Engg. **41(8)**, 729-723.

Browning, C., Pelling, D., and Ledingham, J. M. **(1969).** "An electromagnetic flowmeter for studying changes of cardiac output in unanaesthetized rats," Med. Biol. Engg. Med. **7(5)**, 549-558.

Buell, J. C. **(1988).** "A practical, cost-effective, noninvasive system for cardiac output and hemodynamic analysis," Am. Heart J. **116(2)**, 657-64.

Burbank, D. P., and Webster, J. G. **(1978).** "Reducing skin potential motion artefact by skin abrasion," Med. Biol. Engg. Comp. **16**, 31-38.

Charloux, A., Richard, R., Oswald, M., and Geny, B. **(2000)**. "A new impedance cardiograph device for the non-invasive evaluation of cardiac output at rest and during exercise: comparison with the 'direct' Fick method," Eur. J. Appl. Physiol. **82**, 313-320.

Cheng, Y. P., Huey-Dong, W., Gwo-Jen, J., and Cheng-Yi, W. **(2001).** "Removal of cardiac beat artifact in esophageal pressure measurement via a modified adaptive noise cancellation scheme," Annals Biomed. Engg. **29**, 236-243.

Cherkassky, V. and Kilts, S. **(2001).** "Comparison of wavelet thresholding methods for denoising ECG signals," Lecture Notes in Computer Science **2130**, 625-629.

Christie, J., Sheldahl, L. M., Tristani, F. E., Sagar, K. B., Ptacin, M. J., and Wann, S. **(1987).** "Determination of stroke volume and cardiac output during exercise: comparison of two-dimensional and Doppler echocardiography, Fick oximetry, and thermodilution," Circulation **76**, 539-547.

Cohen, A., and Longini, R. L. **(1971).** "Self-balancing system for medical and physiological instrumentation," IEEE Trans. Biomed. Engg. **18**, 66 – 69.

Cotter, G., Schachner, A., Sasson, L., Dekel, H., and Moshkovitz, Y. **(2006).** "Impedance cardiography revisited," Physiol. Meas. **27(9)**, 817-827.

Daley, P. J., Sagar, K. B., and Wann, L. S. **(1985). "**Doppler echocardiographic measurement of flow velocity in the ascending aorta during supine and upright exercise," Br. Heart J. **54**, 562-567.

Daubechies, I. **(1992)**. *Ten Lectures on Wavelets* (SIAM, Philadelphia).

De Boor, C. **(1978).** *A Practical Guide to Splines* (Springer-Verlag, New York).

DeMarzo, A. P., Lang, R. M., Priemer, R, and Korcarz, C. E. **(1995)**. "Computer method of predicting the reliability of impedance cardiography: stroke volume measurement," Comp. in Cardiol., 497-500.

DeMarzo, A., and Lang, R. M. **(1996)**. "A new algorithm for improved detection of aortic valve opening by impedance cardiography," Comp. in Cardiol., 373-376.

Deshpande, A. K., Jindal, G. D., Jagasia, P. M., Murali, K. V. S., Bharadwaj, P. A., Tahilkar, K. I., and Purulkar, G. B. **(1990)**, "Impedance plethysmography of thoracic region: impedance cardiography," J. Postgraduate Medicine **36(4)**, 207-212.

DeSouza, W. M., and Panerai, R. B. **(1981). "**Variability of thoracic impedance cardiograms in man," Med. Biol. Engg. Comput. **19,** 411-415.

Donoho, D. L. **(1995). "**Denoising via soft thresholding," IEEE Trans. Information Theory **41(3)**, 613–627.

Donoho, D. L., and Johnstone, I. M. **(1998).** "Minimax estimation via wavelet shrinkage," Annals of Statistics **26(3)**, 879-921.

Donoho, D. L., and Johnstone, I. M., Kerkyacharian, G., and Picard, D. **(1995).** "Wavelet shrinkage: Asymptopia?," J. Royal Statistical Society **57(2)**, 301-369.

Du Quesnay, M. C., Stoute, G. J., and Hughson, R. L. **(1987).** "Cardiac output in exercise by impedance cardiography during breath holding and normal breathing," J. Appl. Physiol. **62**, 101-107.

Edmunds, A. T., Godfrey, S., and Tooley, M. **(1982).** "Cardiac output measured by transthoracic impedance cardiography at rest, during exercise and at various lung volumes," Clinical Science **63(2)**, 107-113.

Ernst, J. M., Litvark, D. A., Lonzano, D. L., Caciapp, J. T., and Bernston, G. G. **(1999)**. "Impedance pneumography: Noise as signal in impedance cardiography," Psycho-physiology **36**, 333-338.

Ferrigno, M., Hickey, D. D., Linér, M. H., and Lundgren, C. E. **(1986).** "Cardiac performance in humans during breath holding," J. Appl. Physiol. **60(6)**, 1871-1987.

Fisher, D.C., Sahn, D. J., Friedman, M. J., Larson, D., Valdes-Cruz, L. M., Horowitz, S., Goldberg, S. J., and Allen, H. D. **(1983).** "The mitral valve orifice method for noninvasive two-dimensional echo Doppler determinations of cardiac output," Circulation **67**, 872-827.

Fortein, J., Habenbacher, W., Heller, A., Hacker, A., Grullenberger, R., Innerhofer, J., Passath, H., Wanger, C., Haitchi, G., Flotzinger, D., Pacher, R., and Wach, P. **(2005).** "Non-invasive beat-to-beat cardiac output monitoring by an improved method of thransthoracic bioimpedance measurement," Computers in Biology and Medicine **36(11)**, 1185 -1203.

Gardin, J. M., Kozlowski, J., Dabestani, A *et al.* **(1986).** "Studies of Doppler aortic flow velocity during supine bicycle exercise," Am. J. Cardiol. **57**, 327-332.

Gaw, R. .L, Cornish, B. H., and Thomas, B. J. **(2008).** "The electrical impedance of pulsatile blood flowing through rigid tubes: a theoretical investigation," IEEE Trans. Biomed. Engg. **55(2)**, 721-727.

Geddes, L. A., and Baker, L. E. **(1967).** "The specific resistance of biological material--a compendium of data for the biomedical engineer and physiologist," Med. Biol. Engg. **5(3)**, 271-293.

Geddes, L. E., and Baker, L. E. **(1972).** "Thoracic impedance change following saline injection into right and left ventricles," J. Appl. Physiol. **33**, 278-281.

Gong, Y. **(1995).** "Speech recognition in noisy environments: a survey," Speech Communication **16**, 261–291.

Gotshall, R. W., and Sexson, W. R. **(1994).** "Comparison of band and spot electrodes for the measurement of stroke volume by the bioelectric impedance technique," Crit. Care Med. **22(3)**, 420-425.

Greenberg, B. H., Hermann, D. D., Pranulis, M. F., Lazio, L., and Cloutier, D. **(2000).** Reproducibility of impedance cardiography hemodynamic measures in clinically stable heart failure patients," Congestive Heart Failure **6(2)**, 19-26.

Grimnes, S., and Martinsen, Ø. G. **(2000).** *Bioimpedance and Bioelectricity Basics* (Academic, Bodmin).

Guyton, A.C. **(1991).** *Textbook of Medical Physiology* (8th ed., Saunders, New Delhi).

Hamilton, P. S., and Curley, M. G. **(1997).** "Adaptive removal of motion artifact," *Proc. 19th Ann. Int. Conf. Engg. Medicine and Biology* (*IEEE/ EMBC'97*), 297-299.

Hamilton, P. S., and Tompkins, W. J. **(1986).** "Quantitative investigation of QRS detection rules using the MIT/BIH arrhythmia database," IEEE Trans. Biomed. Engg. **33(12)**, 1157-1165

Harley, A. **(1975).** "Observations on the origin of the impedance cardiogram," Br. Heart J. **37(5)**, 550.

Harley, A., and Greenfield, J. C. **(1969).** "Determination of cardiac output in man by means of impedance plethysmography," Aerospace Medicine **39(3)**, 251-256.

Haykin, S. **(2005)**. *Adaptive Filter Theory* (Pearson, New Delhi).

Haykin, S., and Widrow, B. **(2003).** *Least-mean-square Adaptive Filters* (John Wiley, Hoboken, New Jersey).

Hirakawa, S., Ito, H., Kondo, Y., Kanyama, S., Watanabe, I., Mori, N., and Hayase, S. **(1975).** "Comparison of the cardiac output measurements with electromagnetic flowmeter and dye-dilution technique in dogs, with a note on the comparison between

radiocardiography and ear-dye method in man," Japanese Circulation Journal **9(4)**, 393-402.

Huang, Z., Zheng, Z., and Wu, Y. **(1991).** "Monitoring impedance cardiography by adaptive method during external counterpulsation," *Proc. 13th Ann. Int. Conf. Engg. Medicine and Biology* (*IEEE/ EMBC'91*), 819-820.

Huntsman, L. L., Stewart, D. K., Barnes, S. R., Franklin, S. B., Colocousis, J. S., and Hessel, E. A. (**1983).** "Noninvasive Doppler determination of cardiac output in man. Clinical validation," Circulation **67**, 593-602.

Hurwitz, B. E., Shyu, L.Y., Reddy, S. P., Schneiderman, N., and Nagel, J. H. **(1990)**. "Coherent ensemble averaging techniques for impedance cardiography," *Proc. 3rd Annu. IEEE Symp. Comp. Based Med. System* (Chapel Hill, NC), 228-235.

Jensen, L., Yakimets, J., and Teo, K. K. **(1995)**. "A review of impedance cardiography," Heart & Lung **24 (3)**, 183-193.

Jiang, C. F., and Kuo, S. L. **(2007).** "A comparative study of wavelet denoising of surface electromyographic signals," *Proc. 29th Ann. Int. Conf. Engg. Medicine and Biology* (*IEEE/ EMBC'07*), 1868-1871.

Jindal, G. D., Ananthakrishnan, T. S., Kataria, S. K., Sinha, V., Jain, R. K., Mandlik, S. A., Kini, A. R., Naik, M. A., Singh, S. K., Sanghvi, S. H., Haridarshan, G., Deshpandey, A. K., and Mahajan, U. J. **(2004).** *Electrical Impedance and Plethysmography for Medical Application*, BARC Technical Report (Mumbai, India).

Jindal, G. D., and Babu, J. P. **(1985).** "Calibration of dZ/dt in impedance plethysmography," Med. Biol. Engg. Compt. **23**, 279-280.

Joshi, S. M. **(1993).** "A cardiac output monitor," Supervisor: P. C. Pandey, B.Tech. Project report (unpublished), Electrical Engg., IIT Bombay, India.

Joshi, S. M., and Pandey, P. C. **(1994)**, "A cardiac output monitor using impedance plethysmography," *Proc. Int. Conf. on Recent Advances in Biomedical Engg*., Hyderabad, Jan 6-8, 1994, 157-160.

Kania, M., Fereniec, M., and Maniewski, R. **(2007).** "Wavelet denoising for multi-lead high resolution ECG signals," Measurement Science Review **7(2)**, 30-33.

Karnegis, J. N., and Kubicek, W. G. **(1970)**. "Physiological correlates of the thoracic impedance waveform," American Heart J. **79(4)**, 519-523.

Keim, H. J., Wallace, J. M., Thurston, H., Case, D. B., Drayer, J. I., and Laragh, J. H. **(1976).** "Impedance cardiography for determination of stroke index," J. Applied Physiology **41(5)**, 797-799.

Kerr, A. J., Simmonds, M. B., and Stewart, R. A. **(1998).** "Influence of heart rate on stroke volume variability in atrial fibrillation in patients with normal and impaired left ventricular function," Am. J. Cardiol. **82(12)**, 1496-1500.

Khandpur, R. S. **(1992).** *Handbook of Biomedical Instrumentation* (Tata McGraw Hill, New Delhi).

Kiowski, W., Randall, O. S., Steffens, T. G., and Julius, G. **(1981).** "Reliability of echocardiography in assessing cardiac output: A comparative study with a dye dilution technique," J. Molecular Medicine **59**, 1115-1120.

Kizakevich, P. N., Hazucha, M., Van Hoose, L., Bolick, K., Jochem, W. J., McCartney, M., and McMaster, L. **(1994).** "Reproducibility of impedance cardiogram waveform analysis in lower-body and upper-body exercise," *Proc. IEEE 7th Sym. Comp. Based Med. System*, 181-186.

Kizakevich, P. N., Jochem, W. J., and Jones, A. W. **(1988).** "A personal cardiac bioimpedance monitoring system," *Proc. 10th Ann. Int. Conf. IEEE Engg. Med. Biol. Soc.* (*IEEE/EMBC'98*), 48-50.

Kizakevich, P. N., Teague, S. M., Nissman, D. B., Jochem, W. J., Niclou, R., and Sharma, M. K. **(1993).** "Comparative measures of systolic ejection during treadmill exercise by impedance cardiography and Doppler echocardiography," Biological Psychology **36**, 51-61.

Kokkonis, P. A., and Leute, V. **(1996).** "Least squares splines approximation applied to multicomponent diffusion data," Computational Materials Science **6(1)**, 103-111.

Korhonen, I., Kööbi, T., and Turjanmaa, V. **(1999).** "Beat-to-beat variability of stroke volume measured by whole-body impedance cardiography," Med. Biol. Engg. Comput. **37 (Supplement 1)**, 61-62.

Krivoshei, A., Kukk, V., and Min, M. **(2008).** "Decomposition method of an electrical bio-impedance signal into cardiac and respiratory components," Physiol. Meas. **29**, S15–S25.

Kubicek, W. G. **(1989)**. "On the sourse of peak first time derivative (dZ/dt) during impedance cardiography," Annals Biomed. Engg. **17**, 459-462.

Kubicek, W. G., Karnegis, J. N., Patterson, R. P., Witsoe, D. A., and Mattson, R. H. **(1966).** "Development and evaluation of an impedance cardiac output system," Aerospace Med. **37(12)**, 1208-1212.

Kubicek, W. G., Kinnen, E., Paterson, R. P., and Witsoe, D. A. **(1967)**. "Impedance cardiograph," U. S. Patent No. 3,340,867, issued Sep. 12, 1967.

Kubicek, W. G., Kottke, F. J., Ramos, M. U., Patterson, R. P., Witsor, D. A., Labree, J. W., Remole, W., Layman, T. E., Schoening, H. and Garamela, J. T. **(1974)**. "The Minnesota impedance cardiograph- theory and application," Biomed. Engg., 410-417.

Kuriakose, B. **(2000)**. "An impedance cardiograph," Supervisor: P. C. Pandey, M.Tech. Dissertation (unpublished), Biomedical Engg., Indian Institute of Technology, Bombay, India.

Lababidi Z., Ehmke D. A., Durnin R. E., Leaverton P. E., and Lauer R. M. (**1970).** "The first derivative thoracic impedance cardiogram," Circulation **41(4)**, 651-658.

Lababidi Z., Ehmke D. A., Durnin R. E., Leaverton P. E., and Lauer R. M. (**1971).** "Evaluation of impedance cardiac output in children," Pediatrics **47**, 870-879.

Lamberts, R., Visser, K. R., and Ziljstra, W. G. **(1984)**. *Impedance Cardiography*, (Van Gorcum, Assen, The Netherlands).

Leonard, P. A., Douglas, J. G., Grubb, N. R., Clifton, D., Addison, P. S., and Watson, J. N. **(2006).** "A fully automated algorithm for the determination of respiratory rate from the photoplethysmogram," J. Clin. Monit. Comput. **20(1)**, 33-36.

Lewis, J. F., Kuo, L. C., Nelson, J. G., Limacher, M. C., Quiñones, M. A. **(1984).** "Pulsed Doppler echocardiographic determination of stroke volume and cardiac output: clinical validation of two new methods using the apical window," Circulation **70**,425-431.

Lewis, R. P. **(1975).** "Diagnostic value of systolic time intervals in man," Cardiovascular Clinics **6(3)**, 245-264.

Lewis, R. P., Rittogers, S. E., Froester, W. F., and Boudoulas, H. **(1977).** "A critical review of the systolic time intervals," Circulation **56,** 146-158.

Lewis, T. K. **(1974).** "An investigation into the origin of the impedance cardiogram," Ph.D. Dissertation, Worcester Polytechnic Institute, Worcester, Massachusetts.

Lim, L. M., Akay, M., and Daubenspek, J. A. **(1995).** "Identifying respiratory-related evoked potentials," IEEE Engg. Med. Biol. Mag. **14(2)**, 174-178.

Linton, D. M., and Gilon, D. **(2002)**. "Advances in noninvasive cardiac output monitoring," Anals of Cardiac Anaesthesia **5**, 141-148.

Lisheng, X., Zhang, D., and Kuanquan, W **(2005).** "Wavelet-based cascaded adaptive filter for removing baseline drift in pulse waveforms," IEEE Trans. Biomed. Engg. **52**, 1973-1975.

Liu , H., Yambe, T., Sasada, H., Nanka, S., Tanaka, S., Nagatomi, R., and Nitta, S. **(2004).** "Comparison of heart rate variability and stroke volume variability," Autonomic Neuroscience **116**, 69-75.

Liu, Y. and Pecht, M. G. **(2002).** "Reduction of skin stretch induced motion artifacts in electrocardiogram monitoring using adaptive filtering," *Proc. 28th Ann. Int. Conf. Engg. Medicine and Biology* (*IEEE/ EMBC'02*), 6045-6048.

Mallat S. **(1989).** "A theory for multiresolution signal decomposition: The wavelet representation," IEEE Trans. Pattern Analysis and Machine Intelligence **11(7)**, 674-693.

Malmivuo, J., and Plonsey, R. **(1995)**. *Bioelectromagnetism* (2nd ed., Oxford Univ. Press, New York).

Manigandan, N. S. **(2004)**. "Impedance cardiograph", Supervisor: P. C. Pandey, M.Tech. Dissertation (unpublished), Biomedical Engg., Indian Institute of Technology Bombay, India.

Manus, E. **(1986).** "Respiration and heart rate monitoring apparatus," U. S. Patent No. 4,576,179, issued Mar. 18, 1986.

Marque, C., Bisch, C., Dantas, R., Elayoubi, S., Brosse, V., and Pérot, C. **(2004).** "Adaptive filtering for ECG rejection from surface EMG recordings," J. Electromyography Kinesiology **15(3)**, 310-315.

Matsuno, M., Adachi, S., Nakayama, M., and Watanabe, K. **(1986).** "A bridge circuit for temperature drift cancellation," IEEE Tans. Instru. Meas. **42**, 870-872.

Máttar, J. A., Shoemaker, W. C., Diament, D., Lomar, A., Lopes, A. C., De Freitas, E., Stella, F. P., and Factore, L. A. **(1991).** "Systolic and diastolic time intervals in the critically ill patient," Crit. Care Med. **19(11)**, 1382-1386.

Miyamoto, Y., Takahashi, M., Tamura, T., Nakamura, T., Hiura, T., and Mikami, M. U. **(1981).** "Continuous determination of cardiac output during exercise by the use of impedance plethysmography," Med. Biol. Engg. Comput. **19(5)**, 638-644.

Miyamoto, Y., Tamura, T., and Mikami, T. **(1981).** "Automatic determination of cardiac output using an impedance plethysmography," Biotelem. Patient Monit. **8(4)**, 189-203.

Mneimneh, M. A., Yaz, E. E., Johnson, M. T., and Povinelli, R.J. **(2006).** "An adaptive kalman filter for removing baseline wandering in ECG signals," Computers in Cardiology, 253-256.

Modak, W. C. S., and Banerjee, P. K. **(2004).** "Studies of left ventricular functions by systolic time intervals on exposure to dry immersion," Indian J. Aerospace Med. 48(2), 48-56.

Mohapatra, S. N. **(1981)**, *Noninvasive Cardiovascular Monitoring of Electrical Impedance Technique* (Pitman, London).

Muzi, M., Ebert, T. J., Tristani, F. E., Jeutter, D. C., Barney, J. A., and Smith, J. J. **(1985).** "Determination of cardiac output using ensemble-averaged impedance cardiograms," J. Appl. Physiol. **58**, 200-205.

Naidu, N. K. S. **(2005)**. "Hardware for impedance cardiograph," Supervisor: P. C. Pandey, M.Tech. Dissertation (unpublished), Biomedical Engg., Indian Institute of Technology Bombay, India.

Nakonezny, P. A., Kowalewski, R. B., Ernest, J. M., Hawlkey, L. C., Lozano, D. L., Litvwack, D. A., Bernoston, G. G., Sollers, J. J., Kizakevich, P., Cacioppo, J. T., and Lovallo, W. R. **(2001)**. "New ambulatory impedance cardiography validated against Minnesota impedance cardiograph," Psychophysiology **38**, 465-473.

Nelson, N., and Janerot-Sjöberg, B. **(2001).** "Beat-to-beat changes in stroke volume precede the general circulatory effects of mechanical ventilation: a case report," Crit. Care **5(1)**, 41-45.

Northridge, D. B., Findlay, I. N., Wilson, J., Henderson, E., and Dargie, H. J. **(1990).** "Non-invasive determination of cardiac output by Doppler echocardiography and electrical bioimpedance," Br. Heart J. **63(2)**, 93–97.

Nyboer, J, Kreider, M. M., and Hannapel, L. **(1950).** "Electrical impedance plethysmography: A physical and physiologic approach to peripheral vascular study," Circulation **2**, 811-821.

Nyboer, J. **(1970)**. *Electrical Impedance Plethysmography* (2nd ed., Charles C. Thomas, Springfield, Massachusetts).

Ouyang, J. Gao, X., and Zhang, Y. **(1998).** "Wavelet-based method for reducing respiratory interference in thoracic electrical bioimpedance," *Proc. 20th Ann. Int. Conf. Engg. Medicine and Biology* (*IEEE/ EMBC'98*), 1446-1449.

Palko, T., Bialokoz, F., and Weglarz, J. **(1995)**. "Multifrequency device for measurement of the complex electrical bioimpedance design and application," *Proc. 17th Annu. Int. Conf. IEEE Engg. Med. Biol. Soc.* (*IEEE/ EMBC'95*), 145-146.

Pandey, V. K., and Pandey, P. C. **(2005).** "Improved detection of ventricular ejection time for impedance cardiography," *Proc. Indian Conf. Medical Informatics & Telemedicine* (*ICMIT 2005*), Kharagpur, India, 146-150.

Pandey, V. K., and Pandey, P. C. **(2007).** "Tracking-based baseline restoration circuit for acquisition of bio signals," Electronics Letters **43(6)**, 13-14.

Pandey, V. K., Manigandan, N. S., and Pandey, P. C. **(2004)**. "A tracking based drift cancellation circuit for bio-signal acquisition," *Proc. Int. Conf. Instrumentation* (*INCON2004*), Pune, India, 2004.

Pandey, V. K., Naidu, N. K. S., and Pandey, P. C. **(2005).** "Tracking based baseline restoration for acquisition of impedance cardiogram and other biosignals," *Proc. 27th Ann. Int. Conf. IEEE Engg. Med. Biol. Soc.* (*IEEE/ EMBC'05*), 3486-3489.

Pandey, V. K., Pandey, P. C., and Sarvaiya, J. N. **(2008).** "Impedance simulator for testing of instrument for bioimpedance sensing," IETE J. Research on Biomedical Signal and Image Processing **54(3)**, 203-207.

Pandit, S. V. **(1996).** "ECG baseline drift removal through STFT," *Proc. 18th Ann. Int. Conf. Engg. Medicine and Biology* (*IEEE/ EMBC'96*), 1405-1406.

Pappas, C. G., Wang, X., Connolly, R. J., and Schwaitzberg, S. D. **(1994).** "Impedance cardiography in the measurement of cardiac output: studies in rabbits," J. Surg. Res. **59(4)**, 504-510.

Patterson, R. P. **(1989).** "Fundamentals of impedance cardiography," IEEE Engg. Med. Biol. Mag. **8(1)**, 35-38.

Patterson, R., and Wang, L. **(1998).** "Ventricular volume curve obtained from thoracic impedance measurement," *Proc. 20th Annu. Int. Conf. IEEE Engg. Med. Biol. Soc.* (*IEEE/ EMBC'98*), 444-446.

Patwardhan, K. S. **(1997).** "An impedance cardiograph for stress testing," Supervisor: P. C. Pandey, M.Tech. Dissertation (unpublished), Electrical Engg., Indian Institute of Technology Bombay, India.

Peng, Z. Y., Critchiley, L. A. H., Fok, B. S. P., and James, A. E. **(2004).** "Evaluation of impedance based indices of cardiac contractility in dogs," J. Clinical Monitoring and Computing **18(2)**, 103-109.

Penney, B. C., Patwardhan, N. A., and Wheeler, H. B. **(1985).** "Simplified electrode array for impedance cardiography," Med. Biol. Engg. Comput. **23(1)**, 1-7.

Pennock; B. E. **(1990).** "Method and apparatus for measuring respiratory flow," U. S. Patent No. 4,960,118, issued Oct. 2, 1990.

Perrino, A. C., Lippman, A., Ariyan, C., O'Connor, T. Z., and Luther, M. **(1994).** "Intraoperative cardiac output monitoring: comparison of impedance cardiography and thermodilution," J. Cardiothoracic Vascular Anesthesia **8(1)**, 24-29.

Petrovick M. L., Kizakevich P. N., Stacy R. W., and Haak E. D. **(1980).** "A comprehensive cardiac exercise stress processor for environmental health effects studies," J. Med. Syst. **4(2)**, 137-150.

Qu, M., Zhang, Y., Webster, J. G., and Tompkins, W. J. **(1986).** "Motion artifacts from spot and band electrodes during impedance cardiography," IEEE Trans. Biomed. Engg. **33**, 1029-1036.

Quian Q. R., and Garcia H. **(2003).** "Single-trial event-related potentials with wavelet denoising," Clinical Neurophysiology **114(2)**, 376-90.

Quiñones, M. A., Otto, C. M., Stoddard, M., Waggoner, A., and Zoghbi, W. A. **(2002). "**Recommendations for quantification of Doppler echocardiography: a report from the Doppler Quantification Task Force of the Nomenclature and Standards Committee of the American Society of Echocardiography," J. American Society of Echocardiography **15(2)**, 167-184.

Raaijmakers, E., Faes, T. J. C., Govaerts, H. G., de Vries, P. M. J. M., and Heethar, R. M. **(1995).** "The inaccuracy of Kubicek's one cylinder model in thoracic impedance cardiography," IEEE Trans. Biomed. Engg. **44(11)**, 70-76.

Rao, R., Bopardikar, M., and Ajit S. **(1998)**. *Wavelet Transforms: Introduction to Theory and Applications* (Addison-Wesley, Reading, Massachusetts).

Raza, S. B., Patterson, R. P., and Wang, L. **(1992).** "Filtering respiration and low-frequency movement artefacts from the cardiogenic electrical impedance signal," Med. Biol. Engg. Comput. **30(5)**, 556-561.

Reibold, R. C. **(1974).** "Transducer construction and system for measuring respiration,"U. S. Patent No. 3,782,368, issued Jan. 1, 1974.

Riese, H., Groot, P. F. C., Berg, M. V. D., Kupper, N. H. M., Magnee, E. H. B., and Rohaan, E. J. **(2003).** "Large-scale ensamble averaging of ambulatory impedance cardiograms," Behavior Research Methods, Instruments, & Computers **35(3)**, 467-477.

Rosell, J., and Webster, J. G., **(1995).** 'Signal-to-motion artifacts ratio versus frequency for impedance pneunmography," IEEE Trans. Biomed. Engg. **42**, 321-323.

Rosell, J., Cohen, K. P., and Webster, J. G. **(1995).** "Reduction of motion artifacts using a two-frequency impedance plethysmograph and adaptive filtering," IEEE Trans. Biomed. Engg. **12**, 1044-1048.

Ross, J. S., and Wilson, K. J. W. **(2006).** *Ross & Wilson Anatomy and Physiology in Health and Illness* (10^{th} ed., Churchill Livingstone, London).

Rubal, B. J., Baker, L. E., and Poder, T. C. **(1980).** "Correlation between maximum dZ/dt and parameters of left ventricular performance," Med. Biol. Engg. Comput. **18(5)**, 541-548.

Rasmussen, J. P., Sorensen, B., and Kann, T. **(1975).** "Evaluation of impedance cardiography as a non-invasive means of measuring systolic time intervals and cardiac output." American Heart Journal **19**, 210-218.

Sahakian, A. V. and Kuo, K. H. **(1985).** "Canceling the cardiogenic artifact in impedance pneumography," *Proc. 7^{th} Ann. Int. Conf. Engg. Medicine and Biology* (*IEEE/ EMBC'85*), 855-859.

Sakamoto, K., and Kanai, H. **(1979).** "Electrical characteristics of flowing blood," IEEE Trans. Biomed. Engg. **26**, 686-95.

Saunders, C. E. **(1988).** "The use of transthoracic electrical bioimpedance in assessing thoracic fluid status in emergency department patients," Am. J. Emerg. Med. **6(4)**, 337-340.

Sayadi, O., and Shamsollahi, M. B. **(2008).** "ECG denoising and compression using a modified extended Kalman filter structure," IEEE Trans. Biomed. Engg. **55(9)**, 2240-2248.

Schmidt C., Theilmeier, G., Van Aken, H., Korsmeier, P., Wirtz, S. P., Berendes, E., Hoffmeier, A., and Meissner, A. **(2005).** "Comparison of electrical velocimetry and transoesophageal Doppler echocardiography for measuring stroke volume and cardiac output," British J. Anaesthesia **95 (5)**, 603–610.

Schuessler, T. F., Volta, C. R., Goldberg, P., Gottfried, S. B., Kearney, R. E., and Bates, H. T. **(1995).** "An adaptive filter for the reduction of cardiogenic oscillations on esophageal pressure signals," *Proc. 17^{th} Ann. Int. Conf. Engg. Medicine and Biology* (*IEEE/ EMBC'95*), 885-886.

Secher, N.J., Arnsbo, P., Andersen, H.L., and Thomsen, A. **(1979).** "Measurement of cardiac stroke volume in various body positions in pregnancy and during caesarian section: a

comparison between thermodilution and impedance cardiography," Scandinavian J. of Clinical and Laboratory Investigation **39**, 569-576.

Shankar, T. M. R., and Webster, J. G. **(1984).** "Design of an automatically balancing electrical impedance plethysmograph," J. Clin. Engg. **9**, 129 – 134.

Sherwood, A., Allen, M. T., Fahrenberg, J., Kelsey, R. M., Lovallo, W. R., and Van Dornen, J. P. **(1990).** "Methodological guidelines for impedance cardiography," Phychophysiology **27(1)**, 1-23.

Sherwood, A., McFetridge, J., and Hutcheson, S. **(1998).** "Ambulatory impedance cardiography: A feasibility study," Amer. J. Physiol. **85(3)**, 2365-2369.

Sherwood, A., Royal, S. A., Hutcheson, J. S., and Turner, J. R. **(1992).** "Comparison of impedance cardiographic measurements using band and spot electrodes," Psychophysiology **29(6**), 734-741.

Shyu, L., Lin, Y., Liu, C., and Hu, W. **(2004).** "The detection of impedance cardiogram characteristic points using wavelet transform," Computers in Biology and Medicine **34(2)**, 165-175.

Sidney, B. C., Gopinath, R. A., and Guo, H. **(1998)**. *Introduction to Wavelets and Wavelet Transforms: A Primer* (Prentice-Hall, Upper Saddle River, New Jersey).

Siebert, J., Drabik, P., Lango, R., and Szyndler K. **(2004).** "Stroke volume variability and heart rate power spectrum in relation to posture changes in healthy subjects," Med. Sci. Monit. **10(2)**, 31-37.

Siebert, J., Wtorek, J., and Rogowski, J. **(1999).** "Stroke volume variability-cardiovascular response to orthostatic maneuver in patients with coronary artery diseases," Ann. New York Acad. Sci. **873**, 182-190.

Solomon, D. **(1999).** *Computer Graphics and Geometric Modeling* (Springer, New York).

Song, C. G., and Kim, D. W. **(2003).** "An improved approach for measurement of stroke volume during treadmill exercise," Med. Engg. and Physics **25**, 517-522.

Spiering, W., van Es, P. N., and de Leeuw, P. W. **(1998).** "Comparison of impedance cardiography and dye dilution method for measuring cardiac output," Heart **79(5)**, 437-441.

Sramek, B. B. **(1994).** "Thoracic electrical bioimpedance: basic principle and physiologic relationship," Noninvas. Cardiol. **3(2)**, 83-84.

Sramek, B. B., Rose D. M., and Miyamoto A. **(1983).** "Stroke volume equation with a linear base impedance model and its accuracy, as compared to thermodilution and magnetic flowmeter techniques in humans and animals," *Proc. 6th Int. Conf. on Electrical Bioimpedance*, Zadar, Yugoslavia.

Stahl, V., Fischer, A., and Bippus, R. **(2000).** "Quantile based noise estimation for spectral subtraction and Wiener filtering," *Proc. Int. Conf. on Acoustics, Speech, and Signal Proc.* (*ICASSP'00*), 1875-1878.

Stern, H. C., Wolf, G. K., and Belz, G. G. **(1985).** "Comparative measurements of left ventricular ejection time by mechano-, echo- and electrical impedance cardiography," Arzneimittelforschung **35(10)**, 1582-1586.

Summers, R. L., Shoemaker, W. C., Peacock, W. F., Ander, D. S., and Coleman, T. G. **(2003)**. "Bench to bedside: Electrophysiologic and clinical principles of noninvasive hemodynamic monitoring using impedance cardiography," Acad. Emerg. Med. **10(6)**, 669 – 680.

Summers, R. L., Woodward, L. H., and Kolb, J. C. **(1999).** "Correlation of radiographic cardiothoracic ratio with cardiac function in patients with acute congestive heart failure," Emergency Radiology **6(3)**, 153-156.

Taylor, B. C., Timmons, W. D., and Hines, A. S. **(1999).** "A modeling solution to the origin of the electrical impedance cardiogram," *Proc. 1st Joint BMES/EMBS Conf. Serving Humanity. Advancing Technology,* Oct. 13-16, Atlanta, Georgia, 233.

Thakor, N. V., and Zhu, Y. S. **(1991).** "Applications of adaptive filtering to ECG analysis: noise cancellation and arrhythmia detection," IEEE Trans. Biomed. Engg. **38**, 785-794.

Thijsse, B. J., Hollanders, M. A., and Hendrikse, J. **(1998).** "A practical algorithm for least-squares spline approximation of data containing noise," Computers in Physics **12(4)**, 393-399.

Thomas, A, Vohra, A., and Pollard, B. **(1991).** "The effect of haematocrit on transthoracic electrical impedance and on the calculation of cardiac output by an impedance cardiograph," Intensive Care Med. **17(3)**, 178-180.

Thompson, B., Drazner, M. H., Dries, D. L., and Yancy, C. W. **(2004).** "Is impedance cardiography-derived systolic time ratio a useful method to determine left ventricular systolic dysfunction in heart failure?," J. Cardiac Failure **10(s4)**, S38.

Tiinanen, S., Tulppo, M., and Seppänen, T. **(2008).** "Reducing the effect of respiration in baroreflex sensitivity estimation with adaptive filtering," IEEE Trans. Biomed. Engg. **55(1)**, 51-59.

Tinati, M. A., and Mozaffary, B. **(2006).** "A wavelet packets approach to electrocardiograph baseline drift cancellation," Int. J. Biomed. Imaging **2006**, 1-9.

Tompkins, W. J. **(2002).** *Biomedical Digital Signal Processing* (Prentice Hall, New Delhi).

Tong, D.A., Bartels, K. A., and Honeyager, K. S. **(2002).** "Adaptive reduction of motion artifact in the electrocardiogram," *Proc. 24th Ann. Int. Conf. Engg. Medicine and Biology* (*IEEE/ EMBC'04*), 1403- 1404.

Traugott, F. M., A. W. Quail, and White, S. W. **(1981).** "Evaluation of blood resistivity in vivo for impedance cardiography in man, dog and rabbit," Med. Biol. Engg. Comput. **19**, 547-552.

Treister, N., Wagner, K., and Jansen, P. R. **(2004).** "Reproducibility of impedance cardiography parameters in outpatients with clinically stable coronary artery disease," Am. J. Hypertension **18**, 44S-50S.

Unser, M., and Aldroubi, A. **(1996).** "A review of wavelets in biomedical applications," Proceedings of IEEE **84(4)**, 626-638.

Van De Water, J. M., Miller T. W., Vogel, R. L., Mount, B. E., and Dalton, M. L. **(2003).** "Impedance cardiography: The next vital sign technology?," Chest **123**, 2028-2033.

Vandeer, M. N. J. M., Noordegraaf, A. V., Kamp, O., and DeVries, P. M. J. M. **(1999).** "Noninvasive measurement of cardiac output : Two methods compared in patients with mitral regurgitation," Angiolog **50**, 95-101.

Vander, A. J., Sherman, J. H., and Luciano, D. S. **(1980).** *Human Physiology: The Mechanism of Body Function*, 3rd ed. (McGraw Hill, Toronto).

Varanini, M., Emdin, M., Allegri, F., Raciti, M., Conforti, F., Macerata, A., Taddei, A., Francesconi, R., Kraft, G., Abbate, A. L., and Marchesi, C. **(1991).** "Adaptive filtering of ECG signal for deriving respiratory activity," *Proc. Computers in Cardiology*, 621-624.

Veigl, V. L., and Judy, W. V. **(1983).** "Reproducibility of haemodynamic measurements by impedance cardiography," Cardiovascular Res. **17(12)**, 728-734.

Venkatachalam, L., **(2006)**. "Impedance cardiograph," Supervisor: P. C. Pandey, M.Tech. Dissertation (unpublished), Biomedical Engg., Indian Institute of Technology, Bombay, India.

Verdu, J. **(1994).** "Electrical impedance method for the measurement of stroke volume in man: State of art," A Report, Uni. Tartuensis, Jartu, Estonia, 110-129.

Verhoeve, P. E., Cadwell, C. A., and Tsadok, S. **(1998).** "Reproducibility of noninvasive bioimpedance measurements of cardiac function," J. Cardiac Failure **4**, 53.

Visser, K. R. **(1989).** "Electric properties of flowing blood and impedance cardiography," Ann. Biomed. Engg. **17(5)**, 463-473.

Visser, K. R., Lamberts R., Korsten H. H., and Zijlstra, W.G. **(1976).** "Observations on blood flow related electrical impedance changes in rigid tubes," Pflugers Arch. **366**, 289-291.

Von Borries, R. F., Pierluissi, J. H., and Nazeran, H. **(2005).** "Wavelet transform-based ECG baseline drift removal for body surface potential mapping," *Proc. 27th Ann. Int. Conf. Engg. Medicine and Biology* (*IEEE/ EMBC'05*), 3891-3894.

von Borries, R. F., Pierluissi, J. H., Nazeran, H. **(2006). "**Wavelet transform-based ECG baseline drift removal for body surface potential mapping," *Proc. 27th Ann. Int. Conf. Engg. Medicine and Biology* (*IEEE/ EMBC'06*), 3891-3894.

Wang, K. Q., Xu, L. S., Wang, L., Li, Z. G., and Li, Y. Z. **(2003).** "Pulse baseline wander removal using wavelet approximation," Computers in Cardiology, 605- 608.

Wang, L., and Patterson, R. **(1993).** "Contribution of heart movement and blood volume change of impedance cardiography calculated by human thorax model," *Proc. 15th Annu. Int. Conf. IEEE Engg. Med. Biol. Soc.* (*IEEE/ EMBC'93*), 444-446.

Wang, L., Paterson, R. P., and Raza, S. B. **(1991)**. "Respiratory effects on cardiac related impedance indices measured under voluntary cardio-respiratory synchronization (VCRS)," Med. Biol. Engg. Comput., 505-510.

Wang, X. A., Sun, H. H., Adamson, D., and Van de Water, J. M. **(1989).** "An impedance cardiography system: A new design," Ann. Biomed. Engg. **17(5)**, 535-556.

Wang, Y., Haynor, D. R., and Kim, Y. **(2001).** "A finite-element study of the effect of electrode position on the measured impedance change in impedance cardiography," IEEE Trans. Biomed. Engg. **48**, 1390-1401.

Watanabe, T., Kamide, T., Torii, Y. andOchiai, M. **(1981).** "A convenient measurement of cardiac output by half-taped impedance cardiography," Iyodenshi To Seitai Kogaku (Jap. J. Med. Elec. Biol. Eng.) (Tokyo) **19**, 30–34.

Webster J. G. **(1998).** *Medical Instrumentation-Application and Design* (3rd ed., John Wiley, New Delhi).

Weissman, C., Askanazi, J., Milic-Emili, J., and Kinney, J. M. **(1984).** "Effect of respiratory apparatus on respiration," J. Appl. Physiol. **57**, 475-480.

Widrow, B., and Stearns, S. D. **(2005)**. *Adaptive Signal Processing* (PHI, New Delhi).

Widrow, B., Glover, J. R., McCool, J. M., Kaunitz, J., Williams, C. S., Hearn, R. H., Zeidler, J. R., Dong, E., and Goodlin, R. C. **(1975).** "Adaptive noise cancelling: Principles and applications," *Proc. IEEE* **63(12)**, 1692-1716.

Wilson, A. J., Franks, C. I., and Freeston, I. L. **(1982).** "Methods of filtering the heart-beat artefact from the breathing waveform of infants obtained by impedance pneumography," Med. Biol. Engg. Compt. **20**, 293-298.

Witsoe, D. A., Patterson, R. P., and Kubicek, W. G., **(1969).** *Development and Evaluation of An Impedance Cardiograph System to Measure Cardiac Output and Other Cardiac Parameters,* (NASA Technical Report, Huston, Texas)

Woltjer, H. H., van Der Meer, B. J. M., Bogaard, H. J., and de Vries, P. M. J. M. **(1995).** "Comparison between spot and band electrodes and between two equations for calculations of stroke volume by means of impedance cardiography," Med. Biol. Engg. Comput. **33**, 330-334.

Woltjer, H. H., Arntzen, B. W., Bogaard, H. J., and de Vries, P. M. **(1996).** "Optimalisation of the spot electrode array in impedance cardiography," Med. Biol. Engg. Comput. **34(1)**, 84-87.

Woltjer, H. H., Bogaard, H. J., Bronzwaer, J. G, de Cock, C. C., and de Vries, P. M. **(1996).** "Prediction of pulmonary capillary wedge pressure and assessment of stroke volume by noninvasive impedance cardiography," Am. Heart J. **134(3)**, 450-455.

Xu, L., Zhang, D., and Wang, K. **(2005).** "Wavelet-based cascaded adaptive filter for removing baseline drift in pulse waveforms," IEEE Trans. Biomed. Engg. **55(1)**, 1973-1975.

Yakimets, J., and Jensen, L. **(1995).** "Evaluation of impedance cardiography: comparision of NICCOM3-R7 with Fick and thermodilution method," Heart and Lung **24(3)**, 194-205.

Yamamoto, Y., Tamura, M. S., Mouth, Y., Miyasita, M., and Hamamoto, H. **(1998)**. "Design and implementation for beat-by-beat impedance cardiography," IEEE Trans. Biomed. Engg. **35(12)**, 1086-1090.

Zhang, Y., Qu., M., Webster, J. G., Tompkins, W. J., Ward, B. A., and Bassett, D. R. **(1986).** "Cardiac output monitoring by impedance cardiography during treadmill exercise," IEEE Trans. Biomed. Engg. **33**, 1037-1041.

Zhou, P., and Kuiken T. A **(2006).** "Eliminating cardiac contamination from myoelectric control signals developed by targeted muscle reinnervation," Physiological Measurement **27,** 1311-1327.

Zhou, P., Lowery, M. M., Weir, R. F., and Kuiken, T. A. **(2005).** "Elimination of ECG artifacts from myoelectric prosthesis control signals developed by targeted muscle reinnervation," *Proc. 27th Ann. Int. Conf. Engg. Medicine and Biology* (*IEEE/ EMBC'05*), 5276-5279.

Zhou, W., and Gotman, J. **(2004).** "Removal of EMG and ECG artifacts from EEG based on wavelet transform and ICA," *Proc. 26th Ann. Int. Conf. Engg. Medicine and Biology* (*IEEE/ EMBC'04*), 392- 395.

Author's Resume and Thesis Related Publications

Author's resume

Mr. Vinod Kumar Pandey received his M.Sc. in electronics from Dr. Ram Manohar Lohia Avadh University, Faizabad (Uttar Pradesh) in 2000. Presently, he is pursuing Ph.D. in biomedical engineering at Indian Institute of Technology Bombay. His research interests include electronic digital signal processing, wavelets, biomedical instrumentation, and embedded system design.

PhD thesis related publications

Journals

Sarvaiya J. N., Pandey, P. C., and Pandey, V. K. **(2008). "**An impedance detector for glottography," *IETE J. Research* **55(3)**, 97-102.

Pandey, V. K., Pandey, P. C., and Sarvaiya J. N. **(2008).** "Impedance simulator for testing of instrument for bioimpedance sensing," *IETE J. Research on Biomedical Signal and Image* Processing **54(3)**, 203-207.

Pandey, V. K. and Pandey P. C. **(2007).** "Tracking-based baseline restoration circuit for acquisition of bio signals," *Electronics Letters* **43(6)**, 13-14.

International conferences

Pandey, V. K. and Pandey, P. C. **(2009). "**Wavelet based denoising for suppression of motion artifacts in impedance cardiography," submitted to *Int. Symposium on Emerging Areas in Biotechnology & Bioengineering*, Mumbai, India.

Patil, B. B., Pandey, V. K., and Pandey, P. C. **(2009). "**A microcontroller based thorax simulator for testing and calibration of impedance cardiographs," submitted to *Int. Symposium on Emerging Areas in Biotechnology & Bioengineering*, Mumbai, India.

Pandey, V. K. and Pandey, P. C. **(2007).** "Wavelet based cancellation of respiratory artifacts in impedance cardiography," in *Proc. 15th Int. Conf. Digital Signal Processing* (DSP 2007), Cardiff, UK, 191-194.

Pandey, V. K. and Pandey, P. C. **(2005).** "Cancellation of respiratory artifact in impedance cardiography," in *Proc. 27th Annual Int. Conf. of the IEEE Eng. Med. Biol. Soc.* (IEEE/ EMBC 2005), Shanghai, China, 5503-5506.

Pandey, V. K., Naidu, N. K. S., Pandey, P. C. **(2005).** "Tracking based baseline restoration for acquisition of impedance cardiogram and other biosignals," in *Proc. 27th Annual Int. Conf. IEEE Eng. Med. Biol. Soc.* (IEEE/ EMBC 2005), Shanghai, China, 3486-3489.

National conferences

Pandey, V. K. and Pandey, P. C. **(2005).** "Improved detection of ventricular ejection time for impedance cardiography," in *Proc. Indian Conf. Medical Informatics Telemedicine* (ICMIT 2005), Kharagpur, India, 146-150.

Manigandan, N. S., Pandey, V. K., and Pandey, P. C. **(2003).** "Thoracic simulator for impedance cardiography," in *Proc. National Symposium on Instrumentation.* (NSI 28), Pantnagar, India.

Acknowledgements

With deep regards and profound respect, I take this opportunity to express my deep sense of gratitude and indebtedness to my supervisor Prof. P. C. Pandey for support, inspiring guidance, motivation, and constructive criticism which have made this work possible.

I am grateful to Prof. L. R. Subramanyan for all the support for my work, and specifically for initiating the investigation involving clinical recordings. I am thankful to Dr. Nitin Burkule and his associates in the Echo Lab at the Asian Heart Institute and Research Center, Mumbai, for the whole hearted support and active involvement in the clinical part of the investigations. I am thankful to Prof. R. Lal, Prof. S. Mukherjee, and Prof. S. Chaudhuri, members of the research progress committee for my thesis, for their valuable suggestions and encouragements at various stages of the work. I am also thankful to Dr. G. D. Jindal of BARC Mumbai for many insightful discussions and technical materials.

I would like to thank everyone in the Signal Processing & Instrumentation (SPI) Lab for making my time enjoyable in the lab and the institute. My special thanks go to my friends, Jayan, Deven, Krishnan, Devidas, Milind, Parveen, Pandurang, Vidyadhar, and Mani for encouragement and support, making my life happy and joyful. It indeed has been an honor and privilege to work and live in the wonderful environment of the institute. So many people have enriched my life here and I am surely blessed to have met them all, although I am unable to thank them all.

I am grateful to my parents, parents-in law, my wife Shalini, and other family members for being so supportive and patient, especially for supporting me in the final push and making everything worth it.

I dedicate this thesis to all my teachers.

Vinod Kumar Pandey